Universidad de Valladolid

PROGRAMA DE DOCTORADO EN

INVESTIGACIÓN BIOMÉDICA

TESIS DOCTORAL:

REMODELING OF VASCULAR SMOOTH MUSCLE ION CHANNELS INVOLVED IN PURINERGIC SIGNALING IN ESSENTIAL HYPERTENSION

Presentada por INÉS ÁLVAREZ MIGUEL para optar al grado de Doctora por la Universidad de Valladolid

Dirigida por:

Dr. José Ramón López López

Dra. Mª Teresa Pérez García

ABBREVIATIONS INDEX

$[Ca^{2+}]_i$	Intracellular Ca^{2+} Concentration
Ab	Antibody
AC	Adenylate Cyclase
ACE	Angiotensin Converter Enzyme
ADP	Adenosine Diphosphate
Ang II	Angiotensin II
ANO/TMEM16	Anoctamin Family of Ca^{2+}-Activated Cl^- Channels
ANP	Atrial Natriuretic Peptide
AT1	Angiotensin Receptor Type 1
ATP	Adenosine Triphosphate
BAPTA	1,2-Bis(2-Aminophenoxy)ethane-N,N,N',N'-Tetraacetic Acid
BESTs	Bestrophin Family of Ca^{2+}-Activated Cl^- Channels
BK_{Ca}	Large-Conductance Ca^{2+}-Activated K^+ Channels
BPH	Blood Pressure High Mice Model
BPN	Blood Pressure Normal Mice Model
BSA	Bovine Serum Albumin
CaCCs	Ca^{2+}-Activated Cl^- Channels
CaMKII	Ca^{2+}/Calmodulin-Dependent Protein Kinase II
cAMP	Cyclic Adenosine Monophosphate
CFTR	Cystic Fibrosis Transmembrane Conductance Regulator
cGMP	Cyclic Guanosine Monophosphate
CGRP	Calcitonin Gene-Related Peptide
CHO	Chinese Hamster Ovary Cell Line
ClCa	Cl^- Channel Accessory Proteins
ClCs	Voltage-Gated Cl^- Channels
ClICs	Intracellular Cl^- Channels
Cm	Membrane Capacitance
CO	Cardiac Output

CVP	Central Venous Pressure
DAG	Diacylglycerol
DIDS	4,4′ -Diisothiocyanatostilbene-2,2′ -Disulfonic Acid
DMSO	Dimethyl Sulfoxide
DNA	Deoxyribonucleic Acid
DOCA	Deocorticosterone
EDHF	Endothelium-Derived Hyperpolarizing Factor
EGTA	Ethylene Glycol-bis(2-Aminoethylether)-*N,N,N′,N′*-Tetraacetic Acid
EJPs	Excitatory Junction Potentials
eNOS	Endothelial Nitric Oxide Synthase
E-NTPDase	Extracellular Ectonucleotidase Trisphosphate Diphosphohydrolase
ER/SR	Endoplasmic Reticulum/ Sarcoplasmic Reticulum
E_X	Equilibrium Potential of X Ion
GA	Glutaraldehyde
GABA	γ-Aminobutyric Acid
GC	Guanylyl Cyclase
GFP/YFP/RFP	Green/Yellow/Red Fluorescent Proteins
GPCRs	G-Protein Coupled Receptors
GSD	Ground State Depletion Super-resolution
GTP	Guanosine Triphosphate
ICC	Immunocytochemistry
I_{clamp}	Current-Clamp
I_{ClCa}	Ca^{2+}-Activated Cl^- Current
IK_{Ca}	Intermediate-Conductance Ca^{2+}-Activated K^+ Channels
IP/coIP	Immunoprecipitation/Co-immunoprecipitation
IP_3	Phosphatidylinositol (3,4,5)-Trisphosphate
IP_3R	Phosphatidylinositol (3,4,5)-Trisphosphate Receptor
K_{ATP}	ATP-Dependent K^+ Channels
K_{Ca}	Ca^{2+}-Activated K^+ Channels
K_{IR}	Inward Rectifying K^+ Channels

KO	Knockout Animal Model
K_V	Voltage-Dependent K^+ Channels
LTCCs	L-Type Ca^{2+} Channels
MEA	β-Mercaptoethylamine
mRNA	Messenger Ribonucleic Acid
NA	Noradrenaline
Nif	Nifedipine
NKCCs	Na^+, K^+, Cl^- Cotransporters
NO	Nitric Oxide
OAG	1-Oleoyl-2-Acetyl-sn-Glycerol
P_a	Mean Arterial Pressure
PBS	Phosphate Buffered Saline
PCR	Polymerase Chain Reaction
P_d	Dyastolic Pressure
PFA	Paraformaldehyde
PGI_2	Prostacyclin
PHE	Phenylephrine
PIP_2	Phosphatidylinositol 4,5-Biphosphate
PiP_3K	Phosphatidylinositol-4,5-Biphosphate 3-Kinase
PKA	Protein Kinase A
PKC	Protein Kinase C
PKG	Protein Kinase G
PLA	Proximity Ligation Assay
PLC	Phospholipase C
PP2B	Protein Phosphatase 2B/Calcineurin
P_s	Systolic Pressure
P_X	Permeability of X Ion
Pyr3/6/10	Pyrazole3/6/10 Compounds
PVAT	Perivascular Adipose Tissue
qPCR	Quantitative PCR

Ra	Access Resistance
RAAS	Renin-Angiotensin-Aldosterone System
RNA	Ribonucleic Acid
ROCs	Receptor-Operated Channels
RP18S	Ribosomal Protein 18S
RyR	Ryanodine Receptor Channels
SDS-PAGE	Soidum Dodecyl Sulfate Polyacrilamide Gel Electrophoresis
SEM	Standard Error Of The Mean
SERCA	Sarcoplasmic Reticulum Ca^{2+}-ATPase Pump
SHR	Spontaneous Hypertensive Rat Model
SK_{Ca}	Small-Conductance Ca^{2+}-Activated K^{+} Channels
SMDS	Smooth Muscle Dissociation Solution
SNS	Sympathetic Nervous System
SOCE	Store-Operated Ca^{2+} Entry
SOCs	Stretch-Operated Channels
STOC	Spontaneous Transient Outward Currents
SURs	Sulphonylurea Receptors
TEA	Tetraethylammonium
TPR	Total Peripheral Resistances
TRPA	Transient Receptor Potential Ankyrin Family of Channels
TRPC	Transient Receptor Potential Classic Family of Channels
TRPCV	Transient Receptor Potential Vanilloid Family of Channels
TRPM	Transient Receptor Potential Melastatin Family of Channels
TRPML	Transient Receptor Potential Mucolipin Family of Channels
TRPP	Transient Receptor Potential Polycystin Family of Channels
TRPs	Transient Receptor Potential Channels
UDP	Uridine Diphosphate
UTP	Uridine Triphosphate
V_{clamp}	Voltage-Clamp
Vm	Membrane Potential

VOCCs	Voltage-Operated Ca^{2+} Channels
VPR	Volume Pressure Recording
VRACs	Volume-Regulated Anion Channels
VSM	Vascular Smooth Muscle
VSMCs	Vascular Smooth Muscle Cells
αβ-MeATP	α,β-Methylene ATP

INDEX

1

Introduction

The cardiovascular system, composed of the heart and blood vessels, is responsible for the transport and distribution of nutrients, oxygen and other essential substances to the entire body. It is also responsible for removing the associated metabolic products. Blood flows through arteries, capillaries and veins, allowing a rapid exchange between tissues and vessels. Therefore, a fine control of both heart and blood vessels is crucial to maintain the entire body homeostasis. When this homeostasis is spontaneously disrupted due to heart or vascular disorders, compensatory mechanisms activate to physiologically restore homeostasis. However, when the problem persists or when the organism is not capable to adapt, pathological changes occur leading to cardiovascular diseases, such as chronic cardiac failure, heart attack, stroke and hypertension, among others. Blood vessels play a significant role in keeping the homeostatic equilibrium, due to their involvement in the control of blood flow and arterial pressure.

1. The Vascular wall

The vascular wall of arteries and veins is a heterogeneous, three-layered structure comprising the tunica intima, the tunica media and the tunica adventitia (Figure I1), surrounded by perivascular adipose tissue (PVAT). Each layer presents specific histological, biochemical and functional properties, providing different mechanisms and signaling pathways that contribute to the maintenance of vascular homeostasis and to the regulation of vascular responses in cardiovascular pathologies. Moreover, there are changes in the relative amount of each layer related to arterial size, which also determines the vessel function. Large, conduit arteries are an elastic pressure reservoir, showing a strong adventitia with abundant elastic fibers. On the contrary, resistance vessels (small arteries and arterioles of 100-500 µm and 10-100 µm of diameter in humans, respectively) have a diminished adventitia and a very well developed tunica media. The strong muscular wall of resistance vessels is particularly important due to their capability to alter blood flow in response to metabolic needs.

Tunica adventitia

The tunica adventitia is the complex and heterogeneous outer layer of vascular walls consisting of an extracellular matrix scaffold which contains fibroblasts, lymphatic and blood vessels (“vasa vasorum”), nerves, progenitor cells and immune cells. The adventitia layer regulates many vascular responses in an outside-in way by sensing different cues and directing responses to adventitial cells as well as to media and intima cells (Stenmark *et al.*, 2013). Of special interest is the presence of sympathetic neuronal nerve endings containing varicosities, where Noradrenaline

(NA) and other neurotransmitters are released to regulate local contractility and blood flow (Herring and Paterson, 2018).

Tunica media

In peripheral vessels, the tunica media is located under the adventitia, separated from it by the fenestrated outer elastic lamina (mainly composed by elastin). In arterioles, the tunica media consists of a single layer of smooth muscle cells, while in resistance arteries of larger caliber, cells are arranged in multiple layers organized in spiral form (McGrath *et al.*, 2005). In addition, the tunica media is in close contact with endothelia through myoendothelial gap junctions, providing a functional interaction between both layers (Levy and Pappano, 2007).

Tunica intima

The tunica intima is separated from the media by a fenestrated inner elastic lamina and is composed by a monolayer of endothelial cells. Endothelial cells play crucial roles in many vascular functions, such as vascular permeability, local vascular control, angiogenesis and homeostasis regulation. Therefore, endothelial dysfunction induces several pathological disorders including hypertension, atherosclerosis, stroke and inflammatory syndromes (Herring and Paterson, 2018).

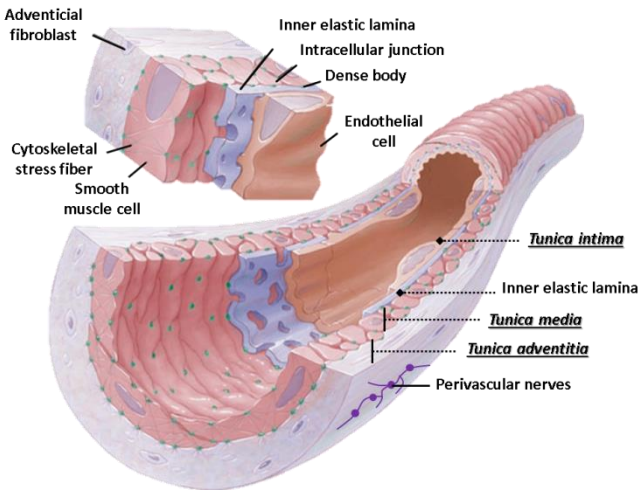

Figure I1. *Structure of arterial vascular wall showing tunica adventitia, tunica media and tunica intima with their associated principal cells (adapted from Martinez-Lemus, 2012).*

2. Biology of Vascular Smooth Muscle Cells (VSMCs)

The vascular wall is an adapting structure that can respond to mechanical, hemodynamic, and neurohumoral challenges. In this way, there is an active control of tissue blood flow that relies largely on the role of the vascular smooth muscle cells (VSMCs). Owing to their contractile properties, VSMCs are responsible for determining the diameter of resistance vessels, controlling blood flow and contributing to the regulation of blood pressure and vascular tone.

2.1 Structure of VSMCs

To carry out their function, VSMCs present several specific structures with different physiological roles: the contractile unit, the sarcoplasmic reticulum, cell junctions and caveolae (Figure I2).

Contractile unit

The cytosol of VSMCs contains thin actin filaments whose endings are interweaved with thick myosin filaments. Unlike the well aligned sarcomeric structure of cardiac or skeletal myocytes, actin filaments in VSMCs are disposed in a lengthwise way and are anchored to both plasma membrane and cytoplasm through dense bands and dense bodies, respectively. These dense bands and bodies, in turn, are linked by intermediate filaments composed of desmin and vimentin proteins. In addition, dense bands are attached to the extracellular matrix by integrins. Altogether, this cytoskeleton structure allows VSMCs to distribute the contraction force through the entire vascular wall (Aaronson, Ward and Wiener, 2004; Gunst and Zhang, 2008). Furthermore, the contractile unit allows VSMCs to maintain a partial contracted state, giving rise to the physiological basal tone that determines vessel resting diameter. Modulation of such tone upon stimulation leads to vasodilator or vasoconstrictor responses.

Sarcoplasmic reticulum (SR)

In VSMCs, SR occupies ~2-6% of cell volume and contains high concentrations of Ca^{2+} (~50 mM). Elements of SR are in close proximity to areas of cell membrane, where several types of ion channels and proteins involved in excitation-contraction coupling have been found (Aaronson, Ward and Wiener, 2004).

Cell junctions and caveolae

Plasma membrane of VSMCs presents numerous tiny invaginations or caveolae involved in cell signaling. Moreover, gap junctions connecting adjacent VSMCs allow the transmission of depolarizations between cells, so that VSMCs form a functional syncytium. In addition, myoendothelial junctions allow the transmission of regulatory signals from endothelial to VSMCs and vice versa, providing complex integrated signaling mechanisms to the control of contractility and vascular tone (Herring and Paterson, 2018).

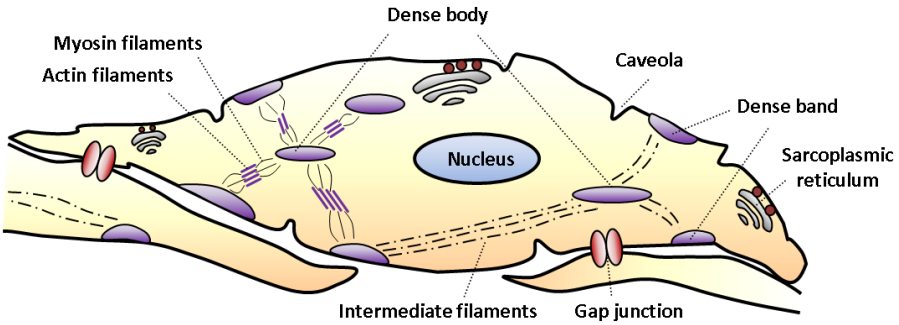

Figure I2. *Structure of a vascular smooth muscle cell.*

2.2. Vascular smooth muscle function and regulation

The vascular system plays very important roles in the regulation of the nutrients and oxygen distribution through the entire body. Propelled by the cardiac force, blood flows through arteries, arterioles and capillaries to get to the most distant cells and tissues. Total blood flow ($L \cdot min^{-1}$) in the cardiovascular system, which is known as cardiac output (CO), represents the blood flow pumped out by the heart. CO depends on the gradient of pressure generated by the heart and on the resistance that the whole vascular system offers to flow. This relationship is known as Darcy´s Law (Herring and Paterson, 2018):

$$CO = \frac{(\bar{P}_a - CVP)}{TPR}$$

Where $\bar{P}_a$ is the mean arterial pressure (mmHg), CVP is the central venous pressure and TPR is the total peripheral resistance. Since CVP is nearly zero, this expression can be simplified to the following equation:

$$CO = \frac{\bar{P}_a}{TPR}$$

Arterial pressure rises steeply and reaches its maximum with the ventricle ejection. This is called systolic pressure (P_s). After that, it gradually declines to a minimum that matches the end of the diastole. This is called diastolic pressure (P_d). Since diastole is longer than systole, mean arterial pressure ($\bar{P}_a$) can be defined as follows:

$$\bar{P}_a = P_d + (P_s - P_d)/3$$

TPR is defined as the resistance to laminar flow and following Poiseuille´s Law, which describes the hydraulic resistance of a tube:

$$R = 8\eta \cdot L/\pi r^4$$

Where, R is the resistance to a laminar flow of a fluid of η viscosity through a tube of L length and r radius. Although Poiseuille´s Law was deduced from the behaviour of Newtonian fluids with laminar flow in rigid tubes, it properly defines the factors that determine R in the circulation, so that it can also be applied with some restrictions to blood vessels. Combining this equation with Darcy´s Law and rearranging terms,

$$\Delta P_a = Q \cdot \frac{8\eta \cdot L}{\pi r^4}$$

From this equation it is evident that small changes in radius result in big effects on mean arterial pressure, constituting an extremely powerful mechanism by which blood vessels regulate both local blood flow and mean arterial pressure (Herring and Paterson, 2018). Smooth muscle cells in the tunica media are the cells responsible for changes in the vascular radius through their contraction-relaxation capabilities. Since the vascular tone defines the vessel radius, VSMCs finely control both $\bar{P}_a$ and blood flow.

2.3. Smooth muscle control of vascular tone.

As mentioned before, vascular tone is defined as the state of contractile tension in the vessel walls, which can be maintained even in the absence of sympathetic innervation. The molecular mechanisms underlying this contractile state are very dependent on the fine control on the membrane potential (Vm) of VSMCs. K^+ channels and L-type Ca^{2+} channels (LTCCs, the most dominant isoforms of voltage-operated Ca^{2+} channels (VOCCs) in VSMCs) are the main channels participating in this control. K^+ channels closing leads to membrane depolarizations, causing LTCCs channels-dependent Ca^{2+} influx, increase of intracellular calcium concentrations ($[Ca^{2+}]_i$) and vasoconstriction, while opening of K^+ channels causes hyperpolarization, LTCCs closing, decrease in $[Ca^{2+}]_i$ and vasodilation (Jackson, 2000; Tykocki, Boerman and Jackson, 2017).

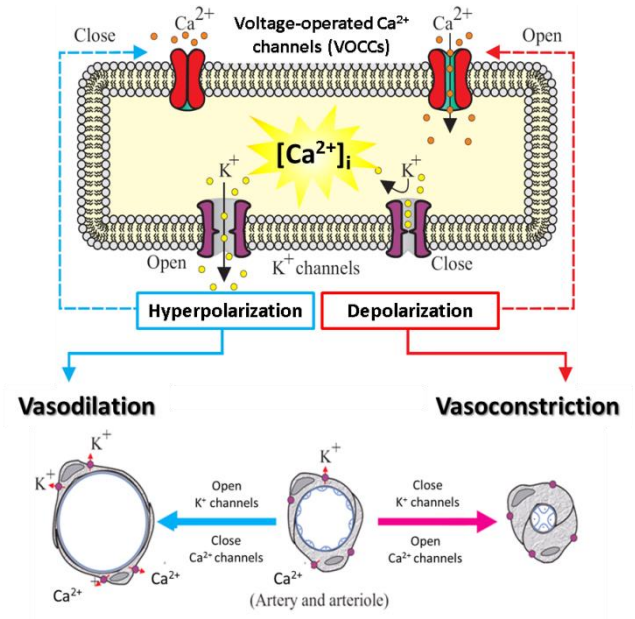

Figure I3. *Regulation of vascular tone by K^+ channels and VOCCs channels. In VSMCs (top), K^+ channels-triggered Vm changes regulate VOCCs-mediated Ca^{2+} influx, causing changes in $[Ca^{2+}]_i$ that lead to vasoconstriction or vasodilation (bottom) of vessels, thus regulating basal vascular tone (adapted from Jackson, 2000).*

In addition to voltage dependent K^+ and Ca^{2+} channels, VSMCs have additional channels involved in the autoregulation of vascular tone. Several members of different K^+ channels families, Ca^{2+}-conducting channels, Cl^- channels, non-selective cation channels and receptor-operated channels (ROCs) expressed in VSMCs have been found to be relevant in this regard (Figure I4). The negative membrane potential of VSMCs (~-50-60 mV) is defined by the intracellular and extracellular $[K^+]$, $[Na^+]$ and $[Cl^-]$ and their relative permeability (~10:4:2, respectively). K^+ channels play crucial roles in the control of vascular tone by influencing membrane potential and so the activity of Ca^{2+} channels. Interestingly, the high $[Cl^-]_i$ in VSMCs (~30-50 mM) determines an E_{Cl} (-26 mV) above the membrane potential, so that activation of chloride channels has a depolarizing effect (Kitamura and Yamazaki, 2001). In the case of ROCs, the main pathway present in VSMCs starts with the activation of a phospholipase-C (PLCβ) dependent of $G_{q/11}$ coupled receptors. Membrane PIP_2 is cleaved by the phospholipase into IP_3 and DAG. IP_3 activates its specific IP_3R receptor on the SR leading to Ca^{2+} release to the cytosol (***pharmacomechanical*** coupling). DAG activates ROCs both, directly and through the PKC signaling pathway, leading to membrane depolarization, VOCCs opening and a further increase of $[Ca^{2+}]_i$ and contraction. Ca^{2+} released from the SR can also activate Ca^{2+}-activated channels (K^+ and Cl^-), finely tuning the changes in Vm

(***electromechanical*** coupling) and therefore the activation of VOCCs, the final level of $[Ca^{2+}]_i$ and the magnitude of contraction (Herring and Paterson, 2018). The structure, function and role of K^+, Ca^{2+}, Cl^- and ROCs families of channels in the vasculature will be discussed in detail in the next sections.

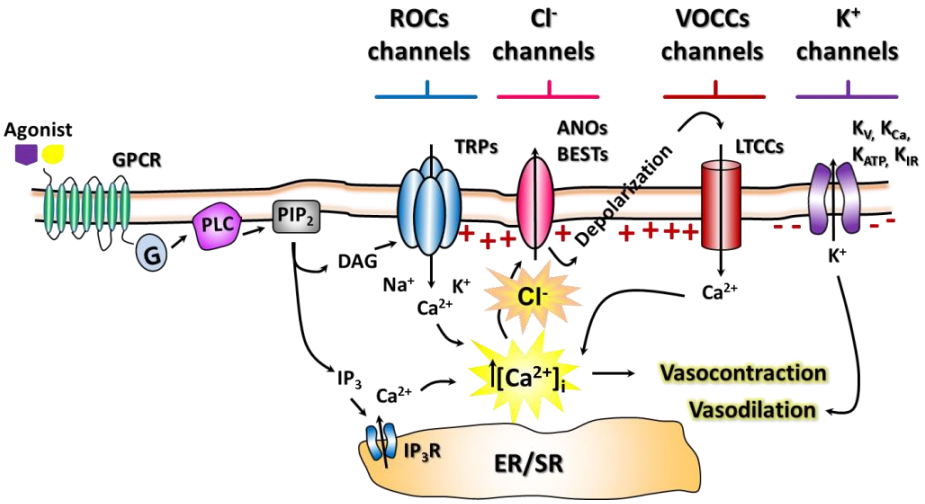

Figure I4. *Contribution of vascular smooth muscle channels to electromechanical and pharmacological coupling in VSMCs.*

Since vascular tone is the key determinant of vessel diameter, it is fine-tuned by ***intrinsic*** and ***extrinsic*** mechanisms that regulate vessels resistance by inducing the appropriate vasoconstriction or vasodilation. The intrinsic mechanisms are those driven by the vascular wall itself and include smooth muscle- and endothelium-derived self-adjusting mechanisms, while extrinsic mechanisms are driven by extravascular mechanisms such as perivascular vasomotor nerves and endocrine factors.

Intrinsic control of vascular tone

Among the intrinsic mechanisms that regulate vascular basal tone, temperature, myogenic response (defined as the vasoconstriction in response of an increase in the arterial pressure), endothelial-derived molecules (NO, PGI_2, endothelium-derived hyperpolarizing factor -EDHF-, and endothelin) and vasoactive autacoids constitute the main ones. NO is synthesized from L-arginine by endothelial nitric oxide synthase (eNOS) and diffuses into smooth muscle where it activates guanylyl cyclase (GC) which in turn catalyzes cyclic guanosine monophosphate (cGMP) production from guanosine triphosphate (GTP). cGMP then activates protein kinase

G (PKG) which reduces $[Ca^{2+}]_i$ causing vasodilation. PGI_2, produced from arachidonic acid, and EDHF act as potent vasodilators on smooth muscle, while endothelin causes vasoconstriction (Herring and Paterson, 2018).

Extrinsic control of vascular tone

Extrinsic control of vascular tone is mainly due to the activity of vasomotor nerves and circulating hormones.

The sympathetic vasoconstrictor nerves contain many varicosities that release NA, adenosine triphosphate (ATP) and neuropeptide Y. NA and ATP acting mainly through α-adrenergic Gq-protein coupled receptors (GPCRs) and purinergic ionotropic receptors, respectively, promote vasoconstrictor responses (Herring and Paterson, 2018, see below). Likewise, a fall in the sympathetic activity causes vasodilation. In addition, in a limited number of tissues, the resistance arteries are innervated by vasodilator fibers together with the ubiquitous sympathetic vasoconstrictor fibers. These vasodilator fibers can be sympathetic, parasympathetic or sensory fibers (Herring and Paterson, 2018). In this regard, it is well established that cutaneous substance P-containing sensory fibers are associated with blood vessels and are, at least in part, responsible for mediating antidromic phenomena such as vasodilation and plasma extravasation. Stimulation of nociceptive C-fibers causes vasodilation due to the release of substance P and calcitonin gene-related peptide (CGRP), leading to the flare responses to a damage. The stimulation of these fibers leads also to mast cells stimulation and histamine release, which potentiates the flare response by increasing microvascular permeability. This spreading flare, together with the local redness and swelling is an important component of the Lewis triple response (the reaction of skin to a mild trauma).

Regarding circulating hormones, the main ones involved in the control of vascular tone are: Adrenaline, Vasopressin, Angiotensin II (Ang II) and atrial natriuretic peptide (ANP). Adrenaline induces vasoconstriction through activation of vascular smooth muscle α-adrenergic receptors (or vasodilation in the skeletal muscle through activation of β-adrenergic receptors); vasopressin, also called antidiuretic hormone, is a potent vasoconstrictor; angiotensin II, produced by the renin-angiotensin-aldosterone system (RAAS), acts directly as a vasoconstrictor agent on vascular smooth muscle and indirectly by enhancing sympathetic activity. It also has an extensive cross-talk with endothelial factors, which is crucial for the angiotensin converting enzyme (ACE) signaling pathway. Finally, ANP acts as a potent vasodilator (Herring and Paterson, 2018).

Therefore, a complex system of different intercommunicated signaling mechanisms is constantly activated to regulate the contractility of VSMCs. The failure of this integrated system leads to specific cardiovascular disorders (v.g. heart attack, stroke, hypertension) or contributes to aggravate systemic syndromes such as obesity or diabetes. The relationships between these diseases and vasculature are complex and multifaceted, including changes in the vessels that directly contribute to the progression of the disease, changes that result from disease progression, and even changes that represent compensatory mechanisms (Tykocki, Boerman and Jackson, 2017).

3. Hypertension

Hypertension is a multifactorial cardiovascular disorder characterized by a chronic, usually progressive, raise in the arterial mean pressure that if it is not properly treated leads to multi-organ lesions in heart, brain and kidneys. Since individual pressure measurements vary individually, repeated values of Ps and Pd exceeding 140/90 mmHg, respectively, are used to diagnose chronic hypertension (Table I1).

Classification	P_s (mmHg)		P_d (mmHg)
Normotension	<120	and	<80
Elevated	120-129	and	<80
Grade 1 hypertension	130-139	or	80-89
Grade 2 hypertension	≥140	or	≥90

Table I1. *Classification of adult blood pressure (adapted from Whelton et al., 2018).*

Hypertension can be divided into essential or primary hypertension, involving 90% of cases, and secondary hypertension, involving the remaining 10%. Essential hypertension is a symptomless, multifactorial genetic disorder, in which inheritance of abnormal genes predisposes an individual to high blood pressure, especially if environmental influences are present, such as salt and alcohol intake, sedentary lifestyle and obesity (Aaronson, Ward and Wiener, 2004). In contrast, secondary hypertension has an identifiable pathologic cause, including hyperaldosteronism and renovascular diseases, which impair volume regulation and activation of renin-angiotensin-aldosterone system; pheochromocytoma, which raises pressure through α-adrenoceptor activation; and pre-eclamptic toxemia, which develops during pregnancy (Herring and Paterson, 2018).

3.1. Etiology of hypertension

Arterial pressure rises because of an imbalance between cardiac output (CO) and total peripheral resistances (TPR). In the early stages, hypertension could be associated with a CO increase with normal or slightly raised TPR, but over time CO reverts to normal values while TPR becomes permanently increased. The molecular, functional and structural changes that lead to this chronic elevation of TPR are not fully understood. Several hypothesis including neurogenic induced hypertension through augmented sympathetic innervation, and also renin-angiotensin-aldosterone induced hypertension have been suggested (Herring and Paterson, 2018). Due to the crucial roles that vascular ion channels play in the control of vascular tone and contractility through their contribution to set resting Vm, the altered expression and function of these VSM channels may contribute to vascular dysfunction and to the pathogenesis of hypertension. However, it is not clear whether these changes occur as part of the disease progression or as compensatory mechanisms to maintain homeostasis. Although there is a huge knowledge about the contribution of VSM channels to the pathophysiology of hypertension, our understanding of their specific roles in vascular dysfunction remains unclear. Some of the difficulties arise from the lack of specific pharmacological blockers against some channels, the huge macromolecular complexes where these channels interact with a wide range of additional proteins, and the broad heterogeneity between vascular tissues and species. Understanding the specific role of a given ion channel to the pathogenesis of hypertension requires the selection of a suitable animal model and the use of multiple approaches.

3.2. Animal models used to study essential hypertension

Due to the complexity of essential hypertension disease, different animal models have been developed to study the molecular mechanisms involved in the hypertension etiology and treatment. These models can be grouped into genetic and non-genetic (Table I2).

Genetic models are in turn divided in genotype-driven models, created by gene overexpression (transgenic) or deletion (knockout) to focus in a gene involved in hypertension, and phenotype-driven models, which involve selective breeding of hypertensive strains and their maintenance over generations. The latter models include the spontaneously hypertensive rat (SHR) model, the salt-sensitive Dahl rat model and the blood pressure high (BPH) mouse model (Lerman *et al.*, 2005).

Non-genetic models have been broadly used to study the effects of induced hypertension on end-organ damage in different species. These models include: 1)

surgically induced hypertension, such as the hypertensive models developed by unilateral constriction of renal artery (1K1C and 2K1C models); 2) pharmacologically induced hypertension, such as deocorticosterone (DOCA)-salt rat model, Angiotensin II- and other vasoactive peptide-infused models; and 3) environmental-induced hypertensive models, such as salt diet- and stress-induced hypertensive models (Lerman *et al.*, 2005).

		Animal model	Pa increase (mmHg)	Time to establish (weeks)	Hypertension type
Genetic Models	Genotype-driven	Transgenic	Variable	Variable	Essential
	Phenotype-driven	SHR	40-60	4-6	
		Salt-Dahl rats	>30	2	Essential
		BPH mice	>30	birth	
Non-Genetic Models	Surgically-induced	2KIC	>50	4	Vascular renal disease
		1KIC	>70	4	
	Pharmacologically-induced	DOCA-salt	>20-35	3	Hyperaldosteronism
		Angiotensin II	>40-50	4-10 days	Essential
		NOS inhibitors	>5-25	4-6	Essential
	Environmentally-induced	High salt diet-induced	>10	4-5 days	
		Stress-induced	10-20	4-6 months	Essential
		Cold-induced	20-40	3	

Table I2. *Different experimental animal models to study hypertension (Lerman et al., 2005).*

BPH mice as a model of essential hypertension

Among these possible models to study hypertension and due to the interest of our research group in the study of the pathophysiology of essential hypertension, we chose the BPN/BPH. The phenotype-driven hypertensive (BPH/2J) mouse model of essential hypertension and its normotensive control (BPN/3J) was early developed by crossbreeding of eight different mouse strains showing high and normal blood pressure measured by the tail-cuff method. Early studies using the high blood pressure (BPH) mouse strain also showed increased heart rate and early mortality (Schlager, 1981; Schlager and Sides, 1997), and later studies found a reduction in the NA content in hypothalamus, amygdala and cerebellum (Schlager, Freeman and

El Seoudy, 1983) and greater contents in the preoptic area and in the superior cervical ganglion (Denoroy *et al.*, 1985), consistent with a neurogenic form of hypertension. Furthermore, evidences of an overactive sympathetic nervous system (SNS) in the BPH strain associated with circadian rhythms confirmed the involvement of neurogenic mechanisms leading to hypertension (Davern *et al.*, 2009, 2010). Additionally, changes in the expression pattern of genes involved in hypertension-related systems, such as adrenal catecholamines and sympathetic function, steroid hormone synthesis and sensitivity, oxidative stress and intermediary metabolism have been described. Some of these gene expression profiles shared a common direction of expression in the two different hypertensive SHR and BPH models, while other revealed differences between the two models, such as adrenal catecholamines synthesis (depressed in SHR, but enhanced in BPH), and the glucocorticoid dependence of SHR (Friese *et al.*, 2005). Furthermore, findings of genes differentially expressed between males and females in the BPH strain suggested that differences in sex hormones influenced the mechanisms that are involved in the onset of hypertension in this mouse model (Chiu *et al.*, 2014), reinforcing the multifactorial and complex nature of hypertension. These observations, together with the existence of a good control strain of the BPH strain (BPN strain), indicate that BPH is a suitable model to study essential hypertension. The examination in detail of the gene expression profile and its associated functional properties in this BPH mouse model could contribute to unravel the mechanisms associated with human essential hypertension.

4. Ion channels in VSMCs.

VSMCs exhibit a large variety of ion channels in their membrane that are involved in the autoregulation of contractility and vascular tone (Tykocki, Boerman and Jackson, 2017). These channels can be grouped in several families: K^+-channels, including voltage-dependent (K_V), Ca^{2+}-activated (K_{Ca}) and inward rectifying K^+ channels (K_{IR} or classical inward rectifiers, and K_{ATP} or ATP-dependent); Ca^{2+} channels, including L-type (LTCCs), T-type, N-type, P/Q-type and R-type subfamilies of channels; receptor-operated channels (ROCs) and stretch-activated channels (SOCs), including transient receptor potential channels (TRPs); and Cl^--channels.

4.1. K^+-channels

In resting VSMCs, $[K^+]_i$ is higher than $[K^+]_o$ due to the electrogenic activity of the Na^+-K^+ pump (~150 mM vs. 5 mM). Driven by this electrochemical gradient, outward K^+ flux contribute to set the negative Vm of VSMCs due to the relative

large permeability to K^+ in resting conditions, thus influencing vascular tone by controlling Vm. Up to four families of K^+ channels have been found in VSMCs.

4.1.1. Voltage-dependent K^+ channels (K_V)

K_V channel family comprises up to twelve members (K_V1-12) arranged in the plasma membrane as tetramers of four pore forming α-subunits. Each subunit has six transmembrane α-helices (S1-S6), with S4 containing the voltage sensor and the P-loop between S5 and S6 forming the channel pore (Figure I5). The N- and C-termini reside in the cytosol and are related with fast and slow channel inactivation, respectively. Differences in the functions of K_V channels depend not only on the structural differences of each family member, but also on their ability to form heteromultimers or to associate with accessory and regulatory subunits (Gutman *et al.*, 2005). These channels are activated in response to membrane depolarizations leading to the K^+ efflux responsible of the consequent return to resting Vm. Therefore, K_V channels can contribute to control the resting Vm and vascular tone. In addition, several vasodilators can activate K_V channels through cAMP-PKA, cGMP-PKG and other endothelium-dependent signaling pathways. They are also responsible of the effect of several vasoconstrictors that close K_V channels through protein $G_{q/11}$-mediated PKC activation and $[Ca^{2+}]_i$ increase.

The role of K_V channels expression and function in the development of hypertension remains unclear. Electrophysiological and expression studies have reported increased, decreased and no changes in expression and K_V channels mediated currents, however, the bulk of literature points to a reduced expression and function of these channels in hypertension, depending on the animal model, vascular bed and type of hypertension (Cox, Folander and Swanson, 2001; Berg, 2003; Cox *et al.*, 2008; Moreno-Domínguez *et al.*, 2009; Jepps *et al.*, 2011).

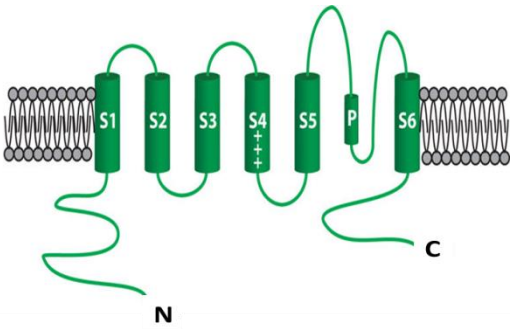

Figure I5. *Structure of the α-subunit of voltage-dependent K^+ channels (K_V) showing the membrane domains S1-S6 with the voltage sensor in S4 and the pore forming P-loop between S5 and S6* (adapted from Jackson, 2017).

4.1.2. Inward rectifying K^+ channels (K_{IR})

Inward rectifying K^+ channels (K_{IR}) derive their name from the characteristic rectification that appears in the current-voltage (I/V) relationship of the currents they carry out (Figure I6). Inward currents (obtained at Vm more negative than the E_K) are much larger than outward currents (obtained at Vm more positive than E_K). This family of K^+ channels comprises the large conductance inward rectifiers (K_{IR}) and the ATP dependent channels (K_{ATP}) (Hibino *et al.*, 2010).

4.1.2.1. Large conductance K_{IR} channels

Large conductance K_{IR} channels are tetramers constituted by four α-subunits, all of which are formed by two transmembrane α-helices (M1 and M2) linked by a P-loop which constitutes the ion-conducting pore. The N- and C-termini domains are localized in the cytosol. The C domain is involved, along with the M2 helix, in the blockade of outward K^+ flux by intracellular Mg^{2+} and polyamines at Vm more depolarized than E_K. Among the seven subfamilies of K_{IR} channels, only $K_{IR}2.1$ (KCNJ2) and K_{IR} 2.2 (KCNJ12) have been found to be highly expressed in VSMCs (Bradley *et al.*, 1999; Zaritsky *et al.*, 2000; Smith *et al.*, 2008).

It is known that several vasoconstrictors acting on the $G_{q/11}$-coupled PLCβ-DAG-PKC signaling cascade can block K_{IR} channels, enhancing vasoconstrictors-induced depolarization and contraction of VSMCs. On the other hand, K_{IR} channels located at the endothelium could also amplify small hyperpolarizations caused by other channels or by small increases in extracellular K^+ concentration, , contributing to the vasodilator response of some stimuli (William F. Jackson, 2017). Although K_{IR} channels are named for the inward rectification of current, it is the small outward "hump" in the current-voltage relationship (i.e., the region of negative slope conductance, figure I6) that is present between the E_K and the resting Vm (∼−40 to −30 mV) of endothelial cells that is important for their physiological function. This negative slope conductance allows outward K_{IR} current to be activated by membrane hyperpolarization, permitting K_{IR} channels to amplify hyperpolarization induced by other K^+ channels and ion transporters. Also, increases in extracellular K^+ concentration activate K_{IR} channels, which transduce this change into membrane hyperpolarization. As endothelial cells have high membrane resistance at resting membrane potential, activation of only a few K_{IR} channels can effectively modulate their membrane potential.

In general, reduced expression and function of K_{IR} channels have been reported in hypertension, although in some cases this K_{IR} channels dysregulation has been accompanied by compensatory mechanisms to maintain homeostasis (Tajada *et al.*, 2012).

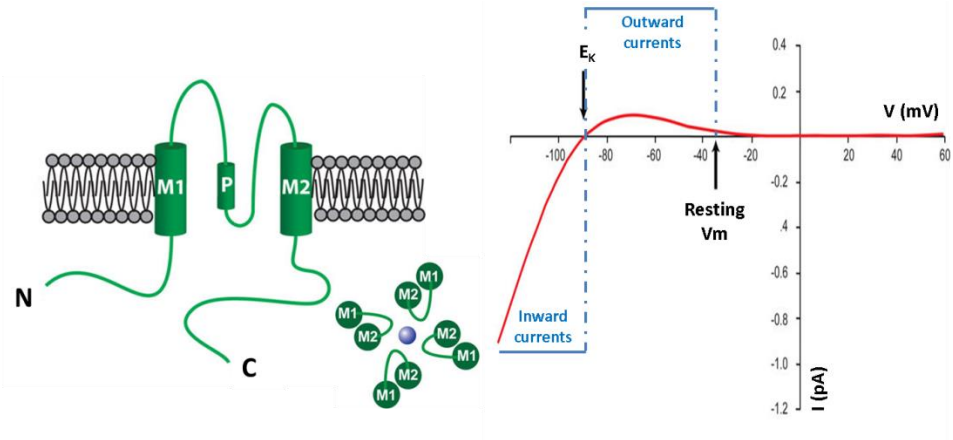

Figure I6. *Structure of inward rectifying K^+ channels (K_{IR}) showing the α-subunit composed by the two membrane domains M1 and M2 linked by P-loop (left) and the top view of four α-subunits with K^+ ion in the middle of the tetramer (bottom). The associated K_{IR} channels behavior depending on the Vm is also depicted (right) (adapted from Jackson, 2017).*

4.1.2.2. ATP-dependent K^+ channels (K_{ATP})

ATP-dependent K^+ channels (K_{ATP}) are named for their sensitivity to ATP, linking membrane excitability and metabolism. A decrease in the $[ATP]_i$ induces the opening of K_{ATP} channels and the consequent hyperpolarization. However, their functional activity can be modulated by additional signaling pathways in an ATP independent manner. The structure of K_{ATP} channels consists of a hetero-octamer composed of a tetramer of pore-forming $K_{IR}6.1$ subunits associated with a tetramer of sulphonylurea receptors (SURs) 2B. SUR2B monomers are formed by seventeen transmembrane α-helices clustered in three groups (TMD0, TMD1 and TMD2) with two intracellular nucleotide-binding fold domains (NBF1 and NBF2) and N- and C-termini outside and inside the cell, respectively (Figure I7) (Babenko, Aguilar-Bryan and Bryan, 1998; Hibino *et al.*, 2010).The $K_{IR}6.1$ subunits have two transmembrane spans and form the channel's pore. The SUR subunits allow nucleotide (ATP and ADP)-mediated regulation of the channel through their NBFs, and are critical in the role of the channel as a sensor of metabolic status. These SUR subunits are also sensitive to sulfonylureas, MgATP, and some other pharmacological channel openers (Foster and Coetzee, 2016). Besides intracellular ATP, K_{ATP} channel activity can be inhibited by vasoconstrictors through several mechanisms: 1) PKC-triggered alteration of channel gating and channel internalization; 2) calcineurin (PP2B)-induced dephosphorylation and 3) G_i-triggered adenylate cyclase (AC) inhibition. Moreover, K_{ATP} channels can also contribute to the action of vasodilators through the cAMP-PKA and cGMP/PKG signaling pathways (Tykocki, Boerman and Jackson, 2017). Several evidences suggest a contribution of the reduced expression and

function of K_{ATP} channels to the genesis of hypertension (Tajada *et al.*, 2012), although another set of studies showed no changes in K_{ATP} channels function in some hypertensive animal models (Tykocki, Boerman and Jackson, 2017).

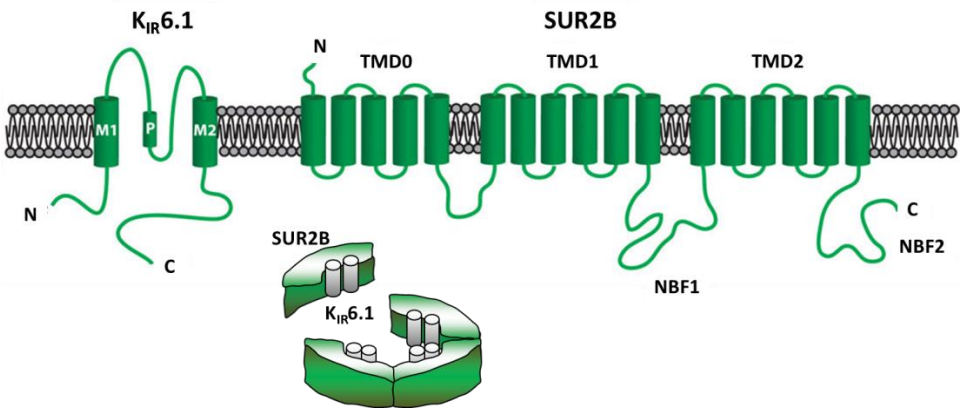

Figure I7. *Structure of ATP-dependent K^+ channels (K_{ATP}). Four $K_{IR}6.1$ subunits associated to four SUR2B subunits comprise the functional hetero-octamer of a K_{ATP} channel (adapted from Babenko, Aguilar-Bryan and Bryan, 1998; Jackson, 2017).*

4.1.3. Ca^{2+}-activated K^+ channels (K_{Ca})

K_{Ca} are K^+ channels activated by increases in $[Ca^{2+}]_i$. K_{Ca} channels comprises two subfamilies according to single channel conductance, voltage sensitivity and pharmacological properties: 1) The large-conductance Ca^{2+}- and voltage-activated channels (BK_{Ca}), which are the most abundant K^+ channels expressed in VSMCs, and 2) the small-conductance Ca^{2+}-activated channels (SK_{Ca}), also found in several vascular beds and mainly expressed in the endothelium . An additional subfamily of intermediate-conductance Ca^{2+}-activated channels (IK_{Ca}) has been reported, but they are only expressed in proliferating VSMCs (Tykocki, Boerman and Jackson, 2017). The structure of the pore-forming α-subunit of BK_{Ca} channels consists of seven transmembrane α-helices (S0-S6) with the P-loop between S5 and S6 forming the ion-conducting pore and several charged residues in S2, S3 and S4 determining the voltage sensor. N-terminus faces the outside of cell, while C-terminus is localized in the cytosol and shows two, tandem regulator of conductance K^+ domains (RCK1 and RCK2) which constitute the Ca^{2+} sensor. Moreover, additional regulatory subunits, such as β1- and γ-subunits, have been reported to associate with BK_{Ca} channels (Figure I8). β1-subunits enhance the Ca^{2+} sensitivity and trafficking of α-subunit and the channel activation, while γ-subunits, which are leucine-rich-repeat containing proteins (LRRCs), increase the voltage and channel activators sensitivities (Tykocki, Boerman and Jackson, 2017). K_{Ca} channels play a

central role in the control of membrane potential and vascular tone and contractility as a coupled unit with VOCCs and Ryanodine receptor (RyR) channels in many VSMCs. Considering the close proximity between plasma and SR membranes, Ca^{2+} influx through VOCCs channels locally activates RyR channels leading to unitary Ca^{2+} release events (Ca^{2+} sparks) from SR. These Ca^{2+} sparks have been shown to regulate K_{Ca} channel open probability leading to K^+ efflux in the form of spontaneous transient outward currents (STOC), causing membrane hyperpolarization, VOCCs channels closing and global $[Ca^{2+}]_i$ decrease. Therefore, this Ca^{2+} spark-STOC pathway seems to be an important negative feedback system in the regulation of membrane potential, vascular tone and contractility (Nelson *et al.*, 1995; Jaggar *et al.*, 1998). Likewise, despite several controversial studies, evidences showed a BK_{Ca} contribution not only to the resting Vm both in health and disease, but also to agonists-induced vasoconstriction by preventing vasospasm in a negative feedback way (Jackson, 2000). In hypertensive animal models, both increase and decrease in the expression and functions of BK_{Ca} channels have been reported to be dependent on animal strains, vascular beds and methodological differences (Tajada *et al.*, 2013; Tykocki, Boerman and Jackson, 2017).

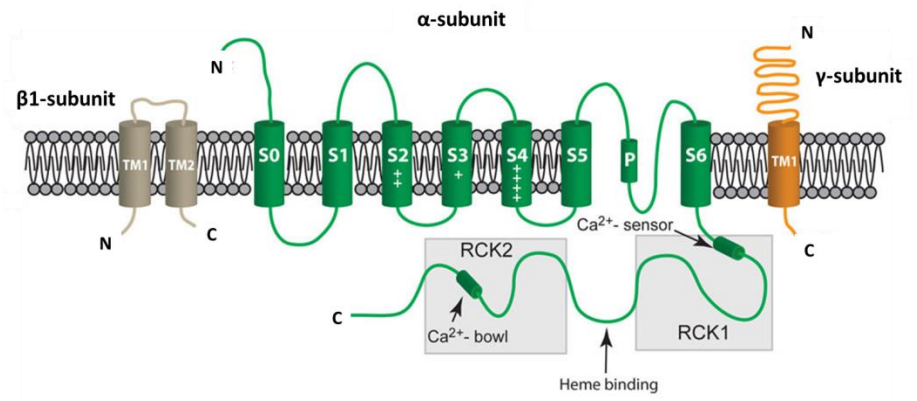

Figure I8. *Structure of large-conductance K^+ channels (BK_{Ca}). α-subunit showing its seven membrane domains (S0-S6) with the voltage sensor in S2, S3 and S4, and its Ca^{2+} sensor in C-terminus along with the regulator conductance K^+ domains (RCK1 and RCK2). Additional regulatory β1- and γ-subunits are also depicted (adapted from Jackson, 2017).*

4.1.4. K^+ channels remodeling in BPH mice

Using BPN and BPH mice, our group has previously determined the functional expression of K^+ channels and their contribution to VSMC excitability. Our results showed that in mesenteric VSMCs of BPH mice there is a remodeling of K_v2 currents, leading to a decreased K_v mediated current amplitude which contributes to the hypertensive phenotype (Moreno-Domínguez *et al.*, 2009). However, while

VSMCs from BPH mice were significantly more depolarized than BPN VSMCs, there were no changes in the contribution of K_v currents to resting Vm, suggestng that the remodeling of K_v2 currents was an adaptative mechanism to prevent larger vasoconstrictor responses. In adition, we found that VSMCs from BPH mesenteric arteries exhibited a significant decrease in the mRNA expression of $K_{IR}2.1$, $K_{IR}4.1$, $K_{IR}6.x$ and SUR2, and a decrease in the current amplitudes mediated by both K_{IR} and K_{ATP} channels. The decreased expresion of both channels did contribute to the more depolarized resting Vm of BPH cells, but only the response to K_{ATP} channel blockers and activators was impaired when arterial tone was tested. Altogether, our data indicate that changes in K_{ATP} channels in resistance arteries could be an important determinant of the hypertensive phenotype in the BPH model (Tajada *et al.*, 2012).

4.2. Voltage-operated Ca^{2+} channels (VOCCs)

Voltage-operated Ca^{2+} channels (VOCCs) are broadly distributed in many tissues and cells. They transduce membrane depolarization into an increase in $[Ca^{2+}]_i$ by activating a Ca^{2+} influx down its large electrochemical gradient. By increasing $[Ca^{2+}]_i$, VOCCs play important roles in the regulation of contractility, vascular tone and gene expression in VSMCs (Jackson, 2000; Ghosh *et al.*, 2017).

4.2.1. Classification of VOCCs

VOCCs were first divided in six different families according to their pharmacology and the electrophysiological characteristics of their currents. L-type Ca^{2+} currents present relative high voltage of activation (from -40 to -30 mV), high single channel conductance, slow voltage-dependent inactivation and are blocked mainly by dihydropyridines. T-type Ca^{2+} currents present more negative voltage of activation (from -70 to -60 mV), rapid voltage-inactivation, small single channel conductance and are relatively insensitive to organic Ca^{2+} blockers. The additional N-, P-, Q- and R-type Ca^{2+} currents, less common in VSMCs, present intermediate currents between L- and T-type and are sensitive to the blockade with several toxins, except R-type currents. These different types of currents have been grouped, in turn, into three subfamilies according to the genes encoding the α1-subunit responsible of carrying the currents: 1) the Ca_V1 subfamily comprising four members ($Ca_V1.1$-1.4) and carrying the high-voltage-activated, long lasting L-type Ca^{2+} currents; 2) the Ca_V2 subfamily, including channels carrying P/Q-($Ca_V2.1$), N-($Ca_V2.2$) and R-type ($Ca_V2.3$) currents; and 3) the Ca_V3 subfamily including members ($Ca_V3.1$-3.3) carrying low-voltage-activated, transient T-type Ca^{2+} currents (Tykocki, Boerman and Jackson, 2017).

4.2.2. Structure of VOCCs

The general structure of VOCCs consists of a complex of α1, α2, β, γ and δ subunits in such a way that the principal α1-subunit (190 kDa) associates with a disulfide-linked α2δ dimer (170 kDa), an intracellular phosphorylated β-subunit (55 kDa) and a transmembrane γ-subunit (33 kDa) (Figure I9) (Catterall, 2011).

The α1-subunit is organized in four repeated motifs (I-IV), each of which containing six transmembrane α-helices (S1-S6) with a loop between S5 and S6 forming the pore. The S4 helix of each motif serves as the voltage sensor and their conformational changes lead to channel opening. The intracellular β-subunit has no transmembrane segments and binds to the intracellular loop between I and II motifs of α1-subunit, while γ-subunit is a glycoprotein with four transmembrane domains and N- and C-termini in the cytosol. The extracellular α2-subunit is attached to the membrane through disulfide linkage to δ-subunit, which is anchored to the membrane through glycophosphatidylinositol. Although α1-subunit is sufficient to render channel functionality, α2δ and specially β-subunits enhance the channel expression and confer more physiological gating properties (Catterall, 2011).

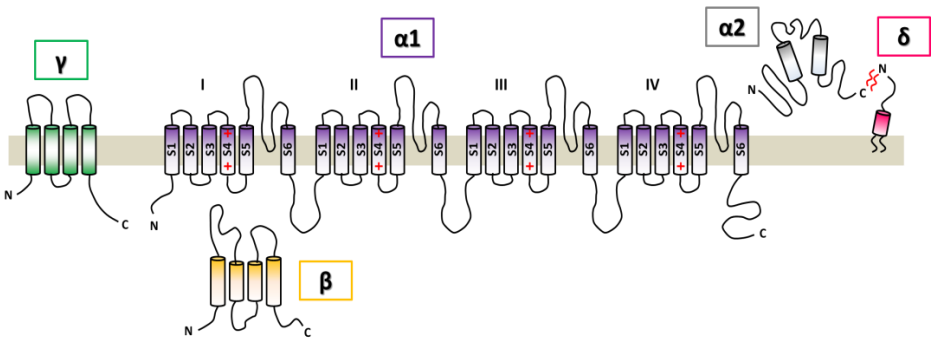

Figure I9. *Structure of L-type Ca^{2+} channels (LTCCs) showing the pore forming α1-subunit, the intracellular regulatory β-subunit, the extracellular disulfide-linked α2δ dimer and the transmembrane γ-subunit (adapted from Catterall, 2011).*

4.2.3. Function of L-type and T-type Ca^{2+} channels in VSMCs

As previously mentioned, L-type Ca^{2+} channels constitute the dominant VOCC channel expressed in VSMCs cells, although evidences of functional T-type Ca^{2+} channels have been also reported. The principal role of these channels is their contribution to the regulation of vascular tone by Vm: depolarizations open L-type Ca^{2+} channels leading to Ca^{2+} influx, increase in $[Ca^{2+}]_i$ and vasoconstriction, whereas hyperpolarization closes these channels, decreases $[Ca^{2+}]_i$ and causes

vasodilation. In addition, L-type Ca^{2+} channels play important roles in the control of myogenic tone and vasomotion (Tykocki, Boerman and Jackson, 2017, see for refrences). Moreover, these channels are regulated not only by changes in Vm but also by additional signaling mechanism, including vasoconstrictor- and vasodilator-dependent signaling pathways. Several evidences showed a directly $G_{q/11}$-induced activation of L-type Ca^{2+} channels independently of changes in Vm and likely through PKC-induced increase of their open-state probability, thus enhancing the agonists-induced vasoconstriction (Del Valle-Rodríguez, López-Barneo and Ureña, 2003; Ureña, del Valle-Rodríguez and López-Barneo, 2007). On the other hand, both activation and blockade of L-type Ca^{2+} channels have been reported in the presence of vasodilators. While, cGMP-PKG signaling pathways appears to block L-type Ca^{2+} channels contributing to vasodilation, vasodilator-induced cAMP-PKA-dependent mechanisms lead to both activation and inhibition of L-type Ca^{2+} channels (Xiong and Sperelakis, 1995).

4.2.4. Remodeling of L-type Ca^{2+} Channels in BPH mice

Strong evidences support an increased expression and function of $Ca_V1.2$ channels in hypertension that contributes to the increased myogenic tone and contractility and to the decreased vasodilator activity, all of which contributing to the increased peripheral vascular resistances. The molecular mechanisms by which hypertensive patients show increased functional expression of LTTCs channels remains unclear, but may be related to an increased trafficking of α-subunit to cell membrane through an increased expression of the modulatory α2δ and β subunits and also through the activation of PiP_3K-γ mediated by $G_{12/13}$-coupled receptors (Bannister *et al.*, 2012; Kharade *et al.*, 2013; Tykocki, Boerman and Jackson, 2017). Using the BPH mouse model, we found a decrease in the global smooth muscle Ca^{2+} influx due to fewer $Ca_V1.2$ channels. However, these $Ca_V1.2$ channels were hyperactive in BPH cells, leading to a larger local Ca^{2+} influx at rest that triggered an increased Ca^{2+} release from intracellular stores (sparks). Moreover, since BK_{Ca} channels from BPH myocytes showed reduced Ca^{2+} sensitivity, their activation by the increased $[Ca^{2+}]_i$ was impaired. The decreased $Ca_V1.2$ currents but higher $Ca_V1.2$ triggered sparks found in BPH VSMCs have been related to differences in the subunit composition of these channels (Tajada *et al.*, 2013). Our results suggest that changes in the molecular composition of both $Ca_V1.2$ and BK_{Ca} channels could explain vascular dysfunction during hypertension in BPH mice.

4.3. Other channels: Receptor-operated (ROCs) and stretch-operated (SOCs) channels and Cl^--conducting channels

In addition to the important roles that both, K^+-conducting channels and voltage-dependent Ca^{2+} channels play to the contribution of membrane potential, vascular tone and contractility, many other families of ion channels have been found to be functionally expressed in VSMCs. In this context, non-selective cation channels and Cl^--conducting channels have been the principal families of ion channels widely studied both, in health and disease.

Non-selective cation channels comprise several families of agonists-activated and stretch-activated channels which are permeable only to cations (K^+, Na^+ and Ca^{2+}). Both, the agonist or the stretching stimulus can activate the channel either directly or indirectly. In the direct activation, the channel is the receptor itself, such as the P2X ATP receptors. In contrast, the indirect activation involves a second messenger chain triggered by an agonist-activated receptor. In this context, several GPCR receptors and the transient receptor potential (TRP) channels, which behave as ROCs, are widely expressed in VSMCs and have been found to be involved in the physiopathology of the vascular system. Receptor activation increases $[Ca^{2+}]_i$ (see above, section 2.3), and the consequent activation of Ca^{2+} sensitive channels modulate membrane potential, the activity of VOCCs and the final contractile responses. As described above, K_{Ca} channels behave as brakes, hyperpolarizing Vm and limiting VOCCs activation. However, Ca^{2+} sensitive Cl^- channels have the opposite effect, producing a membrane depolarization or amplifying in some cases the depolarization induced by ROCs activation, potentiating the activation of VOCCs and generating in some cases action potentials (v.g. in the portal vein). This role of Cl^--conducting channels in the VSMCs arises from the fact that these cells present a high $[Cl^-]_i$ and then, a more depolarized E_{Cl} (above membrane potential) compared to other cell types. Thus, activation of Cl^--conducting channels results in Cl^- efflux and VSMCs depolarization.

Since this Thesis focuses on TRP channels, Ca^{2+} activated Cl^- channels and Purinergic signaling in BPN/BPH mice, a more detailed description of the structure, function and action mechanisms of these receptors and channels will be discussed in the following sections.

5. Receptor-dependent contraction signaling pathways

It has been broadly described that the transmitters released from perivascular nerves and also several factors released from endothelial cells dually contribute to vascular tone control. Most of these molecules modulate vascular tone through the activation of both metabotropic and ionotropic receptors (see above, section 2.3).

Although several differences in the regulatory mechanisms have been found in different vascular beds and in different species, the purinergic signaling has an important dual role in the control of vascular tone and remodeling. Purine and pyrimidine nucleotides lead to complex integrated responses due to the activation of the nineteen different types of purinergic receptors characterized so far, which are divided in two main families: adenosine P1 and P2 receptors (Burnstock, 1978, 1980).

5.1 Adenosine P1 receptors

Adenosine P1 family comprises A_1, A_{2A}, A_{2B} and A_3 receptors and are coupled to $G_{i/o}$ (A_1 and A_3) and to $G_{\alpha s}$ (A_{2A} and A_{2B}) proteins, leading to a reduced and increased cAMP production, respectively. However, evidences showed A_1, A_{2B} and A_3 receptors couple also to $G_{q/11}$ leading to PLCβ signaling cascade activation. A_1 and A_3 receptors display a ~49% of sequence identity, while A_{2A} and A_{2B} receptors are ~45% identical. Adenosine receptors present a typical GPCR structure, consisting in an extracellular N-terminus, seven α-helical membrane spanning domains and an intracellular C-terminus. Consensus sites for N-glycosilation and cysteine containing sites are localized in the extracellular loops. An additional cysteine residue localized in the C-terminus of A_1, A_{2B} and A_3, but not A_{2A}, has been found to be post-transcriptionally modified. Additionally, the intracellular third loop plays an important role in the AC activity and in the receptor internalization (Olah and Stiles, 2000). Besides the differences on species and vascular beds, all adenosine P1 receptors have been found in perivascular nerves, smooth muscle and endothelial cells with A_{2A} and A_{2B} receptors being the most commonly expressed. P1 receptors contribute mostly to vasodilation responses via inhibitory, pre-junctional modulation and also enhancing cAMP-mediated NO production (Burnstock and Ralevic, 2013).

5.2 Purine and pyrimidine P2 receptors

Since the first description of the purinergic signaling by Drury and Szent-Györgyi in 1929 and the first definition of purinergic receptors by Burnstock in 1976, several studies have focused on a possible receptor subdivision based on pharmacological

approaches. Purinergic receptor were divided into P1 and P2 families by Burnstock in 1978 and some time later the P2 family was subdivided into ionotropic P2X receptors and G-protein-coupled P2Y receptors (Burnstock and Kennedy, 1985).

5.2.1 P2X receptors

P2X receptors comprise $P2X_{1-7}$ isoforms, all of which having intracellular N- and C-termini linked by two transmembrane domains (TM1, involved in channel gating; and TM2, lining the ion pore) and a extracellular loop (Brake, Wagenbach and Julius, 1994; Valera *et al.*, 1994; Burnstock, 2007). P2X receptors are ligand-gated channels with variable affinity for ATP and variable conductance for Na^+, K^+ and Ca^{2+}. P2X activation causes widespread cellular responses depending on their cellular subtype expression and on the homo and/or heteromeric structures they form ($P2X_2/P2X_3$, $P2X_4/P2X_6$, $P2X_1/P2X_5$) (North and Surprenant, 2000). Among P2X receptors, $P2X_1$ is the protein most expressed in smooth muscle, followed by $P2X_2$, $P2X_4$ and $P2X_7$, while $P2X_3$, $P2X_5$ and $P2X_6$ receptors are usually absent. In contrast, all the P2X isoforms have been found in endothelial cells with $P2X_4$ receptors being the dominant protein (Ralevic and Dunn, 2015).

5.2.2 P2Y receptors

P2Y family comprises eight isoforms grouped according to their sequence similarity and to their G-protein selectivity (Table I3): $P2Y_1$-like receptors ($P2Y_1$, $P2Y_2$, $P2Y_4$, $P2Y_6$ and $P2Y_{11}$) present a 28-52% sequence identity and couple mainly with G_q, while $P2Y_{12}$-like receptors ($P2Y_{12}$, $P2Y_{13}$ and $P2Y_{14}$) share 45-50% sequence identity and couple mainly with $G_{i/o}$. However, most of the G_q receptors link also to other G-proteins, such as $G_{i/0}$ and $G_{12/13}$ or G_s ($P2Y_{11}$) and show a complex cross-talk with other membrane receptors and channels (Erb and Weisman, 2012).

The structure of P2Y receptors consists of an extracellular N-terminus, seven transmembrane spanning domains involved in the ligand binding, three intracellular loops involved in the G-protein coupling and an intracellular C-terminus containing several protein kinases binding sites.

P2Y receptors are broadly expressed in different tissues and cellular subtypes so that their cellular responses vary based on their ligand specificity, G protein coupling and second messenger system. $P2Y_1$, $P2Y_2$, $P2Y_4$ and $P2Y_6$ receptors are commonly expressed in smooth muscle cells and their coupling to $G_{q/11}$ protein leads to PLC-mediated $[Ca^{2+}]_i$ increase and contraction. In endothelial cells, $P2Y_1$, $P2Y_2$ and $P2Y_6$ are the most abundant receptors, with some vessels expressing $P2Y_4$, and are related to $[Ca^{2+}]_i$ increase and subsequently NO, EDHF and PGI_2 co-releasing, leading to vasodilation. However, vasoconstrictor effects mediated by

P2Y receptors expressed in the endothelial cells have been also described when the endothelium is damaged, leading to local vasospasm (Burnstock and Ralevic, 2013)

Ligand-stimulated activation of P2Y receptors is rapidly desensitized and proteins internalized due to the GPCR kinases (GRK_{1-7}) mediated phosphorylation of intracellular Ser/Thr residues, which are then targeted by β-arrestins ($\beta\text{-}Arr_{1-4}$) leading to receptor endocytosis and recycling. Although all P2Y receptors are β-Arr desensitized and internalized, several differences have been found based on the receptor subtype: all P2Y receptors interact with $\beta\text{-}Arr_2$, while $P2Y_2$ and $P2Y_4$ receptors interact with both $\beta\text{-}Arr_1$ and $\beta\text{-}Arr_2$ (Hoffmann *et al.*, 2008).

The variabilities in the ligand specificity, in the G-protein coupling and the possibility to form homo- or heteromers with P2Y receptors and other proteins lead to a wide variety of P2Y receptor mediated cellular processes, many of them quite relevant in cardiovascular, inflammation and neurotransmission disorders.

P2YRs	Agonist	G protein- Main effector
$P2Y_1$	ADP	**G_q**- PLCβ, Rac, Rho activation
$P2Y_2$	UTP=ATP	**G_q**- PLCβ activation
		G_o- PLCβ, Rac activation
		G_{12}- Rho activation
$P2Y_4$	UTP=ATP	**G_q**- PLCβ activation
		G_o- PLCβ activation
$P2Y_6$	UDP	**G_q**- PLC activation
		$G_{12/13}$- Rho activation
$P2Y_{11}$	ATP	**G_q**- PLCβ activation
		G_s- AC activation
$P2Y_{12}$	ADP	**$G_{i/o}$**- AC inhibition; PLCβ, RhoA activation
$P2Y_{13}$	ADP	**$G_{i/o}$**- AC inhibition; PLCβ, RhoA activation
$P2Y_{14}$	UDP-Glucose	**$G_{i/o}$**- AC inhibition; PLCβ activation

Table I3. *P2Y receptors subtypes, their main agonists and G-protein coupling.*

5.3 Role of P2X and P2Y receptors in the control of vascular tone

Because of the differences found in the expression of purinergic receptors in VSMC and endothelial cells, purinergic signaling can elicit both vasoconstrictor and vasodilator responses. Common to most vessels is that ATP co-released with noradrenaline (NA) from the sympathetic perivascular nerves produces vascular constriction. However, ATP released from endothelium leads to NO and endothelium-derived hyperpolarizing factor (EDHF) production and vasodilation. In addition, UTP and UDP co-released from platelets and damaged endothelial cells lead to vasoconstriction. Obviously, the final response depends on the balance among all these pathways.

ATP and NA are separately co-stored in the perivascular nerves varicosities and are released to the adventitia layer as co-transmitters in variable proportions. ATP is released earlier than NA and induces the initial phase of contraction, while NA is responsible of the long-lasting vasoconstrictions (Burnstock and Ralevic, 2013). Although there are evidences of the expression of both P2X and P2Y receptors in vascular smooth muscle, the availability of good pharmacological tools and the development of genetic KO mice have allowed to describe $P2X_1$ receptors as the main mediators of the fast vasoconstrictor response to ATP released from sympathetic perivascular nerves (Vial and Evans, 2002; Burnstock and Ralevic, 2013). In addition, clusters of $P2X_1$ receptors have been found in close proximity to sympathetic nerve varicosities (Hansen *et al.*, 1999). The ATP-triggered $P2X_1$ activation leads to channel opening, increase of Na^+, K^+ and Ca^{2+} conductance, membrane depolarization and subsequent VOCCs channels-mediated Ca^{2+} entry and contraction, whereas NA triggered responses are slower due to the G-protein coupling and second messenger involvement. Furthermore, both pressure and vessel size are important determinants of the magnitude of the purinergic response: $P2X_1$-triggered contractions dominated in small and medium size arteries, whereas the noradrenergic component dominated in large vessels (Gitterman and Evans, 2001). Likewise, the ATP component in the constriction response was significantly reduced at low arterial pressures (Rummery *et al.*, 2007).

The rapid smooth muscle depolarizations arising from the actions of neurotransmitters are known as fast excitatory junction potentials (EJPs) and are maintained by the continuously release of ATP quanta, while slow depolarizations have a noradrenergic component (Ralevic and Dunn, 2015). On the other hand, NA acting on α_1-adrenergic receptors can promote additional ATP release from smooth muscle cells through pannexin-1 channels (Figure I10), contributing to the integrated complex vasoconstriction response (Billaud *et al.*, 2011). Some of the ATP released can directly act through pre-junctional, inhibitory autoreceptors, such as P2Y receptors and A_1 adenosine receptors, the latter after being rapidly

metabolized to adenosine by ectonucleotidase triphosphate diphosphohydrolases (E-NTPDases) of the VSMCs membrane (Kauffenstein *et al.*, 2010) and by soluble ATPases released from the sympathetic nerves (Figure I10) (Burnstock and Ralevic, 2013).

Purines released from perivascular nerves can also activate endothelial cells via P2Y and $P2X_4$ receptors, leading to NO, EDHF and PGI_2 release, vasodilation and inhibition of platelet aggregation. Furthermore, ATP-triggered ATP release in endothelial cells by shear stress and hypoxia can also activate this vasodilation response in a paracrine way (Figure I10) (Burnstock and Ralevic, 2013). Evidences showed that endothelial dysfunction promotes platelets aggregation and leukocytes accumulation, leading to ATP, ADP and UTP release, which induces local vasospasm through smooth muscle P2Y receptors (Burnstock and Ralevic, 2013).

Smooth muscle cells also express P2Y receptors, which are activated by pyrimidine nucleosides and nucleotides. Although several isoforms ($P2Y_{1,2,4,6}$) have been found in smooth muscle, evidences point to an important contribution of $P2Y_2$ and mainly $P2Y_6$ to the UTP- and UDP-triggered vasoconstrictions (Figure I10) (Vial and Evans, 2002; Bar *et al.*, 2008; Koltsova, Maximov, *et al.*, 2009). Of note, $P2Y_6$ involvement in the control of vascular tone has been recently related to its dimerization with AT1 receptors, promoting Ang II-induced hypertension dependent on age (Nishimura *et al.*, 2016). As in the case of ATP, UTP causes vasodilation when acting in endothelial cells through $P2Y_2$ and $P2Y_4$, but not $P2Y_6$ receptors, via EDHF mechanism (Burnstock and Ralevic, 2013).

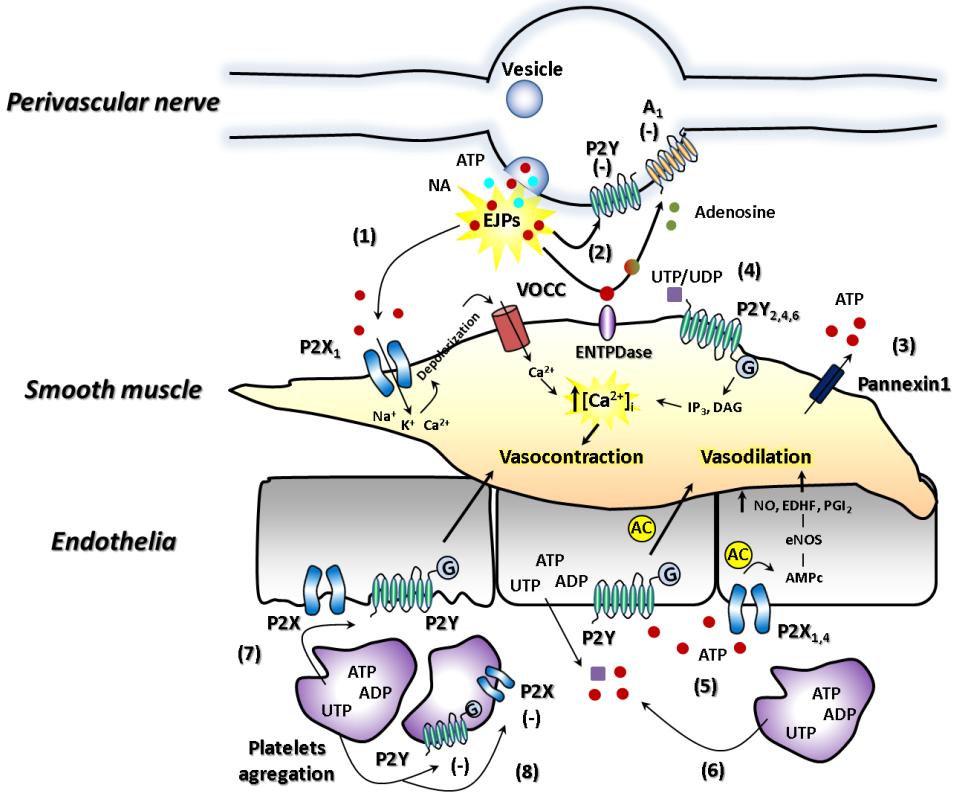

Figure I10. *Summary of the purinergic signaling control of vascular tone. 1, ATP co-released with NA from varicosities enhances EJPs and induces $P2X_1$-mediated depolarization, VOCCs activation, $[Ca^{2+}]_i$ increase and vasoconstriction. 2, ATP released is rapidly metabolized by E-NTPDases to adenosine, which has pre-junctional, inhibitory activities via P2Y and A_1 autoreceptors. 3, ATP is also released from smooth muscle cells via pannexin1. 4, UDP and UTP contribute to vasoconstriction via G-protein coupled $P2Y_{2,4,6}$ receptors. 5, ATP acting on P2Y and $P2X_{1,4}$ receptors in endothelia has vasodilator effects via AC activation of cAMP-triggered NO, EDHF and PGI_2 production. 6, ADP, ATP and UTP released from endothelial and platelets cells contributes to endothelia-mediated vasodilation. However, purines and pyrimidines released from aggregating platelets cause P2X- and P2Y-triggered vasoconstriction. 8, ADP, ATP and UTP have inhibitory effects on platelets in a paracrine way.*

5.4 Role of purinergic signaling in hypertension

Using different in vitro and in vivo models of hypertension, evidences have shown the physiological contribution of different components of the purinergic signaling to the control of vascular tone, rendering purinergic signaling components as new possible therapeutic targets. In this context, several different evidences support a contribution of the purinergic signaling to hypertension development:

- Essential hypertension has been associated with an increased sympathetic nerve activity and with hyperplasia and hypertrophy of arterial walls.

Moreover, purinergic receptors expressed on neuronal tissues mediate sympathetic activity. Antagonists of these receptors are centrally acting potential agents to the treatment of hypertension (Burnstock and Ralevic, 2013).

- Both, the increased contribution of the ATP released from sympathetic perivascular nerves and the purinergic pre-junctional, inhibitory modulation caused EJPs enhancement and a subsequent augmented vasoconstriction. Conversion from a balanced contribution to a potentiated response of ATP over NA has been found in hypertensive subjects, leading to enhanced vasoconstrictions. These findings pointed to a possible use of $P2X_1$ antagonists to the hypertension treatment (Burnstock and Ralevic, 2013).

- ATP released from endothelial cells during shear stress exerted by changes in blood flow acts as a vasodilator through endothelial $P2X_4$ and P2Y receptors, providing new possible treatments to hypertension (S. Wang *et al.*, 2015).

- Recent studies pointed to $P2X_3$ antagonists as promising tools for hypertension treatment by inhibiting sympathetic nerve activity involving the carotid body (Pijacka *et al.*, 2016). Furthermore, $P2X_7$ involvement in hypertension through increased inflammation have been described, pointing to $P2X_7$ antagonists as clinical hypertensive agents (Burnstock, 2017).

- There are evidences showing that adenosine activates renin-angiotensin-aldosterone (RAAS) system in hypertensive subjects. Considering differences in the G protein coupling of P1 receptors, adenosine A_1 antagonists and A_{2A} and A_{2B} agonists have been proposed as possible therapeutic agents to hypertension treatment (Nayak *et al.*, 2015).

- Changes in the functional expression of P1 and P2 receptors in smooth muscle, endothelial and even vascular circulating cells of hypertensive mice models evoked mainly potentiated vasoconstrictor responses. Extracellular purines and pyrimidines also contributed to the hypertensive phenotype not only by their increased release and receptor activation, but also by enhancing proliferation and hypertrophy (Burnstock and Ralevic, 2013).

6. TRP channels

Since the first discovery and characterization of a transient receptor potential (*trp*) gene encoding a cation channel (TRP) related with defective vision in a Drosophila *trp* mutant, several efforts have demonstrated the biodiversity of these channels in terms of tissue distribution, physiological functions and their association with pathological disorders. Twenty-eight mammalian TRP homologs have been described so far and characterized as cationic non-specific channels involved in sensory and signal transduction processes in excitable and non-excitable cells. These TRP channels have been grouped into seven subfamilies, according to their sequence homology (Figure I11): TRPC (canonical), TRPV (vanilloid), TRPM (melastatin), TRPA (ankyrin), TRPML (mucolipin) and the TRPP (polycystin). The additional TRPN (NOMP-C homologues) subfamily is not found in mammals, but expressed in invertebrates and cold-blooded vertebrates (Earley and Brayden, 2015).

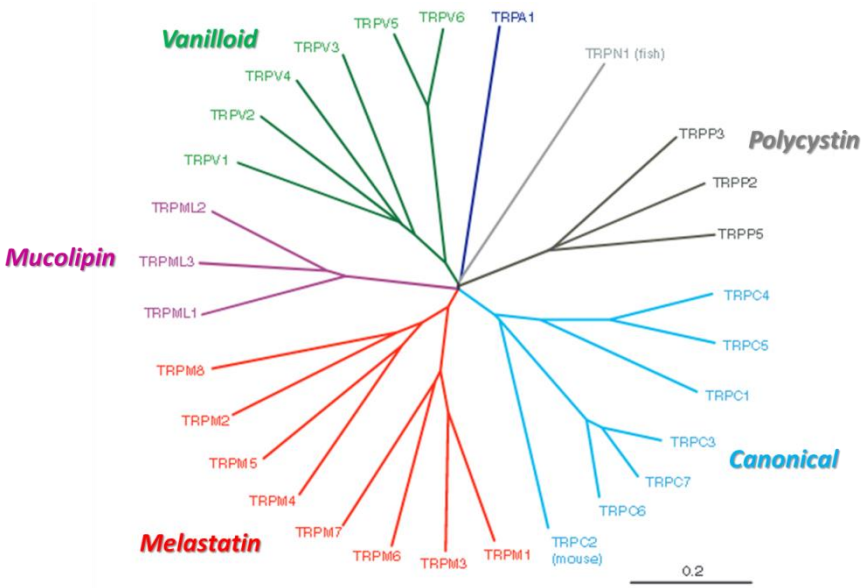

Figure I11. *Phylogenetic tree of the mammal TRP family of channels (adapted from Nilius and Owsianik, 2011).*

6.1 Structure

All TRP channels share a general transmembrane structure consisting of six spanning domains (S1-6) with a pore-forming loop between S5-S6. The intracellular N- and C-termini differ in length and amino acid sequence, providing several well-described motifs involved in channel assembly, activation and regulation. While

numerous ankyrin motifs are present on the N-terminus of TRPC, TRPV and TRPA subunits, calmodulin/IP_3R-binding motifs, Ca^{2+}-binding EF hands, serine-threonine kinase motifs and even a PDZ motif (TRPC4) are present in the C-terminus (Figure I12).

Functional channels arise from the association of four TRP subunits in a homomeric or heteromeric way. The TRPC subfamily has been the most widely studied in terms of subunit assembly: TRPC1 can heteromultimerize with TRPC3, TRPC4, TRPC5, TRPC6 or TRPC7 subunits; TRPC4 and TRPC5 can form heteromultimeric channels as can combinations of TRPC3, TRPC6 and TRPC7 subunits (Hofmann *et al.*, 2002; Earley and Brayden, 2015). Functional associations between TRPV5/TRPV6, TRPM6/TRPM7, and TRPML1/TRPML3 have been also reported. On the other hand, association between subunits of different subfamilies, such as TRPC1/TRPV4 and TRPV1/TRPA1, have also been reported with less supported evidence (Earley and Brayden, 2015).

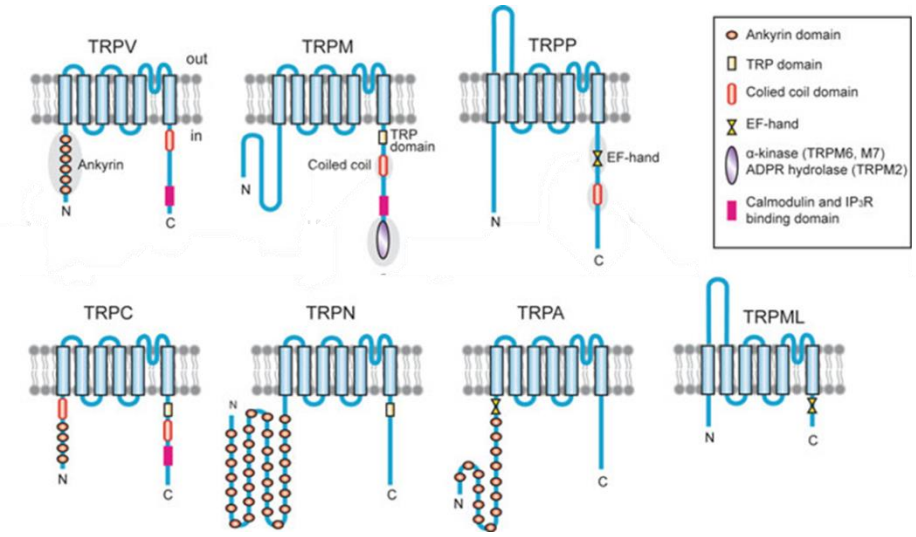

Figure I12. *Membrane topology of the different TRP subfamilies of cationic channels (adapted from Minghui, Yong and Jian, 2011).*

With the electron microscopy advances, a detailed structure of members of different TRP subfamilies, such as TRPC3, TRPM2, TRPV1 and TRPV4 have been described. For TRPC3 subunit, cryoelectron microscopy studies showed an odd high-resolution structure compared to the other TRP channels studied. The overall structure of TRPC3 (200x200x240 Å, 388 kDa for protein and 40.8 kDa for attached glycan) is divided into two components: a dense globular inner core and a sparse outer shell with a mesh-like structure containing many aqueous spaces (Figure I13).

This expanded structure could explain the multi-modal activation, regulation and even association of TRPC3 subunits (Mio *et al.*, 2007; Minghui, Yong and Jian, 2011).

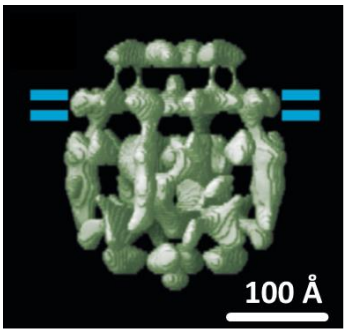

Figure I13. *Cryo-EM of TRPC3 structure. Blue lines indicate putative transmembrane region (Mio et al., 2007).*

6.2 Physiological roles of TRP channels in VSMCs

TRP channels have an important role in several biological processes, such as muscle contraction, cell proliferation, secretion, nociception and many other important processes, by controlling the ion flux across the cell membrane. In addition, several TRP members (TRPP2, TRPM8, TRPV1 and TRPA1) are expressed in intracellular organelles, where participate as modulators of protein trafficking and vesicular ionic homeostasis (Earley and Brayden, 2015). Although TRP channels are described as non-selective cation channels, their relative permeability to different ions (P_{Na}: P_K: P_{Ca}) determine their functional role: while monovalent Na^+ and K^+ cations are particularly important for the control of membrane potential and excitability, divalent Ca^{2+} and Mg^{2+} cations play important roles as second messengers and cofactors. Therefore, the activity of TRP channels can contribute to membrane potential regulation (TRPC, TRPM4), Ca^{2+} signaling (TRPC, TRPV and TRPA1) and Mg^{2+} homeostasis (TRPM6 and TRPM7).

Many studies have identified the functional expression of members of TRPC ($TRPC_{1,3,4,5,6}$), TRPV ($TRPV_{1\text{-}4}$), TRPM ($TRPM_{4,8}$), TRPA ($TRPA_1$) and TRPP ($TRPP_2$) families in smooth muscle and endothelial cells and their involvement in the control of vascular tone, reactivity, permeability and angiogenesis (Earley and Brayden, 2015). Again, TRP-triggered vascular responses depend on the vascular bed, cellular subtype and TRP family. Here we will focus on the roles of TRPC channels in the vasculature.

Membrane potential regulation

Cation influx through TRPC channels promotes different and even opposite vascular responses depending on their cellular subtype expression. Usually, in smooth muscle cells, increased Na^+ and Ca^{2+} permeabilities associated with TRPC channels activation results in membrane depolarization, leading to VOCC channels-triggered Ca^{2+} entry and contraction (Figure I14). $TRPC_{1,3,4,5,6}$ are the principal channels found in VSMCs of different vascular beds and their GPCR receptor- and swelling (TRPC6)-triggered activation have been associated to increased vascular contractility (Earley and Brayden, 2015). Interestingly, TRPC3 channels have been found to be constitutively active, further contributing to resting Vm and myogenic tone (Albert *et al.*, 2006). On the other hand, $TRPC_{1,3,4,5,6}$ channels found in endothelial cells induced endothelium-dependent vasodilation via eNOS-triggered NO production.

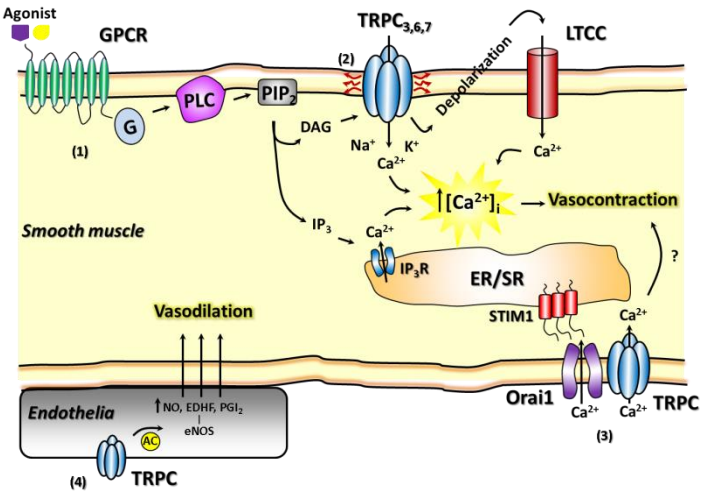

Figure I14. *Scheme of the TRPC-triggered control of vascular tone. 1, agonists-activated GPCRs induce PLC-triggered PIP_2 cleavage leading to IP_3 and DAG production. IP_3 activates IP_3R receptors on ER/SR leading to Ca^{2+} release to cytosol. DAG and also shear stress (2) directly activate $TRPC_{3,6,7}$ leading to cation influx, membrane depolarization and LTTCs channels-mediated Ca^{2+} influx. $[Ca^{2+}]_i$ increase leads to contraction of VSMCs. 3, upon agonist stimulation, Ca^{2+}-depleted stores induce SOCE through STIM1/Orai1 complex and TRPC channels. This TRPC-triggered SOCE has been also proposed to directly activate VSMC constriction. 4, in endothelial cells, TRPC-mediated cation influx, specially Ca^{2+}, leads to eNOS-induced NO, EDHF and PGI_2 production leading to VSMC relaxation.*

Ca^{2+} signaling

Changes in $[Ca^{2+}]_i$ regulate many biological processes, such as muscle contraction, hormone secretion, gene expression and proliferation. Changes in $[Ca^{2+}]_i$ are regulated by the extracellular Ca^{2+} influx, by Ca^{2+} release from intracellular

compartments and by Ca^{2+} extrusion performed by plasma and organelle membrane proteins. In this context, TRP channels with Ca^{2+} permeability influence $[Ca^{2+}]_i$ and subsequent cellular processes acting as ionotropic, metabotropic or store-operated Ca^{2+} channels (Earley and Brayden, 2015).

Agonist-induced GPCR receptor activation causes biphasic changes in $[Ca^{2+}]_i$: the initial transient increase results from the release of Ca^{2+} from the ER/SR, while the second sustained plateau phase is due to Ca^{2+} influx through ROCs. In this context, all members of TRPC family can be activated after stimulation of GPCR receptors and receptor tyrosine kinases (RTKs), through PLCβ and PLCγ, respectively (Clapham, 2003). The PLC-induced cleavage of membrane PIP_2 produces IP_3 and DAG. IP_3 activates its specific IP_3R receptor on ER/SR, leading to Ca^{2+} release to cytosol, while DAG activates PKC and also TRPC3/6/7 channels and heteromeric channels including these subunits in a PKC-independent way (Figure I14) (Hofmann *et al.*, 1999).

SOCE, defined as store-operated Ca^{2+} entry, is another signaling pathway associated to TRP channels, consisting of the refilling of intracellular Ca^{2+} stores upon sustained stimulation of membrane receptors or pharmacologic agents-induced blocking of SERCA. In this context, early studies described several members of the TRPC family, such as TRPC1, TRPC4 and TRPC5 as the SOCE channels. Other members of the TRPC family have also been reported to be involved in the SOCE signaling pathway, such as TRPC3 and TRPC6. However, after the discovery of the STIM1/Orai1 complex formation upon Ca^{2+} store depletion and their characterization as the responsible of SOCE, the consideration of TRPC as SOCE channels have been widely discussed. Later studies focused on the possibility of a direct or indirect interaction of STIM1/Orai1 complex with TRPC channels. Direct interactions between STIM1 and TRPC1, TRPC4 and TRPC5 have been described in different cellular subtypes. These studies described that upon Ca^{2+} stores depletion, the activation of STIM1 proteins lead to their migration toward plasma membrane and direct interaction with TRPC1, enhancing SOCE via TRPC1 channels (Huang *et al.*, 2006; López *et al.*, 2006). On the other hand, indirect interaction between STIM1/Orai1 and TRPC channels has been described for TRPC3 and TRPC6. In this case, STIM1 activation and membrane translocation induced the TRPC1/TRPC3 heteromultimerization, behaving as the SOCE channels. In the same way, TRPC4 and TRPC6 associations induced by the activation and membrane trafficking of STIM1 was also described, pointing to TRPC4/TRPC6 as SOCE channels. This study, however, specified that STIM1 is required only for activation of TRPC channels by agonists, but not for channel activity, thus proposing a new definition of SOCE as channels regulated by store depletion-mediated STIM1 clustering. In this context, all TRPC channels, except TRPC7, behave as SOCE

channels (Yuan *et al.*, 2009). However, another set of studies failed to demonstrate the TRPC involvement in STIM1/Orai1-triggered SOCE pathway, both in heterologous and native systems (Dehaven *et al.*, 2009). Regarding differences obtained in different cell lines and animal models about the role of TRP channels as SOCE channels and their coupling to STIM1/Orai1 complex, more precise functional studies are required. Therefore, considering TRP family as SOCE channels is still in a controversial debate.

6.3. TRPC channels and hypertension

Evidences showed that TRPC3 and TRPC6 channels are the main TRPC members whose dysfunction plays an important role in essential hypertension. Several studies in hypertensive animal models reported a functional increased expression of TRPC3 (Liu *et al.*, 2009; Chen *et al.*, 2010; Noorani, Noel and Marrelli, 2011; Wang *et al.*, 2017) and TRPC6 (Yu *et al.*, 2004; Pulina *et al.*, 2010; Zulian *et al.*, 2010) channels which correlate with enhanced agonists-induced Ca^{2+} influx and contraction. However, whether this increased expression of TRPC channels is cause or consequence of the hypertension remains unclear.

Contrary to what it was expected, $TRPC6^{-/-}$ mice (Dietrich *et al.*, 2005) showed increased vascular tone and increased sensitivity of smooth muscle to vasoconstrictor agonists that resulted in a higher increased mean arterial blood pressure. However, these mice exhibit a clear upregulation of TRPC3 channels that can compensate in different ways the TRPC6 knockout phenotype. TRPC channels also play essential roles in the regulation of myogenic tone, as it was shown by the involvement of TRPC6 channels to the pressure-induced depolarization in cerebral arteries (Welsh *et al.*, 2002). Moreover, increased coupling between TRPC3 and TRPC6 channels with additional proteins, such as other TRP channels, IP_3R receptors (Adebiyi *et al.*, 2010, 2012), Ca^{2+}-activated Cl^- channels (Wang *et al.*, 2016) and many others, enhanced Ca^{2+} influx, contraction and subsequently blood pressure, while the coupling with serine-threonine kinase WNK4 reduced TRPC3-triggered Ca^{2+} entry (Woo *et al.*, 2011).

Therefore, changes in the functional expression of some subtypes of TRPC channels could influence the mechanisms by which VSMCs control vascular tone and contractility, thus promoting vascular dysfunction and increased blood pressure, leading to hypertension. The development of selective pharmacological blockers of TRPC channels could present a potential strategy to prevent and treat essential hypertension (Earley and Brayden, 2015).

7. Chloride channels

In contrast to ions like Na^+ and K^+, in many cell types the electrochemical gradient of Cl^- across the plasma membrane is close to its electrochemical equilibrium, which is expected from a passive distribution across the plasma membrane. However, within VSMCs, the E_{Cl} is normally at a potential more positive than the resting Vm because of active Cl^- accumulation. Hence, opening of Cl^- channels in the plasma membrane causes Cl^- efflux, membrane depolarization, and increased contractile force. VSM Cl^- transporters and Cl^- channels significantly contribute to the physiological regulation of vascular tone and arterial blood pressure, so that changes in their expression and activity could contribute to vascular pathophysiology.

7.1 Classification and structure of Cl^- channels

Cl^- channels are structurally very heterogeneous and no official classification exists. Therefore, following the International Union of Basic and Clinic Pharmacology (IUPHAR) Guides (Alexander *et al.*, 2017), there have been described up to five different families:

- **Voltage-gated Cl^- channels (ClC_{1-7}, ClC_{Ka} and ClC_{Kb}).** ClC_1, ClC_2 and the two ClC_k isoforms are expressed in the plasma membrane. The rest are expressed in endomembranes and behave as Cl^-/H^+ exchangers. ClCs are mainly involved in cell excitability, transepithelial transport, extracellular ion homeostasis, endocytosis and lysosomal function (Jentsch, 2015; Poroca, Pelis and Chappe, 2017).

- **Cystic fibrosis transmembrane conductance regulator (CFTR).** This channel is a membrane ATP-gated Cl^- channel involved in the transepithelial transport of water and electrolyte whose dysfunction leads to cystic fibrosis (Linsdell, 2014).

- **Volume-regulated anion (VRAC) channels.** This family of Cl^- channels participates in the decrease of cell volume upon swelling stimuli by conducting Cl^- efflux. They also participate in membrane excitability, transcellular Cl^- transport, angiogenesis, cell proliferation and so many other cell functions (Nilius and Droogmans, 2003).

- **Large conductance (maxi) Cl^- channels.** This maxi-anion channel, which is widely expressed in many tissues, is activated by swelling stimuli and it has been involved in the control of membrane potential, secretion and cell

volume regulation. Additionally, due to its ability to release small amounts of ATP and glutamate molecules, it has been associated to signal transduction between cells (Sabirov and Okada, 2009).

- **Ca^{2+}-activated Cl^- channels (CaCC).** This family comprises the anoctamin (ANO_{1-10}) and bestrophin ($BEST_{1-4}$) subfamilies. These subfamilies have been well characterized and are involved in numerous cellular functions, including transepithelial transport, control of neuronal and cardiac excitability and regulation of smooth muscle contraction (Matchkov, Boedtkjer and Aalkjaer, 2015). Their structure, vascular function and involvement in hypertension will be discussed in the next sections.

These families of Cl^- channels have been found to be widely expressed in the plasma cell membrane in many tissues, in intracellular membranes and in the cytosol together with an additional family of intracellular Cl^- channels ($ClIC_{1-4}$). This family comprises both soluble and integral membrane isoforms and are likely to have enzymatic and intracellular membrane structural functions (Edwards and Kahl, 2010; Littler Dene *et al.*, 2010).

7.2 CaCCs channels

7.2.1 Bestrophins

BEST channels have been found to form dimers, tetramers and pentamers. Each single protomer comprises four short transmembrane α-helices (TM1-4) and a long intracellular domain formed by five α-helices together with the C-terminus. N- and C-termini are localized in the cytosol, the latter likely involved in Ca^{2+} regulation (Figure I15 A). When pentamerizing, an hydrophilic single pore formed by TM2 domain is followed by an hydrophobic neck involved in the channel gating (Yang *et al.*, 2014). BEST channels are permeable to NO_3^->Br^->Cl^- and permeability to SCN^-, HCO_3^-, GABA and even glutamate has also been reported (Dickson, Pedi and Long, 2014). Of special interest is the BEST3 channel due to its expression in VSMCs from different vascular tissues and its role in the membrane potential regulation by coupling intracellular Ca^{2+} and NO/cGMP pathways through Cl^- outward currents (Matchkov *et al.*, 2008).

7.2.2 Anoctamins

Anoctamin family (ANO or also TMEM16) comprises ten different members, most of them behaving as Ca^{2+}-dependent phospholipid scramblases. However, ANO1/TMEM16A and ANO2/TMEM16B are bona-fide Ca^{2+}-activated Cl^- channels

(CaCCs) (Whitlock and Hartzell, 2017). These CaCCs are formed by eight transmembrane domains with N- and C-termini in the cytosol. The N-terminus presents several calmodulin binding and dimerization motifs, while the C-terminus presents a highly conserved region of unknown functions called Anoctamin domain. Differences in the transmembrane domains linking loops have been proposed: the TM5-TM6 long extracellular loop which reenters the membrane early described has been questioned and replaced by another model proposing a long intracellular loop which also reenters the membrane between TM6-TM7 (Figure I15 B). In any case, this loop have been proposed as the direct Ca^{2+} sensor of the channel (Pedemonte and Galietta, 2014).

ANO1 (TMEM16A) and ANO2 (TMEM16B) appear as closely related members belonging to the same subfamily, while ANO3,4,9 (TMEM16C,D,J) and ANO5,6 (TMEM16E,F) form two separated subgroups, and ANO7,8,10 (TMEM16G,H,K) are distant paralogs of ANO1 (Pedemonte and Galietta, 2014). Evidences showed that ANO channels are activated not only by cytosolic Ca^{2+}, but also by membrane potential in a positive feedback way. More precisely, membrane depolarization enhanced Ca^{2+} sensitivity of the channels.

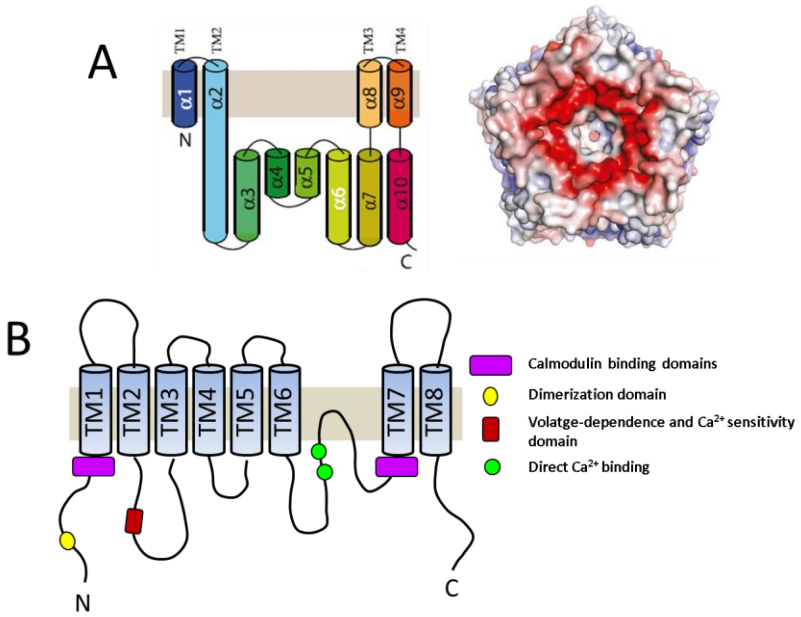

Figure I15. *Structures of BEST and ANO subfamilies of CaCC channels. A, structure of BEST protomer (left) and the outside membrane view (right) of the pentamer form* (from Yang *et al.*, 2014). *B, structure of ANO1 channel based on the more recently proposed model* (adapted from Pedemonte and Galietta, 2014).

7.3 CaCCs and NKCC cotransporters in vasculature

In addition to the important role of VOCCs on the depolarization-triggered Ca^{2+} entry and contraction of VSMCs, Cl^- conductance through VSMCs have been widely explored, although little is still known. As mentioned above, $[Cl^-]_i$ (~50 mM) and Cl^- conductance in VSMCs are larger compared to other cells, such as skeletal and cardiac muscle cells. Intracellular Cl^- accumulation is due in part, but not exclusively, to the activity of the sole isoform of cation-Cl^--cotransporter found in VSMCs, the $Na^+/K^+/2Cl^-$-cotransporter NKCC1. The equilibrium potential for Cl^- in VSMCs cells (~-26 mV) is less negative than their resting potential but is high enough to activate VOCCs and high enough to block spontaneously generated actions potentials in excitable cells. Many studies showed the role of Cl^- conductance activated upon agonists stimulation in the smooth muscle contraction response, however, the exact mechanisms still remain unknown (Kitamura and Yamazaki, 2001).

Both BEST and ANO families of CaCCs have shown to be expressed in vascular vessels, however, their relative contribution to agonists-triggered contraction are different. It has been shown that BEST downregulation has no effect on NA-induced vasoconstriction, suggesting their sole contribution to membrane potential, while downregulation and pharmacological inhibition of ANO1 abolished vasoconstrictor responses (Matchkov, Boedtkjer and Aalkjaer, 2015). Therefore, ANO family, and mainly ANO1 channel, have been the focus of the more recently studies about CaCCs in the vasculature and its associated disorders.

Upon agonist-dependent stimulation, Ca^{2+} released from the intracellular stores activates Cl^- efflux (I_{ClCa}) through ANO1 channels, contributing to membrane depolarization, LTTCs-triggered Ca^{2+} influx and further $[Ca^{2+}]_i$ increase. In addition, ANO1 channels also influenced the stretch-activated Ca^{2+} influx, which is crucial for the myogenic tone response (Bulley *et al.*, 2012). Moreover, the role of ANO1 channels is largely influenced by phosphorylation mechanisms involving Ca^{2+}-dependent kinases and phosphatases, such as CaMKII and calcineurin, respectively, confirming the importance of the amplitude and kinetics of intracellular Ca^{2+} transients to ANO1 functions (Pedemonte and Galietta, 2014). However, it is not clear if a direct phosphorylation of ANO channels leads to I_{ClCa} or an additional regulatory subunit is involved. In this context, Cl^- Channel Accessory (ClCa) family of proteins, such as ClCa1 and ClCa2, has been found to influence the Ca^{2+}-dependent ANO1 activation. ClCa1, described in mammals as a secreted metalloprotease, have been found to enhance ANO1-dependent I_{ClCa} by directly engaging and stabilizing dimeric ANO1 proteins at the membrane surface without increasing its expression (Sala-Rabanal *et al.*, 2015). In contrast, ClCa2 protein, which was found to be anchored to the plasma membrane through C-terminus, directly interacted with

STIM1/Orai1 complex, enhancing SOCE-activated ANO1-dependent I_{ClCa} (Sharma *et al.*, 2018). Another protein-protein interaction involving ANO1 channels was found for TRPC6 channels in cerebral arteries (Wang *et al.*, 2016). In this study, TRPC6 and ANO1 channels were found in close spatial proximity at the plasma membrane and agonist-induced TRPC6 activation lead to local Ca^{2+} signals that activated ANO1-triggered I_{ClCa} and vasoconstriction.

For NKCC1 cotransporter, its main roles in vascular physiology are related to $[Cl^-]_i$ regulation. By controlling $[Cl^-]_i/[Cl^-]_o$ ratio, NKCC1 cotransporter regulates Vm and excitation-contraction coupling. Indeed, NKCC1 blockade attenuated basal tone, myogenic tone and agonists-induced vasoconstriction through Cl^--dependent hyperpolarization and suppression of VOCCs activity (Orlov *et al.*, 2015). These NKCC1-dependent vascular functions were also confirmed using $NKCC1^{-/-}$ KO mice, suggesting the important role of this cotransporter in the vasculature (Koltsova, Kotelevtsev, *et al.*, 2009; Koltsova, Maximov, *et al.*, 2009).

In endothelial cells, I_{ClCa} contributes to cell volume and membrane potential. However, little is known about the endothelial $[Cl^-]_i$. Thus, the hyper- or depolarizing effects of endothelial-triggered I_{ClCa} in the intact vascular wall remains unclear (Matchkov, Boedtkjer and Aalkjaer, 2015).

7.4 Role of ANO1 channels and NKCC1 cotransporter in hypertension

Regarding the role of I_{ClCa} for vascular tone and contractility, several studies have identified some CaCCs, namely ANO1 channels, as potential targets to the treatment of hypertension, although the available data are contradictory. ANO1 upregulation has been characterized and correlated to increases in blood pressure in two different rat models of pulmonary hypertension (Leblanc *et al.*, 2015), as well as in spontaneous hypertension (B. Wang *et al.*, 2015). On the other hand, hypertension-associated downregulation of ANO1 channels due to an increase in the activity of CaMKII was also reported (Wang *et al.*, 2012). Finally, in a mouse model with smooth muscle-specific ANO1 KO, arterial blood pressure was decreased and the development of Ang II-induced chronic hypertension was less severe (Heinze *et al.*, 2014).

The role of NKCC cotransporters in the pathogenesis of hypertension have been differentiated according to primary and secondary hypertension. NKCC1 cotransporter plays an important role in the physiopathology of primary hypertension since is the only isoform expressed in VSMCs, and several mechanisms underlying its role have been proposed. In SHR rats model, both NKCC1 mRNA and protein levels were increased, which involved the NKCC1-dependent $[Cl^-]_i$ regulation, affecting VSMCs contraction and SNS activity. Indeed,

bumetanide-induced NKCC1 blockade on α-adrenergic-dependent vasoconstriction were higher compared to normotensive controls (Lee *et al.*, 2010). Moreover, the higher mRNA and proteins levels also observed in paraventricular nucleus of SHR rats correlated with the higher $[Cl^-]_i$ found in these neurons, resulting in a decreased activity of GABAergic neurons in SHR, compared to controls (Ye *et al.*, 2012). Studies focused on epigenetic regulation of NKCC1 in SHR model concluded that hypomethylation of NKCC1 promoter resulted in its augmented expression and subsequently augmented $[Cl^-]_i$, membrane depolarization and contraction, leading to blood pressure increase (Lee *et al.*, 2010). Moreover, increased activity of NKCC1 cotransporter was also observed in erythrocytes from SHR rats and hypertensive patients, contributing to the long-term increase of blood-pressure. On the other hand, studies performed in $NKCC1^{-/-}$ KO mice revealed a significant decreased in the blood pressure of these animals (Meyer *et al.*, 2002).

8. Hypothesis of study.

Our group has been exploring the contribution of different VSM ion channels to the molecular mechanisms involved in the physiopathology of essential hypertension. Using a genetic, phenotype-driven mouse model of essential hypertension (BPH and their BPN control mice), the functional expression of different families of channels, including K^+ channels and VOCCs, and their contribution to the hypertensive phenotype have been widely explored. However, the contribution of many other families of receptors and ion channels, such as ROCs and SOCs channels are still unknown.

This Thesis aims to explore the role of some ROCs and some GPCR, specifically TRPC channels and P2Y receptors in the genesis of the hypertensive phenotype in BPN/BPH model of essential hypertension.

Since sympathetic nerve activity is increased in this model (see section 3.2), we hypothesize that changes in the activation of the purinergic signaling pathway could be directly contributing to changes in the resting membrane potential and Ca^{2+} influx in VSMCs, leading to $[Ca^{2+}]_i$ increase and promoting the subsequent increased vascular tone and contractility, characteristic of hypertension. The differences between of BPN and BPH in the purinergic response may be the result of changes in the purinergic receptors and/or may be generated by differences in the expression or/and functional activity of TRPC and Ca^{2+} activated Cl^- channels, working downstream in the signaling pathway and fine-tuning the changes in Vm that activate VOCCs opening and vascular contraction.

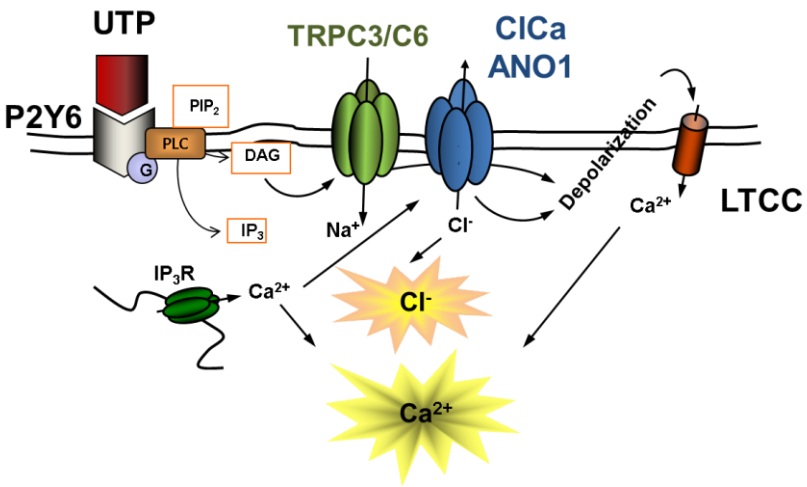

Figure I16. *Scheme of the hypothesis of the purinergic signaling contribution to essential hypertension.*

2

Objectives

OBJECTIVES

This Thesis explores the contribution of Receptor Operated Channels and G protein coupled receptors to the molecular mechanisms involved in hypertension using a genetic mouse model of essential hypertension, the BPN/BPH model. The study focuses specifically in the differences between BPN and BPH mice in the functional contribution of TRPC channels to the hypertensive phenotype at rest and in the context of the activation of the purinergic signaling pathway. The specific goals include:

1. The characterization of ROCs contribution to modulate resting Vm and contractility of BPH mice. To achieve this objective we explored:

   1.1. The functional expression of members of the TRPC family in BPN and BPH mice, and their contribution to vessel contractility.

   1.2. The heteromultimerization profile of TRPC3 and TRPC6 channels and their association with the hypertensive phenotype.

   1.3. The functional expression of members of CaCCs and Cl^- conductance cotransporters involved in the control of Vm and contractility of VSMCs and their functional association with the hypertensive phenotype.

2. The characterization of the purinergic signaling pathway in VSMCs and its relationship with the physiopathology of hypertension. To achieve this objective we explored:

   2.1. The expression profile of several members of P2X and P2Y families of purinergic receptors in VSMCs of BPN and BPH mice.

   2.2. The functional contribution of the purinergic receptors explored to the increased vascular tone and contractility of BPH compared to BPN mice.

3

Materials and Methods

1. Mouse model of essential hypertension

Colonies of hypertensive mice BPH (Blood Pressure High) and their controls BPN (Blood Pressure Normal) from Jackson Laboratories (Jackson Laboratories, Bar Harbor, ME, USA) were maintained by inbreeding crossing in the animal facility of the School of Medicine of Valladolid, under temperature controlled conditions (21°C) and with unlimited access to water and food.

The development of the BPH and BPN strains was performed by crossbreeding of eight different mouse strains that were subjected to phenotypic selection performed by tail-cuff blood pressure measurements. BPH mice showed high blood pressure early in life compared to BPN, which was associated with strain differences in heart rate, heart weight, left ventricular mass, kidney weight and hematocrit (Schlager and Sides, 1997). The development of hypertension in these strains led to an increased heart and left ventricular size (compared to body weight) and an increased heart rate that represented adaptive mechanisms to cope with the increased arterial pressure maintaining the cardiac output. In addition, BPH mouse strain showed lower levels of renin, aldosterone and angiotensin and a short lifespan, compared to BPN (Schlager, 1981; Schlager and Sides, 1997).

All animal protocols were approved by the Institutional care and Use Committee of the University of Valladolid and are in accordance with the European Community guiding principles with respect to the care and use of animals (Directive 2010/63/UE) (Directive, 2010).

2. Tail-cuff measurements

To confirm that BPH and BPN mouse strains maintained their phenotype, blood pressure levels were measured using the CODA® High Throughput Noninvasive Blood Pressure system (Kent Scientific Corporation, Torrington, CT, USA, Figure M1). In addition to the CODA controller, the system has also a far-infrared warming platform, animal holders of different sizes, tail-cuff kits and a computer with database software.

Briefly, aware mice were placed into the animal nose cone holder and carefully secured to avoid the animal being able to turn around, providing unrestricted breathing during measurements. Next, the holders were placed onto the warming platform and the tails were cuffed with the VPR (Volume Pressure Recording) sensor and the occlusion cuff kit without force. The VP recording method consists of inflating the occlusion tail cuff to occlude blood flow and while it is slowly being

deflated, the VPR cuff sensor measures the tail swelling. Systolic blood pressure (P_s) corresponds to the first appearance of tail swelling, while diastolic blood pressure (P_d) is calculated from the rate of tail swelling, and both are identified as the first and second inflections, respectively, of the recording line in the real-time blood pressure graph (Krege *et al.*, 1995; Wang, Thatcher and Cassis, 2017). Mice were acclimated to 32-35°C during 15 min prior to data acquisition. Sessions of recorded measurements were carried out daily during 4-6 consecutive days at the same time. Each session consisted of a total of 40 cycles of inflating steps to a maximum occlusion pressure of 250 mmHg followed by deflating steps of 15 s. The first 5 cycles were used for acclimation and were not included for the analysis. Values of 15 µL were fixed as the minimum tail volume for data acquisition. Mice were first trained at least 2 days prior to data acquisition, as we found that this was enough to ensure extreme reliable and reproducible measurements from session to session.

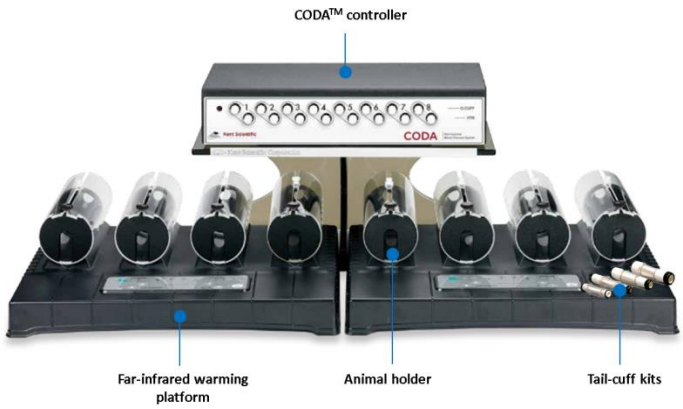

Figure M1. *CODA® High Throughput Noninvasive Blood Pressure system*

3. Animals surgery

BPN and BPH mice ranging from 16 to 58 weeks old (average 36.2 ± 2.4 weeks for BPN and 34.6 ± 1.7 weeks for BPH) and weighing 29.33 ± 0.23 g for BPN and 24.37 ± 0.24 g for BPH (n=69-80, P<0.001) were anesthetized by isoflurane inhalation (5% O_2 at 2.5 $Lmin^{-1}$) and sacrificed by cervical dislocation. Mesenteric arteries were obtained as described previously (Moreno-Domínguez *et al.*, 2009). Briefly, a laparotomy was performed to obtain the small intestine, which was placed in a Sylgard®-coated plate filled with ice cold (4°C) oxygenated (95% O_2-5% CO_2) smooth muscle dissociation solution (SMDS)- 10µM Ca^{2+} (Table M1).

Composition	SMDS (mM)	SMDS 10 µm Ca^{2+} (mM)
NaCl	120	120
KCl	4.2	4.2
$NaCHO_3$	25	25
KH_2PO_4	0.6	0.6
$MgCl_2 \cdot 6H_2O$	1.2	1.2
Glucose	11	11
$CaCl_2$	-	0.010
pH	7.4	

Table M1. *Smooth muscle dissociation solution.*

Subsequently, arteries were cleaned of connective and adipose tissues under a dissecting microscope. The characteristic V-shaped intersection of arteries was taken into account to distinguish them from the veins (Figure M2). 2nd and 3rd order mesenteric arteries were collected and processed in different ways: 1) Frozen at -80°C for further RNA extraction, 2) used directly for myography studies and 3) used to obtain freshly isolated VSMCs.

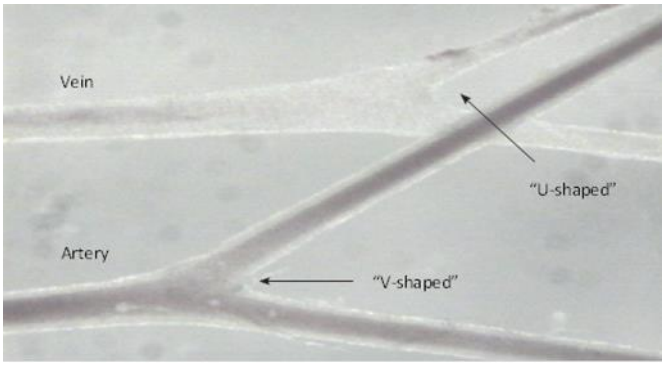

Figure M2. *V-and U-shaped intersection of artery and vein.*

4. RNA isolation and real-time PCR

To explore the mRNA expression pattern of receptors and channels, real-time PCR was performed in mesenteric arteries from BPN and BPH mice. The protocols used consist of several consecutive steps:

a) RNA samples homogeneization and isolation

Total RNA isolation was carried out using the TRIzol® Reagent (Ambion, Life Technologies Corporation) and the Precellys® (Bertin Instruments, France) homogenization methods followed by the PureLink® DNase treatment (Ambion, Life Technologies Corporation), following the manufacturer´s instructions (Figure M3). Briefly, 2nd and 3rd mesenteric arteries from 4-5 mice were denuded of endothelial layer by scraping with a pipette tip and cut in fragments less than 3 mm length. Then, samples were homogenized in TRIzol® Reagent using the CK14 and CK28 Precellys® kit, which consists of tubes containing two sizes of ceramic beads designed for hard tissue homogenization, and a Precellys® tissue homogenizer. By adding chloroform, RNA was then separated in an aqueous layer and precipitated using isopropanol. After washing twice, PureLink® DNase treatment (Ambion, Life Technologies Corporation) was carried out following the manufacturer´s instructions. Finally, RNA was stored at -80°C or used within the day to check the RNA purity and integrity.

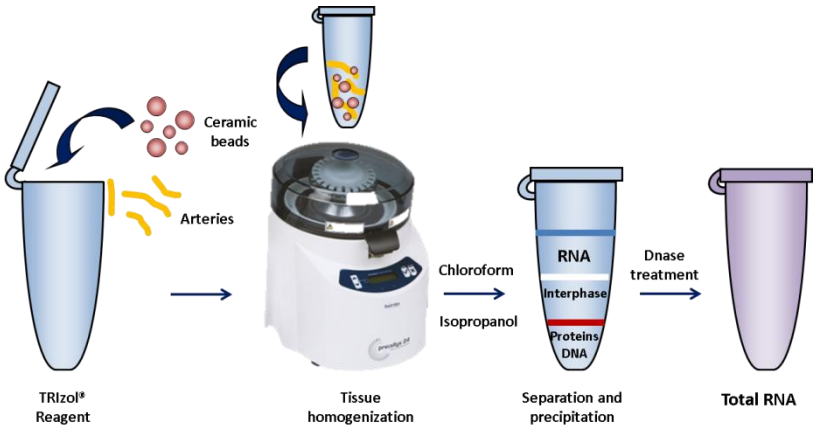

Figure M3. *Total RNA isolation scheme.*

b) RNA quantification

To obtain high efficiency and purity in RNA during the isolation step, many factors, such as the type of tissue, sample handling during surgery, extraction and storage, have to be considered. To check the correctness of these procedures, the quality of the purified RNA was confirmed both by agarose gel electrophoresis and by measuring the absorbance using a spectrophotometer (NanoDrop ND-1000, Thermo Scientific). The equation of Beer-Lambert correlates absorbance to concentration as following:

$$A = E \cdot b \cdot c$$

Where, A is the measured absorbance (or optical density, OD, in absorbance units A), E is the molar extinction coefficient (in $M^{-1} \cdot cm^{-1}$), b is the sample thickness (in cm) and c is the analyte concentration ($mol \cdot L^{-1}$).

When measuring nucleic acids concentration, this equation is rearranged to:

$$c = \frac{A \cdot e}{b}$$

Where c is the nucleic acid concentration (in $ng \cdot \mu L^{-1}$), A is the absorbance (in absorbance units, A), e is the molar extinction coefficient (in $ng \cdot cm \cdot \mu L^{-1}$) and b is the sample lenght (in cm).

Values of optical density ratio A260/280>2 are generally accepted as "pure RNA", while ratio values less than 2 are indicative of contamination. Finally, quantified RNA was treated with RNAse-Free DNAse I (Ambion) to remove possible genomic DNA contamination from the samples.

c) Reverse transcription

The reverse transcription reaction was used to obtain cDNA (RT^+) from purified RNA samples using the reverse transcriptase enzyme MuLvRT, allowing more stable samples to be obtained. With MuLvRt enzyme, a complementary cDNA strand of a single-stranded RNA template is created using the reaction mix described in table M2 (in PCR buffer):

Composition	RT^+ Reaction mix	RT^- Reaction mix
Purified RNA	500-700 ng	200-350 ng
Random hexamers	2.5 µM	2.5 µM
$MgCl_2$	5 mM	5 mM
dNTPs	4 mM	4 mM
RNAse inhibitor	1 u μL^{-1}	
MuLvRT	2.5 u μL^{-1}	

Table M2. *Reaction mix for experiment (RT^+) and genomic control (RT^-) conditions. The final volume of the reaction was 80 µl for the RT^+ and 20µl for RT^-*

The reaction mixture was subjected to the following temperature-controlled reverse transcription cycle (Figure M4): 10 min at 25°C, 60 min at 42°C, and finally 5 min at 99°C. The amplified cDNA (RT^+) was immediately stored at -20°C.

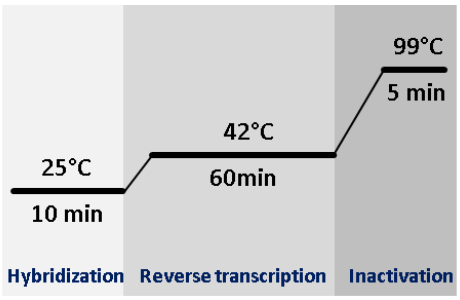

Figure M4. *cDNA synthesis protocol working scheme*

d) Amplification by real-time PCR

Gene relative expression was explored by real-time PCR using the TaqMan Assay (Applied Biosystems, Life Technologies), which is based on the 5´ nuclease activity of the Taq polymerase on a fluorogenic-labeled probe (Figure M5). This TaqMan probe is constructed with a fluorescent dye and a quencher, both bound to the 5´ and 3´ ends, respectively. While the probe is intact, the quencher reduces the fluorescence emitted by the dye by fluorescence resonance energy transfer. When the probe anneals to the target DNA and the 5´ nuclease activity of Taq polymerase cleaves the reporter dye, the emitted fluorescence increases. This fluorescence intensity is proportional to the amount of target DNA accumulated during PCR reaction.

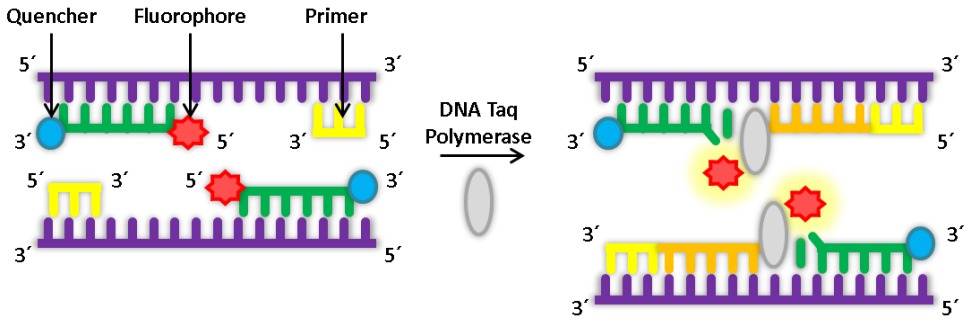

Figure M5. *TaqMan probe action mechanism.*

The previously obtained cDNAs were processed at the Genomic Service of the Parque Científico de Madrid (Spain) using TaqMan Low Density Arrays (TLDA, Applied Biosystems, Life Technologies Corporation). The selected receptor and ion channels genes to explore are described in Table M3. The array also included an endogenous control gene (18S rRNA) to correct for the amount of cDNA, and a

smooth muscle marker (calponin) and an endothelial cell marker (eNOS), to check the purity of smooth muscle tissue.

Gen name	Protein	Applied Biosystems identification number
P2rx1	P2RX1	Mm00435460_m1
P2rx4	P2RX4	Mm00501787_m1
P2ry1	P2RY1	Mm02619947_s1
P2ry2	P2RY2	Mm00435472_m1
P2ry2s1	P2RY2	Mm02619978_s1
P2ry4	P2RY4	Mm00445136_s1
P2ry6	P2RY6	Mm01275473_m1
P2ry6s1	P2RY6	Mm02620937_s1
Trpc1	TRPC1	Mm00441975_m1
Trpc2	TRPC2	Mm00441984_m1
Trpc3	TRPC3	Mm00444690_m1
Trpc4	TRPC4	Mm00444284_m1
Trpc6	TRPC6	Mm01176083_m1
Trpc7	TRPC7	Mm00442606_m1
Clca1	CLCA1	Mm01320697_m1
Clca2	CLCA2	Mm00724513_m1
Clcn3	CLCN3	Mm01348786_m1
Slc12a2	NKCC1	Mm01265951_m1
Tmem16a	TMEM16A/ANO1	Mm00724407_m1
Cnn1 (Calponin 1, smooth muscle)	CNN1	Mm00487032_m1
Gapdh (Glyceraldehide-3P-dehydrogenase)	GAPDH	Mm99999915_g1
Nos3 (Nitric oxide synthase 3, endothelial)	NOS3	Mm00435217_m1
Gus (β-glucuronidase)	Gus	**

Table M3. *Genes whose relative expression was explored using TLDA assay. ** Probes designed in our laboratory.*

A small fraction of cDNAs were used to explore gene expression using TaqMan probes designed in our laboratory in a Rotor-Gene RG3000 (Corbett Life Science, Quiagen) and the results were then compared to those obtained using TLDA arrays. The designed primer sets and TaqMan probes were:

mGAPDH	Primer 5´-3´	5'-TGTGTCCGTCGTGGATCTG-3'
	Primer 3´-5´	5'- GATGCCTGCTTCACCACCTT-3
	TaqMan probe	5'-FAM-TGGAGAAACCTGCCAAGTATGATGACATCA-BHQ2-3
mGus	Primer 5´-3´	5'-CAATGGTACCGGCAGCC-3'
	Primer 3´-5´	5'-AAGCTAGAAGGGACAGGCATGT-3'
	TaqMan probe	5'-FAM-TACGGGAGTCGGGCCCAGTCTTG-BHQ2-3
RPL18	Primer 5´-3´	5'-CAATGGTACCGGCAGCC-3'
	Primer 3´-5´	5'-AAGCTAGAAGGGACAGGCATGT-3'
	TaqMan probe	5'-FAM-TACGGGAGTCGGGCCCAGTCTTG-BHQ2-3

Amplifications were performed in a total volume of 20 µL, using 10 µL of Absolute qPCR mix (ABgene, Thermo Fisher Scientific Inc.), 1 µL of each forward and reverse primers, 1 µL of probe and 1 µL of cDNA. The reaction conditions used were as indicated in Figure M6.

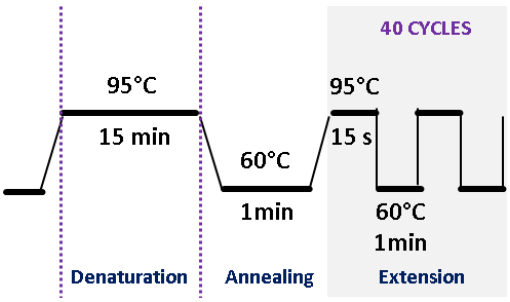

Figure M6. *Amplification protocol.*

e) Relative quantification and quality control

For the analysis of the TaqMan assay, a cycle threshold (Ct) for each curve is determined. At the beginning of the qPCR reaction, a basal unspecific fluorescence is detected. Setting a threshold over this background signal within the exponential phase of the amplification curve provides Ct, or the cycle number at which the emitted fluorescence surpasses (cuts) the threshold (Figure M7). Ct is defined as

the number of cycles required to produce a significant fluorescence increase compared to the baseline signal, and it is inversely proportional to the initial amount of cDNA.

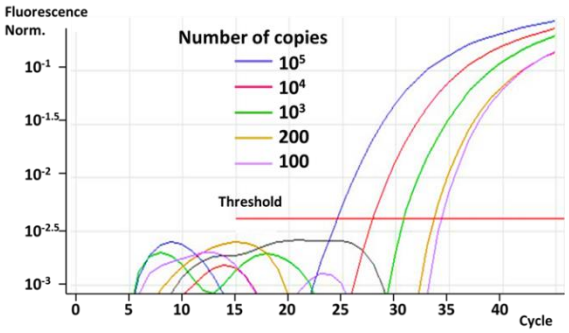

Figure M7. *Example of qPCR amplification plots for the endogenous control RPL18 with serial dilution of a sample, providing a different starting number of cDNA copies. Fluorescence is plotted in a log scale and the threshold value can be manually adjusted.*

Data analysis was performed using the relative quantification method (Livak and Schmittgen, 2001), known as fold-increase method or $2^{-\Delta\Delta Ct}$, based on the comparison of the Ct values of different genes normalized to those of the endogenous controls (Housekeeping genes), such as rRNA 18S and Gapdh.

$$\Delta C_t = C_{t,channel} - C_{t,control}$$

In order to perform this normalization, the efficiency of the amplification of both, the experimental gene and the endogenous control must be close to 1 and differ less than 10%. An efficiency of 1 means that the amount of DNA template doubles in each cycle. To determine the efficiency of the reaction, we performed a PCR with serial dilutions of one sample and obtained the Ct value for each dilution. Representing Ct against the number of copies of each dilution, we can fit a line to these data and calculate its slope (Figures M7 and M8). From this slope, we obtain efficiency as described in figure M8. The expression TLDA assays used were validated by the manufacturer. According to their specifications, the efficiency of the amplification reactions for all genes was 1, and differed by less than 10%.

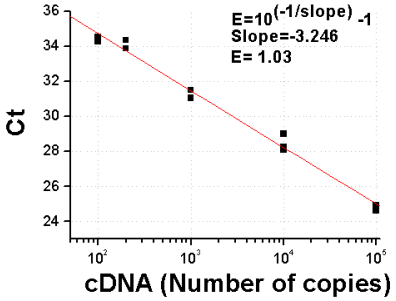

Figure M8. *An example of a standard curve showing the threshold cycle (Ct) on the y-axis and the starting quantity of cDNA target on the x-axis. Slope value is used to calculate the efficiency of the reaction as indicated in the equation. Gene studied was Gapdh.*

After obtaining for each gene its relative expression (ΔC_t value) in preparations, (BPN and BPH tissues) we compared them to get $\Delta\Delta C_t$ with the following equation:

$$\Delta\Delta C_t = \Delta C_{t,sample} - \Delta C_{t,calibrator}$$

Where the sample represents the experimental tissue (BPH) and the calibrator is the control tissue (BPN). With this quantification method, we define a calibrator (in our case BPN tissue) and we determine the changes in our "problem" preparation (the BPH samples) as fold increase or fold decrease with respect to the expression values of the calibrator. To represent these values, we used the logarithm of $2^{-\Delta\Delta Ct}$. Hence, a value of 0 means that there is no change in expression; whilst positive values indicate a higher expression in BPH and negative values indicate a higher expression in BPN tissue.

For statistical comparisons, the ΔCt obtained in each sample ($\Delta C_{t,channel} - \Delta C_{t,control}$) were subtracted from the mean ΔCt of the calibrator to provide S.E.M. Each data point was obtained from duplicate determinations from at least three different assays. In the cases where gene expression was not detected in one of the conditions, a C_t value of 40 was used in order to do the comparisons.

5. Pressure Myography

5.1. Pressure Myography fundaments

Pressure Myography is a technique that allows studying the pathophysiological properties and functions of vascular vessels in vitro. By cannulating a small segment of a vessel, pressure myography simulates the physiological conditions of temperature, pH and intraluminal pressure of in vivo vessels. Designing different protocols, this system allows investigation of myogenic tone, of effects of endothelial secretions or the pharmacological effects on vasoconstrictor and vasodilator responses to different drugs and stimuli. Although the pressure myography mounting procedure could stress the vascular tissue, the vessels still retain many of their in vivo characteristics, which allow extrapolating the results to the in vivo behavior of the entire vascular bed.

In this study, the pressure myography technique has been applied to investigate the role of different molecular components of the VSMCs membrane to the vascular tone. Using pharmacological approaches, vascular responses of mouse mesenteric arteries were investigated under near physiological conditions. Both

constriction and dilation could be readily measured as changes in the vessel´s diameter via digital video-edge detection.

5.2. Pressure Myography System

The pressure myograph system (Danish Myo Technology, Aarhus, Denmark) used to study the functional responses of mesenteric arteries consists of several parts: myography pressure unit, pressure regulator interface, vacuum system, DMT microscope and DMT Software (Figure M9).

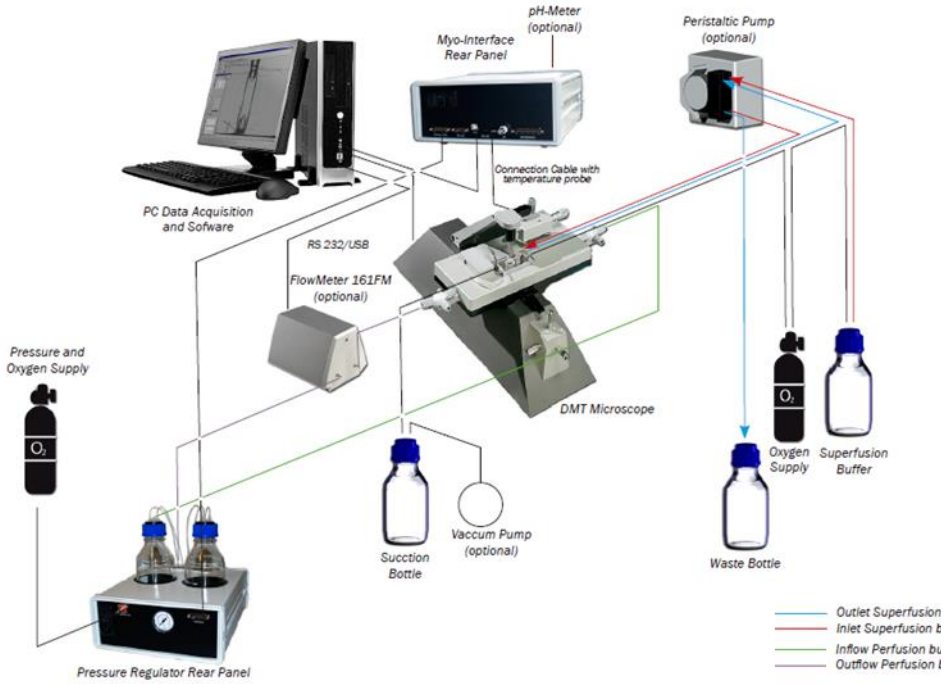

Figure M9. *Scheme of the complete Pressure Myograph System (Model 111P).*

5.2.1. Myography pressure unit

The pressure myography unit contains a bath chamber with two removable glass pipettes with a tip of 0.5 mm. Each pipette is connected to a pressure transducer (P1 and P2 in figure M10) that generates an electrical signal as a function of the pressure imposed by the liquid inside each pipette, based on a Wheatstone bridge circuit. The intraluminal liquid pressure is generated by the external pressure regulator interface connected to the perfusion inlet and outlet of the pressure unit. In addition, the force transducer coupled to the outlet pipette senses changes in the longitudinal force. Finally, the myo chamber cover includes ports for

superfusion, vacuum and oxygenation, also allowing the access for temperature or pH probes or application of reagents and drugs.

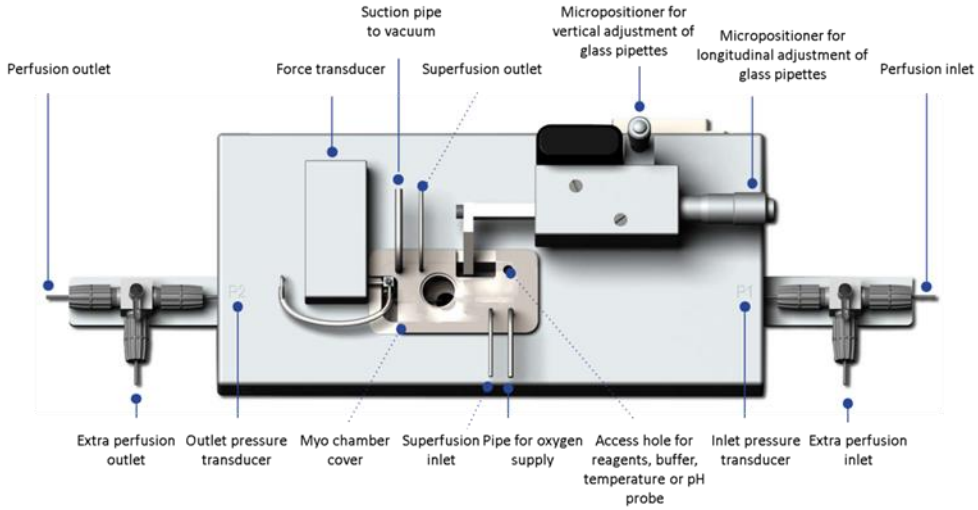

Figure M10. *Myography pressure unit scheme.*

5.2.2. Pressure regulator interface

The perfusion flow is controlled by the Pressure Regulator via the Myo-interface and the MyoView™ Software. The system consists of two separated circuits, one for air and the other one for buffer that transfers the flow and pressure setting signals from the Myo-interface to the pressure unit by the control of the air pressure in each circuit.

5.2.3. Vacuum system

The vacuum system includes a vacuum pump connected to the Myo chamber cover via a suction bottle, maintaining a constant Myo chamber volume of 6 ml.

5.2.4. DMT microscope

The DMT microscope (model 111P) is an inverted microscope equipped with a Zeiss Achromat 10X/0.25 objective and build-in CCD camera. The pressure unit is coupled above the DMT microscope and secured with a lever. The three micro positioners on the front adjust the objective focus in the X Y Z directions. The DMT-microscope has a build-in infrared light source to avoid the influence of background light of the surroundings.

5.2.5. DMT Software

The data acquisition and analysis was carried out using the MyoView™ Software. This software obtains real-time images by measuring the differences in light intensity passing through the walls of a vessel mounted in the pressure unit. In addition, it allows controlling the pressure regulator interface, the force transducer, temperature and pH.

5.3. Pressure Myography procedure

Segments of 2nd and 3rd order of mesenteric arteries cleaned of connective and adipose tissues were mounted in the pressure myograph unit as following: First, the Myo chamber was filled with preheated (37°C) and oxygenated (5% CO_2-95% air) physiological saline Myography Solution (Table M4) and the inlet and outlet glass pipettes were purged of air by imposing a negative pressure using the vacuum system. Next, the arteries were cannulated and fixed to the P1 inlet pipette and, after removing the endothelial tissue by passing air bubbles through the artery segment, they were filled with Myography Solution. Then, the arteries were cannulated and fixed to the P2 outlet pipette avoiding stretching and stressing the vessels. After that, the pressure myograph unit was coupled to the DMT microscope and the Myo chamber cover was carefully placed. The oxygenated superfusion and the vacuum system were connected to control the final chamber volume (6 ml) and the temperature sensor was placed to maintain 37°C during the whole experiment. The arteries were slowly pressurized from 10 to 70 mmHg in oxygenated (5% CO_2-95% air) Myography Solution. This gradually pressurization was carried out in 10 mmHg pressure increase steps every 5 min, reaching the final physiological pressure of 70 mmHg. We choose this value because it is a pressure slightly below the mean arterial pressure and most likely closed to the physiological pressure values in the mesenteric bed (Fenger-Gron, Mulvany and Christensen, 1995). Then, the arteries were incubated at 37°C without intraluminal flow for at least 20 min to equilibrate before starting the data acquisition.

Composition	Myography Solution (mM)	Myography Solution-60mM K^+ (mM)
NaCl	120	65
KCl	5	60
$NaCHO_3$	25	25
Na_2HPO_4	1.18	1.18
$MgSO_4$	1.17	1.17
Glucose	10	10
EDTA	1	1
$CaCl_2$	2.5	2.5
pH	7.4	

Table M4. *Myography Solutions.*

The viability of the mounted arteries was evaluated by their vasoconstriction effect in response to Myography-60 mM KCl Solution or 0.5-1µM Phenylephrine, and endothelium removal was confirmed by the absence of dilation in response to 10 µM Acetylcholine.

5.4. Pressure Myography protocols

The myography protocols performed in this study were based on the analysis of external diameter changes of the mounted arteries elicited by different drugs. To normalize the vasoconstrictor or vasodilator effects of the drugs, 10 µM of Nifedipine was added at the end of the experiment to determine the maximal vessel diameter upon relaxation and Myography-60 mM KCl Solution was used to determine the minimal diameter. When the vasoconstrictor response of drugs was tested, the following equation was used:

$$vasoconstriction\ effect\ (\%) = \frac{D_{Nifedipine} - D_x}{D_{Nifedipine} - D_{K^+}} \cdot 100$$

Where $D_{Nifedipine}$ is the maximal vessel diameter, D_x is the diameter reached in presence of the drug and D_{K^+} is the diameter value reached by Myography-60 mM KCl Solution.

To test the vasodilation response, a previous vasoconstriction state of the artery was performed using 1-10 µM Phe or UTP followed by the addition of the vasodilator drugs. In this case, the normalization was performed using the equation:

$$vasodilation\ effect\ (\%) = \frac{D_x - D_{Phe/UTP}}{D_{Nifedipine} - D_{Phe/UTP}} \cdot 100$$

Where D_x is the diameter reached by the drug, $D_{Phe/UTP}$ is the diameter value of the previous vasoconstriction state and $D_{Nifedipine}$ is the maximal vessel diameter.

The analysis of pressure myography data and the fitting of concentration-response curves of the drugs were performed using Origin® 7 Software.

6. VSMC isolation

Mesenteric arteries were subjected to a two sequential enzymatic incubations at 37°C to obtain freshly isolated VSMCs, according with previously described protocols (Moreno-Domínguez *et al.*, 2009; Tajada *et al.*, 2012). After a first incubation in a 37°C preheated SMDS-Ca^{2+} free solution containing 0.8 mg·ml^{-1} papain, 1 mg·ml^{-1} BSA and 1 mg·ml^{-1} dithiothreitol (Table M5, solution A) during 15 min, arteries were transferred to a 37°C preheated SMDS-10 µM Ca^{2+} solution supplemented with 0.6 mg·ml^{-1} collagenase F and 1 mg·ml^{-1} BSA (Table M5, solution B) during 6 min. Then, arteries were washed three times with ice cold SMDS-10 µM Ca^{2+} solution and were mechanically dissociated using a wide-bore glass pipette to obtain freshly isolated VSM cells. Single cells were maintained at 4°C and used within the same day for either protein expression assays or electrophysiological recordings.

Composition	A solution (mg ml^{-1} SMDS)	B solution (mg ml^{-1} SMDS-10µM Ca^{2+})
BSA	1	1
DTT	1	-
Papain	0.8	-
Collagenase F	-	0.6
pH	7.4	
time	15’	6’

Table M5. *A and B SMDS solutions to VSMCs dissociation.*

7. Protein expression

The study of the protein expression profile of molecular components of the VSMCs contributes to elucidate their role in the vascular vessels properties and functions. Based on the specific strong association antibody-epitope, different antibodies have been used alone or in combination to investigate the protein expression, localization and association of several molecular components of VSMCs. The primary and secondary antibodies used are listed in Table M6.

Protein expression studies have been carried out both in native VSMCs and in heterologous expression systems (CHO: Chinese Hamster Ovary cell line). Several techniques have been used, including immunocytochemistry (ICC), co-immunoprecipitation (coIP), Proximity Ligation Assay (PLA) and Ground State Depletion Superresolution (GSD).

	Antibody	Source	Reference	Applications
primary	anti-TRPC3	goat	ACC-016 (Alomone Labs)	ICC, coIP, PLA, GSD
	anti-TRPC3	rabbit	NBP1-70352 (Novus Biologicals)	PLA, GSD
	anti-TRPC6	Goat	NBP1-00142 (Novus Biologicals)	PLA, GSD
	anti-TRPC6	rabbit	ACC-017 (Alomone Labs)	ICC, coIP, PLA, GSD
	anti-P2Y6	rabbit	APR-011 (Alomone Labs)	PLA, GSD
	anti-ANO1 (S-20)	goat	sc-69343 (Santa Cruz Biotechnology)	GSD
secondary	Alexa 594 anti-rabbit	goat	A-11012 Molecular Probes	ICC
	Alexa 488 anti-goat	donkey	A-11055 Molecular Probes	ICC
	Alexa 568 anti-rabbit	goat	Molecular Probes	GSD
	Alexa 647 anti-goat	donkey	Molecular Probes	GSD
	Peroxidase-conjugated anti-rabbit	goat	Dako	coIP
nuclei	Hoechst		33342 (Life Technology)	ICC,

Table M6. *Primary and secondary antibodies used. ICC: Immunocytochemistry; PLA: Proximity Ligation Assay; Co-IP: Co-Immunoprecipitation; GSD: Ground State Depletion.*

7.1. Immunocytochemistry

The immunocytochemistry technique allows detecting protein expression pattern. In addition, nuclear staining with Hoechst facilitates interpretation of the image results. Using primary monoclonal or polyclonal antibodies that specifically recognize their epitopes and fluorescence-coupled secondary antibodies

recognizing the first ones, the signal can be amplified and easily detected. We used the following primary and secondary antibodies and the nuclei staining at the indicated concentrations: rabbit anti-TRPC3 (4.5 $\mu g \cdot ml^{-1}$), rabbit anti-TRPC6 (4.5 $\mu g \cdot ml^{-1}$), rabbit anti-P2Y6 (4.5 $\mu g \cdot ml^{-1}$), goat Alexa 594 anti-rabbit (1:1000) and Hoechst 33342 (1:2000).

7.1.1. Immunocytochemistry procedure

For the staining of CHO cells overexpressing some of the proteins of interest, transfected CHO cells plated on 12 mm diameter poly-lysine coated coverslips were fixed with freshly made 4% paraformaldehyde in PBS for 15-20 min. After washing three times with PBS 1X, cells were permeabilized in PBTx (0.1% Triton X-100 in PBS) for 20 min and blocked with 1% BSA in PBTx during 10 min. Then, cells were incubated with the primary antibodies for 1-2 hour in a humidified chamber, washed three times with blocking solution and incubated with the secondary antibodies for 30-60 min protected from light, both incubations in blocking solution. After three washes with PBS and one with ddH_2O, the nuclei were labelled with Hoechst 33342 and coverslips were mounted using Vectashield (Vector Laboratories, Inc., Burlingame, CA, USA).

For native VSM cells, several modifications of the above protocol were introduced: 1) Fresh isolated VSMCs were plated on 12 mm poly-lysine coverslips during 1 hour before starting. 2) After fixing the cells as described, samples were incubated in 100 mM Glycine solution for 15 min before washing and permeabilization. 3) The blocking step was performed with PLA Blocking Solution (Duolink® In Situ Kit, Sigma-Aldrich) at 37°C for 1 hour. 4) Primary antibodies were diluted in 0.01% Odissey® Blocking Buffer in PBS and incubation was carried out overnight at 4°C.

Samples were maintained at 4°C protected from light until visualization at the appropriate wavelengths using confocal microscopy.

7.2. Co-immunoprecipitation (coIP)

Co-immunoprecipitation (coIP) is an extension of the classical immunoprecipitation (IP) technique that allows detecting protein-protein interactions. Based on the strong protein-antibody interaction, natural protein associations or overexpressed complex can be jointly precipitated and analyzed with immunoblot. With proteins carrying an epitope tag that can be easily detected with commercially available antibodies or beds, coIP technique allows to easily purify the tag protein as well as other macromolecules bound to the target. Therefore, IP is focused on the primary target or antigen and coIP is focused on secondary targets or interacting proteins.

In this study, coIP assays were performed using agarose GFP-Trap_A beads (Chromotek, Planegg-Martinsried, Germany) that recognized the YFP of the hTRPC3-YFP fusion protein (see CHO cell line section). For the immunoblotting assays, the primary antibodies used were rabbit anti-TRPC3 (4.5 $\mu g \cdot ml^{-1}$) or rabbit anti-TRPC6 (4.5 $\mu g \cdot ml^{-1}$), and the secondary antibody used was horseradish peroxidase-conjugated anti-rabbit (dilution 1:20000).

7.2.1. CoIP procedure

CoIP assays were performed in CHO cells transfected with hTRPC3-YFP and TRPC6 plasmids, alone or in combination, using agarose GFP-Trap_A beads following the manufacturer's instructions (Chromotek, Planegg-Martinsried, Germany). CHO transfected cells were collected in Modified RIPA Buffer (MRB, Table M7) supplemented with Proteases Inhibitor Cocktail (Roche, Basel, Switzerland) and incubated on ice for 15 min. Then cells were centrifuged at 12000 g, at 4°C for 10 min to obtain the CHO cell lysate. This cell lysate was incubated with gentle shaking at 4°C for 2-3 h with the GFP-Trap_A beads previously equilibrated in MRB. Cell lysate was washed with MRB (3x) and then with high NaCl-MRB buffer (3x) and stored in MRB buffer at -20°C.

Composition	MRB (mM)	MRB-750 mM NaCl (mM)
NaCl	150	750
Tris pH 8	50	50
NP-40	1%	1%
Sodium deoxycholate	0.2%	0.2%
pH	7.5	7.5

Table M7. *CoIP solutions.*

For the immunoblot analysis, the cell lysate was diluted in XT Reducing Agent and XT Sample Buffer (Bio-Rad, Hercules, CA, USA) and incubated at 95°C for 5 min. Then, a SDS-PAGE electrophoresis was carried out on 10% polyacrylamide gels to separate the different co-purified proteins. After that, proteins were transferred onto a nitrocellulose membrane and blocked with 5% non-fat dry milk in TTBS buffer (0.1% Tween 20 in Tris-buffered saline) for 1 h. Membranes were then incubated with primary antibodies at 4°C overnight and then with secondary antibodies for 1 h, both incubations in blocking solution. Finally, protein signals were detected using a VersaDoc 4000 Image System (Bio-Rad) with chemiluminiscence reagents (SuperSignal West Femto Maximum Sensitivity Substrate; Pierce, Rockford, IL, USA) and quantification was carried out by

densitometric analysis of each antibody band normalized to its corresponding β-actin signal using Quantity One software (Bio-Rad).

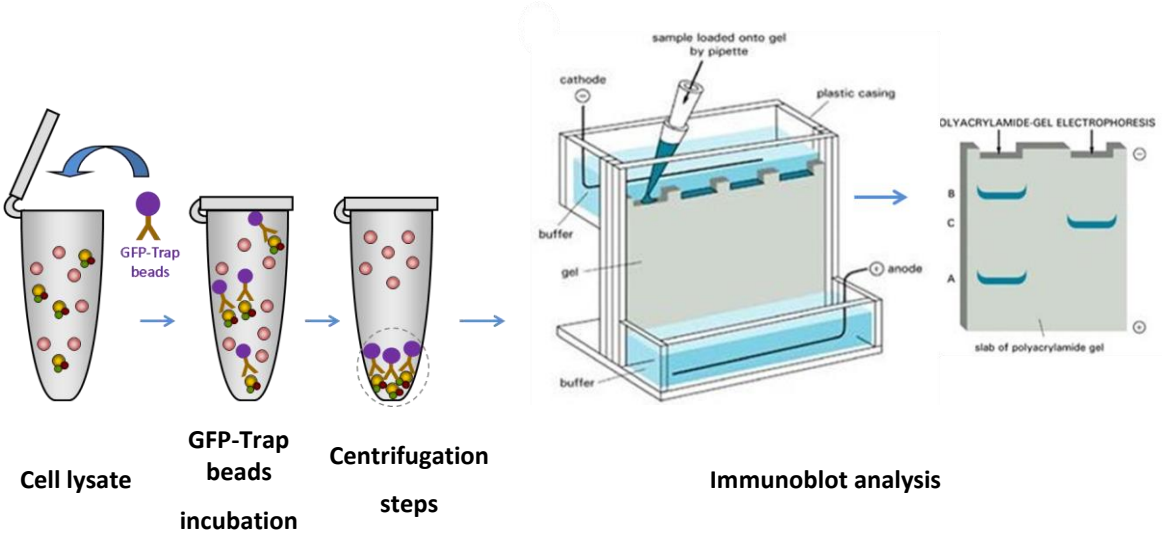

Figure M11. *CoIP working scheme.*

7.3. Proximity Ligation Assay (PLA)

The Proximity Ligation Assay (PLA) is a technique for detection of protein or macromolecules associations. This technique identifies association of the target molecules in the order of zeptomoles ($40 \cdot 10^{-21}$ mol) (Fredriksson *et al.*, 2002). In a more detailed way (Figure M12), samples are fixed, blocked and incubated with two primary antibodies against the targets raised in different species. When adding the secondary antibodies which have complementary PLA probes attached, if they are in close proximity (at least 40 nm), a hybridization using Ligase can be performed. Then, a rolling-circle amplification (RCA) reaction is performed using fluorescence labelled nucleotides and Polymerase. Finally, the signal from each pair of PLA probes can be easily detected as individual spots by fluorescence microscopy.

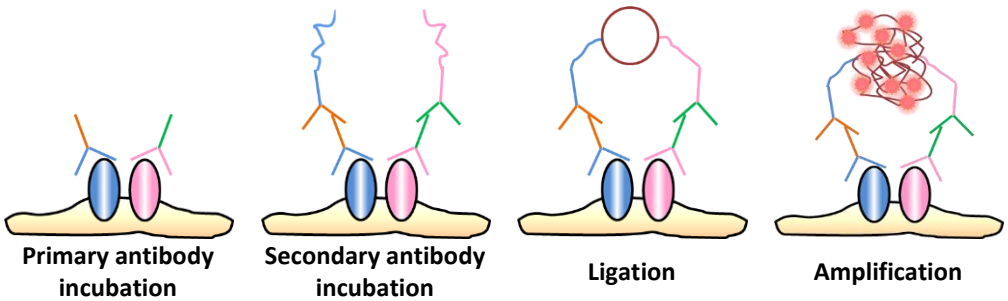

Figure M12. *Working scheme of PLA assay technique.*

PLA is a highly specific technique (Fredriksson *et al.*, 2002) that can be used for detection and quantification of protein interactions. In this study, PLA technique has been used to identify the composition of multimeric channels (defining homo and heteromeric channel associations) as well as interactions between ion channels, receptors and cotransporters in native VSMCs. The primary antibodies and the working concentrations used were: rabbit anti-TRPC3 (4.5 $\mu g \cdot ml^{-1}$, Alomone), goat anti-TRPC3 (dilution 1:200, Novus Biologicals), rabbit anti-TRPC6 (4.5 $\mu g \cdot ml^{-1}$, Alomone), goat anti-TRPC6 (dilution 1:200, Novus Biologicals), rabbit anti-$P2Y_6$ (4 $\mu g \cdot ml^{-1}$, Alomone), goat anti-ANO_1 (dilution 1:200, Santa Cruz).

7.3.1. PLA procedure

Protein associations were explored with PLA technology using Duolink® In Situ Kit (Sigma-Aldrich) following the manufacturer´s instructions. Briefly, freshly isolated VSMCs were settled in 12 mm diameter coverslips, at room temperature for 1 hour. Then VSMCs were fixed with 4% paraformaldehyde for 20 min and then treated with 100 mM Glycine during 15 min. After washing three times with PBS 1X, cells were permeabilized using PBTx (0.1% Triton X-100 in PBS) during 20 min and then blocked with Duolink® In Situ Blocking Solution, at 37°C during 20 min. Afterwards, samples were incubated with two primary antibodies (dilution 1:200 in 0.01% Odissey® Blocking Buffer in PBS) raised in different species, at 4°C overnight. For negative controls, samples were incubated only with one primary antibody. After washing three times with Wash Buffer A, cells were incubated with the Duolink® In Situ PLA Probes (PLUS and MINUS), at 37°C during 1 hour. Then, cells were washed three times with Wash Buffer A, 1U/µl Ligase was added (dilution 1:40) and samples were incubated at 37°C during 30 min. After washing with PBS (3x), amplification was performed using 10U/µl Polymerase (1:80 dilution in Duolink® In Situ Detection Reagents Orange) at 37°C during 100 min. After that, samples were washed twice in wash Buffer B for 10 min and once in 0.01% wash Buffer B for 1 min. Finally, samples were completely dried, mounted using Duolink® In Situ Mounting Medium and kept at 4°C protected from light until visualization using confocal microscopy.

The immunofluorescence image acquisition was performed using a SP5 Confocal Microscope (Leica Microsystems, Wetzlar, Germany) at the appropriate wavelength. For comparisons between different conditions, image acquisition was performed using the same settings for all the conditions studied. ImageJ (Fiji 1.51g) software was used for image analysis.

7.4. Ground State Depletion (GSD) Super-resolution microscopy

7.4.1. GSD Super-resolution fundaments

Ground State Depletion (GSD) microscopy is a super-resolution technique that allows localizing single molecules with high precision and create a high resolution image below the diffraction limit. The principle of single-molecule detection-based super-resolution is based on the different states of energy in which activated fluorophores can be (Figure M13). In conventional fluorescence microscopy, delocalized electrons of fluorophores can be transferred from a ground state (S_0) to an excited state (S_1) and, as they oscillate back into the S_0, they emit fluorescence. In GSD Super-resolution technique, this oscillation cycle is modified by switching the fluorophores to off-states, reducing the amount of simultaneously emitting excitable fluorophores that become spatially and temporally distinct from neighboring fluorophores. Then, the fluorophores in off-states can return back to S_0 and fluoresce again, while other molecules switch to off-states (Fölling *et al.*, 2008; Dixon *et al.*, 2017).

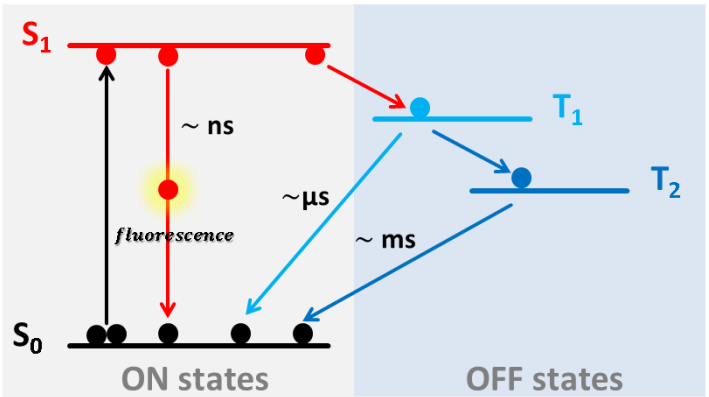

Figure M13. *GSD Super-resolution microscopy based principle.*

The burst of fluorophores can be fitted to a Gaussian curve whose centroid corresponds to the exact position of each fluorophore and, by collecting all the single fluorophore information of several thousands of separated images, a GSD Super-resolution image with sub-diffraction-limit resolution is reconstructed (Figure M14). The quality of the GSD Super-resolution images obtained depends on the numerical aperture (NA) of the lens, the wavelength of light used for excitation and, crucially, the fluorophore properties: number of photons per switched event, the on-off duty cycle, photostability and number of switching cycles. Using fluorophores with high photon yield per switching event and low on-off duty cycle

provides both high localization precision and density. Furthermore, the imaging buffer conditions and properties can modified the switching properties of fluorophores and the quality of the reconstructed image (Dempsey *et al.*, 2011; Dixon *et al.*, 2017).

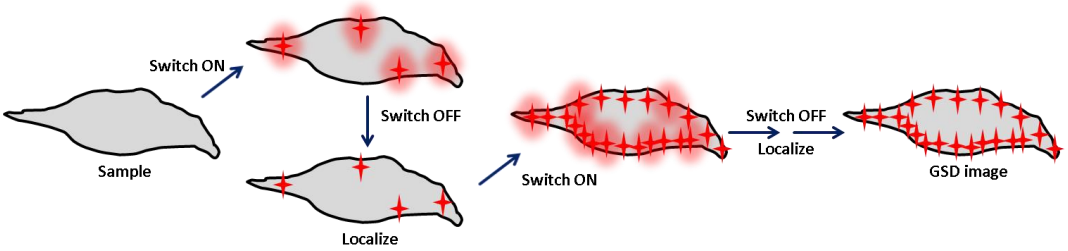

Figure M14. *Scheme of ON-OFF switching cycles and GSD Super-resolution image reconstruction.*

GSD Super-resolution technique was used to explore the exact localization of single molecules, such as purinergic receptors and TRPC channels, on the membrane of VSMCs. In addition, the association and clustering properties of these membrane proteins was also studied. Using immunocytochemistry fundaments with different antibody combinations, it was possible to obtained GSD reconstructed images showing the protein distribution of these receptors and channels with high resolution.

7.4.2. GSD Super-resolution System

The GSD Super-resolution system used in this study consists of several parts: inverted microscope, TIRF/GSD module, high power lasers, external light source and acquisition software (Figure M15).

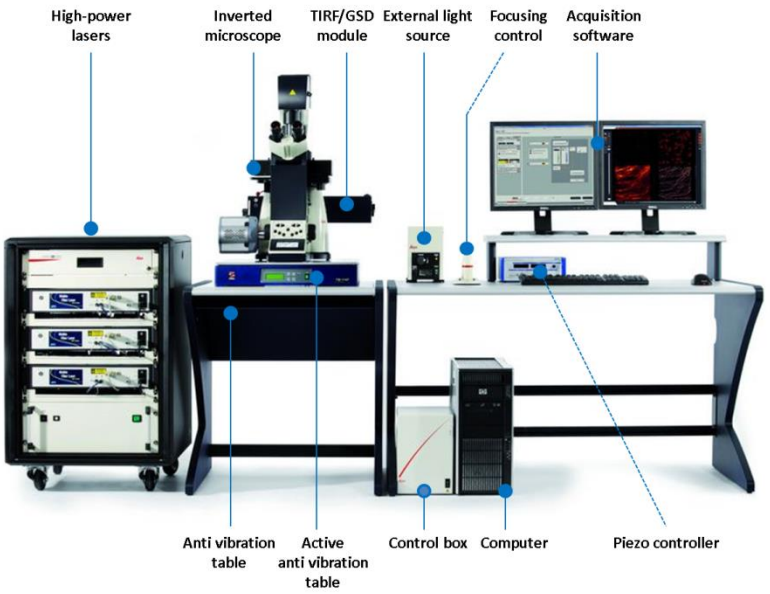

Figure M15. *GSD Super-resolution system.*

a) Inverted microscope

A DMI6000B inverted microscope (Leica Mycrosystems, IL, USA) was used for Super-resolution measurements. Images were acquire using 160x HCX PL APO (NA=1.47) oil-immersion lens and an Andor iXon3 897 EMCCD Camera coupled to the inverted microscope. The inverted microscope with all of the attached components were placed on an anti vibration table.

b) TIRF/GSD module

A DMi8 S TIRF module (Leica Mycrosystems, IL, USA) coupled to the inverted microscope was used to switch from TIRF to GSD conditions. This TIRF/GSD module enables to control the TIRF penetration depth and the illumination angle of the samples, allowing the acquisition of super-resolution images with high power illumination options.

c) Sample SuMo stage

A sample Suppressed Motion (SuMo) 11888439 stage (Leica Mycrosystems, IL, USA) coupled to the inverted microscope was used to minimize possible drifts, ensuring stability during acquisition.

d) High power lasers

The GSD Super-resolution system is equipped with high-power lasers with the following wavelengths: 488 nm, 532 nm and 642 nm. The measured intensities at the focal plane of each one are 1.4 $kW \cdot cm^{-2}$, 2.1 $kW \cdot cm^{-2}$ and 2.1 $kW \cdot cm^{-2}$, respectively. In addition, the system comprises a 405 nm laser to control the single molecule switching behaviour (backpumping).

e) External light source

An external EL6000 light source (Leica Mycrosystems, IL, USA) connected to the inverted microscope via a liquid light guide was used to enhance fluorescence imaging. By using an alignment-free, mercury metal halide bulb, it keeps heat away from the sample and the microscope.

f) Acquisition software

For the image acquisition, LAS X (Leica Mycrosystems, IL, USA) software was used. This software allows controlling the focus in all the XYZ directions, switching between TIRF and GSD imaging modes, and stablishing the setting conditions for acquiring images. In addition, it allows analyzing the high resolution reconstructed images.

7.4.3. GSD Super-resolution procedure

GSD Super-resolution requires labelling the proteins of interest with fluorophores, which can be done with the conventional immunocytochemistry technique. Using commercial primary and secondary antibodies, specific mounting media and GSD Super-resolution software, the on-off duty cycles of fluorophores can be easily controlled to obtain a single molecule reconstructed GSD image.

a) GSD Super-resolution immunostaining protocol

Freshly isolated VSMCs were settled on 25x25 mm square coverslips at room temperature during 1 h and then cells were fixed with PFA-GA (3% paraformaldehyde-0.1% glutaraldehyde in PBS) at room temperature for 10 min. After washing three times with PBS, cells were reduced with 0.1% $NaBH_4$ in ddH_2O at room temperature during 5 min. Then, cells were blocked with SBTx blocking solution (20% Sea Block-0.25% Triton-X 100 in PBS) for 1 h at room temperature. After removing SBTx solution, samples were incubated with 10 $\mu g \cdot mL^{-1}$ of the primary antibodies: rabbit anti-$P2Y_6$, goat anti-TRPC3, rabbit anti-TRPC3 and rabbit anti-TRPC6, in SBTx solution, at 4°C overnight. After washing three times, cells were

incubated with 2 µg·mL^{-1} of the secondary antibodies Alexa 647 donkey anti-goat and Alexa 568 goat-anti rabbit, at room temperature for 1 h protected from light. Then, samples were washed three times with PBS and postfixed using 0.25% GA in PBS at room temperature during 10 min. Finally, samples were washed three times with PBS and kept at 4°C in 3 mM azide and protected from light until image acquisition.

b) GSD Super-resolution sample mounting

In GSD Super-resolution, fluorophores are required to be fluorescent only a fraction of time to be individually localized. For this purpose, the imaging buffer contains two components: β-Mercaptoethylamine (MEA, Cysteamine, Sigma Aldrich), to induce photoswitching of the fluorophore, and an oxygen-scavenging system (Glucose-oxidase+Catalase), to reduce the effects of photobleaching. The previously described (Dempsey *et al.*, 2011) imaging buffer used in this study was prepared as following (Table M8):

Composition	**MEA (mM)**	**Diluting buffer B (mM)**	**GLOX (mM)**	**Imaging buffer 10 mM (mM)**	
MEA	100			**GLOX**	
Glucose		10% w/v		Glucose oxidase	0.56 mg mL^{-1}
NaCl		10		Catalase	0.34 µg mL^{-1}
Tris 1M pH 8		50	10	**MEA**	10
Glucose oxidase			56 mg mL^{-1}	**Buffer B**	Vf
Catalase			3.4 mg mL^{-1}		
pH	8 (HCl)				

Table M8. *Imaging buffer components for GSD Super-resolution microscopy. Left, separately stored aliquots of the components of the imaging buffer. Right, imaging buffer, freshly prepared.*

100 mM-MEA aliquots of 1mL were stored frozen at -20°C, and centrifuged-(14000 rpm, 3 min) GLOX (Glucose-oxidase+Catalase) aliquots were kept at 4°C, both used within 1-2 weeks. The imaging buffer has to be freshly prepared and used within 1-2 h due to the acidification caused by the enzymatic reactions, preventing changes in the photophysics properties of the fluorophores.

To mount the samples, slides of 76x26x1.5 mm with a depression of 15-18 mm diameter and 0.6-0.8 mm depth (neoLab®, Germany) were used. Firstly, imaging buffer was placed on the depression and then coverslips with cells were carefully mounted, avoiding formation of air bubbles. Finally, coverslip was fixed using the yellow and blue components of silicone-glue Twinsil® (Picodent, Wipperfürth,

Germany), previously mixed in a 1:1 volume quantity. After 5-10 min, the glue was hardened and samples were mounted on the inverted microscope.

c) GSD Super-resolution acquisition protocol

For the GSD Super-resolution acquiring, images were acquired firstly with 642 laser and then with 532 laser, using a penetration depth of 130 nm and a TIRF angle of 66.32°. For VSMCs cells, the threshold value to eliminate background, nonspecific signals, was stablished in 85 events·pixel^{-1} and the minimum number of events per image were fixed at 8. A minimum of 30000 images per laser were acquired to obtain the GSD reconstructed image.

7.4.4. GSD Super-resolution analysis

Three different analyses were performed from the GSD reconstructed images: shortest intermolecular distance analysis and cluster size and density analysis.

a) Shortest intermolecular distance analysis

An object-based analysis to measure the shortest distance between purinergic receptors and TRPC channels was performed using the JACoP plug-in of the ImageJ software (National Institute of Health, NIH). This previously described analysis is based on image segmentation by connexity analysis (Henis *et al.*, 2003; Bolte and Cordelieres, 2006; Mercado *et al.*, 2014). Briefly, all the adjacent pixels of a reference pixel with intensity above a set threshold limit are considered to be part of the same structure as the reference pixel. After segmentation, these individual particles are represented by centroids, defined as the geometrical centre of each particle including its global shape. With JACoP plugin, the shortest distances between centroids are analyzed for each laser-activated GSD reconstructed image. Analyzing the data using frequency histograms fitted to a Gaussian curve of two or three components, these measurements allowed stablishing colocalization between particles.

b) Cluster size and density analysis

Cluster size (in µm^2) and density (in particles·µm^2) analysis were performed using the ImageJ software for each individual laser-activated GSD reconstructed image.

8. CHO cell line culture and maintenance

Chinese Hamster Ovary (CHO) cell line was used as an in vitro model to explore the role of different transfected ion channels present in native cells. This epithelial-like cell line was initiated in 1957 (Gamper, Stockand and Shapiro, 2005) and several subclones have been developed since then. Their easy culture and maintenance, high transfection efficiency and very low expression of endogenous ion channels make CHO cells specially valuable for electrophysiological studies.

CHO cells were maintained in Dulbecco´s modified Eagle´s medium supplemented with 10% fetal bovine serum, penicillin-streptomycin (100 $U \cdot ml^{-1}$ each) and 2 mM L-glutamine at 37°C in a 5% CO_2 humidified atmosphere. CHO cells were grown as a monolayer in poly-lysine-coated coverslips prior to transiently transfection using TransIT-X2® System (Mirrus, Madison, WI, USA) following the manufacturer´s instructions. Cells were trasnfected with: 1 µg of DNA of hTRPC3-YFP (yellow fluorescent fusion protein) kindly provided by Dr Klauss Groschner, (University of Graz, Austria), 1 µg of a bicistronic plasmid expressing ratTRPC6 and green fluorescent protein (GFP) as separate proteins (a gift from DR Jason Yuan, University of Arizona, USA), or 0.5 µg of each. Cells were used within 24-72 h postransfection for immunocytochemistry, coIP and electrophysiological studies.

9. Electrophysiology: patch-clamp technique

9.1. Patch-clamp fundamentals

Patch-clamp is a technique used to study ionic currents in individual isolated living cells. An electrical potential difference (V_m) across the cell membrane is generated by the selective ion permeability of the membrane, and it is maintained by the Na^+-K^+ pump. The ion channels and transporters of the lipid membrane behave as conductors (G_m), meaning that they represent the pathways for ionic current (I) to flow. These three parameters (Vm, I and Gm) are related by the Ohm´s law:

$$\Delta V_m = IR_m = \frac{I}{G_m}$$

In resting conditions, the ΔV_m between the inner and outer sides of lipid membrane depends on the concentrations of ions to which the membrane is permeable and on their permeabilities (p_{ion}). In most mammalian cells, K^+, Na^+ and Cl^- make the largest contribution to the resting membrane potential (V_m), described as the steady-state condition with no net flow of electrical current across the membrane. Therefore, V_m follows the Goldman-Hodgkin-Katz (GHK) equation:

$$V_m = \frac{RT}{F} \ln \left(\frac{p_K[K^+]_o + p_{Na}[Na^+]_o + p_{Cl}[Cl^-]_i}{p_K[K^+]_i + p_{Na}[Na^+]_i + p_{Cl}[Cl^-]_o} \right)$$

For performing the patch-clamp recordings, a micropipette (a glass tube filled with an electrolyte solution and containing an AgCl recording electrode connected to an amplifier) is brought into contact with the cytosol of an isolated cell. Another electrode (reference or bath electrode) is placed in a bath surrounding the cell. An electrical circuit can be formed between the recording and reference electrode with the cell of interest in between, and changes in ion flows across the cell membrane can be measured.

9.2. Patch-clamp set-up

a) Perfusion chamber

The perfusion chamber consists of a polycarbonate chamber (RC-24E, Warner Instruments, Hamden, CT, USA) attached to an aluminum platform (P1, Warner Instruments) and a glass coverslip perfectly sealed to the bottom of the chamber. The small volume (~200 µL) of the chamber is controlled by an inlet and an outlet connected to a perfusion system, allowing quick solution changes. Cells are placed on the bottom of the chamber either directly or previously attached to glass coverslips.

b) Perfusion system

The perfusion system consists of six reservoirs controlled by electrovalves. Solutions from reservoirs perfuse by gravity at a rate of 1-2 ml·min^{-1} through silicone tubes and converge in one tube to reach the perfusion chamber. The outlet tube connected between the chamber and the vacuum pump system facilitates the quick solution changes of the chamber.

c) Inverted microscope

IX70 (Olympus, Tokyo, Japan) and Eclipse TE300 (Nikon, Tokyo, Japan) inverted microscopes were used for patch-clamp experiments. pE-100 Light Source systems (CoolLED, UK) attached to each microscope were used when patching transfected CHO cells. Both microscopes were also adapted with a support for the electrode holder (2.0 mm 64-840 QSW, Warner Instruments), the perfusion chamber and the macro and micromanipulation system. The macro manipulator system is attached to the holder through the amplifier headstage (AU CV201, Axon Instruments).

d) Micro and macromanipulators

The macro (PSC-500 Series, Burleigh, Newton, NJ, USA) and micromanipulators (423 Series, Newport, Irvine, CA, USA) used for electrophysiological studies allows finely controlling the distance between the micropipette and the cell. The macro manipulator allows localizing the micropipette and moving it closer to the cell and the micromanipulator permits stablishing contact between the pipette tip and the cell membrane. Adjustments in the three XYZ spatial axes can be performed.

e) Vibration isolation table

The vibration isolation table (63-544 microg, TMC, Peabody, MA, USA) works based on air cushions placed on the table legs that support a heavy table top. This table top is kept afloat using a gas source from a nitrogen tank. The inverted microscope is placed on the table top, isolating it from external vibrations. The vibration isolation table is essential for stable recordings to avoid crushing the pipette to the bottom of the chamber or detaching the pipette from the cell. Moreover, the microscope, the perfusion system and the macro and micromanipulators are placed inside a Faraday cage to isolate from external electric fields.

f) Amplifiers

The Axopatch-200 and the Multiclamp 700A (Axon Instruments, Inc., Foster City, CA, USA) amplifiers used in this study allow amplifying the signal and also to control several recording settings: current/voltage clamp switching, offset control, capacitance and series resistance compensations, holding potential settings, gain and other useful controls.

g) Digitizers

Digidata 1322A and 1440A (Axon Instruments) were the devices used to convert de analogical recorded data (AD) to digital data (DA) and vice versa. In addition, these interfaces enable the communication between the cell signals, the amplifier and the computer software, by using AxoScope software. Analogical signals generated by cells are converted to digital format by the analog-digital converter of digitizers. Similarly, digital signals and protocols generated by the computer are converted to analogic by the digital-analog converter of Digidata.

h) Patch-clamp software

pClamp 10.2® software (Axon Instruments) was used to communicate the AD/DA conversion interface to the computer and to perform the patch-clamp data

analysis. This software comprises several subroutines, and we used mainly two of them: Clampex® subroutine, to design stimulation protocols and acquire the data, and Clampfit® subroutine to analyze the recorded data.

9.3. Micropipette manufacturing system

Borosilicate glass capillaries with outer and inner diameters of 2.00 and 1.12 mm, respectively, and an inner filament (1B200F-4, World Precision Instruments, Inc., UK) were used as for making micropipette electrodes. The inner filament helps with the filling of the pipette by increasing capillary properties and avoiding bubble formation. Two micropipettes were obtained from each capillary by pulling them, and after that, the tips were fire-polished to obtain a smooth surface and increase their resistance.

PP-83 vertical puller (Narishige, Tokyo, Japan) and P-97 automatic puller (Sutter Instruments, Novato, CA, USA) were used to stretch borosilicate glass capillaries. The vertical puller heats the capillaries using a heating coiled resistance and stretches them in two successive steps. With the automatic puller, the capillaries are clamped at both ends and a resistance placed between the clamps heats and stretches the capillaries following a previously fixed cycle protocol. This protocol consists of several heating and successive stretching cycles by setting several parameters, such as pulling, velocity, resistance cooling time and air flow pressure. By controlling these parameters, electrodes can be obtained with a greater reproducibility.

9.4. Patch-clamp procedure

Electrophysiological recordings were carried out in CHO transfected cells and in native VSMCs from mesenteric arteries. Freshly isolated VSMCs were placed in the perfusion chamber and allowed to adhere to the chamber bottom at room temperature for 15 min. For CHO cells, the coverslip of transfected cells was directly placed in the chamber. Then, the perfusion system, previously purged with the bath solutions, was connected to the inlet of the chamber and the vacuum was activated. The glass micropipette filled with internal solution (Tables M11 and M12) was attached to the AgCl electrode and fixed to the pipette holder. Using the macromanipulator, the micropipette electrode was placed above the selected cell and, with the micromanipulator, got in contact with the cell to make a high resistance (GΩ) seal. We monitored the resistance of the pipette using the subroutine Seal Test of the software Clampex®, which continuously records the current in response to a pulse of -10 mV (Figure M17). After gigaseal formation, the holding potential was made negative, close to resting membrane potential of cells

(-40 mV for VSMCs and -60 mV for CHO cells). At this point we are in the cell-attached configuration of the patch-clamp technique. Patch-clamp technique can be used in several different configurations (Figure M16). In this work we use the whole-cell configuration for voltage-clamp measurements and the perforated-patch configuration for current-clamp studies.

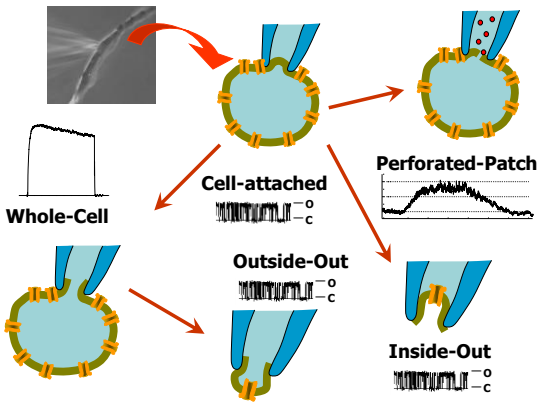

Figure M16. *Different configurations of the patch-clamp technique.*

With the voltage-clamp, we control the membrane potential with an electronic feedback system that measures the cell membrane potential and compares it with the potential established in the experimental protocol. Differences between both potentials are immediately corrected with an injection of current, that mirrors (with opposite direction) the ionic current that we are registering. To reach the whole-cell configuration we start from the point in which we got the gigaseal formation (cell-attached configuration). After this, a negative pressure is applied to the tube connected to the micropipette electrode, disrupting the seal and allowing the access to intracellular solution. This can be detected by the large capacitative transient that appears when the gigaseal is broken (Figure M17). The amplitude and the time course of these peaks were used to estimate the series resistance or access resistance (Ra) and membrane capacitance (Cm) of the cells. A good recording typically has a stable seal over 1 GΩ, Ra of less than 20 MΩ (and usually much smaller, below 10 MΩ) and constant cell capacitance and resistance during all recording. In this configuration we achieve electrical continuity between the recording electrode and the inside of the cell. Since the cell volume is negligible compared to the volume of the internal solution in our pipette, we considered the composition of the medium in the intracellular side of the membrane identical to that of our internal solution.

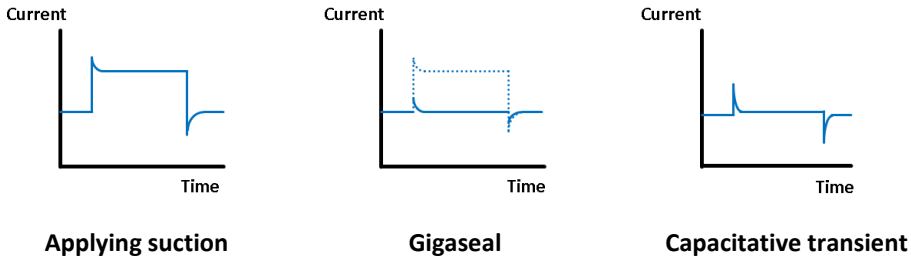

Figure M17. *Current response vs time when forming the GΩ seal and accessing the patched cell.*

9.5. Patch-clamp protocols

The patch-clamp protocols are different depending on whether we use voltage-clamp measurements (fixing the membrane potential to study ionic currents) or current-clamp (fixing the currents to study membrane potential variations).

9.5.1. Voltage-clamp measurements

To study changes in currents across the membrane, voltage-clamp (V_{clamp}) technique was used in whole-cell configuration, as previously described. As mentioned above, using whole-cell configuration, the pipette solution directly contacts cytoplasm and replaces it, so it is important to use pipette solutions similar to intracellular one with the appropriate modifications to study the ion conductance of interest.

The voltage-protocols used with V_{clamp} technique consisted mainly on voltage-ramps (Figure M18). 1s depolarizing ramps from -150 mV to +80 mV from a holding potential of -10 mV were applied every 10 s under control conditions or in the presence of agonists or blockers. When this protocol was used with intracellularly applied antibodies, the access resistance (Ra) and the membrane capacitance (Cm) were continuously monitored and recorded by applying the membrane test algorithms of Clampex 10 software throughout the experiment. Only cells with GΩ seal and stable Ra and Cm values were considered for analysis. Data were acquired at a frequency of 5 kHz and filtered at 2 kHz.

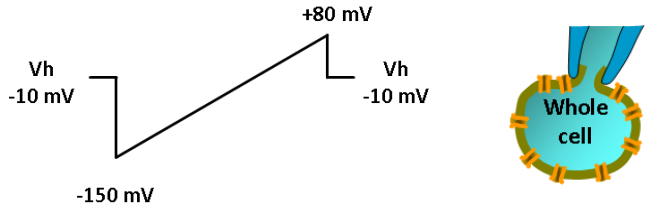

Figure M18. *Ramps protocol used for V_{clamp} measurements in whole-cell configuration.*

9.5.2. Current-clamp measurements

To study changes in the membrane potential induced by agonists and blockers, current-clamp (I_{clamp}) technique was used in perforated-patch configuration. With I_{clamp} technique, if we do not inject current (I=0) we record the resting membrane potential. Unlike in the voltage clamp mode, where the membrane potential is held at a level determined by the experimenter, in current-clamp mode the membrane potential is free to vary, and the amplifier records the voltage the cell generates either spontaneously or as a result of stimulation.

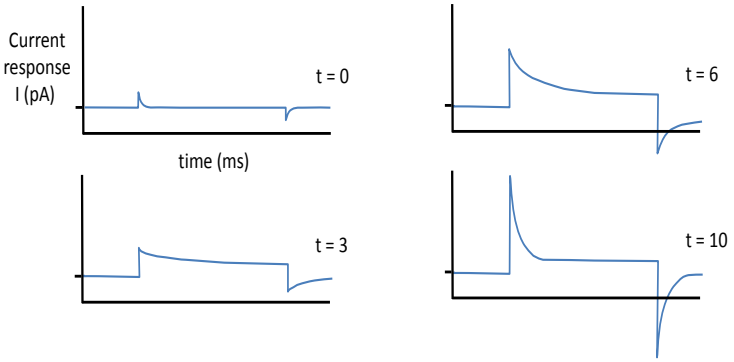

Figure M19. *Stablishment of perforated-patch configuration. The gigaseal is formed at t=0 min. The patch initially appears to become leaky and then the capacitative transients are developed* (modified from Molleman, 2003).

Using amphotericin B, small holes permeable to monovalent ions (but not larger molecules and second messengers) are formed on the cell membrane, allowing the contact between both sides of membrane while preserving the intracellular milieu. Thus, when the GΩ seal is stablished, the presence of amphotericin B (300 $\mu g \cdot mL^{-1}$) in the pipette solution leads to the perforated-patch configuration within minutes, and this can be monitored by the slow increase of the capacitative transients together with the decrease of the Ra through the pipette (Figure M19). Recording of membrane potential changes in response to different agonists and blockers was initiated when the Ra values fall below 20 MΩ. At this point, the amplifier can be switched to current-clamp mode (I=0) to record membrane potential. The high Ca^{2+} content of the pipette solution ensures the correct performance of the perforated-patch technique, as accidental rupture of the patch (changing to whole-cell configuration) leads to a sudden Ca^{2+} load and cell death. These recordings were carried out in a gap-free acquisition mode.

9.6. Patch-clamp solutions

The bath and pipette solutions used to study the contribution of purinergic receptors, TRPC channels and chloride channels currents in VSMCs and CHO cells are described in the following sections.

a) Solutions for TRPC current recordings

External solution. The TRPC external solution was designed to explore unspecific cationic currents in VSMCs and includes nicardipine to block VOCCs channels, $CsCl_2$ to block K_v currents and DIDS and Niflumic acid to block Ca^{2+}-activated Cl^- currents. For CHO cells, standard solution 1X was used (Table M9).

Internal solution. The TRPC internal solution was designed to let 100 nM of free Ca^{2+} and includes $CsCl_2$ to block K_v currents. This solution was prepared adding all components but Mg-ATP and setting a pH of 7.0. Next, keeping the solution at 4°C on ice, ATP was added and pH was brought to 7.2 using KOH. Aliquots of 1 mL were stored at -80°C. Internal solution was filtered before use and always kept on ice. When intracellularly antibodies were needed, the antibody (4.5 $\mu g \cdot mL^{-1}$) was added to the filtered internal solution (Table M10).

Composition	TRPC external solution (mM)	STD 1X solution (mM)
NaCl	141	141
$CaCl_2$	1.8	1.8
$MgCl_2 \cdot 6H_2O$	1.2	1.2
KCl		4.7
$CsCl_2$	5	
Glucose	10	10
Hepes	10	10
Nicardipine	5 µM	
DIDS	100 µM	
Niflumic acid	100 µM	
pH	7.4 (NaOH)	

Table M90. *Bath solutions for TRPC recordings.*

Composition	TRP internal Solution (mM)	Perforated-patch internal solution (mM)
$CsCl_2$	10	
Cs-Aspartate	110	
NaCl	10	
$CaCl_2$	3.2	8
Mg-ATP	2	
KCl		10
K-Glutamate		95
Hepes	10	10
BAPTA	10	
Amphotericin B		300 µg mL^{-1}
pH	7.2 (CsOH)	7.2 (KOH)

Table M10. *Intracellular solutions for TRPC recordings.*

b) Solutions for Ca^{2+}-activated Cl^- current (I_{ClCa}) recordings

External solution. The I_{ClCa} external solution was designed to explore the Ca^{2+}-activated Cl^- currents in VSMCs. This solution includes $CsCl_2$ and tetraethylammonium chloride (TEA) to block K^+ currents and nicardipine to block VOCCs channels (Table M11).

Internal solution. The I_{ClCa} internal solution was designed to let 500 nM of free Ca^{2+} and includes $CsCl_2$, Cs-Aspartate and TEA to block K^+ currents. ATP was added to ice-cold solutions and then pH was adjusted. Aliquots of 1 mL were stored frozen at -80°C and filtered before filling the pipette electrode (Table M11).

c) Solutions for perforated-patch recordings

For I_{clamp} measurements, we used the standard solution 1X in the bath (Table M9) and the perforated-patch internal solution (Table M10) in the pipette. This internal solution could be stored at 4°C as it does not contain ATP. When filling the pipette electrode, the pipette tip was first dipped in filtered perforated-patch internal solution (without amphotericin B) and then backfilled with the same solution containing amphotericin B. Amphotericin-B solutions were prepared freshly every 2 hours by adding 4 µl of a stock 50 µg/µl of Amphotericin B in DMSO to 500 µl of filtered internal solution. The solution was then sonicated to allow amphotericin to come into solution and kept at room temperature protected from light.

Composition	I_{ClCa} external Solution (mM)	I_{ClCa} internal Solution (mM)
NaCl	131	
$CaCl_2$	1.8	7.22
$MgCl_2 \cdot 6H_2O$	1.2	
$CsCl_2$	5	10
Cs-Aspartate		110
TEA Cl	10	10
Mg-ATP		2
Glucose	10	
Hepes	10	10
EGTA		10
Nicardipine	5 µM	
pH	7.4 (NaOH)	7.2 (CsOH)

Table M11. *Electrophysiological solutions for Ca^{2+}-activated Cl^- channels.*

9.7. Data processing and analysis

Electrophysiological data acquisition and part of the analysis were performed with the Clampfit subroutine of the pCLAMP software (Axon Instruments) and with Origin 7.5 software (OriginLab Corp., Northampton, MA, USA).

10. Statistical analysis

Statistical analysis was performed using R software (R Foundation for Statistical Computing, Austria). Data are expressed as mean values ± standard error of the mean (SEM) from several different experiments.

For pressure measurements, pressure myography, electrophysiology and PLA data, statistical comparisons were performed using the Student´s two-tailed t-test for paired or unpaired data or ANOVA with Bonferroni tests, depending on experimental design. For quantitative PCR data, Student´s t-test was performed in the case of normal distribution (i.e. a Saphyro-Wilks test with $p>0.05$), whilst a pairwise Mann-Whitney-Wilcoxon test (i.e. a non-parametric test) was applied to determine whether the differences between groups of pooled data were statistically significant. All through the Results section, values of $p<0.05$ are represented with one asterisk, while values of $p<0.01$ and $p<0.001$ were represented with two and three asterisks, respectively.

4

Results

1. Essential Hypertension mouse model.

The contribution of purinergic receptors, TRPC and Ca^{2+}-activated chloride (CaCCs) channels to the increased vascular tone in hypertension was explored using the BPN/BPH mice model of essential hypertension.

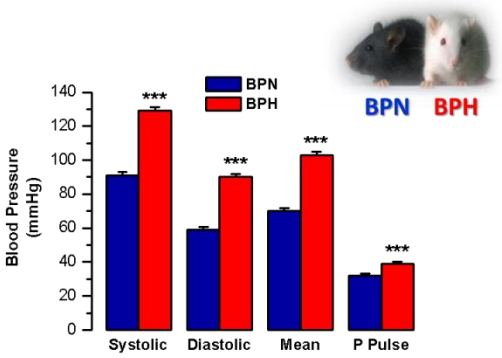

Figure R1. *Systolic, diastolic and mean arterial blood pressures and pulse pressure in BPN and BPH mice. Each bar represents the mean ± SEM, n=24 and n=16 of BPN and BPH mice, respectively. *** P<0.001 compared to BPN.*

BPN and BPH arterial blood pressures were measured by Volume Pressure Recording method using a tail-cuff system. Systolic, diastolic, mean pressures and pulse pressure were obtained from BPN and BPH mice between 10 and 40 weeks of age and were consistently higher (~30 mmHg) in BPH compared to BPN mice (Figure R1). Within the ranges of age studied, no time-dependent changes in blood pressure were observed in either group.

1.2. Characterization of vascular reactivity to sympathomimetic agonists in BPH phenotype.

BPH VSM cells have a more depolarized resting membrane potential when compared with BPN cells. The values obtained in this work, measured in BPN and BPH freshly isolated VSMCs under current-clamp (I=0) perforated-patch configuration were -48.8 ± 1.1 and -40.7 ± 0.7 mV respectively (n=76 cells from 35 BPN, and n=97 cells from 38 BPH) , in good agreement with previous data obtained in our laboratory (Moreno-Domínguez *et al.*, 2009; Tajada *et al.*, 2012).

Mesenteric arteries from BPH mice showed also a higher myogenic tone compared to BPN vessels (Tajada *et al.*, 2012). The role of different ionic channels underlying these differences between BPN and BPH arteries has been thoroughly characterized in our laboratoty (all references from the lab). However, vascular

tone is physiologically regulated by many modulators that activate G_q-coupled receptors, and the possible differences between BPN and BPH mice have not been studied yet. The sympathetic nervous system (SNS) is a main regulator of vessel tone by releasing Noradrenaline (NA) that stimulates VSMCs contraction activating the α_1-adrenergic receptors present in these cells. Nevertheless, activation of these receptors does not entirely mimic the physiological activation of sympathetic neuronal contraction due to the release of other neurotransmitters such as ATP (Hirst and Edwards, 1989; Mulvany and Aalkjaer, 1990; Wier and Morgan, 2004). In order to explore the differences between BPN and BPH responses to NA, the effect of Phenylephrine (PHE), a specific α_1-adrenergic receptor agonist, on vessels tone was investigated by pressure myography using segments of 2nd and 3rd order mesenteric arteries pressurized to 70 mmHg (Figure R2).

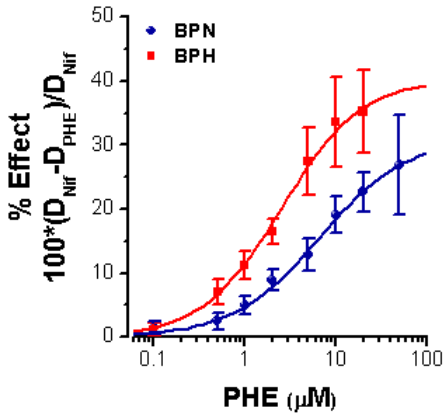

Figure R2. *Vasoconstriction response elicited by PHE. Dose-response curves of PHE were obtained in BPN (blue) and BPH (red) mesenteric arteries. Data represents mean ± SEM, n=5-12 BPN mice and n=3 of BPH mice. **p<0.01 when applying ANOVA and Bonferroni tests.*

Concentration-response curves of the PHE-elicited vasoconstrictor effects were obtained in BPN and BPH mice (Figure R2) and fitted to a Hill function curve as follows:

$$E = E_{max} \cdot \frac{[PHE]^n}{{E_{50}}^n + [PHE]^n}$$

Where, E_{max} represents the maximum vasodilator effect, E_{50} represents the [PHE] that gives the 50% of the maximum effect and n represents the Hill coefficient. BPH

arteries are more reactive to PHE, evidenced by a higher E_{max} (40.3% vs. 31.2%) and a lower E_{50} (2.51 µM vs. 6.64 µM). In both cases, the Hill coefficient (0.99 and 0.90) and the correlation R^2 coefficient (0.99 and 0.99), the last related to the fitting method, were close to 1.

These results demonstrate that BPH arteries exhibit a greater reactivity to an α_1-adrenergic agonist, pointing to differences in the signaling pathway between BPN and BPH mice not explored yet. For that reason, we decided to explore ion channels participating in the α_1-adrenergic signaling pathway-induced contraction which could contribute to the more depolarized Vm and the greater reactivity in BPH cells, such as the transient receptor potential classic ($TRPC_{1-7}$) family of channels.

2. Role of TRPC channels in essential hypertension.

2.1. mRNA expression profile of TRPC channels

In order to study the contribution of the non-specific cationic TRPC channels to the BPH phenotype, their mRNA expression profile was explored by qPCR. Resistance vessels, such as mesenteric arteries, and femoral and aorta tissues from BPN and BPH mice were used. The genes explored included members of the TRPC family ($TRPC_{1-7}$) and several control genes, such as calponin as a control of VSMC, endothelial nitric oxide synthase (eNOS) as a control of endothelial contamination, and ribosomal protein 18S (RP18S) as an endogenous control for the qPCR technique. We explored both the relative abundance (expressed as $2^{-\Delta Ct}$) and the differences in expression observed in BPH mice compared to BPN (expressed as $\log 2^{-\Delta\Delta Ct}$).

All members of the family, with the exception of TRPC5 and TRPC7, were expressed in the three vascular beds, although channel expression was larger in resistance (mesenteric) than conduit (femoral and aorta) arteries (See figure R3 and note the different scale for the femoral an aorta data). While TRPC1 expression was dominant in conduit arteries, expression of TRPC1, 3, 4 and 6 was very similar in mesenteric arteries. When differences in expression between BPN and BPH were studied (Figure R3, right panel), the only channel overexpressed in BPH cells was TRPC3. Differences in expression are represented as $\log 2^{-\Delta\Delta Ct}$, so that 0 values indicate no change in mRNA expression, positive values mean higher expression in BPH and negative values mean the opposite.

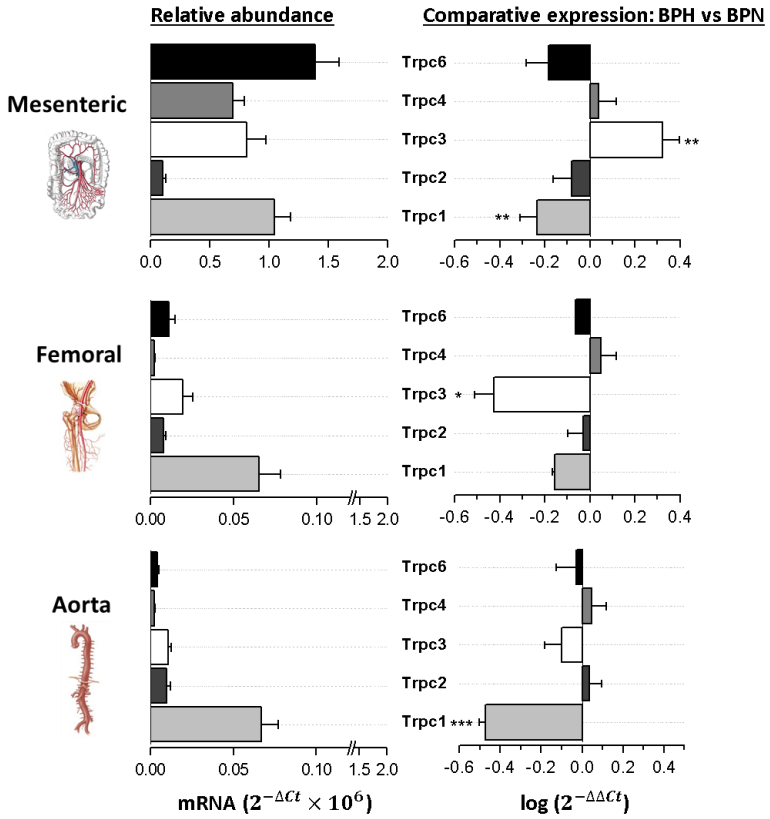

Figure R3. *Changes in the mRNA expression profile of TRPC family of channels in BPN and BPH arteries. Left panels show the relative abundance of TRPC family channels in VSMC of mesenteric, femoral and aorta arteries expressed as* $2^{-\Delta Ct}$*, where* $\Delta Ct = Ct_{channel} - Ct_{18S}$*. Right panels show differences in the TRPC channels expression in BPH arteries using BPN as calibrator calculated as* $2^{-\Delta\Delta Ct}$*, where* $\Delta Ct = \Delta Ct_{BPH} - \Delta Ct_{BPN}$*. Positive values mean increased expression whilst negative values mean decreased expression. Each bar is mean±SEM, n=10. **P<0.01.*

Since TRPC channels expression is higher in resistance vessels (which functionally contribute more to set blood pressure), and TRPC3 is overexpressed in those vessels in BPH mice when compared with BPN, we decided to explore the possible contribution of TRPC3 channels to the hypertensive phenotype in mesenteric arteries. We used a pharmacological approach, testing several pyrazole compounds (Pyr3, Pyr6 and Pyr10) that have been described as putative blockers of the TRPC channels (Kiyonaka *et al.*, 2009; Schleifer *et al.*, 2012), to explore the contribution of TRPC3 channels to vascular tone using pressure myography and electrophysiology. While Pyr3 and Pyr10 have been proposed as selective blockers of DAG-activated TRPC3 channels, Pyr6 seems to exhibit greater potency inhibiting Orai-mediated Ca^{2+} entry (Schleifer *et al.*, 2012).

2.2. TRPC3 contribution to vascular tone.

Endothelium-denuded arteries were pressurized to 70 mmHg and precontracted with PHE (5-10 µM) in order to activate TRPC channels and assess the vasodilatory response elicited by the pyrazole compounds. Pyr applications at different concentrations were performed in the continuous presence of PHE, and at the end of the experiment nifedipine (10 µM) was applied to determine the maximum passive vessel diameter (Figure R4 A).

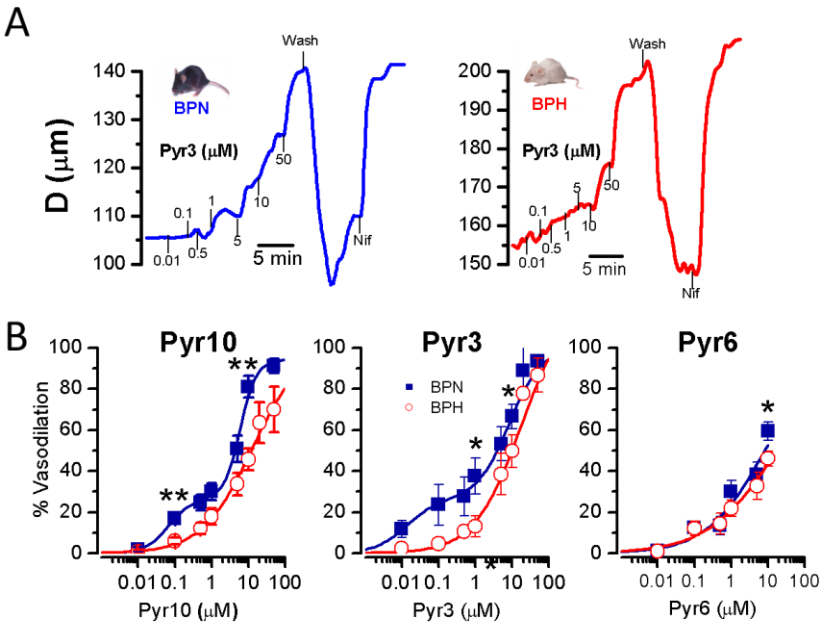

Figure R4. Effects of Pyr compounds on the vascular tone in BPN and BPH mesenteric arteries. A, representative examples of the vasodilator effect of Pyr3 in BPN (left) and BPH (right) mesenteric arteries. Arteries were pressurized to 70 mmHg and precontracted with PHE (5 µM) before Pyr applications at the indicated concentrations (µM). At the end of the experiment, Nif (10 µM) was added to obtain the maximum passive diameter. B, concentration-response vasodilator effect of Pyr10, Pyr3 and Pyr6 in BPN (blue) and BPH (red) PHE-precontracted mesenteric arteries. Data were normalized to the maximal diameter values obtained with Nif and expressed as percentage of relaxation (see Methods). Each point is mean ± SEM, n=5-9 arteries in each group. *p<0.05, **p<0.01

Concentration-response curves were obtained for each Pyr compound in BPN and BPH arteries, and data were fitted to a Hill function (Figure R4 B). Pyr3 and Pyr10 elicited a concentration-dependent vasodilator response which was more effective in BPN mesenteric arteries. In fact, the Hill fitted curves for Pyr3 and Pyr10 in BPN arteries were best fitted with two different components (Table R1), being the high-affinity one responsible for ~30% of the total response. This high-affinity component was not present in BPH. We hypothesized that this component

represents the specific blockade of TRPC3 channels described in the literature, while the low-affinity corresponds to some unspecific effect. In contrast to the effects seen with Pyr3 and Pyr10, Pyr6 vasodilation was less potent and no significant differences between BPN and BPH at lower concentrations were found.

	BPN			BPH	
	Kd_1 (μM)	Kd_2 (μM)	R^2	Kd (μM)	R^2
Pyr3	0.013	8.3	0.99	20	0.99
Pyr10	0.067	5.97	0.99	10	0.99
Pyr6	-	8.16	0.95	20	0.98

Table R1. *Kd values (μM) for each Pyr compound. Kd_1 values refer to the high affinity component of the Hill fitted curve.*

If we assume that the main target of Pyr3 and Pyr10 are TRPC3 channels, the larger vasodilator effects of these drugs at concentrations ≤10 μM in BPN arteries would suggest an increased functional role of TRPC3 channels in these arteries. These results were certainly not anticipated by the mRNA expression studies, although several facts could explain the apparent discrepancy. First, it is possible that mRNA changes in expression do not correlate with changes in protein. Second, the differences in the Pyr3/10 effects could reflect differences not only in the number of channels present in the membrane but also in the subunit composition of the TRPC tetramers. Since TRPC6 and TRPC1 expression was smaller in BPH mesenteric arteries (see figure R3), and it is well known that TRPC3 and TRPC6 form heteromultimers in physiological conditions (Hofmann *et al.*, 2002; Earley and Brayden, 2015), we decided to explore the second possibility using electrophysiological and immunocytochemical approaches, previously validated in heterologous expression system.

2.3. Characterization of the Pyr10 sensitivity of TRPC3 and TRPC6 channels in a heterologous expression system.

The dependence of the effect of Pyr10 on the composition of the TRPC tetramers was explored by characterizing the effect of Pyr10 on the non-selective cationic currents recorded in the CHO cell line overexpressing TRPC3, TRPC6 or both (TRPC3/6). Depolarizing ramps from -150 mV to +80 mV were used in transfected and mock transfected CHO cells in resting conditions and in the presence of Pyr10 (10 μM). In addition, as TRPC3 and TRPC6 mediated currents can be activated by several GPCR as well as by pressure-induced membrane stretch (Gonzales *et al.*, 2014; Wilson and Dryer, 2014), we tested the effect of Pyr10 on currents activated by a hypotonic stimulus (70% STD 1X solution, HS, see Methods).

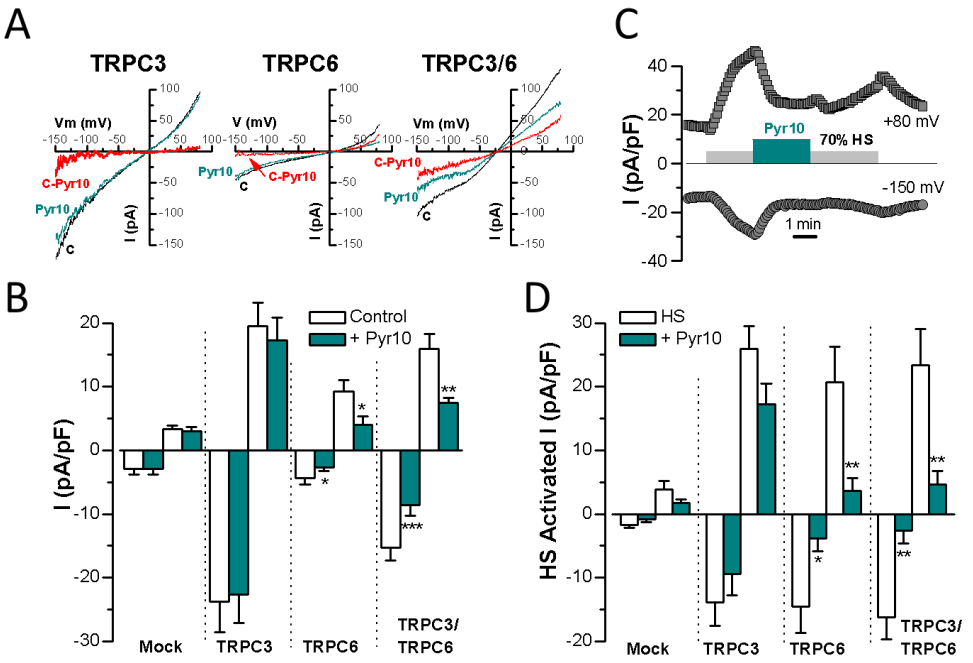

Figure R5. *Functional contribution of TRPC3 and TRPC6 channels to basal and stretch-activated, non-selective cation currents in CHO cells. A, representative traces of currents recorded in unstimulated CHO cells transfected with TRPC3, TRPC6 or TRPC3/6 channels. The effect of the Pyr10 (10 µM) application (Pyr10, green) and the subtracted Pyr10-sensitive current (C-Pyr10, red) are also shown. B, bar plots showing averaged currents amplitudes (pA/pF) measured at -150 mV (lower bars) and +80 mV (upper bars) in each condition and also in mock cells. Data are mean ± SEM, n=7-23 cells in each condition. C, representative time course experiment showing the effect of Pyr10 on the stretch-activated currents recorded at -150 mV and +80 mV in a TRPC3/6 transfected CHO cell. D, summary of the Pyr10 effect on stretch-activated currents recorded at -150 mV (lower bars) and +80 mV (upper bars) for each condition. Data are mean ± SEM, n=13-22 cells in each condition.*

Cationic currents of variable amplitudes were recorded in mock transfected CHO cells and in cells transfected with TRPC3, TRPC6 or TRPC3/6 channels. In all cases, basal currents were significantly larger in transfected cells (Figure R5 B). Figure R5 A shows representative current traces of cells transfected with TRPC3, TRPC6 or both, in control conditions and in the presence of Pyr10 (10 µM). The figure also shows the Pyr10-sensitive currents (red), obtained by subtracting the current obtained in the presence of Pyr from the current obtained in the absence of the blocker (C-Pyr10). Control currents were higher in TRPC3 than in TRPC6 transfected cells and showed an intermediate behavior in TRPC3/6 transfected cells. Regarding the effect of Pyr10, data showed that only cells expressing TRPC6 channels (alone or with TRPC3) were sensitive to Pyr10 (figure R5 B). Since TRPC3 and TRPC6 are activated when cells are stretched, we also tested the effect of Pyr10 on stretch-activated CHO cells. Typical traces obtained in whole-cell experiments recording

the current peak density at -150 mV and +80 mV, before and after Pyr10 application, are shown in figure R5 C. As expected, HS application elicited a reversible increase in the recorded currents similar in the three conditions studied (TRPC3-, TRPC6- and TRPC3/6-transfected cells), significantly larger than the obtained in untransfected cells. Interestingly, as in the case of basal currents, the blocking effect of Pyr10 (10 µM) on HS-activated currents was obtained only when TRPC6 channels were present (figure R5 D).

Taken together, these data strongly suggested that Pyr10 is actually a TRPC6 channel blocker, in clear disagreement with previous data in the literature where Pyr10 has been described as specific for TRPC3 channels (Schleifer *et al.*, 2012). In our hands, Pyr10 is indeed a TRPC6 blocker, and since this blockade occurred either in TRPC6 or TRPC3/6 transfected cells, it could be hypothesized that Pyr10 behaves as a TRPC current blocker of TRPC6 homotetramers and also of TRPC6 heteromultimers with other TRPC channels, such as the TRPC3.

In order to confirm the presence of those heteromultimers in the CHO cells transfected with TRPC6 and TRPC3 channels, we performed co-immunoprecipitation assays using GFP-Trap® beads that bind to the TRPC3-YFP fusion protein. The antibodies against TRPC3 and TRPC6 channels used for the immunoblotting step were first tested with immunocytochemistry in TRPC3- or TRPC6-transfected CHO cells. Figure R6 shows the specificity of both antibodies as well as the membrane expression of both TRPC channels.

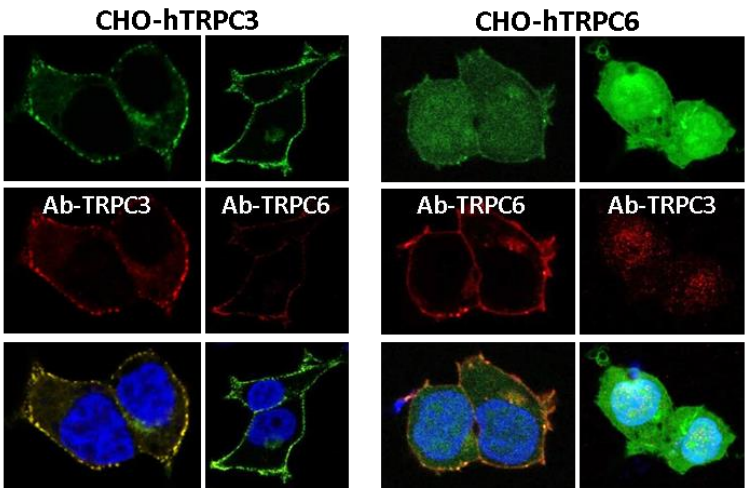

Figure R6. *Immunostaining evidence of the location and association of TRPC3 and TRPC6 channels in CHO cells. Representative confocal images of immunolabelling using anti-TRPC3 and anti-TRPC6 antibodies (middle images) in TRPC3-YFP (left) and TRPC6-GFP (right) transfected (upper images) CHO cells. Immunostaining was predominant at the cell membrane and correlated with YFP (fusion protein)-labelling for TRPC3 (lower images). No cross-reactivity was observed in either case.*

Figure R7 shows a typical co-immunoprecipitation experiment in which TRPC3 channels could be detected in the pull-downs obtained from both TRPC3 and TRPC3/6 transfected cells, strongly suggesting that TRPC3 and TRPC6 associate to form heteromultimers. As expected, TRPC6 could only be detected in the pull-downs obtained from the TRPC3/C6 transfected cells.

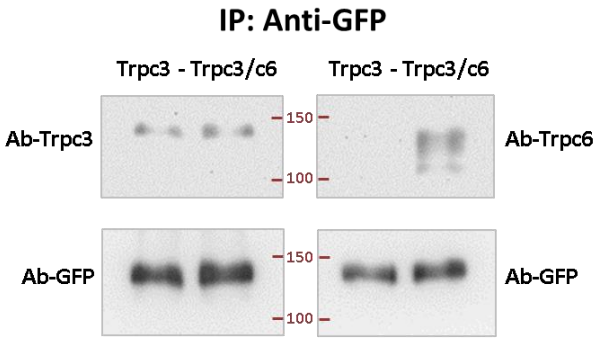

Figure R7. *TRPC3-YFP and TRPC3-YFP/TRPC6 transfected cells were co-immunoprecipitated using GFP-Trap beads and immunoblotted with anti-GFP (as load control), anti-TRPC3 and anti-TRPC6. Data are representative of two independent experiments.*

These experiments demonstrate that Pyr10 is a tool for studying TRPC6 channels, either as homo or heteromultimers. To our knowledge, there is not a similar pharmacological tool to explore specifically TRPC3 channel function. However, since anti-TRPC3 antibodies have shown a good specificity when tested in immunocytochemical and western-blot experiments, we decided to explore if they could affect functionally TRPC3 channels when applied intracellularly in a patch-clamp pipette. Therefore, whole-cell patch-clamp experiments were performed in transfected and mock CHO cells adding to the pipette solution anti-TRPC3 or anti-GFP/RFP (as negative control, see Methods).

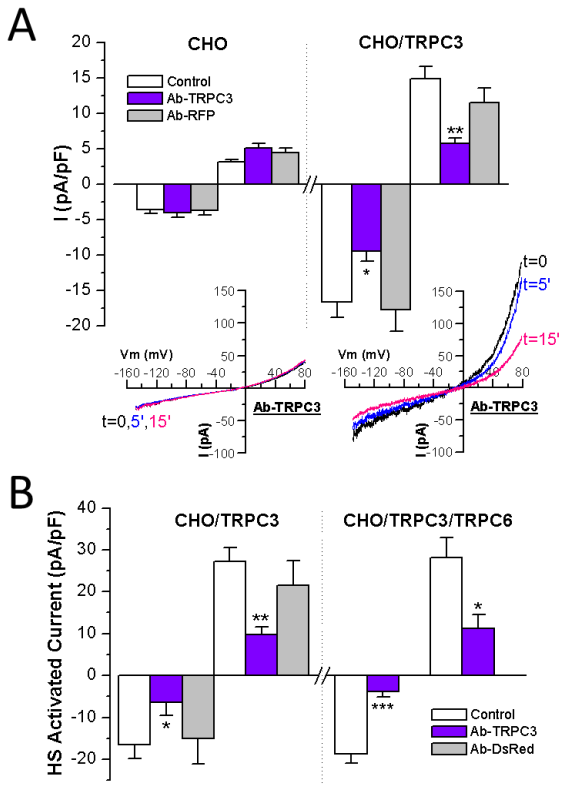

Figure R8. *Use of antibodies to determine functional contribution of TRPC3 and TRPC6 channels in CHO cells. A, blocking effect of the intracellularly applied antibodies on whole-cell currents in TRPC3-transfected (right) and mock CHO (left) cells. Bars are average basal current densities at -150 mV (lower bars) and +80 mV (upper bars) after 5-10 min of recording in control pipette solution or in presence of the indicated antibodies. Data are mean ± SEM, n=9-14 cells from at least four different experiments. The inset plots show representative current traces obtained at the indicated times in a mock (left) or in a TRPC3-transfected (right) cell with anti-TRPC3 in the pipette solution. B, same protocol of intracellularly applied antibodies used on stretch-activated currents with HS solution in TRPC3- and TRPC3/6-transfected cells. Bars are mean ± SEM, n=8-10 cells.*

No changes in basal current amplitudes were observed in transfected and mock cells when using control antibodies up to 10 min of recording, while a significantly reduction in transfected cells was observed when dialyzing with anti-TRPC3 (Figure R8 A). Similar results were obtained when the effect of antibodies was tested on HS-activated currents (Figure R8 B). The effect of anti-TRPC3 antibodies was also tested in cells transfected with TRPC3/6 (Fig R8 B). In this case, the effect was also evident, suggesting that the antibody was also effective on heteromultimeric channels.

2.4. Characterization of TRPC3/6 heteromultimers in VSMCs from BPN and BPH mice.

We have shown that Pyr10 and anti-TRPC3 antibodies were good tools for exploring TRPC6 and TRPC3 mediated currents, respectively, although they could not provide information about possible changes in heteromultimeric composition when both channels are present. This is the case of native VSMCs from mesenteric arteries. However, the larger expression of TRPC3 and lower expression of TRPC6 mRNA in BPH cells could translate into a different composition of TRPC3/6 heteromultimers in these cells, and this could have functional consequences in the control of vascular tone. To test this hypothesis, Proximity Ligation Assays (PLA, see Methods) were carried out in freshly isolated VSMCs from BPN and BPH mesenteric arteries using combinations of anti-TRPC3 and anti-TRPC6 antibodies raised in different species. Since PLA gives positive signals with proteins that are closer than 40 nm, it can detect the presence of heteromultimers in the membrane, although the existence of clusters of channels can not be excluded (see the Discussion section). Nevertheless, and for the sake of simplicity, the possible associations that could be found in a single tetramer, and how they would be detected with the three tested combinations of antibodies (C3/C3, C6/C6 and C3/C6), are depicted in the figure R9. Briefly, the combination C3/C6 labels only the heteromultimers, whilst the combinations C3/C3 and C6/C6 detect not only homomultimers but also heteromutimers with more than one subunit of the corresponding channel.

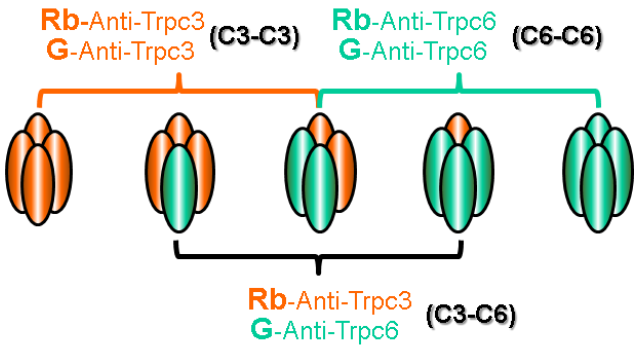

Figure R9. *Scheme of the C3-C3, C6-C6 and C3-C6 possible associations that can be recognized using PLA.*

Figure R10 A shows representative confocal images of the punctae distribution obtained in BPN and BPH native cells for the three tested combinations of antibodies. Labelling the cells with two different anti-TRPC3 antibodies (C3-C3 combination) or combining anti-TRPC3 and anti-TRPC6 antibodies (C3-C6

combination) produced a significantly higher number of puncta per cell in BPH than in BPN cells. In contrast, the labelling with two different TRPC6 antibodies (C6-C6 combination) was significantly smaller. Average values of the punctae density normalized to the cell size for all the described combinations are depicted in figure R10 B. Since C3/C3 and C6/C6 labelling are mutually exclusive, and the combination of both would label all possible associations of TRPC3 and TRPC6 channels, the percentage of heteromultimers with more than a TRPC3 (C3>1) or TRPC6 (C6>1) in BPN and BPH cell can be estimated from the C3/C3 and C6/C6 data (Figure R10 C).

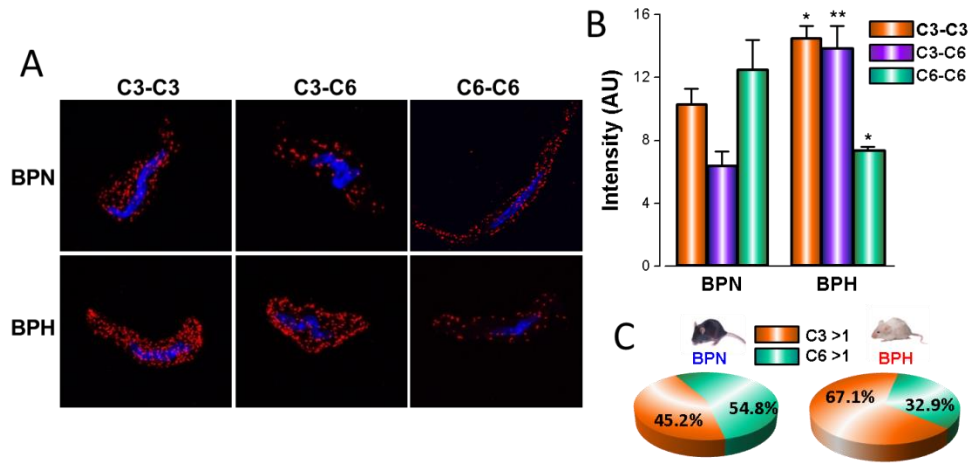

Figure R10. *Differences in TRPC assembly in BPN and BPH mesenteric VSMCs. A, representative confocal images of the punctae distribution in BPN (upper) and BPH (lower) native VSMC cells. B, bar plot showing the average of density punctae of each condition represented in (A). Data are mean ± SEM, n=36-64 cells in each condition from four different experiments. *p<0.05, **p>0.01 compared to BPN. C, interpretation of the summary data, considering 100% as the sum of C3-C3 or C6-C6 and assuming C3-C6 is included in both.*

Although these experiments do not provide accurate information about the total expression of TRPC3 or TRPC6 channels in the cells, they allow us to conclude that heteromultimers are more abundant in BPH cells, and that the TRPC3/TRPC6 ratio in those multimers is higher than in BPN cells.

2.5. Characterization of the functional contribution of TRPC3 and TRPC6 multimeric associations in native VSMC cells from BPN and BPH mice.

All data presented so far suggest a higher TRPC3 contribution, either as homo or heteromultimers, to the BPH phenotype. To test this hypothesis from a functional point of view, we characterized the TRP mediated currents in freshly isolated native VSMCs with the whole-cell configuration of the patch-clamp technique using Pyr

compounds (to block TRPC6 channels) or intracellular anti-TRPC3 antibodies (to block TRPC3 channels). Cationic currents were elicited with a ramp voltage protocol (see Methods) either on non-stimulated VSMCs (basal currents) or after the application of different agonists activating GPCRs (Receptor Operated Currents, ROCs).

2.5.1. Characterization of basal TRPC currents.

Ionic currents were recorded in the presence of TRP bath solution (see Methods). Basal current amplitudes at -150 mV were significantly larger in BPH than in BPN cells, even when current amplitudes were corrected for cell size (-8.1 ± 0.5 pA/pF in BPH vs. -6.4 ± 0.7 pA/pF in BPN, figure R11 B), since BPH cells were significantly larger than BPN (16.9 ± 0.6 pF, n=61 cells from 25 BPH; vs. 13.9 ± 0.5 pF, n=36 cells from 16 BPN). On the contrary, the effect of Pyr3 and Pyr10 on current amplitude was smaller in BPH cells. Figure R11 A shows representative records obtained in cells from both mice, and Figure R11 C represents the Pyr3 ad Pyr10 sensitive currents expressed as percentage of total current, measured at -150 mV.

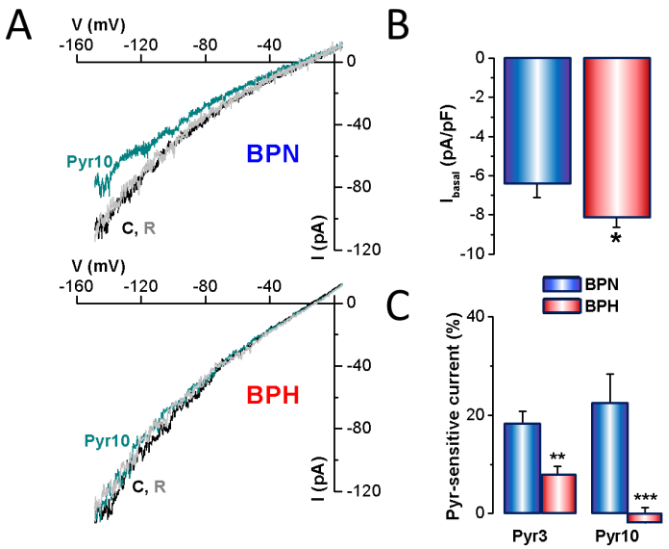

Figure R11. *Pyr sensitivity of TRPC-mediated basal currents in native VSMCs. A, representative current-voltage traces of a BPN and a BPH native cells in TRP solution (C), in presence of Pyr10 (10 µM) and after washout of the blocker (R). B, bar plot showing averaged current amplitudes at -150 mV for BPN and BPH cells. Data are mean ± SEM, n=40-60 cells from 16-25 mice in each condition. *p<0.05. C, bar plot showing the average fraction of Pyr3- and Pyr10- sensitive current at -150 mV. Data are mean ± SEM, n=10-23 cells from 7-13 mice in each condition.**p<0.01; ***p<0.001.*

For these recordings, the composition of intra and extracellular solutions was designed to minimize or block any other currents (see Methods). Also, particular care was taken to study inly cells with high resistance seals and very good access, so that the contribution of other unspecific, leak conductances is negligible. With these assumptions, the larger TRP currents recorded in BPH cells could certainly contribute to the more depolarized Vm characteristic of that phenotype, and the Pyr effects suggested a smaller contribution of TRPC6 channels to the cationic currents in BPH cells, in clear agreement with the results obtained in the PLA experiments and with the smaller expression of TRPC6 mRNA in VSMCs from mesenteric arteries. Those experiments also suggested a higher contribution of TRPC3 channels in BPH cells. To confirm this last point, the effect of intracellularly applied anti-TRPC3 antibody on whole-cell currents was analyzed in native BPN and BPH cells. A ramp protocol from -150 mV to +80 mV was applied in cells where the antibody anti-TRPC3 (or an antibody control, anti-RFP) was included in the pipette solution. Ramps were applied every 10 s, and the time course of the current amplitudes at -150 mV and +80 mV was studied, being t=0 the beginning of the whole-cell recording (figure R12 A). In the presence of anti-TRPC3 antibody in the pipette, basal current amplitude of BPH cells decreased by 25% and by 39% after 5 and 10 min of recording, respectively. No changes were observed when applying anti-RFP or no antibody. The effects of the anti-TRPC3 antibody were very small in BPN cells, being only significant in BPH cells (figure R12 B).

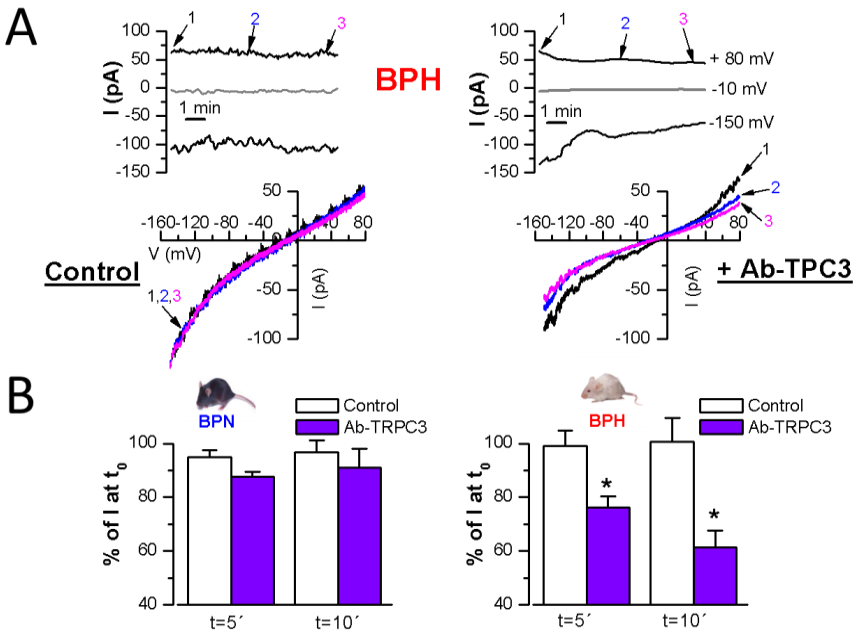

Figure R12. *Effect of anti-TRPC3 antibody on TRPC3-mediated currents in BPN and BPH cells. A, representative traces of the current amplitudes at the indicated voltages in a BPH cell recorded with anti-RFP (left) or with anti-TRPC3 (right) antibodies in the pipette solution. Current-voltage ramp traces 1, 2 and 3 corresponding to 0, 5 and 5 min of recording are depicted. B, average current amplitudes represented as the fraction of the initial current with both, anti-TRPC3 or control antibodies, are shown for BPN and BPH cells. Each bar is mean ± SEM, n=7-14 cells in each group. For the control group, untreated cells and anti-RFP treated cells were pooled together. *p<0.05.*

These results strongly suggest that TRPC3 contribution to the cationic currents in native VSMCs is higher in BPH when compared to BPN mice.

2.5.2. Characterization of Receptor activated TRPC currents.

We have demonstrated so far differences in the contribution of TRPC3/6 channels to basal currents in BPN and BPH VSMCs. Next, we explored these differences when these currents were activated with different agonists, such as ATP (30 µM), UTP (50 µM), Phenylephrine (10 µM) or the DAG-analogue OAG (100 µM). These agonists were applied to activate ROCs, and the effect of Pyr3/10 (10 µM) was investigated to explore the contribution of TRPC6 channels to the currents (Figure R13).

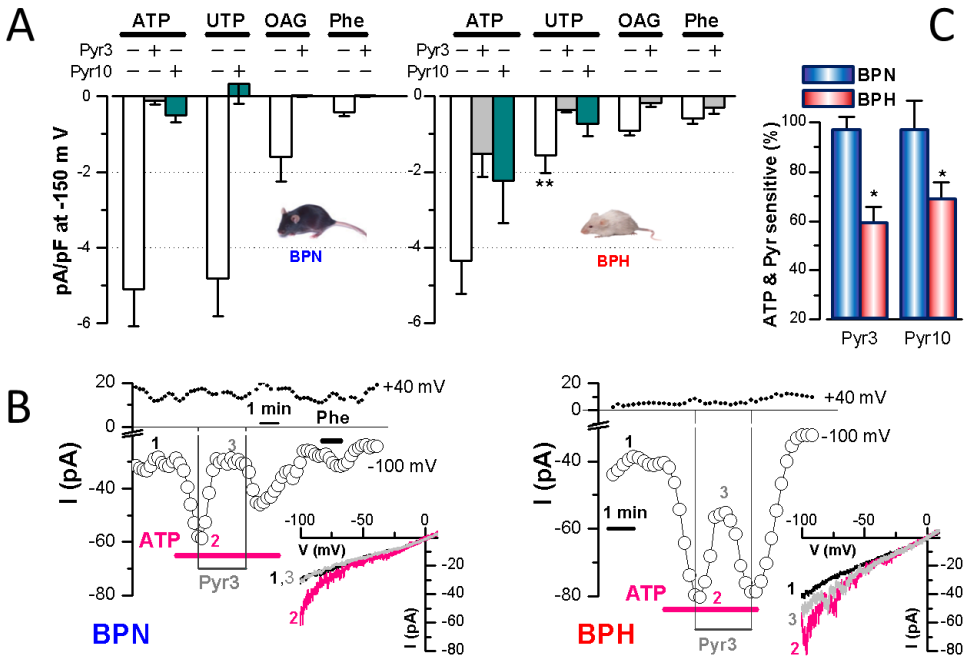

Figure R13. *Effect of Pyr blockers on agonist-activated currents in native VSMCs. A, summary data of 30 µM-ATP-, 50 µM-UTP-, 100 µM-OAG- and 10 µM-PHE-activated currents alone or in the presence of 10 µM-Pyr3/10 recorded with a ramps protocol from -150 mV to +80 mV. Each bar is the mean ± SEM, n=17-36 cells for agonist-induced currents and n=6-14 cells for Pyr3/10 blockade. **p<0.01 compared with UTP-activated currents in BPN cells. B, representative current amplitude traces recorded in the presence of 30 µM ATP alone or with 10 µM Pyr3 at the indicated voltages in a BPN (left) and a BPH (right) cell. Inset plots showing current-voltage traces in control (1) conditions, in the presence of ATP (2) or ATP+Pyr3 (3). C, bar plot showing the fraction of ATP-activated current that can be blocked by Pyr3 or Pyr10 in BPN and BPH cells. *p<0.05 compared to BPN.*

ROCs amplitude showed no significant differences between BPN and BPH cells for all the studied agonists, except for UTP, which elicited significantly smaller currents in BPH cells. However, a remarkable difference was obtained when comparing the blocking effect of Pyr compounds. Although Pyr3/10 almost fully abolished ROCs in BPN cells, a significant fraction of the activated currents was insensitive to these drugs in BPH cells. Figure R13 B shows representative traces obtained in BPN and BPH cells when ATP was used to elicit ROCs.

Taken together, expression and functional studies performed so far strongly suggest a significant change in the contribution of TRPC3 and TRPC6 channels to the VSMCs electric phenotype in BPH mice. TRPC3/6 mediated currents are larger in BPH cells, and so is the ratio of TRPC3/TRPC6. This “shift” towards a more dominant role of TRPC3 channels could contribute in part to the increased vascular

tone present in the BPH phenotype. However, these differences between BPN and BPH cells do not explain all the differences observed when ROCs were studied, especially when UTP was used as agonist.

Since electromechanical coupling is very relevant for controlling vascular tone (Herring and Paterson, 2018) and TRPC3/C6 are just one element in the activation cascade from the receptor to contraction, we decided to explore in detail the purinergic signaling cascade both in BPN and BPH mesenteric arteries in order to better contextualize the observed changes in TRPC3/6 channel.

3. Differences in the purinergic signaling cascade between BPN and BPH VSMCs.

3.1. Functional contribution of P2XR and P2YR receptors to vascular tone.

Purinergic signaling is particularly relevant in the physiology of vascular smooth muscle cells, since it is involved in the sympathetic control of the vessel tone. NA and ATP co-released by sympathetic nerves mediates vasoconstriction in a biphasic way. First, there is a transient response mediated mainly by the P2X purinergic receptors which is followed by a sustained response mediated by the α_1-adrenoreceptors (von Kügelgen and Starke, 1968; Sneddon and Burnstock, 1985). However, the contribution of the purinergic and adrenergic components to the overall vasoconstrictor response to nerve stimulation is not homogeneous in the different vascular beds. In large arteries, the response is essentially adrenergic, while in smaller arteries the response is mediated predominantly through P2X receptors (Gitterman and Evans, 2001). In addition to these responses mediated by the neurogenic release of ATP, it is well known that other nucleotides, like UTP, mediate vasoconstrictor responses through the activation of P2Y receptors, and these receptors have been described to play a relevant role in the myogenic response of small vessels (Kauffenstein *et al.*, 2016).

To investigate the possible differences in the purinergic signaling pathways between BPN and BPH VSMCs, vascular responses to different agonists and blockers of those pathways were first explored by pressure myography. Mesenteric arteries (2^{nd} or 3^{rd} order) were pressurized to 70 mmHg and concentration-response curves of ATP and UTP were obtained to discriminate between P2X- and P2Y-mediated responses, respectively.

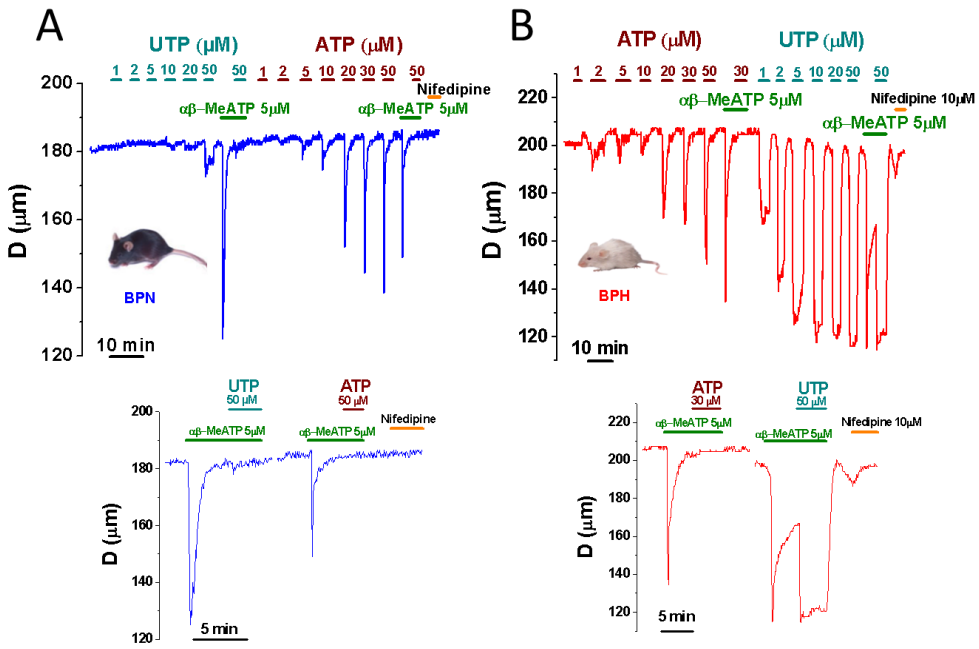

Figure R14. *Differences in the vasoconstrictor response to ATP and UTP in BPN and BPH mesenteric arteries. A, B, representative examples showing the ATP- and UTP-mediated effects on the vascular tone of BPN (A) and BPH (B) mesenteric arteries. The inset plots show the ATP- and UTP-mediated effects on 10 μM αβ-MeATP- activated arteries.*

Figure R14 shows typical experiments carried out in BPN (left) and BPH (right) arteries. In both cases, UTP and ATP were applied sequentially in several steps with increasing concentrations, from 1 to 50 μM. Whilst ATP responses were transient, and very similar in BPN and BPH cells (10 μM ATP: 18.3 ± 2.1 % vs. 16.7 ± 2.7 % of vasoconstriction, p=0.68, n=7-16 arteries from 8 BPN and 5 BPH mice, respectively), vasoconstrictor effects of UTP were sustained and significantly larger in BPH mesenteric arteries (Figures R15 and R16 A). At the end of each sequence, the higher concentration of the agonist was tested in the presence of αβ-MeATP (10 μM), an agonist of $P2X_1$ that elicits a fast and transient response due to receptor desensitization. These responses are shown in the lower part of the figure at a magnified time scale. Concentration-response curves obtained for ATP and UTP in several arteries were averaged, and data were plotted and fitted to a Hill function curve as follows:

$$E = E_{max} \cdot \frac{[NTP]^n}{{E_{50}}^n + [NTP]^n}$$

Where, E_{max} represents the maximum effect, [NTP] represents the concentration of the tested nucleotide triphosphate, E_{50} represents the concentration of the agonist that gives the 50% of the maximum effect and n represents the Hill coefficient. The best fitting parameters are shown in the following table (Table R2):

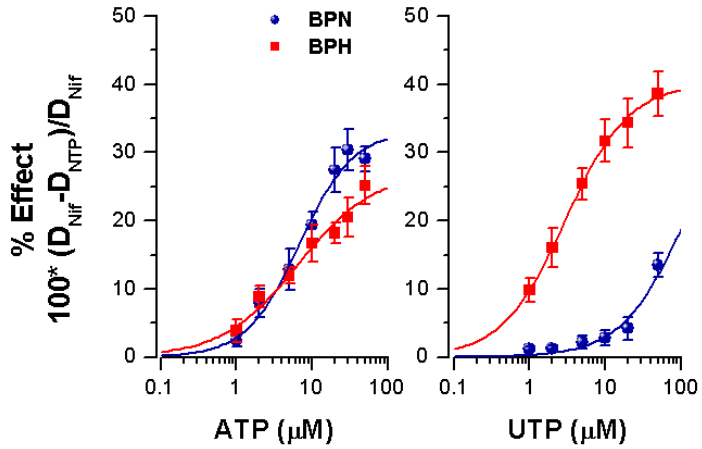

Figure R15. *Dose-response vasoconstrictor effect of ATP (left) and UTP (right) in BPN (blue) and BPH (red) mesenteric arteries. Data were normalized to maximal diameter values obtained with Nif (10 μM) and are expressed as percentage of vasoconstriction (see Methods). Each point is mean ± SEM, n=5-16 arteries in each group. p<0.001 in UTP curves when applying ANOVA and Bonferroni test.*

	BPN				BPH			
	E_{max} (%)	E_{50} (μM)	n	R^2	E_{max} (%)	E_{50} (μM)	n	R^2
ATP	33.2±7.5	6.8±3.8	1.2±0.4	0.99	27.2±11.8	6.4±8.5	0.9±0.4	0.98
UTP	-	~115*	-	0.84	40.2±8.6	2.9±1.8	1±0.4	0.99

Table R2. *Main kinetics parameters obtained after fitting ATP and UTP dose-response curves to a Hill function. *Since proper fitting to the Hill function was not possible in BPN cells, the apparent E_{50} was stimated carrying out a fitting procedure assuming E_{max} and n values identical to those obtained in BPH.*

In the presence of αβ-MeATP, a maximal dose of ATP did not elicit any response, suggesting that ATP vasoconstriction is essentially mediated by $P2X_1$ purinergic receptors. Moreover, whilst the effects of ATP are very similar in BPN and BPH arteries, BPN cells are almost insensitive to UTP stimulation (as the concentration-response curve in these arteries is shifted to the right almost two orders of magnitude). This larger response to UTP in BPH mice was clearly not anticipated from the results obtained when the effect of UTP on TRPC currents was studied (Figure R13).

Since the constrictor responses to UTP are in all likelihood mediated by the $P2Y_{1-7}$ family of purinergic receptors, the striking difference in the response between BPN and BPH arteries suggests a more relevant contribution of P2Y purinergic receptors to the vascular tone in BPH mice. To determine the members of the P2Y family of purinergic receptors involved, we tested the effects of the agonists and blockers described in Table R3:

	$P2X_1$	$P2Y_1$	$P2Y_2$	$P2Y_4$	$P2Y_6$
ATP			=UTP	=UTP	
UTP			=ATP	=ATP	
UDP					>UTP
αβ-MeATP					
MRS 2578					
PSB0474					
UTPγS					

Table R3. *Specific physiological (top) and synthetic (bottom) agonists (green) and blockers (red) previously described in the literature used to explore purinergic receptors involved in UTP-mediated signaling cascade in BPN and BPH arteries (from Lewis and Evans, 2000; Malmsjö et al., 2000; Sugihara et al., 2011).*

Average results are shown in figure R16. The vasoconstrictor effects of UTP (mainly through $P2Y_2$/$P2Y_4$) and UDP (mainly through $P2Y_6$) were much larger in BPH than in BPN arteries. However, due to the fast break down of UTP to UDP, the UTP-mediated effects obtained could represent, at least in part, UDP-mediated effects. Therefore, the more stable synthetic UTP-analog UTPγS and the specific $P2Y_6$ synthetic agonist PSB0474 were tested at 10 μM. Both elicited larger vasoconstrictions in BPH. In addition, the effect of the specific $P2Y_6$ blocker MRS 2578 (10 μM) was tested on the responses induced by UDP or PSB0474, and in both

cases a partial blockade was obtained. Taken together, these data suggest that UTP-elicited vasoconstrictor effects are mainly mediated by $P2Y_6$ receptors, with a smaller contribution of $P2Y_2$ and/or $P2Y_4$ receptors.

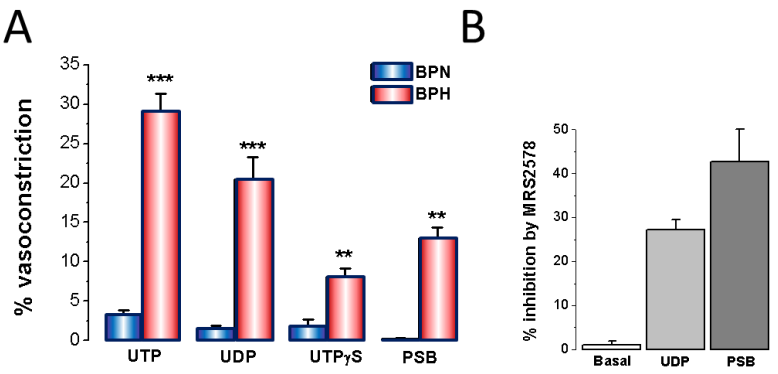

Figure R16. *Involvement of $P2Y_6$ purinergic receptors in UTP-mediated responses in BPH. A, bar plot showing differences in the vasoconstriction responses mediated by the indicated P2Y agonists (10 μM) in BPH and BPN mesenteric arteries. Each bar is mean ± SEM, n=2-16 arteries in each group. **p<0.01; ***p<0.001, compared to BPN. B, bar plot showing blocking effect of MRS 2578 (10 μM) on BPH arteries precontracted with UDP and PSB (10 μM). Each bar is mean ± SEM, n=2 arteries.*

To further investigate the different contribution of the purinergic receptors to the hypertensive phenotype, their mRNA expression pattern was explored by qPCR (Figure R17). qPCR data showed mRNA expression of $P2X_1$ and $P2X_4$ and $P2Y_1$, $P2Y_2$, $P2Y_4$ and $P2Y_6$ purinergic receptors. Even though P2X mRNA levels were much larger than P2Y (note the different scale for each family), mRNA expression was identical in BPN and BPH arteries when comparing the mRNA expression pattern. However, significantly higher expressions of $P2Y_2$ and $P2Y_6$ and lower expression of $P2Y_1$ receptors were observed in BPH VSMCs. These data agreed with the hypothesis of a higher expression of P2Y receptors contributing to the larger UTP-mediated effects in the BPH phenotype.

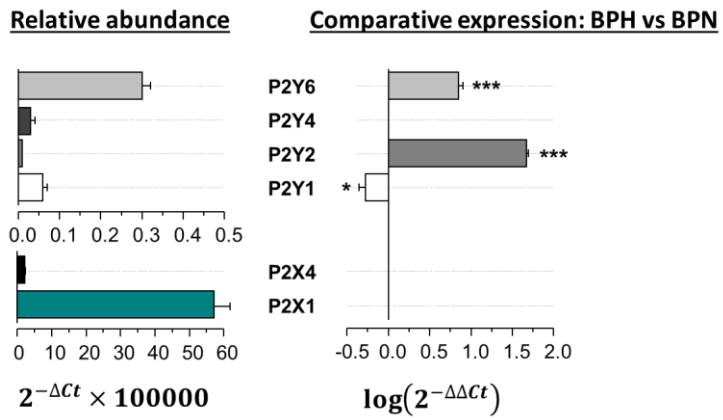

Figure R17. *mRNA expression profile of P2X and P2Y purinergic receptors in BPN and BPH mesenteric arteries. Left, relative abundance of purinergic receptors in BPN mesenteric arteries normalized to the amount of RP18S. Data are expressed as* $2^{-\Delta Ct}$*, where* $\Delta Ct = Ct_{receptor} - Ct_{18S}$*. Right, changes in P2X and P2Y receptors expression in BPH compared to BPN. Differences are expressed as* $log\ (2^{-\Delta\Delta Ct})$*, where* $\Delta\Delta Ct = \Delta Ct_{BPH} - \Delta Ct_{BPN}$*, meaning that positive, negative and 0 values indicate increased, decreased and no change mRNA expression, respectively. Each bar is the mean ± SEM, n=4 mice in each group. *P<0.05; ***P<0.001.*

Nevertheless, the good correlation of changes in P2Y receptor expression and UTP responses between BPN and BPH cell is clearly at odds with the effect of UTP on TRP currents. Therefore, we decided to explore the UTP signaling pathway in more detail, to better understand the differences between BPN and BPH phenotypes and in order to clarify the role of TRP in this signaling pathway.

3.2. Characterization of the P2Y signaling pathway in the BPH phenotype.

P2Y receptors are members of the GPCR receptors superfamily, coupled to PLC activation through G_q proteins. DAG and IP_3 produced by the PLC-mediated PIP_2 breakdown induces TRPC3/6 activation and Ca^{2+} release from intracellular stores, respectively, leading altogether to an intracellular [Ca^{2+}] increase. This increased $[Ca^{2+}]_i$ triggers activation of Ca^{2+}-activated Cl^- channels (CaCCs) and membrane depolarization (Figure I4). While the described differences in $P2Y_{2/6}$ expression are consistent with the greater contractile response to UTP in BPH arteries, our electrophysiological studies showing a larger activation of TRPC currents in BPN do not fit in this scheme. There are two questions that we need to answer to solve this apparent paradox, and we explored two other levels of the signaling pathway to try to answer them.

Q1. Why do we see less UTP-mediated TRPC currents in BPH cells if we have more receptors and more channels?

We explored the coupling between $P2Y_6$ receptors and TRPC3/6 channels. Differences in their location and association could shed light on question 1, as we could have a less efficient signaling in spite of having more proteins. These data are shown in section 3.2.1.

Q2. How can we have a larger contractile response to UTP while activating smaller TRPC currents?

We studied the expression and contribution of other channels, (CaCCs channels) to UTP-mediated responses. A different contribution of both channels (TRPC and CaCCs) in BPN and BPH cells to UTP responses could explain the changes in contraction. We explore this hypothesis on section 3.2.2.

3.2.1. P2Y6 and TRPC3/6 coupling.

We speculate that the smaller efficacy of UTP activating TRP currents, despite having more receptors and more channels in BPH cells, could be due to differences in the physical association (v.g. in membrane microdomains) between P2Y receptors and TRPC channels. To explore this hypothesis, Ground State Depletion (GSD) Super-resolution and PLA studies were performed in BPN and BPH VSMCs.

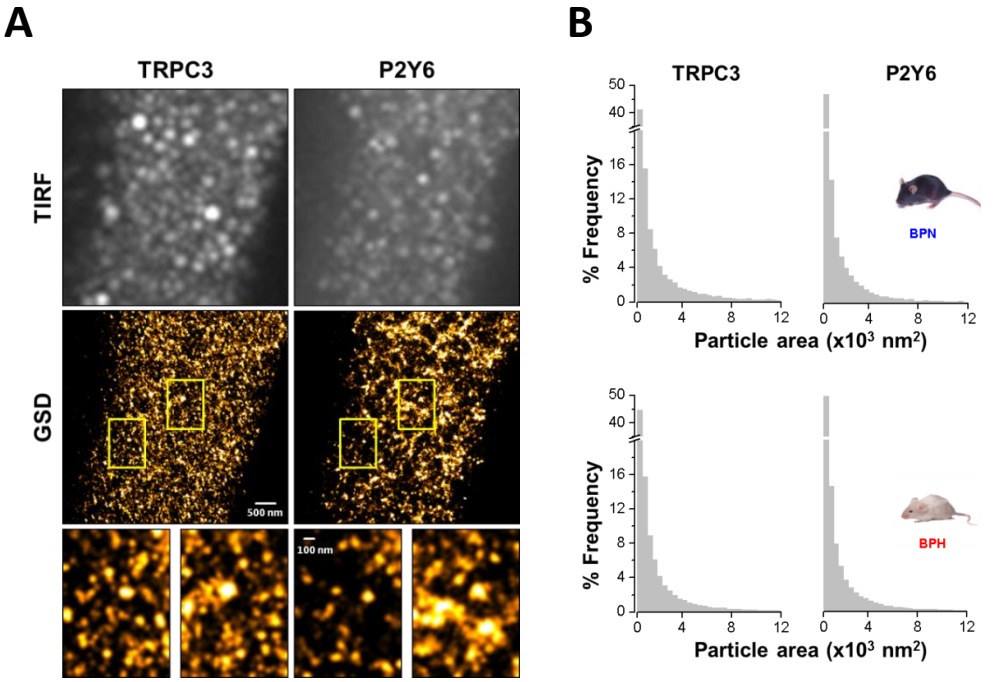

Figure R18. *Spatial organization of TRPC3 channels and P_2Y_6 receptors in BPN and BPH VSMC cells. A, representative TIRF (top) and GSD (bottom) super-resolution microscopy images showing the spatial organization of TRPC3 and $P2Y_6$ in a BPH cell. The magnification of the areas shown in yellow boxes is also depicted. B, histograms showing the areas of TRPC3 and $P2Y_6$ clusters in BPN and BPH cells.*

GSD Super-resolution data (Figure R18) revealed that TRPC3 channels and $P2Y_6$ receptors were broadly distributed in clusters with a large variety of sizes both in BPN (TRPC3, 2036.67 ± 23.60 nm; $P2Y_6$, 1788.29 ± 22.11 nm) and BPH (TRPC3, 1717.31 ± 9.39 nm; $P2Y_6$, 1632.61 ± 12.38 nm) VSMC cells. Sites of close proximity between TRPC3 channels and $P2Y_6$ receptors could be observed (Figure R19) and were analyzed by fitting the lowest intermolecular distance between both proteins to a Gaussian function of two components with centers at ~53.9 and ~109.2 nm in BPN, and ~44.8 and ~81.3 nm in BPH. There is a small population of TRPC3 channels and $P2Y_6$ receptors that seem to be further apart in BPN cells. The closer proximity between TRPC3 channels and $P2Y_6$ receptors observed in BPH is compatible with an enhanced coupling between both signaling pathways. Nevertheless, since the lowest distances are not very different, and most of them seemed to be close enough to be detected by PLA, an additional test of protein association was performed using PLA assay by labelling TRPC3/6 channels and $P2Y_6$ receptors in BPN and BPH cells (Figure R20).

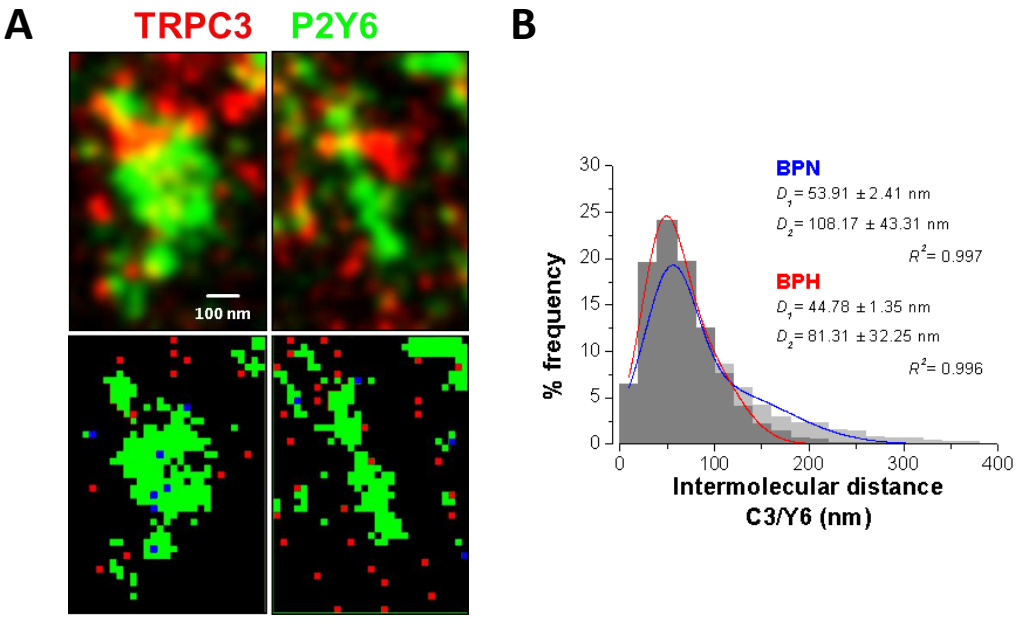

Figure R19. *Expanded merged GSD images showing sites of close interaction between TRPC3 and $P2Y_6$. A, images of the associated object-based colocalization (bottom) between TRPC3 (red centroids) and $P2Y_6$ (green regions). Colocalization centroids (blue) are also depicted. B, plot showing the lowest intermolecular distances between TRPC3 and $P2Y_6$ centroids in BPN (n=3713 particles from 3 cells) and BPH (n=8299 from 8 cells). Data were fit to a Gauss function of two components.*

PLA data revealed close proximities between $P2Y_6$ receptors and TRPC3 or TRPC6 channels in BPN and BPH cells. The C3-Y6 condition showed higher punctae than the C6-Y6 condition in both preparations. In addition, there are significantly higher punctae for C3-Y6 condition in BPN. Since the PLA technique is more sensitive than the GSD super-resolution to disclose distances below 40 nm, these results are compatible with a higher coupling between P2Y receptors and TRPC3/C6 channels in BPN cells, despite the smaller expression of those proteins, and could explain in part the larger activation of TRP currents by UTP recorded in BPN cells.

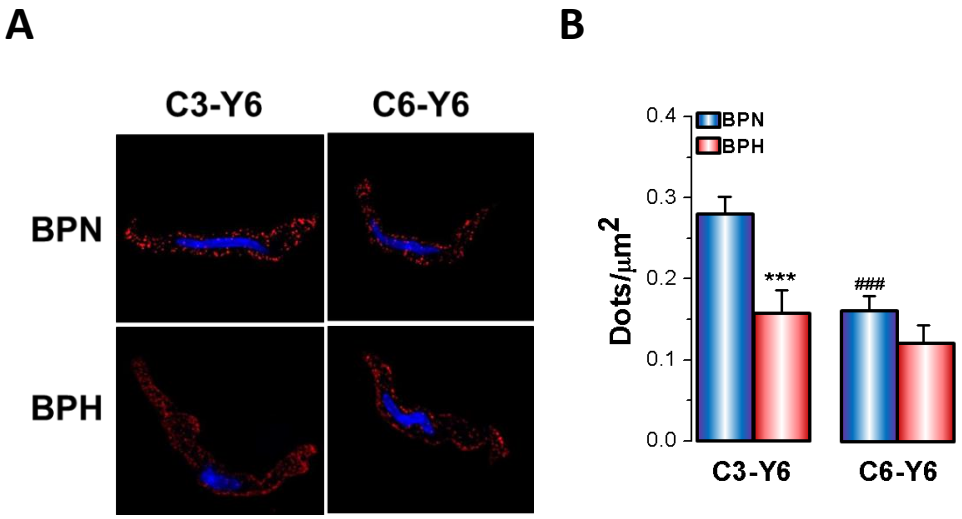

Figure R20. *Differences in the association pattern between TRPC3/6 channels and $P2Y_6$ receptors in VSMCs. Representative confocal images (A) of the summarized (B) C3-Y6 and C6-Y6 associations obtained in BPN and BPH cells. Each bar is mean ± SEM, n=40-60 cells in each group. ***p<0.001, compared to BPN. ###p<0.001, compared to C3-Y6.*

However, the fact that UTP elicited very small depolarizations and smaller vasoconstrictions in BPN compared to BPH, despite the larger activation of TRP currents, suggests additional components in the UTP-activated $P2Y_6$ signaling pathway responsible for the larger depolarization and the bigger response to UTP in BPH arteries. One of such components could be the CaCCs.

3.2.2. Ca^{2+}-activated Cl^- channels involvement in the UTP-activated $P2Y_6$ signaling pathway.

Several members of the membrane CaCCs channels have been found in VSMCs (see Introduction for references). To evaluate their contribution to the UTP response, we measured the UTP activated currents in two different recording conditions (Figure R21). One of them was designed to maximize the TRP component, blocking

CaCCs with Niflumic acid (100 µM), DIDS (100 µM) and 10 mM EGTA. These currents are labelled in the figure R21 as I_{TRP}. The other was designed to record any current activated by the agonist, adding no blockers and keeping the intracellular calcium buffered at ~500 nM. These currents likely represent the activation of both TRP and CaCCs channels and are labelled in the figure R21 as $I_{TRP/CaCC}$. Examples of typical experiments of each condition are shown in Figure R21A. Results demonstrate that although I_{TRP} currents are smaller in BPH, as previously shown (Figure R13), $I_{TRP/CaCC}$ are significantly larger in BPH cells, strongly suggesting that differences in CaCC channels between BPN and BPH could contribute to explaining the differences in the UTP response.

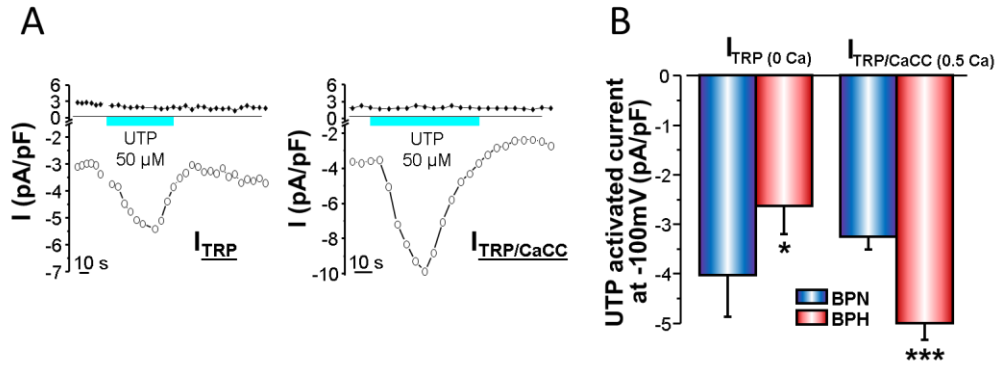

Figure R21. *Differences in the UTP effects on whole-cell currents in BPN and BPH VSMCs. A, representative traces of UTP-elicited effects on the peak current recorded at -150 mV and +80 mV in each condition in BPH cells. B, summary of the UTP-sensitive current recorded at -150 mV in BPN and BPH cells. Each bar is mean ± SEM, n=96 and n=73 cells from BPN and BPH, respectively. **p<0.01.*

In this context, we explored the mRNA expression pattern of several members of the known families of CaCCs channels in mesenteric arteries from BPN and BPH mice. We explored also the expression of some proteins that contribute to the $[Cl^-]_i$ control, such as the Na^+, K^+, Cl^- cotransporter $NKCC_1$ and the voltage-activated Cl^- channel ClCN3 (Figure R22). qPCR data showed higher mRNA expression of $ClCa_1$ and ANO_1 channels in BPH compared to BPN mesenteric arteries, while no changes of $ClCa_2$, $ClCN_3$ and the $NKCC_1$ cotransporter were observed. These data are in good agreement with the larger activation of CaCC currents in BPH cells and point out to ANO1 as a good molecular correlate of that difference between BPN and BPH cells.

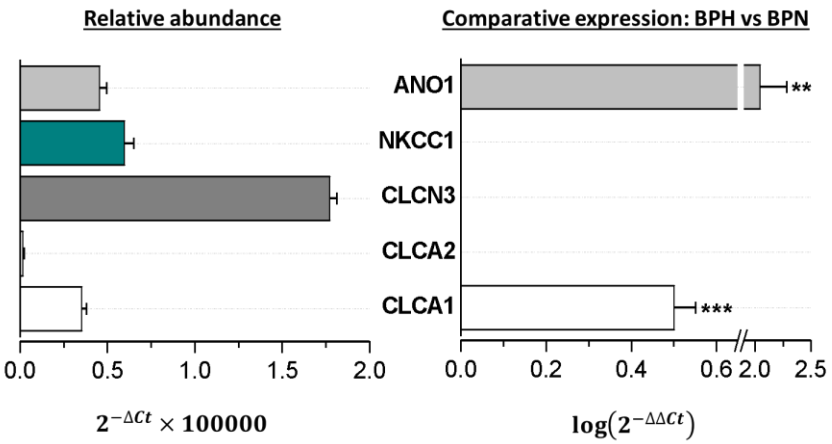

Figure R22. *Differences in the mRNA expression profile of several Ca^{2+}-activated Cl^- channels and Na^+, K^+, Cl^- cotransporters in BPN and BPH mesenteric VSMCs. Left, relative abundance of the indicated channels and cotransporters in BPN VSMCs from mesenteric arteries normalized to the amount of RP18S. Data are expressed as $2^{-\Delta Ct}$, where $\Delta Ct = Ct_{receptor} - Ct_{18S}$. Right, changes in mRNA expression in BPH compared to BPN. Differences are expressed as $log\ (2^{-\Delta\Delta Ct})$, where $\Delta\Delta Ct = \Delta Ct_{BPH} - \Delta Ct_{BPN}$, meaning that positive, negative and 0 values indicate increased, decreased and no change mRNA expression, respectively. Each bar is the mean ± SEM, n=4 mice in each group. **P<0.01; ***P<0.001.*

These data suggest that an increased contribution of CaCCs activation in BPH cells could explain the enhanced UTP-induced contraction in the hypertensive arteries. If this were the case, we would expect to see differences between BPN and BPH cells in the depolarization induced by UTP and in the sensitivity of that response to the effect of TRP or CaCC blockers. To test this hypothesis, we measured the effect of UTP and different blockers on membrane potential with the perforated-patch configuration of the current-clamp technique. Average results are shown in Figure R23 A, whilst Figure R23 B shows two typical records obtained in a BPN and a BPH cell. The effect of high extracellular K^+ (60 mM) was used to determine cell integrity. Under these conditions the reversal potential for K^+ will be around -20 mV (for an estimated $[K^+]_i$ of 130 mM). We can see that there are other cationic conductances that contribute to set resting Vm in VSMCs since the values recorded were always more positive than the calculated E_K. Although the two cells in the example seem to be different, there were not statistical differences between BPN and BPH cells in the Vm value reached with 60 mM K^+ stimulation (-11,14 ± 0,75 mV in BPH vs -10,93 ± 1,4 in BPN, p=0,9, n= 21-40 cells).

UTP produced a significantly larger depolarization in BPH cells, in line with the differences in the response to UTP between BPN and BPH arteries. In fact, the depolarization obtained in BPN cells was almost undetectable in many cells. Also, as expected for channels that are open at resting membrane potential, the blockade of TRPs and CaCCs produced a significant hyperpolarization both in BPN

and BPH cells. The hyperpolarization induced by Pyr3 was significantly larger in BPH cells, in agreement with a larger expression of TRP channels in those cells. The effect of Niflumic Acid was not different, but the effect of the specific inhibitor of ANO1, also called T16Ainh, was significantly larger in BPH, in good agreement with the expression data.

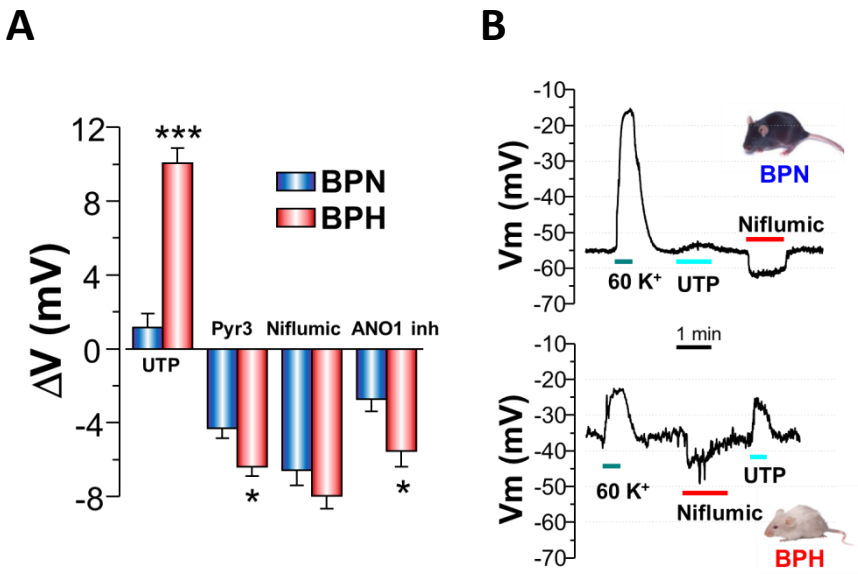

Figure R23. *Differences on the effects of UTP and the blockers of TRPC3/6 and CaCCs channels on resting membrane potential in BPN and BPH cells. A, bar plot showing the UTP (50 μM)-induced depolarizations and Pyr3 (10 μM)-, Niflumic (100 μM)- and ANO1 inhibitor (10 μM)-induced hyperpolarizations in BPH compared to BPN cells. Each bar is the mean ± SEM, n=5-54 cells in each group. *P<0.05; ***P<0.001. B, Representative traces of the effect of UTP and Niflumic on Vm in a BPN and a BPH cell from A. Depolarizations induced by KCl (60 mM) as a control of cell stability are also depicted.*

If we compare the effect of TRP or CaCC blockade on membrane potential, there are no apparent differences, suggesting that both channel families are contributing to set the membrane potential. In fact, the larger effects of Pyr3 in BPH cells suggest that TRP could contribute to the characteristic depolarized basal state of BPH VSMCs. However, when the effect of TRP or CaCC blockers are tested on UTP-induced depolarization in BPH cells, the different contribution of those channels to the response is striking (Figure R24). All inhibitors affected the depolarization induced by UTP, suggesting that all channels contribute to that response, but the magnitude of the effect was very different. Pyr3 showed a very small effect, whilst Niflumic Acid and/or the specific blocker of ANO1 completely abolished (or even reverted) the effect of UTP. These results pointed clearly to CaCCs as important

players in the response to UTP and suggested that the differences in the expression of these channels are at the core of the differences in the purinergic pathway between BPN and BPH mice.

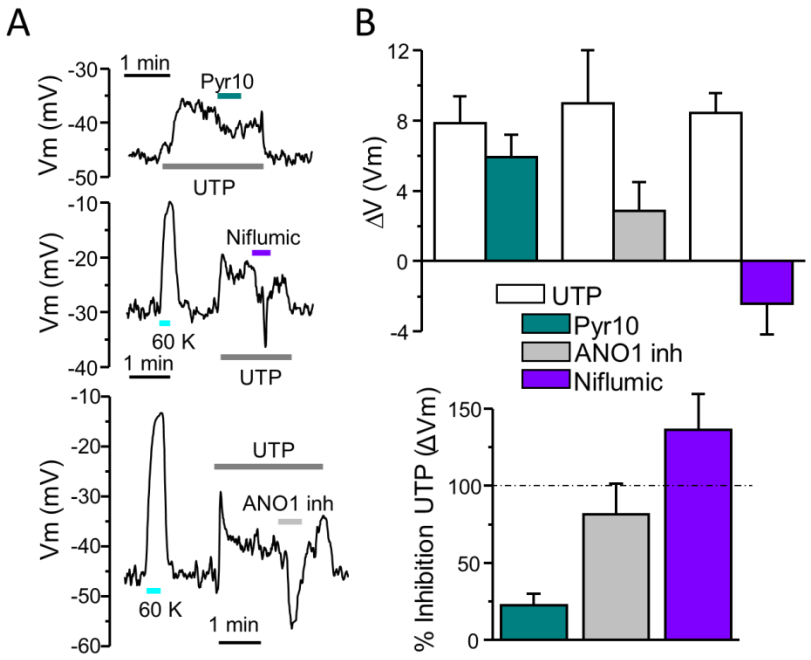

Figure R24. *Differences in the contribution of TRPC3/6 and CACCs channels to the UTP-induced depolarization in BPN and BPH cells. A, representative traces of the blocking effects elicited by Pyr3 (10 µM), Niflumic Acid (100 µM) and ANO1 inhibitor (10 µM) on UTP-induced depolarizations. As a control of the cell stability KCl (60 mM)-induced depolarizations are also depicted. B, bar plots showing the summarized blocking effects expressed as absolute values (top) and percentage (bottom) on UTP-induced depolarizations in BPN and BPH cells. Each bar is the mean ± SEM, n=5-10 cells in each group.*

5

Discussion

In the present study, using the BPN/BPH model of essential hypertension, we have explored the contribution of TRPC channels to the hypertensive phenotype. Furthermore, since TRPC channels are prototypic examples of Receptor Operated Channels (ROCs), we have investigated the differences between normal and hypertensive mice in the vascular responses to the α-adrenergic and the purinergic signaling pathways, the two GPCR pathways mainly associated with the sympathetic stimulation of resistance arteries. Using different approaches, we have explored differences in the expression profile of members of the purinergic P2X and P2Y families of receptors and we have functionally characterized their relative contribution to the hypertensive phenotype. Focusing on the UTP-mediated activation of purinergic signaling pathway, we have also explored downstream members, such as TRPC and CaCCs channels that, by their direct or second messenger-mediated coupling to purinergic signaling, could be enhancing the integrated response of vasculature. Thus, although we have separately explored the different contribution of these families of receptors and ion channels to the BPH vs BPN phenotype, the obtained results must be interpreted in the context of the integrated responses of arterial vessels to understand the complexity of the hypertensive phenotypic change.

1. TRPC Channels in the BPN/BPH model

TRPCs channels have been widely described as ROCs that contribute to modulate the membrane potential and the contractility of vasculature (Earley and Brayden, 2015). In this Thesis we have explored the mRNA expression profile of TRPC channels in several vascular beds of BPN and BPH mice. All channels, but TRPC5 and TRPC7, are expressed in VSMCs from both mice strains. Overall, mRNA expression is more than 20 times larger in resistance (mesenteric) than in conduit (femoral and aorta) arteries, and whilst TRPC1 is the more highly expressed channel in conduit arteries, TRPC1/3/4/6 mRNAs are more abundant in the mesenteric bed. When the expression levels are compared between BPN and BPH mesenteric VSMCs, it is evident that TRPC3 are the only channels that are overexpressed in the hypertensive cells (Figure R3). On the contrary, TRPC1 and TRPC6 are downregulated (although only data for TRPC1 is statistically significant). TRPC1 channels are mainly involved as SOCs (Nesin and Tsiokas, 2014; Ambudkar, de Souza and Ong, 2017), so we decided to focus on TRPC3 and TRPC6 channels as the main candidates to carry out ROCs in mesenteric VSMCs. Since these channels have been described to form functional multimeric channels in several tissues (Hofmann *et al.*, 2002; Earley and Brayden, 2015), we also hypothesized that in

addition to their different expression levels, changes in the composition of homo- or heterotetramers of these two channels could contribute to the genesis of the hypertensive phenotype. In any case, these differences should determine different, and experimentally discernible, biophysical, pharmacological and functional properties of TRPC channels in BPN and BPH VSMCs.

Pyr-compounds are the only available blockers described in the literature as putative blockers of TRPC3 channels (Kiyonaka *et al.*, 2009; Schleifer *et al.*, 2012). We tested the effect of three of these compounds (Pyr10, Pyr3 and Pyr6) on the vascular tone induced in mesenteric arteries by the stimulation with the α1 agonist Phenylephrine (Figure R4). Pyr10 and Pyr3 exhibited a powerful vasodilatory effect both in BPN and BPH arteries. Nevertheless, the effect is clearly different at concentrations below 10 μM, where vasodilation is larger in BPN than in BPH arteries.

However, since the specificity for TRPC channel blockers has not been thoroughly tested in the literature, we have tried out several methodological approaches to investigate the functional contribution of TRPC channels in a heterologous expression system (CHO cells) overexpressing TRPC3, TRPC6 or both. In this way we have determined that pyrazole compounds (Pyr3 and Pyr10) are effective blockers of TRPC mediated currents when CHO cells are transfected with TRPC6 channels, either alone or with TRPC3 (Figure R5). As TRPC3 and TRPC6 associate forming heteromultimers (Figure R7), the simplest interpretation of the effect of pyrazole compounds is to assume that the presence of TRPC6 subunits in the channel tetramer is a requirement for the inhibitory effect of these compounds. If this interpretation is correct, pyrazole compounds are effective blockers of TRPC6 channels, and could be used in native cells to estimate the contribution of these channels to the effects mediated by TRPC channels. This interpretation is also consistent with the smaller vasodilatory effect of these compounds in BPH arteries, where, according to mRNA data, we have increased TRPC3 and decreased TRPC6 expression.

These results clearly contradict the previously reported selective blocking effect on TRPC3 channels of Pyr10 and Pyr3. Although these reported effects on native TRPC3 channels (Kiyonaka *et al.*, 2009; Schleifer *et al.*, 2012) are compatible with the presence of TRPC3/6 heterotetramers in those preparations, we do not have a clear explanation for the discrepancy. Nevertheless, several differences in the experimental methodology can be highlighted. We have characterized the effects of Pyr on TRPC3, TRPC6 or TRPC3/6 overexpressed in CHO cells by exploring both basal and stretch-activated whole-cell currents with the patch-clamp technique, while previous reports have used TRPC3-transfected HEK293 (and/or HEK293T) cells and have estimated channel activity indirectly from changes in $[Ca^{2+}]_i$ upon

stimulation of endogenous muscarinic receptors with carbachol (Schleifer *et al.*, 2012). Noteworthy, it has been described that HEK cells endogenously express TRPC3 and TRPC6 channels (Bugaj *et al.*, 2005). In addition, we have analyzed the acute effects of Pyr compounds when applied in the external solutions both in basal conditions and in the presence of the stimulus, while previous reports explored the Pyr-elicited effects, mainly Pyr3, upon chronic pre-treatment before stimulation. Thus, it is quite possible that differences associated to the endogenous expression of TRPC3 and TRPC6 channels in different cell lines and/or differences associated to the response of the blockers related to the specific activation pathway could explain the observed discrepancies.

Since Pyr compounds turned out to be experimental tools to check the functional contribution of TRPC6 channels, we explored the possibility of using antibodies against TRPC3 channels to study the functional contribution of those channels. Although the only available antibodies recognize intracellular epitopes of the channel and their use must be limited to patch-clamp experiments where the intracellular medium is accessible, this experimental approach has proven to be instrumental to block TRPC3 mediated currents when these channels were overexpressed in CHO cells (Figure R8).

Non-selective cationic currents recorded in VSMCs isolated from BPN or BPH mesenteric arteries are significantly different in magnitude and in their sensitivity to Pyr compounds and anti-TRPC3 antibodies. The larger currents recorded in BPH cells in the absence of receptor activation (basal activity, Figure R11B), the smaller sensitivity to Pyr compounds (Figurer R11C) and the larger effect of anti-TRPC3 antibodies (Figure R12B) strongly correlate with the larger expression of TRPC3 in BPH VSMCs. Certainly, these differences can contribute to explain the more depolarized resting Vm of VSMCs cells from BPH, the increased vascular reactivity observed in BPH mesenteric arteries (Moreno-Domínguez *et al.*, 2009) and the larger effect of Pyr compounds observed in mesenteric arteries form BPN mice.

The results obtained with this electrophysiological approach in native cells are supported by data obtained with the Proximity Ligation Assay (PLA) technique. PLA data demonstrate a larger proportion of TRPC3-containing channels (and the consequent smaller proportion of TRPC6 subunits) in BPH cells (Figure R10). These findings are consistent with a larger number of TRPC3 homotetramers and/or heteromultimeric TRCP3/6 complexes in VSMCs from BPH mice. Early evidences previously reported that TRPC heteromultimerization, such as the case of TRPC6/7, showed distinct functional properties than the homomultimeric association (Hofmann *et al.*, 2002; Maruyama *et al.*, 2006). Thus, a better understanding of the mechanisms by which TRPC subunits combine to form functional ion channels complexes is essential to evaluate their contribution to endogenous cation

currents. In many cases, the use of KO animal models helps to understand the role of a particular channel, but this is not the case of TRPC3 or TRPC6 channels. Several studies using single, double TRPC3/6 and up to quadruple KO of TRPCs channels concluded that TRPC functions are a result of the combined activity of multiple TRPC proteins and that the interfering with one single TRPC channel does not imply an alteration in the functional responses, thus indicating possible redundancies in the function of TRPC channels (Sexton *et al.*, 2016). However, in good agreement with the results obtained in this Thesis, a study using TRPC6 KO mice showed changes in the vascular phenotype consisting of increased vascular reactivity and blood pressure, which was a result of a compensatory upregulation of TRPC3 channels. From these data, we could conclude that TRPC3 and TRPC6 channels are not freely interchangeable and that they have distinct and non-redundant roles in the vasculature (Dietrich *et al.*, 2005).

2. GPCR signaling Pathways in the BPN/BPH model: The sympathetic drive

Noradrenaline (NA) and ATP are co-released by sympathetic neurons in the vicinity of VSMCs contributing to the physiological setting of vascular tone. NA induces contraction by activating α1 receptors whilst ATP activates a complex set of purinergic receptors (ionotropic and metabotropic). Pressure myography data show differences in agonists-induced vascular responses between BPN and BPH mice when the α1 agonist PHE is used (Figure R2), but not when the agonist is ATP (Figure R15, left panel). These results are compatible with the reported sympathetic hyper sensitivity of BPH mice (Davern *et al.*, 2009, 2010) and point to the α1 receptor signaling pathway as the more probable culprit of the differences. We have tested the functional impact of TRPC currents on these responses investigating ROCs elicited by PHE, ATP and OAG in BPN and BPH VSMCs (Figure R13). ROCs are not significantly different in magnitude although the sensitivity to Pyr compounds strongly suggests that the TRPC channels mediating the response are mainly TRPC3 in BPH and TRPC6 in BPN, as expected from the expression data. Nevertheless, the different role of TRPC3 and TRPC6 channels contributing to Vm depolarization when PHE (or NA) are the agonists has not been characterized in detail and needs to be further explored.

ATP-induced ROCs are much bigger than ROCs elicited by PHE or OAG (Figure R13). This difference can be easily explained if we consider that ATP is activating also P2X ionotropic receptors. In fact, when the effect of ATP is characterized using

myography, almost 100% of the contractile response can be attributed to the P2X receptors, since ATP does not elicit a contractile response when P2X receptors have been desensitized with αβ-MeATP (Figure R14). These results are in good agreement with the large expression of P2X receptors, compared with P2Y (see below), but are difficult to reconcile with the large effect of Pyr compounds on ATP induced currents, both in BPN and BPH cells (Figure R13C). Although the simplest explanation for these results is to assume some unspecific effect of Pyr compounds on P2X currents, we have not fully characterized the biophysical properties of ATP currents to thoroughly test this possibility.

3. GPCR signaling Pathways in the BPN/BPH model: The UTP divergence

The more striking result that we obtained comparing ROCs currents in BPN and BPH VSMCs was the effect of UTP (Figure R13A), since non-specific cationic currents elicited by this agonist are twice as big in BPN mice. Surprisingly, larger currents do not correlate with bigger responses in terms of vessel contraction, and in fact, BPN mesenteric arteries are almost insensitive to UTP stimulation, with apparent EC_{50} over 100 µM (Figure R14 and R15), whilst BPH arteries respond to much lower UTP concentrations (EC_{50}~3µM). Nevertheless, in agreement with the results obtained with other agonists, the effect of Pyr10 suggests that these UTP activated currents are mainly mediated by TRPC6 channels in BPN and by TRPC3 channels in BPH mice. Physiologically, UTP is released from platelets and endothelial damaged cells, and these remarkable differences in the response of mesenteric arteries can be relevant defining the vascular phenotype of the hypertensive animals.

Several studies in the literature demonstrate some discrepancies in the contribution of TRPC3 channels to the UTP-activated responses. UTP-induced depolarizations and contraction were found to be mediated by TRPC3 channels in cerebral arteries of adult rats (Reading *et al.*, 2005), as well as in rat cardiomyocytes where TRPC3/7 channels were found to be involved in ATP/UTP-mediated responses (Alvarez *et al.*, 2008). In contrast, dual signaling pathways through $P2X_1$-like receptors, and in a less degree through P2Y receptors, but not via TRPC3 channels, appear to be the main molecular mechanisms by which extracellular UTP constricted rat aorta, mesenteric and cerebral arteries (Sugihara *et al.*, 2011). In this latter study, UTP-elicited inward currents could not be blocked by Pyr3 nor intracellularly applied anti-TRPC3 antibodies, although it could be due to the weak TRPC3 expression they found in rat vasculature.

None of these reported differences in the contribution of TRPC channels to the UTP signaling pathway in different species and vascular beds give us any clue to explain our discrepant results in the BPN/BPH model of essential hypertension. Nevertheless, we have explored several hypotheses to explain the lack of correlation between the size of the non-specific cationic currents elicited by UTP and the obtained amount of vessel contraction: (1) A different functional expression of purinergic receptors, (2) a different interaction of UTP receptors and TRPC channels and (3) a significant role of other channels different from TRPC modulating membrane potential.

3.1. Expression of purinergic receptors in the BPN/BPH model.

In agreement with data available in the literature regarding other mouse strains, mRNA expression studies performed in mesenteric arteries from BPN mice showed the presence of $P2X_1$, $P2X_4$, $P2Y_1$, $P2Y_2$, $P2Y_4$ and $P2Y_6$ purinergic receptors (Figure 17R). P2X mRNA levels are over ~200 times bigger than P2Y mRNA, and $P2X_1$ and $P2Y_6$ are the mRNAs more abundant in each family. Interestingly, whilst there are no differences in the expression levels of P2X receptors between BPN and BPH arteries, there is an increased expression of $P2Y_2$ and $P2Y_6$ and a decreased expression of $P2Y_1$ purinergic receptors in the BPH mice (Figure R17).

The functional contribution of P2Y receptors to the contractile response elicited by UTP was explored in BPH mesenteric arteries with pressure myography using several selective agonists and blockers of different purinergic receptors. UTP (a non-selective agonist of P2Y receptors) at 10 μM elicited a response close to maximal in BPH arteries (~30%, Figure R15 and R16). UDP and UTPγS, at the same concentration as UTP, elicited responses that represented a ~70% and ~28% of the UTP response, respectively. If we take into account that UDP is a selective agonist of $P2Y_6$ and UTPγS of $P2Y_{2/4}$ receptors, it seems reasonable to assume that those percentages could approximately reflect the contribution of those receptors to the overall P2Y response. However, the response obtained with 10 μM PSB0474 represents only a ~50% of the UTP response, although at that concentration PSB0474 is supposed to be highly selective to $P2Y_6$. Additionally, partial blockade of UDP and PSB0474 mediated responses were obtained using the specific blocker of $P2Y_6$ receptors MRS2578 (Figure R16B). Taking together, these data suggested a strong contribution of $P2Y_6$ purinergic receptors to the UTP and UDP mediated vasoconstrictor responses in BPH mice and point to the differences in the expression of this receptor as a partial explanation of the differences observed between BPN and BPH regarding the UTP responses. Nevertheless, part of the response to UTP is also mediated by $P2Y_{2/4}$. Certainly, the proper quantitative characterization of the relative contribution of each P2Y receptor would have

required a more detailed characterization of the concentration-response curves and the relative efficacies of each agonist.

All data commented above demonstrate that P2Y receptors are functionally relevant in BPH, and almost irrelevant in BPN arteries (Figures R15 and R16), although UTP is clearly more effective activating ROCs through TRPC channels in BPN mice (Figure R13). These results clearly pose two interesting questions. First, how more P2Y receptors in BPH cells elicited less activation of TRPC currents. And second, how UTP can induce bigger contractile responses activating less TRPC currents. To answer the first question we explored the possibility of a different coupling between P2Y6 receptors and TRPC channels due to a different spatial distribution. To answer the second, we investigated if, in addition to TRPC channels, there were other channels recruited by P2Y6 activation that could be contributing to UTP effects on membrane potential and vascular tone, specially in BPH cells.

3.2 Membrane location of UTP receptors and TRPC channels.

One possible explanation of the lack of correlation between the amount of P2Y receptors and TRPC currents could be a weaker coupling between receptors and channels due to different membrane localization (more distant) of the proteins. GSD Super-resolution imaging has revealed that both, TRPC3 and $P2Y_6$ receptors are expressed in BPN and BPH cells forming clusters of similar sizes (Figure R18). The distribution of minimal intermolecular distances between receptors and channels seems to be very similar in BPN and BPH mice (40-50 nm), although there is a small fraction of $P2Y_6$- and TRPC3-containing clusters which were more distant in BPN (~100 nm) than in BPH (~80 nm) VSMCs cells (Figure R19). The proximity of the receptor and channel clusters is confirmed by PLA studies, although this technique demonstrate a higher punctae distribution for both $P2Y_6$/TRPC3 and $P2Y_6$/TRPC6 associations in BPN compared to BPH cells (Figure R20), even when pre-incubating samples with UTP to activate purinergic signaling pathway (data not shown). The PLA technique gives positive results when proteins are closer than 40 nm, a figure very close to the limit of GSD resolution. Therefore, the results obtained with both techniques seemed to point to a closer location of $P2Y_6$ and TRPC3/6 proteins in BPN cells. We can speculate that proximity correlates with coupling, since DAG diffusion could be more efficient for activating TRPC channels if receptors are closer to channels, although further studies are required to confirm if the differences observed between BPN and BPH are functionally relevant.

3.3 Contribution of CaCCs channels to the UTP signaling pathway in the BPH phenotype

Although TRPC channels are activated by agonist and are responsible for a significant amount of the ROCs, it is well known that in vascular smooth muscle the activation of GPCR coupled to Gq proteins increases $[Ca^{2+}]_i$, and then many calcium dependent proteins, such as Ca^{2+} activated chloride channels (CaCCs). Since the ionic composition of the recording solutions used in the experiments discussed above were designed to block CaCCs, we performed another batch of experiments studying UTP activated currents in the absence of blockers of chloride channels and with high Ca^{2+} in the pipette, to facilitate the activation of CaCCs. With these recording conditions, UTP activated currents should be the sum of the activation of both, TRPC channels and CaCCs, and the comparison with currents recorded without CaCCs theoretically would allow us to define the role of CaCCs. These experiments are shown in Figure R21, and the results turned out to be not as easy to interpret as initially supposed:

- UTP activated currents recorded in BPN VSMCs when TRPC and CaCCs are available ($I_{TRP/CaCC}$) are not significantly different from those recorded when CaCCs are blocked (I_{TRP}). Contrary to that, in BPH VSMCs, $I_{TRP/CaCC}$ are almost twice as big as I_{TRP}.

- $I_{TRP/CaCC}$ are significantly larger in BPH cells.

The simplest interpretation of differences between I_{TRP} and $I_{TRP/CaCC}$ in each group of animals is to consider that CaCCs are not functionally present in BPN VSMCs (since $I_{TRP} \sim I_{TRP/CaCC}$), whilst they represent half of the total current recorded in BPH VSMCs. However, this explanation is unlikely, since $I_{TRP/CaCC}$ currents are sensitive to CaCC blockers both in BPN (Figure D1) and BPH VSMCs. Another possibility could be related with a possible modulation of TRPC currents by intracellular calcium. There are several reports documenting the sensitivity of non-specific cationic currents and those mediated by some known channels like TRPC3 to extracellular and intracellular calcium (see Lichtenegger and Groschner, 2014 for a review). The modulation by intracellular calcium is more controversial, but there is some evidence showing that TRPC3 currents are bigger when calcium entry is moderately buffered with EGTA and much smaller when forming heterotetramers with TRPC1 (Lintschinger *et al.*, 2000). To our knowledge, a detailed characterization of the intracellular calcium dependence of TRPC3/C6 has not been carried out, but in the light of the results depicted in figure R21, it is reasonable to postulate that TRPC currents are smaller in the presence of intracellular calcium.

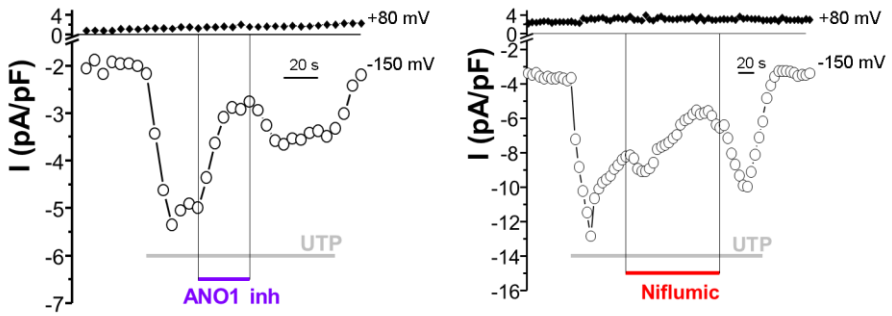

Figure D1. *Effects of CaCCs blockers (10 µM) on UTP (50 µM)-activated currents in a BPN VSMC cell.*

In any case, the lack of correlation between the size of UTP activated currents and the UTP effect on vessel contractility disappears when TRPC and CaCC mediated currents are recorded together ($I_{TRP/CaCC}$), since they are significantly larger in BPH: Larger currents would produce bigger depolarizations, more activation of voltage-dependent calcium channels and more contraction (Figures R14 and R15). In fact, that is the case, since UTP elicited robust and weak depolarizations in BPH and BPN VSMCs, respectively (Figure R23A). However, it is surprising that UTP almost has no effect on BPN VSMCs membrane potential because the size of UTP activated currents (I_{TRP} or $I_{TRP/CaCC}$) is far from being negligible. The result is even more unexpected if we take into account that TRPC channels and CaCCs contribute in basal conditions to membrane potential, as demonstrated by the fact that Pyr compounds or CaCC blockers (Niflumic Acid or ANO1 inhibitor) hyperpolarize both BPN and BPH VSMCs. Is interesting to note that although the effect of blocking basal currents on membrane potential is significantly larger in BPH cells than in BPN cells when Pyr-compounds or ANO-1 inhibitors are used, and although the effect of both inhibitors is quantitatively very similar in BPH cells (Figure R23), the inhibition of CaCCs is much more effective blocking the depolarization induced by UTP in BPH cells (Figure R24).

These results strongly suggest that CaCCs are the main mediators of the depolarization elicited by UTP and point to differences in the expression of CaCCs between BPN and BPH mice. This difference exists at the mRNA level (Figure R22) since mesenteric arteries from BPH mice have a significantly larger expression of the CaCC channel ANO-1 (TMEM16A) and its associated subunit ClCa1 (Sala-Rabanal *et al.*, 2015). Nevertheless, we do not have a satisfactory explanation for the lack of correlation between the activation of TRPC3/6 currents by UTP and the level of changes obtained in membrane potential. It has been described that TRPC3 and TRPC6 channels associate with large conductance Ca^{2+}-activated K^+ channels

(BK_{Ca}) in cultured podocytes (Kim, Alvarez-Baron and Dryer, 2009) and that TRPC1 channels associated with the same channels in vascular smooth muscle cells (Kwan *et al.*, 2009): Ca^{2+} entry trough TRPC channels would activate BK_{Ca} channels and the hyperpolarizing effect of such activation would brake the depolarizing effect of TRPC activation. Certainly, this type of interaction could explain at least in part the lack of correlation between TRPC currents and membrane potential, especially if the association between TRPC and BK_{Ca} channels is dependent on the activation of a signaling pathway. Obviously, the association of TRPC3/6 channels and BK channels must be demonstrated in the BPN/BPH model, and this is a venue certainly worth studying in the future if we consider the already described differences between BPN and BPH mice regarding BK_{Ca} function (Tajada *et al.*, 2013).

Besides differences in tissues and species specificities, CaCCs channels are activated in smooth muscle both, by Ca^{2+} released from the SR and by Ca^{2+} entry via VOCCs, SOCs and ROCs (Leblanc *et al.*, 2015). In addition, it has been shown (Nelson *et al.*, 1995; Jaggar *et al.*, 1998; Yip *et al.*, 2018) that the release of Ca^{2+} from intracellular stores can activate Spontaneous Transient Currents mediated by K^+ (Outward, STOC) and Cl^- (Inward, STICS) channels. In this context, it is quite possible that the hyperpolarizations beyond resting Vm obtained with ANO1 inhibitor or Niflumic Acid during UTP stimulation (figure R24) could be due to the Ca^{2+}-triggered activation of $I_{K(Ca)}$, since it has been previously reported that Niflumic Acid-mediated blockade of $I_{CaCC)}$ enhanced the evoked Ca^{2+} release from intracellular stores without altering its spontaneous release, thus enhancing Ca^{2+}-activated $I_{K(Ca)}$ and hyperpolarization (Hogg, Wang and Large, 1994). It is tempting to speculate that whilst the relative amount of STOCs and STICs could regulate resting membrane potential, the activation of GPCR could activate ROCs (TRPC3/6) and Ca^{2+} release from the SR, activating CaCCs, depolarizing the plasma membrane and activating VOCCs, depending on the intensity of the response of the relative activation of CaCCs and BK channels. This Thesis, and previous work of our lab (Moreno-Domínguez *et al.*, 2009; Tajada *et al.*, 2012, 2013), demonstrate that all these channels are differently expressed in BPN and BPH mice, contributing to set the hypertensive phenotype, although we still do not have a clear picture of the fine tuning of the spatiotemporal relationships of all of them upon the stimulation of all the relevant receptors. Since in a nonlinear system such as VSMCs, subtle differences in one parameter could produce big changes in the final output depending on the state of other parameters in the system, a proper understanding of the final integrated response requires a good understanding of all relevant changes in the system.

In conclusion, it seems that in BPH mesenteric arteries UTP activates a $P2Y_6$-dependent signaling pathway leading to the associated Ca^{2+} release from

intracellular stores, which in turn may activate the opening of membrane CaCCs channels, mainly ANO1 channels, leading to Cl^- efflux and subsequent membrane depolarization. Since these channels do not inactivate (Large and Wang, 1996), the continuous evoked depolarization contribute to the opening of VOCCs channels, leading to Ca^{2+} influx and $[Ca^{2+}]_i$ increase, thus enhancing vasoconstriction.

Several reports have described in detail the kinetics of ANO1-triggered inward currents using pharmacological approaches, with Niflumic Acid and ANO1 inhibitor (Hogg, Wang and Large, 1994; Large and Wang, 1996; Davis *et al.*, 2013; Bradley *et al.*, 2014; Leblanc *et al.*, 2015), and KO and siRNA-silencing mechanisms (Bulley *et al.*, 2012; Dam *et al.*, 2014; Heinze *et al.*, 2014). In all these studies, low unitary conductance (1.2-3.5 pS) of CaCCs channels were confirmed in several smooth muscle and non-smooth muscle tissues. However, differences in the mean open time were reported, with smaller values obtained in excised patches compared to intact cells. In addition, they also reported an increased probability of open channels upon depolarization, but not an increase in the single-channel conductance (Large and Wang, 1996), that seemed to be voltage-dependent with membrane depolarization increasing the efficacy of Ca^{2+} in activating the channels (Leblanc *et al.*, 2015).

Previous studies have also reported the vasodilator effects of Niflumic Acid and ANO1 inhibitor on agonist precontracted arteries (Large and Wang, 1996; Remillard and Leblanc, 2000; Davis *et al.*, 2013). However, almost all of them explored the contribution of ANO1 channels on the Norepinephrine-, Angiotensin II and vasopressin-elicited vasoconstrictions. In fact, the role of chloride channels in Noradrenaline induced responses is well documented, and several studies demonstrated that a reduction in $[Cl^-]_o$ by partial substitution for aspartate or SCN^- inhibited NA-induced oscillations in vascular tone (vasomotion) in rat mesenteric arteries (Boedtkjer *et al.*, 2008). Nevertheless, few reports exist investigating the role of these channels on the UTP-triggered purinergic signaling on vascular contractility (Mitchell *et al.*, 2012). Most of the available studies on UTP-triggered activation of ANO1 channels focused their efforts on epithelial secretion mechanisms (Rock *et al.*, 2009; Dutta *et al.*, 2011). We have not yet characterized the effect of CaCCs inhibitors in the response of UTP in BPH arteries, but we have tested their effect on the response to PHE in BPN, as shown in Figure D2. In agreement with the data obtained in other preparations, the contractile response elicited by the activation of α1-adrenergic receptors is very sensitive to CaCCs blockers.

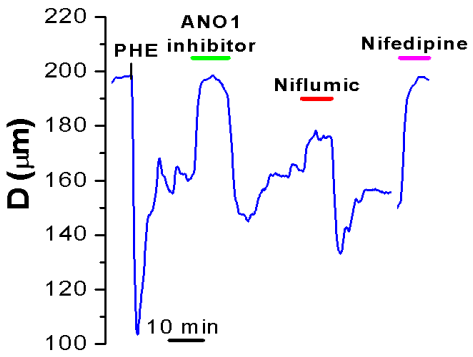

Figure D2. *Effects of CaCCs (10 µM) blockers on PHE (10 µM)-induced vasoconstriction in a BPN mesenteric artery.*

We did not perform a full characterization of the sensitivity of the contractile response in BPN and BPH arteries to these inhibitors, but we hypothesize that the higher responsiveness to PHE typical of BPH (Figure R2) could be also due to a higher role of CaCCs in the α1-adrenergic signaling pathway in BPH mice. In fact, we hypothesize that some of the differences in the kinetic and the intensity of the responses to the activation of different Gq-coupled receptors are related to a different contribution of ROCs mediated by TRPC channels and depolarizing currents mediated by CaCCs, especially ANO1. This hypothesis needs to be confirmed with further experiments, quantitatively characterizing the role of TRPC3/6 and ANO1 in the response elicited by different relevant agonists.

Although qPCR results showed a higher mRNA expression of ANO1 channels in BPH cells, and current-clamp experiments demonstrated a higher contribution of those channels to set the resting Vm in basal conditions and upon stimulation with UTP (Figures R22 and R23), we did not carry out in this Thesis a full characterization of the sensitivity to ANO1 inhibitors of UTP-elicited inward currents. These studies need to be done, but they must be properly designed in order to take into account the complex kinetic behavior of these channels. It is known that changes in $[Cl^-]_o$ modulate the gating kinetics and the permeation properties of the channel both in resting (Contreras-Vite *et al.*, 2016) and in UTP-activated conditions (Muraki, Imaizumi and Watanabe, 1998). A decrease in $[Cl^-]_o$ lead to a decrease in the Cl^- conductance of the channels and $[Cl^-]_o$ has a dual effect on the kinetics of activation, being monoexponential at low concentrations and biexponential at large concentrations (Large and Wang, 1996; Muraki, Imaizumi and Watanabe, 1998; Contreras-Vite *et al.*, 2016).

In addition to this role of $[Cl^-]_o$ modulating the channel conductance and the kinetic properties of ANO1, $[Cl^-]_i$ in VSMCs is also of paramount importance, since the Cl^- equilibrium potential is very close to Vm and changes in $[Cl^-]_i$ would determine the net effect of the opening of chloride channels on resting Vm. Intracellular Cl^- is not at equilibrium in VSMCs as its concentration depends on the activity of several transporters such as NKCC1 (see the Introduction section). Changes in the activity of this cotransporter can influence $[Cl^-]_i$, Cl^- driving force and then the subsequent effect on Vm of ANO1 activity.

Previous studies on hypertensive animal models have reported a higher mRNA and protein expression of NKCC1 cotransporter associated to an increased functional activity and a larger contribution to myogenic tone and agonists-induced vasoconstriction (Meyer *et al.*, 2002; Lee *et al.*, 2010; Ye *et al.*, 2012; Orlov *et al.*, 2015). In addition, the blockade or even the lack of this cotransporter led to decreases in the agonists-induced vasoconstriction and in the mean blood pressure, as shown in studies using bumetanide and in studies in $NKCC1^{-/-}$ KO models (Meyer *et al.*, 2002; Koltsova, Kotelevtsev, *et al.*, 2009; Lee *et al.*, 2010; Ye *et al.*, 2012). We did not find any difference in the mRNA expression of NKCC1 between BPH and BPN mice (Figure R22), although preliminary functional studies revealed a relevant role of NKCC1 modulating PHE-induced constrictions of BPN mesenteric arteries (Figure D3). We are in the process of characterizing the effect of blocking NKCC1 in BPN and BPH mice, aiming to understand the relationship between $[Cl^-]_i$, CaCC activity and the hypertensive phenotype in response to different agonists.

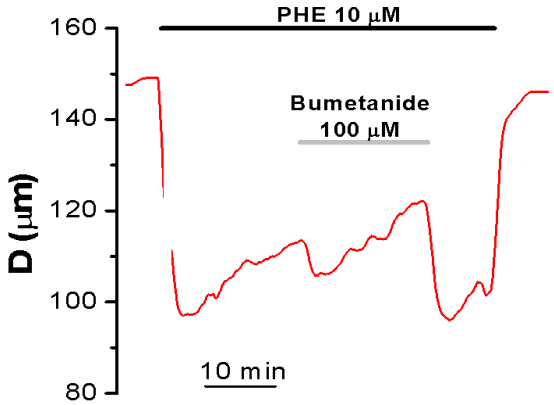

Figure D3. *Vasodilator effect of the NKCC1 blocker bumetanide on PHE-induced vasoconstriction in a BPH mesenteric artery.*

Taken together, our results suggest a clear involvement of TRPC3/C6 and CaCCs (mainly ANO1) in setting the more depolarized resting Vm of BPH VSMC cells. In addition, the role of both channels in the contractile responses induced by GPCR agonists seems to be agonist dependent and quite different in BPN and BPH mice. UTP activation of the $P2Y_6$-dependent purinergic signaling pathway increases membrane DAG (opening TRPC3/C6 channels) and $[Ca^{2+}]_i$ (opening ANO1). The activation of both conductances depolarizes the membrane potential, activates VOCCs, further increases $[Ca^{2+}]_i$ and induces the final contractile response. However, this response is only relevant in BPH arteries, since UTP is almost unable to elicit a response in BPN animals. Although ANO1 channels are good candidates to explain part of the differences between BPN and BPH responses to UTP, it is quite remarkable how subtle changes in the expression of all the players involved in the response to the same agonist produce such a big difference in the final output. A full understanding of the subtle differences that lead to the hypertensive phenotype of BPH mice requires a detailed characterization of the quantitative contribution of all the ionic channels involved in the control of membrane potential during the activation of different GPCRs by different agonists, especially if we consider that other G proteins, in addition to Gq are also relevant. This characterization is certainly part of a future project that will deepen our understanding of the differences between BPN and BPH mice, giving new quantitative insights that will have the huge advantage of allow a full integrative analysis of the results, since all subtle differences can be contextualized in the same model of hypertension.

6

Conclussions

1. BPH mice show a moderate essential hypertensive phenotype, which associates with an increased vascular tone and sympathetic activity. BPH mesenteric arteries exhibit larger responses to the α1-adrenergic agonist PHE than BPN arteries, whilst there are no differences in the effect of ATP.

2. Differences in the expression of TRPC3 and TRPC6 channels, which are the molecular correlate of the ROCs currents, can explain the differences in the α1-adrenergic responses. The mRNA expression profile of TRPC channels demonstrate a larger expression of TRPC3 and a lower expression of TRPC6 channels in VSMCs from mesenteric BPH arteries.

3. Pyr compounds (10 and 3) and anti-TRPC antibodies are good tools to investigate the functional role of TRPC channels in native systems. Control experiments carried out in a heterologous expression system (CHO cells) have validated the use of Pyr compounds as blockers of TRC6 channels, and anti-TRPC3 antibodies as blockers of TRPC3 channels.

4. The effect of Pyr compounds on PHE induced vasoconstriction is larger in BPN arteries, in good agreement with the higher expression of TRPC6 in those cells.

5. Basal TRPC currents in BPH VSMCs are larger, more sensitive to intracellular anti-TRPC3 antibody and less sensitive to Pyr3/10 blockers than in BPN cells. Altogether, these results suggest a higher contribution of TRPC3 channels to basal currents in BPH VSMCs.

6. PLA and immunocytochemical experiments demonstrate a different profile of TRPC3/C6 association in BPH VSMCs. BPH cells have a higher expression of TRPC3 channels in the membrane, either as homo or as heterotetramers with TRPC6, whilst TRPC6 homomultimers predominate in BPN VSMCs.

7. PHE, ATP and OAG-activated currents are similar in BPN and BPH VSMCs, while UTP activated ROCs are smaller in BPH VSMCs. The closer proximity between TRPC3/6 channels and $P2Y_6$ UTP receptors in BPN VSMCs suggested by PLA and Super-resolution imaging techniques could explain these differences. However, ROCs elicited with all the stimuli are less sensitive to Pyr compounds in BPH cells, which agree with the higher expression of TRPC3 channels in these cells.

8. Pressure myography studies show that ATP induced vasoconstriction is mainly mediated through $P2X_1$ receptors activation and is unchanged in BPH arteries. In contrast, UTP effect is much larger in BPH vessels. The increased expression and functional contribution of $P2Y_6$ receptors in BPH mesenteric VSMCs can account for this effect of UTP.

9. In current-clamp experiments, UTP induced depolarization of VSMCs cells is significantly larger in BPH cells. This effect is insensitive to Pyr10 but can be inhibited by CaCCs blockers such as Niflumic acid and ANO1-inhibitor. There is also a larger contribution of CaCCs to UTP activated currents in BPH cells, and a

larger mRNA expression of ANO1 and its regulatory subunit $ClCa_1$. These results strongly suggest that UTP-induced depolarization is mediated by the activation of ANO1 channels.

10. GPCR signaling pathways in BPN/PBH mice are mediated by the integrated coupling between GPCRs and TRPC3/6 and ANO1 channels, although the relative importance of those channels seems to be receptor dependent. Although both TRPC and ANO1 channels contribute to set the resting Vm of VSMCs, ANO1 channels are the essential mediators of the UTP-induced depolarizations. In this context, differences in the functional expression and/or the coupling between GPCRs and TRPC and CaCCs channels could contribute to the increased reactivity of BPH arteries, pointing out to all these proteins as new potential therapeutic targets for the treatment of essential hypertension

7

References

REFERENCES

Aaronson, P. I., Ward, J. P. T. and Wiener, C. M. (2004) *The Cardiovascular System at a Glance*. 2nd edn. Oxford: Blackwell Publishing.

Adebiyi, A. *et al.* (2010) 'Isoform-selective physical coupling of TRPC3 channels to IP3 receptors in smooth muscle cells regulates arterial contractility', *Circulation Research*, 106(10), pp. 1603–1612.

Adebiyi, A. *et al.* (2012) 'An elevation in physical coupling of type 1 inositol 1,4,5-trisphosphate (IP3) receptors to transient receptor potential 3 (TRPC3) channels constricts mesenteric arteries in genetic hypertension', *Hypertension*, 60(5), pp. 1213–1219.

Albert, A. P. *et al.* (2006) 'TRPC3 properties of a native constitutively active Ca2+-permeable cation channel in rabbit ear artery myocytes', *Journal of Physiology*, 571(2), pp. 361–369.

Alexander, S. *et al.* (2017) *Concise Guide to Pharmacology 20178/2018: Other ion channels.*, *Br J Pharmacol*.

Alvarez, J. *et al.* (2008) 'ATP/UTP activate cation-permeable channels with TRPC3/7 properties in rat cardiomyocytes', *American journal of physiology. Heart and circulatory physiology*, pp. 21–28.

Ambudkar, I. S., de Souza, L. B. and Ong, H. L. (2017) 'TRPC1, Orai1, and STIM1 in SOCE: Friends in tight spaces', *Cell Calcium*. Elsevier Ltd, 63, pp. 33–39.

Babenko, A. P., Aguilar-Bryan, L. and Bryan, J. (1998) 'A view of SUR/K IR 6.X, K ATP channels', *Annual Review of Physiology*, 60, pp. 667–687.

Bannister, J. P. *et al.* (2012) 'Transcriptional upregulation of α2δ-1 elevates arterial smooth muscle cell voltage-dependent Ca2+ channel surface expression and cerebrovascular constriction in genetic hypertension', *Hypertension*, 60(4), pp. 1006–1015.

Bar, I. *et al.* (2008) 'Knockout Mice Reveal a Role for P2Y 6 Receptor in Macrophages , Endothelial Cells , and Vascular Smooth Muscle Cells', *Molecular Pharmacology*, 74(3), pp. 777–84.

Berg, T. (2003) 'The vascular response to the K+channel inhibitor 4-aminopyridine in hypertensive rats', *European Journal of Pharmacology*, 466(3), pp. 301–310.

Billaud, M. *et al.* (2011) 'Pannexin1 regulates α1-adrenergic receptor-mediated vasoconstriction', *Circulation Research*, 109(1), pp. 80–85.

Boedtkjer, D. M. B. *et al.* (2008) 'Vasomotion has chloride-dependency in rat mesenteric small arteries', *Pflugers Archiv European Journal of Physiology*, 457(2), pp. 389–404.

Bolte, S. and Cordelieres, F. P. (2006) 'A guided tour into subcellular colocalisation analysis in light microscopy', *Journal of Microscopy*, 224(3), pp. 13–232.

Bradley, E. *et al.* (2014) 'Pharmacological characterization of TMEM16A currents', *Channels*, 8(4), pp. 308–320.

Bradley, K. K. *et al.* (1999) 'Kir2.1 encodes the inward rectifier potassium channel in rat arterial smooth muscle cells', *J Physiol*, 515 (Pt 3(1999), pp. 639–651.

Brake, A. J., Wagenbach, M. J. and Julius, D. (1994) 'New structural motif for ligand-gated ion channels defined by an ionotropic ATP receptor', *Nature*. Nature Publishing Group, 371, p. 519.

Bugaj, V. *et al.* (2005) 'Functional properties of endogenous receptor- and store-operated calcium influx channels in HEK293 cells', *Journal of Biological Chemistry*, 280(17), pp. 16790–16797.

Bulley, S. *et al.* (2012) 'TMEM16A/ANO1 channels contribute to the myogenic response in cerebral arteries', *Circulation Research*, 111(8), pp. 1027–1036.

Burnstock, G. (1978) 'No Title', in Straub, R. and Bolis, L. (eds) *A basis for distinguishing two types of purinergic receptor, in Cell Membrane Receptors for Drugs and Hormones: a Multidisciplinary Approach*. New York.: Raven Press, pp. 107–118.

Burnstock, G. (1980) 'Purinergic nerves and receptors', *Progress in biochemical pharmacology*, 16, p. 141—154.

Burnstock, G. (2007) 'Purine and pyrimidine receptors', *Cellular and Molecular Life Sciences*, 64(12), pp. 1471–1483.

Burnstock, G. (2017) 'Purinergic Signaling in the Cardiovascular System', *Circulation Research*, 120(1), pp. 207–228.

Burnstock, G. and Kennedy, C. (1985) 'Is there a basis for distinguishing two types of P2-purinoceptor?', *General Pharmacology*, 16(5).

Burnstock, G. and Ralevic, V. (2013) 'Purinergic Signaling and Blood Vessels in Health and Disease', *Pharmacological Reviews*, 66(1), pp. 102–192.

Catterall, W. A. (2011) 'Voltage-Gated Calcium Channels', *Cardiac Electrophysiology: From Cell to Bedside*, pp. 12–24.

Chen, X. *et al.* (2010) 'Increased rhythmicity in hypertensive arterial smooth muscle is linked to transient receptor potential canonical channels', *Journal of Cellular and Molecular Medicine*, 14(10), pp. 2483–2494.

Chiu, C. L. *et al.* (2014) 'Identification of genes with altered expression in male and female Schlager hypertensive mice', *BMC Medical Genetics*, 15(1), pp. 2–7. doi: 10.1186/s12881-014-0101-x.

Clapham, D. E. (2003) 'TRP channels as cellular sensor', *Nature*, 426(December), pp. 517–524.

Contreras-Vite, J. A. *et al.* (2016) 'Revealing the activation pathway for TMEM16A chloride channels from macroscopic currents and kinetic models', *Pflugers Archiv European Journal of Physiology*, 468(7), pp. 1241–1257.

Cox, R. H. *et al.* (2008) 'Voltage gated K+channel expression in arteries of Wistar-Kyoto and spontaneously hypertensive rats', *American Journal of Hypertension*, 21(2), pp. 213–218.

Cox, R. H., Folander, K. and Swanson, R. (2001) 'Differential Expression of Voltage-Gated K+ Channel Genes in Arteries From Spontaneously Hypertensive and Wistar-Kyoto Rats', *Hypertension*, 37(5), pp. 1315–1322.

Dam, V. S. *et al.* (2014) 'TMEM16A knockdown abrogates two different Ca2+-activated Cl - currents and contractility of smooth muscle in rat

mesenteric small arteries', *Pflugers Archiv European Journal of Physiology*, 466(7), pp. 1391–1409.

Davern, P. J. *et al.* (2009) 'Role of the sympathetic nervous system in schlager genetically hypertensive mice', *Hypertension*, 54(4), pp. 852–859.

Davern, P. J. *et al.* (2010) 'Cardiovascular reactivity and neuronal activation to stress in Schlager genetically hypertensive mice', *Neuroscience*. Elsevier Inc., 170(2), pp. 551–558.

Davis, A. J. *et al.* (2013) 'Potent vasorelaxant activity of the TMEM16A inhibitor T16Ainh-A01', *British Journal of Pharmacology*, 168(3), pp. 773–784.

Dehaven, W. I. *et al.* (2009) 'TRPC channels function independently of STIM1 and Orai1', *Journal of Physiology*, 587(10), pp. 2275–2298.

Dempsey, G. T. *et al.* (2011) 'Evaluation of fluorophores for optimal performance in localization-based super-resolution imaging', *Nature Methods*, 8(12), pp. 1027–1040.

Denoroy, L. *et al.* (1985) 'Catechoimine concentrations in discrete brain nuclei and sympathetic tissues of genetically hypertensive mice', 340, pp. 148–150.

Dickson, V. K., Pedi, L. and Long, S. B. (2014) 'Structure and insights into the function of a Ca2+-activated Cl-channel', *Nature*. Nature Publishing Group, 516(7530), pp. 13–218.

Dietrich, A. *et al.* (2005) 'Increased vascular smooth muscle contractility in TRPC6-/-mice', *Molecular and cellular biology*, 25(16), p. 6980.

Directive, E. U. (2010) '63/EU of the European parliament and of the council of 22 September 2010 on the protection of animals used for scientific purposes', *Official Journal of the European Union*, 276, pp. 33–74.

Dixon, R. E. *et al.* (2017) 'Ground State Depletion Super-resolution Imaging in Mammalian Cells', *Journal of Visualized Experiments*, (129), pp. 1–9.

Dutta, A. K. *et al.* (2011) 'Identification and functional characterization of TMEM16A, a Ca2+-activated Cl-channel activated by extracellular nucleotides, in biliary epithelium', *Journal of Biological Chemistry*, 286(1), pp. 766–776.

Drury, A. N. and Szent-Györgyi, A. (1929) 'The physiological activity of adenine compounds with especial reference to their action upon the mammalian heart', *The Journal of Physiology*, pp. 213–237.

Earley, S. and Brayden, J. E. (2015) 'Transient Receptor Potential Channels in the Vasculature', *Physiological Reviews*, 95(2), pp. 645–690.

Edwards, J. C. and Kahl, C. R. (2010) 'Chloride channels of intracellular membranes', *FEBS Letters*, 584(10), pp. 2102–2111.

Erb, L. and Weisman, G. A. (2012) 'Coupling of P2Y receptors to G proteins and other signaling pathways', *Wiley Interdisciplinary Reviews: Membrane Transport and Signaling*, 1(6), pp. 789–803.

Fenger-Gron, J., Mulvany, M. J. and Christensen, K. L. (1995) 'Mesenteric blood pressure profile of conscious, freely moving rats.', *The Journal of Physiology*, 488(3), pp. 753–760.

Fölling, J. *et al.* (2008) 'Fluorescence nanoscopy by ground-state depletion and single-molecule return', *Nature Methods*, 5(11), pp. 943–945.

Foster, M. N. and Coetzee, W. A. (2016) 'K_{ATP} Channels in the Cardiovascular System', *Physiological Reviews*, 96(1), pp. 177–252.

Fredriksson, S. *et al.* (2002) 'Protein detection using proximity-dependent DNA ligation assays. Nature Biotechnology 20, 473 - 477 (2002).', *Nat Biotechnol*, 20(5), pp. 473–477.

Friese, R. S. *et al.* (2005) 'Common genetic mechanisms of blood pressure elevation in two independent rodent models of human essential hypertension', *American Journal of Hypertension*, 18(5), pp. 633–652.

Gamper, N., Stockand, J. D. and Shapiro, M. S. (2005) 'The use of Chinese hamster ovary (CHO) cells in the study of ion channels', *Journal of Pharmacological and Toxicological Methods*, 51(3 SPEC. ISS.), pp. 177–185.

Ghosh, D. *et al.* (2017) 'Calcium channels in vascular smooth muscle cells', *Advances in Pharmacology*, 78, pp. 49–87.

Gitterman, D. P. and Evans, R. J. (2001) 'Nerve evoked P2X receptor contractions of rat mesenteric arteries; dependence on vessel size and lack of role of L-type calcium channels and calcium induced calcium release', *British Journal of Pharmacology*, 132(6), pp. 1201–1208.

Gonzales, A. L. *et al.* (2014) 'A PLCγ1-Dependent, Force-Sensitive Signaling Network in the Myogenic Constriction of Cerebral Arteries', *Science Signaling*, 7(327).

Gunst, S. J. and Zhang, W. (2008) 'Actin cytoskeletal dynamics in smooth muscle: a new paradigm for the regulation of smooth muscle contraction', *AJP: Cell Physiology*, 295(3), pp. C576–C587.

Gutman, G. A. *et al.* (2005) 'International Union of Pharmacology. LIII. Nomenclature and molecular relationships of inwardly rectifying potassium channels', *Pharmacological reviews*, 57(4), pp. 473–508.

Hansen, M. A. *et al.* (1999) 'P(2X) (purinergic) receptor distributions in rat blood vessels', *Journal of the Autonomic Nervous System*, 75(2–3), pp. 147–155.

Heinze, C. *et al.* (2014) 'Disruption of vascular Ca2+activated chloride currents lowers blood pressure', *The Journal of clinical investigation*, 124(2), pp. 675–86.

Henis, Y. I. *et al.* (2003) 'Co-localization analysis of complex formation among membrane proteins by computerized fluorescence microscopy', *J Microsc*, 212(July), pp. 122–131.

Herring, N. and Paterson, D. J. (2018) *Levick´s Introduction to Cardiovascular Physiology*. 6th edn. Edited by C. Press and T. and F. Group.

Hibino, H. *et al.* (2010) 'Inwardly Rectifying Potassium Channels: Their Structure, Function, and Physiological Roles', *Physiology Reviews*, 90, pp. 291–366.

Hirst, G. D. and Edwards, F. R. (1989) 'Sympathetic neuroeffector transmission in arteries and arterioles', *Physiological Reviews*, 69(2), pp. 546–604.

Hoffmann, C. *et al.* (2008) 'Agonist-selective, receptor-specific interaction of human P2Y receptors with ??-arrestin-1 and -2', *Journal of Biological Chemistry*, 283(45), pp. 30933–30941.

Hofmann, T. *et al.* (1999) 'Direct activation of human TRPC6 and TRPC3 channels by diacylglycerol', *Nature*. Macmillan Magazines Ltd., 397, p. 259.

Hofmann, T. *et al.* (2002) 'Subunit composition of mammalian transient receptor potential channels in living cells.', *Proc Natl Acad Sci U S A*, 99(11), pp. 7461–7466.

Hogg, R. C., Wang, Q. and Large, W. A. (1994) 'Action of niflumic acid on evoked and spontaneous calcium- activated chloride and potassium currents in smooth muscle cells from rabbit portal vein', *Br J Pharmacol*, 112, pp. 977–984.

Huang, G. N. *et al.* (2006) 'STIM1 carboxyl-terminus activates native SOC, Icrac and TRPC1 channels', *Nature Cell Biology*. Nature Publishing Group, 8, p. 1003.

Jackson, W. F. (2000) 'Ion Channels and Vascular Tone', *Hypertension*, 35(1), pp. 173–178.

Jackson, W. F. (2017) 'Boosting the signal: Endothelial inward rectifier K+channels', *Microcirculation*, 24(3), pp. 1–11.

Jackson, W. F. (2017) 'Potassium Channels in Regulation of Vascular Smooth Muscle Contraction and Growth', pp. 89–144.

Jaggar, J. H. *et al.* (1998) 'Ca 2+ channels, ryanodine receptors and Ca 2+ -activated K + channels: a functional unit for regulating arterial tone', *Acta Physiologica Scandinavica*, 164, pp. 577–587.

Jentsch, T. J. (2015) 'Discovery of CLC transport proteins: Cloning, structure, function and pathophysiology', *Journal of Physiology*, 593(18), pp. 4091–4109.

Jepps, T. A. *et al.* (2011) 'Downregulation of Kv7.4 channel activity in primary and secondary hypertension', *Circulation*, 124(5), pp. 602–611.

Kauffenstein, G. *et al.* (2010) 'NTPDase1 (CD39) controls nucleotide-dependent vasoconstriction in mouse', *Cardiovascular Research*, 85(1), pp. 204–213.

Kauffenstein, G. *et al.* (2016) 'Central Role of P2Y6 UDP Receptor in Arteriolar Myogenic Tone', *Arteriosclerosis, thrombosis and Vascular Biology*, 36(8), pp. 1598–1606.

Kharade, S. V. *et al.* (2013) 'The β3 subunit contributes to vascular calcium channel upregulation and hypertension in angiotensin II-infused C57BL/6 mice', *Hypertension*, 61(1), pp. 137–142.

Kim, E. Y., Alvarez-Baron, C. P. and Dryer, S. E. (2009) 'Canonical transient receptor potential channel (TRPC)3 and TRPC6 associate with large-conductance Ca2+-activated K+ (BKCa) channels: role in BKCa trafficking to the surface of cultured podocytes.', *Molecular Pharmacology*, 75(3), p. 466 LP-477.

Kitamura, K. and Yamazaki, J. (2001) 'Chloride Channels and Their Functional Roles in Smooth Muscle Tone in the Vasculature.', *The Japanese Journal of Pharmacology*, 85(4), pp. 351–357.

Kiyonaka, S. *et al.* (2009) 'Selective and direct inhibition of TRPC3 channels underlies biological activities of a pyrazole compound', *Proceedings of the National Academy of Sciences*, 106(13), pp. 5400–5405.

Koltsova, S. V., Kotelevtsev, S. V., *et al.* (2009) 'Excitation-contraction coupling in resistance mesenteric arteries: Evidence for NKCC1-mediated pathway', *Biochemical and Biophysical Research Communications*. Elsevier Inc., 379(4), pp. 1080–1083.

Koltsova, S. V., Maximov, G. V., *et al.* (2009) 'Myogenic tone in mouse mesenteric arteries: Evidence for P2Y receptor-mediated, Na+, K+, 2Cl-cotransport-dependent signaling', *Purinergic Signalling*, 5(3), pp. 343–349.

Krege, J. H. *et al.* (1995) 'A Noninvasive Computerized Tail-Cuff System for Measuring Blood Pressure in Mice', *Hypertension*, 25(5), p. 1111 LP-1115.

von Kügelgen, I. and Starke, K. (1968) 'Noradrenaline and adenosine triphosphate as co-transmitters of neurogenic vasoconstriction in rabbit mesenteric artery', *The Journal of Phisiology*, pp. 479–493.

Kwan, H. Y. *et al.* (2009) 'TRPC1 associates with BKCachannel to form a signal complex in vascular smooth muscle cells', *Circulation Research*, 104(5), pp. 670–678.

Large, W. a and Wang, Q. (1996) 'Characteristics and physiological role of the Ca(2+)-activated Cl- conductance in smooth muscle.', *The American journal of physiology*, 271(2 Pt 1), pp. C435–C454.

Leblanc, N. *et al.* (2015) 'Molecular and Functional Significance of Ca^{2+} -Activated Cl^{-} Channels in Pulmonary Arterial Smooth Muscle', *Pulmonary Circulation*, 5(2), pp. 244–268.

Lee, H. A. *et al.* (2010) 'Promoter hypomethylation upregulates Na+-K+-2Cl-cotransporter 1 in spontaneously hypertensive rats', *Biochemical and Biophysical Research Communications*. Elsevier Inc., 396(2), pp. 252–257.

Lerman, L. O. *et al.* (2005) 'Animal models of hypertension: An overview', *Journal of Laboratory and Clinical Medicine*, 146(3), pp. 160–173.

Levy, M. N. and Pappano, A. J. (2007) 'Cardiovascular Physiology', in *Cardiovascular Physiology*. 9th edn. Philadelphia: Mosby, Elsevier.

Lewis, C. J. and Evans, R. J. (2000) 'Lack of run-down of smooth muscle P2X receptor currents recorded with the amphotericin permeabilized patch technique, physiological and pharmacological characterization of the properties of mesenteric artery P2X receptor ion channels', *British Journal of Pharmacology*, 131(8), pp. 1659–1666.

Lichtenegger, M. and Groschner, K. (2014) 'TRPC3: A Multifunctional Signaling Molecule', in Nilius, B. and Flockerzi, V. (eds) *Mammalian Transient Receptor Potential (TRP) Cation Channels: Volume I*. Berlin, Heidelberg: Springer Berlin Heidelberg, pp. 67–84.

Linsdell, P. (2014) 'Functional architecture of the CFTR chloride channel', *Molecular Membrane Biology*. Taylor & Francis, 31(1), pp. 1–16.

Lintschinger, B. *et al.* (2000) 'Coassembly of Trp1 and Trp3 proteins generates diacylglycerol- and Ca2+-sensitive cation channels', *Journal of Biological Chemistry*, 275(36), pp. 27799–27805.

Littler Dene, R. *et al.* (2010) 'The enigma of the CLIC proteins: Ion channels, redox proteins, enzymes, scaffolding proteins?', *FEBS Letters*. Wiley-Blackwell, 584(10), pp. 2093–2101.

Liu, D. *et al.* (2009) 'Increased transient receptor potential canonical type 3 channels in vasculature from hypertensive rats', *Hypertension*, 53(1), pp. 70–76.

Livak, K. J. and Schmittgen, T. D. (2001) 'Analysis of relative gene expression data using real-time quantitative PCR and the 2-ΔΔCT method', *Methods*, 25(4), pp. 402–408.

López, J. J. *et al.* (2006) 'Interaction of STIM1 with endogenously expressed human canonical TRP1 upon depletion of intracellular Ca2+ stores', *Journal of Biological Chemistry*, 281(38), pp. 28254–28264.

Malmsjö, M. *et al.* (2000) 'The stable pyrimidines UDPbetaS and UTPgammaS discriminate between the P2 receptors that mediate vascular contraction and relaxation of the rat mesenteric artery.', *British journal of pharmacology*, 131(1), pp. 51–6.

Martinez-Lemus, L. A. (2012) 'The dynamic structure of arterioles', *Basic and Clinical Pharmacology and Toxicology*, 110(1), pp. 5–11.

Maruyama, Y. *et al.* (2006) 'Heteromultimeric TRPC6-TRPC7 channels contribute to arginine vasopressin-induced cation current of A7r5 vascular smooth muscle cells', *Circulation Research*, 98(12), pp. 1520–1527.

Matchkov, V. V. *et al.* (2008) 'Bestrophin-3 (vitelliform macular dystrophy 2-like 3 protein) is essential for the cGMP-dependent calcium-activated chloride conductance in vascular smooth muscle cells', *Circulation Research*, 103(8), pp. 864–872.

Matchkov, V. V., Boedtkjer, D. M. and Aalkjaer, C. (2015) 'The role of Ca2+activated Cl-channels in blood pressure control', *Current Opinion in Pharmacology*. Elsevier Ltd, 21, pp. 127–137.

McGrath, J. C. *et al.* (2005) 'New aspects of vascular remodelling: The involvement of all vascular cell types', *Experimental Physiology*, 90(4), pp. 469–475.

Mercado, J. *et al.* (2014) 'Local control of TRPV4 channels by AKAP150-targeted PKC in arterial smooth muscle', *The Journal of General Physiology*, 143(5), pp. 559–575.

Meyer, J. W. *et al.* (2002) 'Decreased blood pressure and vascular smooth muscle tone in mice lacking basolateral Na(+)-K(+)-2Cl(-) cotransporter.', *American journal of physiology. Heart and circulatory physiology*, 283(5), pp. H1846–H1855.

Minghui, L., Yong, Y. and Jian, Y. (2011) 'Structural Biology of TRP Channels', in Islam, M. S. (ed.) *Transient receptor Potential Channels*, pp. 1–23.

Mio, K. *et al.* (2007) 'The TRPC3 Channel Has a Large Internal Chamber Surrounded by Signal Sensing Antennas',

Journal of Molecular Biology. Elsevier Ltd, 367(2), pp. 373–383.

Mitchell, C. *et al.* (2012) 'A Ca 2+-dependent chloride current and Ca 2+ influx via Ca v1.2 ion channels play major roles in P2Y receptor-mediated pulmonary vasoconstriction', *British Journal of Pharmacology*, 166(4), pp. 1503–1512.

Molleman, A. (2003) 'Patch Clamping: An Introductory Guide to Patch Clamp Electrophysiology.', *Wiley*, p. 186.

Moreno-Domínguez, A. *et al.* (2009) 'De novo expression of Kv6.3 contributes to changes in vascular smooth muscle cell excitability in a hypertensive mice strain', *Journal of Physiology*, 587(3), pp. 625–640.

Mulvany, M. J. and Aalkjaer, C. (1990) 'Physiological Reviews of Small Arteries', *Physiological reviews*, 70(4), pp. 921–961.

Muraki, K., Imaizumi, Y. and Watanabe, M. (1998) 'Effects of UTP on membrane current and potential in rat aortic myocytes', *Eur.J Pharmacol.*, 360, pp. 239–247.

Nayak, S. *et al.* (2015) 'Characterization of Dahl salt-sensitive rats with genetic disruption of the A2B adenosine receptor gene: implications for A2B adenosine receptor signaling during hypertension', *Purinergic Signalling*, 11(4), pp. 519–531.

Nelson, M. T. *et al.* (1995) 'Relaxation of Arterial Smooth-Muscle by Calcium Sparks', *Science*, 270(5236), pp. 633–637.

Nesin, V. and Tsiokas, L. (2014) 'TRPC1', in Nilius, B. and Flockerzi, V. (eds) *Mammalian Transient Receptor Potential (TRP) Cation Channels: Volume I*. Berlin, Heidelberg: Springer Berlin Heidelberg, pp. 15–51.

Nilius, B. and Droogmans, G. (2003) 'Amazing chloride channels: An overview', *Acta Physiologica Scandinavica*, 177(2), pp. 119–147.

Nilius, B. and Owsianik, G. (2011) 'The transient receptor potential family of ion channels', *Genome Biol*, 12(3), p. 218.

Nishimura, A. *et al.* (2016) 'Purinergic P2Y 6 receptors heterodimerize with angiotensin AT1 receptors to promote angiotensin II – induced hypertension', 9(411), pp. 1–13.

Noorani, M. M. Z., Noel, R. C. and Marrelli, S. P. (2011) 'Upregulated TRPC3 and downregulated TRPC1 channel expression during hypertension is associated with increased vascular contractility in rat', *Frontiers in Physiology*, JUL(July), pp. 1–9.

North, R. A. and Surprenant, A. (2000) 'Pharmacology of Cloned P2X receptors', (2), pp. 79–99.

Olah, M. E. and Stiles, G. L. (2000) 'The role of receptor structure in determining adenosine receptor activity', *Pharmacology and Therapeutics*, 85(2), pp. 55–75.

Orlov, S. N. *et al.* (2015) 'NKCC1 and NKCC2: The pathogenetic role of cation-chloride cotransporters in hypertension', 2(2), pp. 186–196.

Pedemonte, N. and Galietta, L. J. V. (2014) 'Structure and Function of TMEM16 Proteins (Anoctamins)', *Physiological Reviews*, 94(2), pp. 419–459.

Pijacka, W. *et al.* (2016) 'Purinergic receptors in the carotid body as a new drug target for controlling hypertension', *Nature Medicine*, 22(10), pp. 1151–1159.

Poroca, D. R., Pelis, R. M. and Chappe, V. M. (2017) 'ClC channels and transporters: Structure, physiological functions, and implications in human chloride channelopathies', *Frontiers in Pharmacology*, 8(MAR), pp. 1–25.

Pulina, M. V *et al.* (2010) 'Upregulation of Na ƨ and Ca 2 ƨ transporters in arterial smooth muscle from ouabain-induced hypertensive rats', (6).

Ralevic, V. and Dunn, W. R. (2015) 'Purinergic transmission in blood vessels', *Autonomic Neuroscience: Basic and Clinical*. Elsevier B.V., 191, pp. 48–66.

Reading, S. A. *et al.* (2005) 'TRPC3 mediates pyrimidine receptor-induced depolarization of cerebral arteries.', *American journal of physiology. Heart and circulatory physiology*, 288(5), pp. H2055-61.

Remillard, C. V and Leblanc, N. (2000) 'Role of Ca 2 1 - and swelling-activated Cl 2 channels in a 1 -adrenoceptor-mediated tone in pressurized rabbit mesenteric arterioles', 46(August), pp. 557–568.

Rock, J. R. *et al.* (2009) 'Transmembrane protein 16A (TMEM16A) is a Ca2+ -regulated Cl- secretory channel in mouse airways', *Journal of Biological Chemistry*, 284(22), pp. 14875–14880.

Rummery, N. M. *et al.* (2007) 'ATP is the predominant sympathetic neurotransmitter in rat mesenteric arteries at high pressure', *Journal of Physiology*, 582(2), pp. 745–754.

Sabirov, R. Z. and Okada, Y. (2009) 'The maxi-anion channel: A classical channel playing novel roles through an unidentified molecular entity', *Journal of Physiological Sciences*, 59(1), pp. 3–21.

Sala-Rabanal, M. *et al.* (2015) 'Secreted CLCA1 modulates TMEM16A to activate Ca2+-dependent chloride currents in human cells', *eLife*, 2015(4), pp. 1–14.

Schlager, G. (1981) 'Longevity in spontaneously hypertensive mice', *Experimental Gerontology*, 16(4), pp. 325–330.

Schlager, G., Freeman, R. and El Seoudy, A. A. (1983) 'Genetic study of norepinephrine in brains of mice selected for differences in blood pressure', *Journal of Heredity*, 74(2), pp. 97–100.

Schlager, G. and Sides, J. (1997) 'Characterization of hypertensive and hypotensive inbred strains of mice', *Laboratory animal science*, 47(3), p. 288—292.

Schleifer, H. *et al.* (2012) 'Novel pyrazole compounds for pharmacological discrimination between receptor-operated and store-operated Ca(2+) entry pathways.', *British journal of pharmacology*, 167(8), pp. 1712–22.

Sexton, J. E. *et al.* (2016) 'The contribution of TRPC1, TRPC3, TRPC5 and TRPC6 to touch and hearing', *Neuroscience Letters*. Elsevier Ireland Ltd, 610, pp. 36–42. doi: 10.1016/j.neulet.2015.10.052.

Sharma, A. *et al.* (2018) 'CLCA2 is a positive regulator of store- operated calcium entry and TMEM16A', pp. 1–20.

Smith, P. D. *et al.* (2008) 'K_{IR} channels function as electrical amplifiers in rat vascular smooth muscle', *The Journal of Physiology*, 586(4), pp. 1147–1160.

Sneddon, P. and Burnstock, G. (1985) 'ATP as a co-transmitter in rat tail artery', *European Journal of Pharmacology*, 106, pp. 149–152.

Stenmark, K. R. *et al.* (2013) 'The Adventitia: Essential Regulator of Vascular Wall Structure and Function', *Annual Review of Physiology*, 75(1), pp. 23–47.

Sugihara, M. *et al.* (2011) 'Dual signaling pathways of arterial constriction by extracellular uridine 5'-triphosphate in the rat.', *Journal of pharmacological sciences*, 115, pp. 293–308.

Tajada, S. *et al.* (2012) 'High blood pressure associates with the remodelling of inward rectifier K^+ channels in mice mesenteric vascular smooth muscle cells', *The Journal of Physiology*, 590(23), pp. 6075–6091.

Tajada, S. *et al.* (2013) 'Down-regulation of CaV1.2 channels during hypertension: How fewer CaV1.2 channels allow more Ca2+ into hypertensive arterial smooth muscle', *Journal of Physiology*, 591(24), pp. 6175–6191.

Tykocki, N. R., Boerman, E. M. and Jackson, W. F. (2017) 'Smooth Muscle Ion Channels and Regulation of Vascular Tone in Resistance Arteries and Arterioles', *Compr Physiol*, 7(2), pp. 485–581.

Ureña, J., del Valle-Rodríguez, A. and López-Barneo, J. (2007) 'Metabotropic Ca2+channel-induced calcium release in vascular smooth muscle', *Cell Calcium*, 42(4–5), pp. 513–520.

Valera, S. *et al.* (1994) 'A new class of ligand-gated ion channel defined by P2X receptor for extracellular ATP', *Nature*. Nature Publishing Group, 371, p. 516.

Del Valle-Rodríguez, A., López-Barneo, J. and Ureña, J. (2003) 'Ca2+ channel-sarcoplasmic reticulum coupling: A mechanism of arterial myocyte contraction without Ca2+ influx', *EMBO Journal*, 22(17), pp. 4337–4345.

Vial, C. and Evans, R. J. (2002) 'P2X(1) receptor-deficient mice establish the native P2X receptor and a P2Y6-like receptor in arteries.', *Molecular pharmacology*, 62(6), pp. 1438–45.

Wang, B. *et al.* (2015) 'Overexpression of ANO1/TMEM16A, an arterial Ca2+-activated Cl- channel, contributes to spontaneous hypertension', *Journal of Molecular and Cellular Cardiology*. Elsevier B.V., 82, pp. 22–32.

Wang, B. *et al.* (2017) 'Enhanced mitochondrial transient receptor potential channel, canonical type 3-mediated calcium handling in the vasculature from hypertensive rats', *Journal of the American Heart Association*, 6(7).

Wang, M. *et al.* (2012) 'Downregulation of TMEM16A calcium-activated chloride channel contributes to cerebrovascular remodeling during hypertension by promoting basilar smooth muscle cell proliferation', *Circulation*, 125(5), pp. 697–707.

Wang, Q. *et al.* (2016) 'Local coupling of TRPC6 to ANO1/TMEM16A channels in smooth muscle cells amplifies vasoconstriction in cerebral arteries',

American Journal of Physiology - Cell Physiology, 310(11), pp. C1001–C1009.

Wang, S. *et al.* (2015) '$P2Y_2$ and Gq/G_{11} control blood pressure by mediating endothelial mechanotransduction', *The Journal of clinical investigation*, 125(8), pp. 3077–3086.

Wang, Y., Thatcher, S. E. and Cassis, L. A. (2017) 'The Renin-Angiotensin-Aldosterone System', 1614, pp. 69–73.

Welsh, D. G. *et al.* (2002) 'Transient receptor potential channels regulate myogenic tone of resistance arteries', *Circulation Research*, 90(3), pp. 248–250.

Whelton, P. K. *et al.* (2018) '2017 ACC/AHA/AAPA/ABC/ACPM/AGS/APhA/ ASH/ASPC/NMA/PCNA Guideline for the Prevention, Detection, Evaluation, and Management of High Blood Pressure in Adults: A Report of the American College of Cardiology/American Heart Association Task Force on Clinical Pr', *Journal of the American College of Cardiology*, 71(19), pp. e127–e248.

Whitlock, J. M. and Hartzell, H. C. (2017) 'Anoctamins/TMEM16 Proteins: Chloride Channels Flirting with Lipids and Extracellular Vesicles', *Annual Review of Physiology*, 79(1), pp. 119–143.

Wier, W. G. and Morgan, K. G. (2004) '$α$1-Adrenergic signaling mechanisms in contraction of resistance arteries', in *Reviews of Physiology, Biochemistry and Pharmacology*. Berlin, Heidelberg: Springer Berlin Heidelberg, pp. 91–139.

Wilson, C. and Dryer, S. E. (2014) 'A mutation in TRPC6 channels abolishes their activation by hypoosmotic stretch but does not affect activation by diacylglycerol or G protein signaling cascades.', *American journal of physiology. Renal physiology*, 306(9), pp. 1018–25.

Woo, H. *et al.* (2011) 'Serine-threonine kinase with-no-lysine 4 (WNK4) controls blood pressure via transient receptor potential canonical 3 (TRPC3) in the vasculature', *Pnas*, 4, pp. 3–8.

Xiong, Z. and Sperelakis, N. (1995) 'Regulation of L-Type Calcium Channels of Vascular Smooth Muscle Cells', 91(1), pp. 75–91.

Yang, T. *et al.* (2014) 'Structure and selectivity in bestrophin ion channels', *Science*, 346(6207), pp. 355–359.

Ye, Z.-Y. *et al.* (2012) 'NKCC1 Upregulation Disrupts Chloride Homeostasis in the Hypothalamus and Increases Neuronal Activity-Sympathetic Drive in Hypertension', *Journal of Neuroscience*, 32(25), pp. 8560–8568.

Yip, K.-P. *et al.* (2018) 'Intraluminal pressure triggers myogenic response via activation of calcium spark and calcium-activated chloride channel in rat renal afferent arteriole', *American Journal of Physiology-Renal Physiology*, 315(6), pp. F1592–F1600.

Yu, Y. *et al.* (2004) 'Enhanced expression of transient receptor potential channels in idiopathic pulmonary arterial hypertension', *Proceedings of the National Academy of Sciences*, 101(38), pp. 13861–13866.

Yuan, J. P. *et al.* (2009) 'STIM1 heteromultimerizes TRPC channels to determien their function as store-operated channels', *Nature*, 9(6), pp. 636–645.

Zaritsky, J. J. *et al.* (2000) 'Targeted Disruption of Kir2.1 and Kir2.2 Genes Reveals the Essential Role of the Inwardly Rectifying K+ Current in K+-Mediated Vasodilation', *Circulation Research*, 87(2), pp. 160–166.

Zulian, A. *et al.* (2010) 'Upregulation of Na ε / Ca 2 ε exchanger and TRPC6 contributes to abnormal Ca 2 ε homeostasis in arterial smooth muscle cells from Milan hypertensive rats', pp. 624–633.

8

Resumen

RESUMEN FINAL

1. Introducción

La hipertensión arterial (HTA) es una enfermedad crónica que se caracteriza por un aumento sostenido de la presión sanguínea arterial, siendo un factor de riesgo determinante de diversas patologías cardiovasculares, neurológicas y renales. El 90% de los casos de HTA se diagnostican como hipertensión esencial, de origen genético y sujeto a factores ambientales y estilos de vida como sedentarismo, tabaquismo, ingesta de alcohol, dieta y obesidad (Aaronson, Ward and Wiener, 2004). El 10% restante de los casos de HTA se diagnostican como hipertensión secundaria, cuyo origen deriva de problemas de causa patológica conocida, incluyendo hiperaldosteronismo, patologías renovasculares, feocromocitoma o toxemia preeclámptica, entre otros (Herring and Paterson, 2018).

Fisiológicamente, la presión arterial está finamente regulada por el sistema cardiovascular mediante el control del gasto cardíaco (CO) y las resistencias periféricas totales (TPR). Inicialmente, la HTA esencial se asocia a un aumento del CO con valores normales o ligeramente elevados en las TPR; sin embargo, con el transcurso del tiempo, el CO revierte a sus valores fisiológicos mientras que los valores que definen las TPR se mantienen crónicamente elevados. El estado y la actividad contráctil de las células que componen la capa de músculo liso vascular (VSMCs), concretamente en arterias y arteriolas, son los principales determinantes de las TPR. Normalmente, los vasos sanguíneos se encuentran en un estado de contracción parcial denominado tono vascular que determina el diámetro del vaso en condiciones basales. En respuesta a estímulos, el cambio en el estado contráctil de las VSMCs determina la contracción y dilatación de los vasos, regulando de esta forma de manera muy eficiente el flujo sanguíneo en los distintos lechos vasculares. Este tono vascular basal depende directamente del potencial de membrana (Vm) de las células VSMCs, finamente regulado por los canales de K^+ y los canales de Ca^{2+} dependientes de voltaje (VOCCs), de manera que la despolarización de las VSMCs da lugar a contracción vascular, mientras que los estímulos hiperpolarizantes producen vasodilatación. En trabajos previos de nuestro grupo, se ha identificado la contribución de diferentes canales de K^+ y canales VOCCs al desarrollo de la hipertensión en el modelo murino de hipertensión esencial BPH/BPN. Sin embrago, existen otros muchos canales y receptores de membrana cuya contribución en la patogénesis de la hipertensión esencial aún se desconoce.

2. Objetivos

El objetivo principal de esta Tesis consiste en caracterizar la contribución funcional de los canales activados por receptor (ROCs) y de los receptores acoplados a proteínas G (GPCR) en la patogénesis de la hipertensión arterial esencial en el modelo murino de hipertensión BPH/BPN. Concretamente, el estudio se ha centrado en caracterizar las diferencias en la contribución de los canales TRPC al fenotipo hipertenso en condiciones basales, así como tras estimulación de la cascada de señalización purinérgica.

3. Material y Métodos

Para la realización de esta Tesis, se ha utilizado principalmente el modelo de ratón BPH/BPN. Se trata de un modelo genético de HTA esencial, obtenido a partir del cruce de distintas cepas de ratón seleccionadas fenotípicamente. De este modo se han obtenido ratones con fenotipo hipertensivo moderado (BPH) y sus respectivos controles (BPN), compartiendo un fondo genético similar. Todos los protocolos aplicados a los animales utilizados en esta Tesis han sido aprobados por el Comité de Ética en Experimentación Animal de la Universidad de Valladolid, acorde con la Guía de Principios de la Comunidad Europea relativa a la protección de animales utilizados para experimentación y otros fines científicos (Directiva 2010/63/UE).

Además, se ha utilizado la línea celular CHO como sistema heterólogo de expresión génica de distintos vectores que codifican para canales TRPC, lo que nos ha permitido caracterizar de forma aislada la expresión y el patrón de asociación de dichos canales, así como sus propiedades electrofisiológicas.

Mediante estudios de expresión génica (PCR cuantitativa) y estudios de expresión y asociación de proteínas (inmunocitoquímica, co-IP, PLA, GSD Super-resolution…) hemos caracterizado las diferencias, a nivel molecular, de los canales iónicos y receptores de membrana entre los fenotipos BPH y BPN. La caracterización funcional se ha llevado a cabo mediante estudios de electrofisiología en células aisladas y estudios de miografía de presión en arterias mesentéricas. Con la técnica de patch-clamp hemos caracterizado las corrientes iónicas a través de los canales de membrana, así como la contribución de dichos canales al Vm, y con los estudios de miografía de presión hemos caracterizado la contribución de dichos canales y receptores de membrana a las diferencias en la contractilidad vascular entre BPH y BPN.

4. Resultados

Los resultados obtenidos en la caracterización del modelo de hipertensión BPH mostraron un incremento moderado en los valores de presión arterial, valores de potencial de membrana de las VSMCs en reposo más despolarizados y una mayor respuesta contráctil al agonista α_1-adrenérgico Phenilephrine (PHE) respecto los ratones control BPN, sugiriendo que el incremento de la actividad simpática contribuye al aumento del tono vascular en nuestro modelo.

Los resultados de expresión génica obtenidos en células VSMCs procedentes de arterias mesentéricas de ratones BPH mostraron un aumento de la expresión de los canales TRPC3 y una disminución de los canales TRPC6 respecto el fenotipo BPN. Además, mediante los estudios realizados en células CHO, validados posteriormente en células VSMCs, caracterizamos la actividad electrofisiológica de los canales TRPC3/C6, así como las diferencias en el patrón de expresión y formación de heteromultímeros TRPC3/C6. Para esta caracterización funcional hemos utilizado el bloqueo mediante anticuerpos específicos anti-TRPC3 aplicados intracelularmente para determinar la contribución de los canales TRPC3, y el bloqueo farmacológico con los compuestos Pyr3/10 para estudiar la contribución de los canales TRPC6. Nuestros resultados son consistentes con un aumento de la contribución funcional de los canales TRPC3 en células BPH, tanto en condiciones basales como en respuesta a la estimulación por distintos agonistas. Las corrientes basales fueron mayores en células BPH y sólo ellas fueron sensibles al bloqueo con anticuerpos anti-TRPC3. Por otro lado, las corrientes inducidas por agonistas se bloquearon en su totalidad por Py3/10 en células BPN, y sólo parcialmente en células BPH, sugiriendo una mayor expresión de canales TRPC6 en normotensos. Así mismo, los resultados obtenidos mediante miografía de presión mostraron un mayor efecto vasodilatador de los compuestos Pyr3/10 en arterias mesentéricas de ratones BPN pre-contraídas con el agonista PHE. Finalmente, los estudios de PLA apoyaron estos datos funcionales, revelando una mayor expresión de canales TRPC3 en BPH, tanto como homomultímeros TRPC3 como heteromultímeros TRPC3/C6, frente a una mayor expresión de homomultímeros TRPC6 en BPN, datos que también concuerdan con los resultados obtenidos en el patrón de expresión de mRNA. En conjunto, los resultados obtenidos en el estudio de la caracterización de los canales TRPC como ROCs en nuestro modelo BPH/BPN nos sugieren una mayor contribución de los canales TRPC3 al fenotipo hipertenso.

Por otro lado, cuando comparamos la amplitud de las corrientes ROC mediadas por TRPC en respuesta a distintos agonistas en células BPN y BPH, sólo encontramos diferencias en el caso de UTP. Las corrientes TRPC inducidas por el agonista UTP fueron significativamente mayores en células BPN. Sin embargo, los estudios de caracterización funcional de la señalización purinérgica mostraron un mayor efecto

vasoconstrictor de UTP mediado principalmente por receptores $P2Y_6$ en el fenotipo BPH, y un aumento en la expresión de mRNA de $P2Y_6$ en BPH; .

Una posible explicación a esta observación (hay más canales TRPC3 y más receptores $P2Y_6$ en las células BPH y, sin embargo, las corrientes TRPC activadas por UTP son menores) podría ser una diferencia en el acoplamiento entre los receptores y los canales. Los estudios de PLA y Super-resolución (GSD) mostraron una mayor proximidad entre canales TRPC3 y receptores purinérgicos $P2Y_6$ en células BPN, lo que podría explicar en parte el aumento de corrientes ROC activadas por UTP obtenido en BPN.

Finalmente, el aumento de la respuesta vasoconstrictora en las arterias BPH, a pesar de tener una menor corriente TRPC inducida por UTP, podría explicarse por la contribución a esta respuesta vasoconstrictora de otros canales además de los TRPCs. Observamos que la aplicación de UTP en BPH produce una despolarización del potencial de membrana mucho mayor que en BPN, y en ambos casos, se inhibe de forma parcial por Pyr10 y casi totalmente en presencia de bloqueantes de los canales de Cl^- activados por Ca (CaCCs) como Ácido Niflúmico o el inhibidor de los canales Anoctamina 1 (ANO1-Inhibitor).

Así mismo, los estudios electrofisiológicos de las corrientes totales activadas por UTP mostraron una mayor contribución de los canales CaCCs en el fenotipo BPH, acorde con el mayor patrón de expresión de mRNA del canal ANO1 y su subunidad reguladora ClCa1. Estos resultados indican que los canales CaCCs contribuyen de manera importante a la respuesta mediada por UTP, y sugieren que las diferencias en la expresión de estos canales pueden explicar las diferencias en la señalización purinérgica entre las células de BPN y BPH.

5. Discusión y Conclusiones

El modelo BPH es un modelo de hipertensión esencial moderada asociado a un aumento del tono vascular y a un incremento de la actividad simpática. Puesto que los canales TRPCs son el prototipo de los canales activados por receptor (ROCs), hemos investigado las diferencias en las repuestas vasculares a agonistas α_1-adrenérgicos y purinérgicos, ya que son las dos vías de señalización más importantes asociadas a la estimulación simpática en arterias de resistencia. Los patrones de expresión de mRNA y asociación proteica de los canales TRPC mostraron un aumento en la expresión de TRPC3, asociado como homomultímeros o heteromultímeros con TRPC6, en BPH; mientras que la asociación de homomultímeros TRPC6 fue predominante en BPN. Además, el aumento de expresión de TRPC3 se correlaciona con la mayor actividad basal del canal en células BPH.

Por otro lado, lo estudios control llevados a cabo en células CHO demostraron que tanto los compuestos Pyr3/10 como los anticuerpos anti-TRPC3 son buenas herramientas farmacológicas para el estudio del papel funcional de los canales TRPC en sistemas nativos. De esta manera, mientras que los anticuerpos anti-TRPC3 fueron capaces de bloquear selectivamente las corrientes basales a través de TRPC3, los compuestos Pyr3/10 bloquearon la actividad del canal TRPC6. Estos resultados fueron posteriormente validados en células nativas, de manera que se obtuvo un mayor efecto bloqueante con los anticuerpos anti-TRPC3 y una menor sensibilidad al bloqueo mediado por los compuestos Pyr3/10 en BPH; mientras que los efectos de Pyr3/10 fueron mayores en BPN. Por tanto, estos datos nos sugieren una mayor contribución de los canales TRPC3 al fenotipo hipertenso.

La caracterización funcional de la respuesta activada por UTP en el modelo BPH nos sugiere que está principalmente mediada por los receptores purinérgicos $P2Y_6$. Además, existe una gran contribución de los canales CaCCs, concretamente del canal ANO1, a la despolarización inducida por UTP en BPH, lo que concuerda con la mayor expresión de mRNA de ANO1 y su subunidad reguladora ClCa1.

En conjunto, nuestros resultados sugieren que los cambios en la expresión tanto delos canales TRPC como de los canales CaCCs contribuyen a fijar un potencial de membrana más despolarizado en las células BPH, y por tanto una mayor vasoconstricción basal. Además, la contribución de estos dos tipos de canales a las respuestas inducidas por agonistas de receptores acoplados a proteínas G (GPCR) es diferente en BPH y BPN y además es dependiente del tipo de agonista. Así, la activación por UTP de los receptores $P2Y_6$ da lugar a un amento de DAG, que activa canales TRPC3/6, y a un aumento de calcio intracelular, que activa los canales ANO1. La activación de ambos canales da lugar a una despolarización que desencadena la respuesta contráctil. Sin embargo, esta respuesta es mucho mayor en las arterias BPH debido, en gran parte, al aumento de la contribución funcional de los canales CaCCs en células BPH. En este contexto, cambios pequeños en la expresión y/o el acoplamiento de los distintos elementos de la vía de señalización (GPCR, TRPC y CaCCs) pueden dar lugar a diferencias importantes en la respuesta final, sugiriendo que estas proteínas pueden representar nuevas dianas terapéuticas para la prevención y el tratamiento de la hipertensión esencial.

9

Annex

J Physiol 595.5 (2017) pp 1497–1513

The Journal of Physiology

Differences in TRPC3 and TRPC6 channels assembly in mesenteric vascular smooth muscle cells in essential hypertension

Inés Álvarez-Miguel, Pilar Cidad, M. Teresa Pérez-García* and José Ramón López-López*

Departamento de Bioquímica y Biología Molecular y Fisiología e Instituto de Biología y Genética Molecular (IBGM), Universidad de Valladolid y Consejo Superior de Investigaciones Científicas (CSIC), Valladolid, Spain

Key points

- Canonical transient receptor potential (TRPC)3 and TRPC6 channels of vascular smooth muscle cells (VSMCs) mediate stretch- or agonist-induced cationic fluxes, contributing to membrane potential and vascular tone.
- Native TRPC3/C6 channels can form homo- or heterotetrameric complexes, which can hinder individual TRPC channel properties. The possibility that the differences in their association pattern may change their contribution to vascular tone in hypertension is unexplored.
- Functional characterization of heterologously expressed channels showed that TRPC6-containing complexes exhibited Pyr3/Pyr10-sensitive currents, whereas TRPC3-mediated currents were blocked by anti-TRPC3 antibodies.
- VSMCs from hypertensive (blood pressure high; BPH) mice have larger cationic basal currents insensitive to Pyr10 and sensitive to anti-TRPC3 antibodies. Consistently, myography studies showed a larger Pyr3/10-induced vasodilatation in BPN (blood pressure normal) mesenteric arteries.
- We conclude that the increased TRPC3 channel expression in BPH VSMCs leads to changes in TRPC3/C6 heteromultimeric assembly, with a higher TRPC3 channel contribution favouring depolarization of hypertensive VSMCs.

Abstract Increased vascular tone in essential hypertension involves a sustained rise in total peripheral resistance. A model has been proposed in which the combination of membrane depolarization and higher L-type Ca^{2+} channel activity generates augmented Ca^{2+} influx into vascular smooth muscle cells (VSMCs), contraction and vasoconstriction. The search for culprit ion channels responsible for membrane depolarization has provided several candidates, including members of the canonical transient receptor potential (TRPC) family. TRPC3 and TRPC6 are diacylglycerol-activated, non-selective cationic channels contributing to stretch- or agonist-induced depolarization. Conflicting information exists regarding changes in TRPC3/TRPC6 functional expression in hypertension. However, although TRPC3-TRPC6 channels can heteromultimerize, the possibility that differences in their association pattern may change their functional contribution to vascular tone is largely unexplored. We probe this hypothesis using a model of essential hypertension (BPH mice; blood pressure high) and its normotensive control (BPN mice; blood pressure normal). First, non-selective cationic currents through homo- and heterotetramers recorded from transfected Chinese hamster ovary cells indicated that TRPC currents were sensitive to the selective antagonist Pyr10 only when TRPC6

*These authors contributed equally to this work.

DOI: 10.1113/JP273327

was present, whereas intracellular anti-TRPC3 antibody selectively blocked TRPC3-mediated currents. In mesenteric VSMCs, basal and agonist-induced currents were more sensitive to Pyr3 and Pyr10 in BPN cells. Consistently, myography studies showed a larger Pyr3/10-induced vasodilatation in BPN mesenteric arteries. mRNA and protein expression data supported changes in TRPC3 and TRPC6 proportions and assembly, with a higher TRPC3 channel contribution in BPH VSMCs that could favour cell depolarization. These differences in functional and pharmacological properties of TRPC3 and TRPC6 channels, depending on their assembly, could represent novel therapeutical opportunities.

(Received 23 August 2016; accepted after revision 7 November 2016; first published online 12 November 2016)
Corresponding author M. T. Pérez García: Departamento de Bioquímica y Biología Molecular y Fisiología, Universidad de Valladolid, Edificio IBGM, c/ Sanz y Forés n° 3, 47003 Valladolid, Spain. Email: tperez@ibgm.uva.es

Abbreviations BPH, blood pressure high; BPN, blood pressure normal; CHO, Chinese hamster ovary; DAG, diacylglycerol; GFP, green fluorescent protein; GPCR, G-protein coupled receptors; HS, hypotonic stimulus; KO, knockout; LTCC, L-type Ca^{2+} channel; PLA, proximity ligation assay; ROCs, receptor operated channels; SOCs, store-operated channels; RFP, red fluorescent protein; RPB, modified radioimmunoprecipitation assay buffer; SMDS, smooth muscle dissociation solution; TRP, transient receptor potential; TRPC channels, canonical transient receptor potential channels; VSMCs, vascular smooth muscle cells.

Introduction

Smooth muscle cells of blood vessels (vascular smooth muscle cells; VSMCs) act as critical determinants of blood pressure by modulating the vessel diameter and hence blood flow. Most importantly, vascular disease resulting in high blood pressure is among the most common causes of death and disability in the western world.

Ion channels initiate and regulate contraction and VSMC tone, modulating intracellular [Ca^{2+}] levels. The identification of ion channel genes expressed in VSMCs has significantly improved our knowledge of the signalling pathways leading to VSMC contraction, as well as their possible contribution to pathophysiological conditions. Although L-type, voltage-dependent Ca^{2+} channel (LTCC) is the primary pathway for Ca^{2+} influx in VSMC, non-selective cation channels have also been identified as important players in the regulation of vascular tone, either modulating membrane potential or providing a Ca^{2+} entry pathway independent of the activation of LTCCs (Albert & Large, 2006).

The molecular correlates of the non-selective cation channels expressed in VSMCs are members of the transient receptor potential (TRP) family. TRP channels are activated by vasoconstrictors, by membrane stretch and by Ca^{2+} store depletion (Dietrich *et al.* 2006; Nilius & Honoré, 2012), and the canonical TRP (TRPC) family has been proposed as the molecular constituent of receptor- and stretch-operated channels (ROCs and SOCs, respectively) that link the diacylglycerol (DAG) signalling cascade pathway to the activation of LTCCs. The seven TRPC family members can be classified into subfamilies on the basis of their amino acid similarity. Among them, the TRPC3/6/7 subfamily has been proposed as the DAG-activated ROCs (Hofmann *et al.*, 1999, 2002), although TRPC7 channels have not been found in the vasculature (Earley & Brayden, 2015).

Despite years of study characterizing the biophysical properties and the functional roles of TRPC3 and TRPC6 channels, surprisingly little is known regarding their contribution to vasoconstriction and vasorelaxation in arteries. Several reasons contribute to the paucity of these studies, including their lack of distinct biophysical properties and the shortage of selective pharmacological blockers. Moreover, the use of small interfering RNA approaches to study these channels in cultured VSMCs has provided information that is not easy to interpret in terms of the contribution of the channels to the regulation of VSMCs contractility because cultured VSMCs undergo phenotypic modulation and show lost contractile properties (Owens *et al.* 2004). In recent years, knockout (KO) animals and more selective pharmacological agents have provided better approaches for studying the contribution of these channels to vascular tone. However, no conclusive results could be obtained from TRPC3 and TRPC6 KO animals. Neither agonist-induced, nor pressure-evoked contraction was reduced in arteries from TRPC6-KO mice because upregulation of TRPC3 channels provided a compensatory vasoconstrictor mechanism in these animals (Dietrich *et al.* 2005). Although these channels have been described in VSMCs from many arteries, as for TRPC3-KO, the TRPC3-deficient mice phenotype shows an impaired vasodilatation related to the lack of endothelial TRPC3 channels (Senadheera *et al.* 2012; Yeon *et al.* 2014). In any case, the combination of several of these approaches enables the distinction of the contributions of these two channels to vascular tone in different vascular beds. TRPC6 channels are linked to pressure-induced (myogenic) vasoconstriction

and can also be activated by a variety of G-protein coupled receptors (GPCR) ligands (Mederos y Schnitzler *et al.* 2008; Gonzales *et al.* 2014; Earley & Brayden, 2015). However, the mechanisms linking stretch or mechanical stimuli to TRPC6 channels activation remain controversial. Although some studies suggest that TRPC6 channels could be intrinsically mechanosensitive (Wilson & Dryer, 2014), other laboratories conclude that TRPC6 channel gating in response to stretch is an indirect effect resulting from the mechanical activation of GPCR (Sharif-Naeini *et al.* 2008; Gonzales *et al.* 2014). An interesting proposal that can solve this controversy sugggests that both mechanisms could be acting in a synergistic way, so that simultaneous receptor-mediated and mechanical stimulation could amplify calcium influx through TRPC6 channels (Inoue *et al.* 2009). TRPC6 channel exhibits mechanosensitivity only after its receptor-mediated activation via PLC/diacylglycerol and PLA2/ 20-HETE pathways.

TRPC3 channels contribute to basal tone and to agonist-induced vasoconstriction but do not appear to have a role in the myogenic response (Reading *et al.* 2005; Dietrich *et al.* 2006). However, these studies also show some discrepancies regarding the expression and the functional contribution of these channels in different preparations and leave several relevant questions unanswered. In particular, the characterization of the unique contributions of these two channels in pathophysiological contexts with an altered vascular tone has not been defined. An increased expression of TRPC3 channels in conduit arteries from hypertensive animals has been reported (Liu *et al.* 2009; Noorani *et al.* 2011), although their expression and functional contribution in VSMCs from resistance arteries remain a matter of debate (Reading *et al.* 2005; Adebiyi *et al.* 2012; Senadheera *et al.* 2012). Also, the upregulation of TRPC6 channels (with normal TRPC3 channel expression) has been described in mesenteric arteries in other hypertension models (Linde *et al.* 2012).

Aside from the different models and vascular beds used, these discrepancies can be related to the fact that the contribution of TRPC3 and TRPC6 channels in native VSMCs is dependent on their association as homo- or heterotetrameric complexes. Because TRPC3 and TRPC6 expression overlaps in most VSMC tissues and their physical interaction has been demonstrated (Hofmann *et al.* 2002; Beech *et al.* 2004; Shin *et al.* 2011), TRPC3/6 heterotetramers may be the molecular correlate of the native receptor-operated non-selective cationic influx in VSMCs. For this reason, the characterization of endogenous TRPC channels in native cell is challenged by the possibility of heteromultimeric associations that can hinder the contribution of an individual TRPC channel (Maruyama *et al.* 2006). In this regard, the possibility that differences in their association pattern may change their functional contribution to vascular tone is unexplored.

In the present study, we probe this hypothesis using a model of essential hypertension (BPH mice; blood pressure high) and its normotensive control (BPN mice; blood pressure normal) (Schlager & Sides, 1997). We observed changes in the expression of TRPC3 mRNA in mesenteric VSMCs from BPH animals, and we aimed to define its possible contribution to the hypertensive phenotype by determining the functional and pharmacological profile of TRPC3 and TRPC6 homo- and heterotetramers, combining studies in native VSMCs, in heterologous expression systems, and in whole arteries. The data obtained indicate that changes in TRPC3 channels expression determine differences in TRPC3 and TRPC6 proportions and assembly, leading to a higher TRPC3 channel contribution in BPH VSMCs that could favour cell depolarization in the hypertensive phenotype.

Methods

Ethical approval

All animal protocols were approved by the Institutional Care and Use Committee of the University of Valladolid, and are in accordance with the European Community guiding principles with respect to the care and use of animals (Directive 2010/63/UE).

Mice protocols

Colonies of BPH and BPN mice (Jackson Laboratories, Bar Harbor, ME, USA) were housed in the animal facility of the School of Medicine of Valladolid, under temperature-controlledconditions (21 °C) and with unlimited access to water and food. Blood pressure was measured in awake mice with a tail-cuff pressure meter (LSI Letica Scientific Instruments, Barcelona, Spain) as described previously (Tajada *et al.* 2012). BPN and BPH mice used in the present study were paired in terms of age, ranging from 16 to 58 weeks (average 36.2 ± 2.4 weeks for BPN and 34.6 ± 1.7 weeks for BPH). However, the weight of BPN animals was significantly larger that BPH mice of matching ages (29.33 ± 0.23 g for BPN *vs.* 24.37 ± 0.24 g for BPH, $n = 69$–80, $P < 0.001$), as described previously (Moreno-Domínguez *et al.* 2009). Mice were deeply anaesthetized by isoflurane inhalation (5% at 2.5 l min^{-1} O_2) and killed by decapitation. Mesenteric arteries were obtained as described previously (Moreno-Domínguez *et al.* 2009). Briefly, arteries were carefully dissected and cleaned of connective and endothelial tissues in cold (4 °C) oxygenated (95% O_2–5% CO_2) smooth muscle dissociation solution (SMDS)–10 μM Ca^{2+} (120 mM NaCl, 4.2 mM KCl, 25 mM $NaCHO_3$, 0.6 mM KH_2PO_4, 1.2 $MgCl_2$ and 11 mM glucose, pH 7.4). Subsequently, arteries were

either frozen at −80 °C for further RNA extraction or used directly for myography measurements or to obtain freshly dispersed VSMCs.

Chinese hamster ovary (CHO) cells culture and transfection

CHO cells were maintained in Dulbecco's modified Eagle's medium supplemented with 10% foetal bovine serum, penicillin-streptomycin (100 U ml^{-1} each) and 2 mM L-glutamine at 37 °C in a 5% CO_2 humidified atmosphere. CHO cells were grown as a monolayer in poly-L-lysine-coated coverslips prior to transiently transfection by using TransIT-X2® System (Mirus, Madison, WI, USA) in accordance with the manufacturer's instructions. Cells were transfected with 1 μg of DNA of hTRPC3-YFP (kindly provided by Dr Klaus Groschner, University of Graz, Austria), 1 μg of ratTRPC6-green fluorescent protein (GFP) (a gift from Dr Jason Yuan, U of Arizona) or 0.5 μg of each. Cells were used 24–72 h after transfection.

RNA extraction

RNA extraction was carried out from 30–40 mesenteric arteries from five or six BPN and BPH mice (Cidad *et al.* 2010). After cleaning of connective, adipose and endothelial tissues, total RNA from arteries was isolated with a MELT™ Total RNA Isolation System Kit (Ambion, Inc., Thermo Fisher Scientific, Waltham, MA USA) in accordance with the manufacturer's instructions. After DNAse I (Ambion, Inc.; Thermo Fisher Scientific) treatment, 500–750 ng of RNA was used for the reverse transcription reaction (2.5 U μl^{-1} MuLvRT, 1 U μl^{-1} RNase inhibitor, 2.5 μM random hexamers, 1 × PCR buffer, 5 mM $MgCl_2$ and 4 mM mixed dNTPs; Applied Biosystems, Thermo Fisher Scientific) at 42 °C for 60 min to obtain cDNA. Real-time PCR was carried out using TaqMan Low-Density Arrays (Applied Biosystems; Thermo Fisher Scientific) and an ABI Prism 7900HT sequence detection system (Applied Biosystems) at the Genomic Service of the CNIC (Madrid, Spain). Data were analysed with the threshold cycle (Ct) relative quantification method (ΔΔCt) (Livak & Schmittgen, 2001). We analysed two different housekeeping genes: ribosomal protein 18 s (RP18s) and Gapdh. RP18s is included in the arrays such that is also an internal control of the reaction. By contrast, Gapdh serves as an external control because its expression is determined from the same samples in an independent reaction. Because the data obtained with the two housekeeping genes showed no significant differences in expression between BPN and BPH samples, expression data were normalized by the level of ribosomal RNA 18S transcript. The relative abundance of the genes was calculated from $2^{(-\Delta Ct)}$, where $\Delta Ct = Ct_{Channel}\text{-}Ct_{18S}$. Differences between BPN and BPH samples were calculated from $2^{(-\Delta\Delta Ct)}$, where $\Delta\Delta Ct = \Delta Ct_{BPH} - \Delta Ct_{BPN}$. In this way, the levels of mRNA in BPH samples are expressed as changes relative to BPN: $2^{(-\Delta\Delta Ct)} = 1$ will indicate the absence of changes between both preparations; increased expression is denoted by a $2^{(-\Delta\Delta Ct)} > 1$; and decreases are indicated by $2^{(-\Delta\Delta Ct)} < 1$. A more intuitive expression can be obtained when changes are expressed as log $2^{(-\Delta\Delta Ct)}$ (Fig. 1): positive values indictate a higher expression in BPH mice, whereas negative values indicate a lower expression compared to BPN mice.

Myography measurements

Segments of third-order mesenteric arteries were mounted in a pressure myograph system (Danish Myo Technology, Aarhus, Denmark). The arteries were cannulated between two borosilicate glass pipettes and fixed with nylon filaments at both ends. Then, the artery segment was air bubbled to remove endothelial tissue and filled with physiological saline solution (120 mM NaCl, 2.5 mM $CaCl_2$, 1.17 mM $MgSO_4$, 5 mM KCl, 1.18 mM Na_2HPO_4, 25 mM $NaHCO_3$, 1 mM EDTA, 10 mM glucose, pH 7.4 adjusted with 5% CO_2–95% air), which was maintained throughout the duration of the experiment. The arteries were pressurized to 70 mmHg in physiological saline solution and incubated at 37 °C for at least 20 min to equilibrate before starting the measurements. The viability of mesenteric arteries was evaluated by their ability to constrict in response to phenylephrine, and the endothelium denudation was confirmed in control experiments by the absence of dilatation in response to 10 μM ACh. Data regarding the external diameter were collected with a CCD camera placed in an inverted microscope (Danish Myo Technology) and were analysed using MyoView software (Danish Myo Technology). The vasodilatory effect of the Pyr compounds was tested in phenylephrine (5–10 μM) precontracted arteries. At the end of each experiment, vessels were superfused with a solution containing 10 μM nifedipine to determine the maximal vessel diameter upon relaxation. Dose–response curves of chemical agents were calculated with the formula $100 \times (D - D_{Phe})/(D_{Nif} - D_{Phe})$ and fitted by either one or two Hill functions.

VSMC isolation

Fresh VSMC cells were obtained after two sequential enzymatic incubations at 37 °C of second- and third-order mesenteric arteries in accordance with previously described methods (Moreno-Domínguez *et al.* 2009; Tajada *et al.* 2012). The first digestion was carried out in SMDS-Ca^{2+}-free solution containing 0.8 mg ml^{-1} papain (Worthington Biochemical Corp., Lakewood, NJ,

USA), 1 mg ml^{-1} BSA (Sigma-Aldrich, St Louis, MO, USA) and 1 mg ml^{-1} dithiothreitol (Sigma-Aldrich) and the second one was performed in SMDS-10 μM Ca^{2+} supplemented with 0.6 mg ml^{-1} collagenase F (Sigma-Aldrich) and 1 mg ml^{-1} BSA. Subsequently, the tissues were washed three or four times in SMDS-10 μM Ca^{2+} and were mechanically dissociated with a wide-bore glass pipette to obtain freshly isolated VSMC cells. Single cells were maintained at 4 °C until patch clamp recordings or protein expression assays.

Protein expression assays

Protein expression in VSMC and CHO cells was studied by immunocytochemistry and immunoprecipitation assays, as well as by a proximity ligation assay (PLA). For the immunocytochemistry assay, transfected CHO cells plated on poly-lysine coated coverslips were fixed with 4 % paraformaldehyde in PBS for 15 min, permeabilized in PBTx (PBS, 0.1% Triton X-100) and blocked with PBTx with 1% of BSA for 10 min. Then, cells were incubated first with the primary antibody: rabbit anti-TRPC3 (4.5 μg ml^{-1}; ACC-016; Alomone Labs, Jerusalem, Israel) or rabbit anti-TRPC6 (4.5 μg ml^{-1}; ACC-017; Alomone) and then with the secondary antibody: Alexa 594 goat anti-rabbit (dilution 1:1000; Molecular Probes, Carlsbad, CA, USA), both in blocking solution. The nuclei were labelled with Hoechst 33342 (dilution 1:2000; Life Technologies, Grand Island, NY, USA) and coverslips were mounted with Vectashield (Vector Laboratories, Inc., Burlingame, CA, USA).

For the immunoprecipitation assay, cell lysate from transfected CHO cells was collected in modified radio-immunoprecipitation assay buffer (MRB) (150 mM NaCl, 50 mM Tris, pH 8, 1% NP-40 and 0.2% sodium deoxycholate, pH 7.4 adjusted with NaOH) with Proteases Inhibitor Cocktail (Roche, Basel, Switzerland). Then, the cell lysate was incubated at 4 °C with

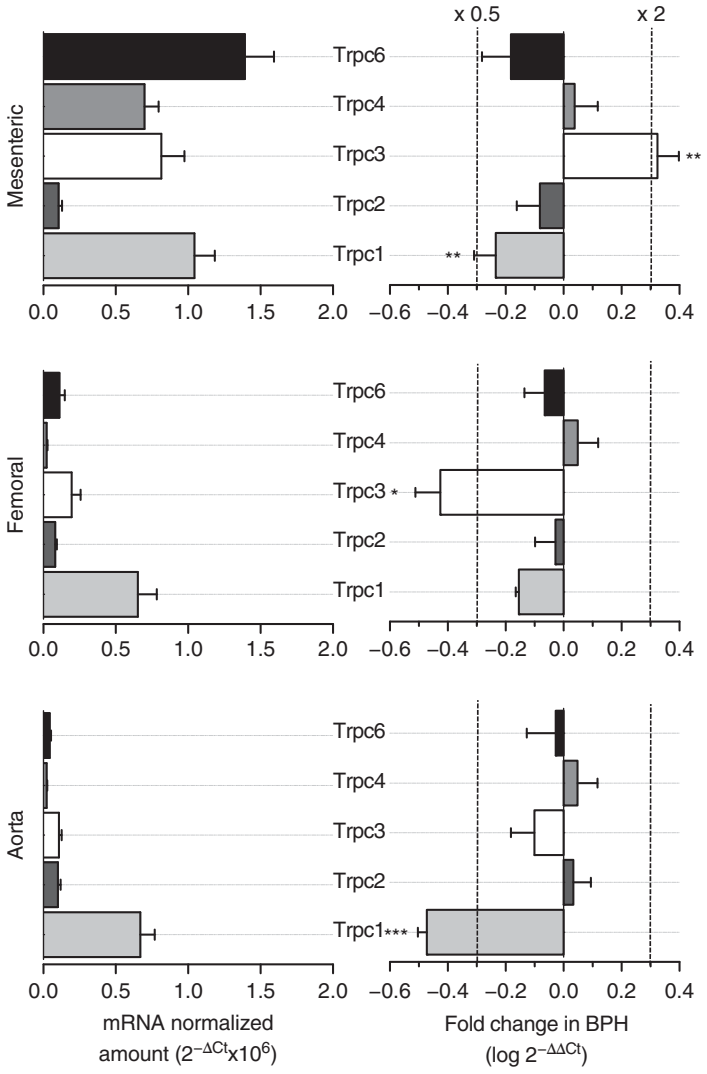

Figure 1. mRNA profile of TRPC channels in BPN and BPH VSMCs
Left: relative abundance of TRPC family channels in VSMC from BPN mesenteric, femoral and aorta arteries normalized by the amount of RP18S. Data are expressed as $2^{-\Delta Ct}$, where $\Delta Ct = Ct_{channel} - Ct_{18S}$. Right: showing, for each vascular bed, the changes in TRPC channels expression in BPH arteries using BPN arteries as the calibrator. Differences are expressed as log ($2^{-\Delta\Delta Ct}$) where $\Delta\Delta Ct = \Delta Ct_{BPH} - \Delta Ct_{BPN}$. With the log scale, a value of 0 represents no change, increases in expression are depicted as positive changes, and decreased expression appears as a negative value. For reference, the values of a two-fold increase or a two-fold decrease are indicated by the dotted lines. Each bar is the mean ± SEM, $n = 6$–10 values from at least three independent experiments. All through the figures $^*P < 0.05$; $^{**}P < 0.01$; $^{***}P < 0.001$.

gentle shaking for 2–3 h with the GFP-Trap_A beads in accordance with the manufacturer´s instructions (Chromotek, Planegg-Martinsried, Germany) and, after washing three times with MRB buffer and with high NaCl-MRB buffer (750 mM), samples were maintained at −20 °C until analysis by western blotting. For immunoblot analysis, protein samples were diluted in XT Reducing Agent and XT Sample Buffer (Bio-Rad, Hercules, CA, USA) and incubated at 95 °C for 5 min. They were then separated by SDS-PAGE on 10% polyacrylamide gels and transferred onto nitrocellulose membrane, which was then blocked with 5 % non-fat dry milk in 0.1 % Tween 20 in Tris-buffered saline for 1 h. Membranes were incubated with the primary antibodies in blocking solution: rabbit anti-TRPC3 (4.5 μg ml^{-1}; Alomone) or rabbit anti-TRPC6 (4.5 μg ml^{-1}; Alomone), at 4 °C overnight. Next, membranes were incubated with the secondary antibody: horseradish peroxidase-conjugated anti-rabbit IgG (dilution 1:20000; Dako, Glostrup, Denmark) for 1 h. Protein signals were detected using a VersaDoc 4000 Image System (Bio-Rad) with chemiluminescence reagents (SuperSignal West Femto Maximum Sensitivity Substrate; Pierce, Rockford, IL, USA).

Protein association in native VSMC cells was explored with PLA technology using the Duolink® In Situ kit (Sigma-Aldrich) in accordance with the manufacturer´s instructions. Briefly, freshly isolated native cells were incubated in 12 mm diameter dishes at 37 °C in a 5% CO_2 humidified atmosphere for 1 h prior to be fixed with 4 % paraformaldehyde in PBS. After washing, cells were permeabilized with 0.2% Triton x-100 in PBS and blocked with the kit´s blocking solution at 37 °C for 1 h. Then, cells were incubated with different combinations of first intracellular antibodies: rabbit anti-TRPC3 (1 μg ml^{-1}; Alomone), goat anti-TRPC3 (1 μg ml^{-1}; NBP1-70352; Novus Biologicals, Littleton, CO, USA), rabbit anti-TRPC6 (1 μg ml^{-1}; Alomone) and goat-anti-TRPC6 (1 μg ml^{-1}; NBP1-00142; Novus Biologicals) at room temperature overnight. Cells were then labelled with Doulink® In Situ PLA probes: anti-goat PLUS and anti-rabbit MINUS for 1 h at 37 °C and, subsequently, ligation and amplification reactions were carried out in accordance with the manufacturer ´s instructions. Samples were mounted with Vectashield with DAPI to stain the nuclei and maintained at 4°C until visualization at the appropriate wavelengths using an SP5 confocal microscope (Leica Microsystems, Wetzlar, Germany). Control experiments employed only one primary antibody.

Electrophysiological recordings

Electrophysiological measurements were carried out at room temperature (20–25°C) using a whole-cell configuration of the patch clamp technique. CHO transfected cells were perfused with a bath solution (Standard$_e$ solution) containing (in mM) 141 NaCl, 1.8 $CaCl_2$, 1.2 $MgCl_2$, 4.7 KCl, 10 glucose an d10 Hepes, pH 7.4 (NaOH). For recordings of freshly isolated VSMCs, we used a TRP external solution containing (in mM) 141 NaCl, 1.8 $CaCl_2$, 1.2 $MgCl_2$, 5 CsCl, 10 glucose, 10 Hepes, 0.005 nicardipine, 0.1 DIDS and 0.1 niflumic acid (pH 7.4 with NaOH). Borosilicate glass patch pipettes of 3–10 MΩ of resistance were filled with an internal solution (TRP internal solution) containing (mM) 10 CsCl, 110 Cs aspartate, 10 NaCl, 3.2 $CaCl_2$, 10 Hepes, 10 BAPTA, 2 MgATP, pH 7.2 (with CsOH) and with an estimated free [Ca^{2+}] of 100 nM. When indicated, rabbit anti-TRPC3 or TRPC6 or rat anti-red fluorescent protein (RFP) (Chromotek) antibodies were included at a final concentration of 4 μg ml^{-1}. Current–voltage relationships were obtained with 1 s ramp protocols from −150 mV to +80 mV from a holding potential of −10 mV, under control conditions or in the presence of the different activators or blockers. A 70% Standard$_e$ solution was applied as hypotonic stimulus (HS). For the experiments with intracellularly applied antibodies, the access resistance (Ra) and the membrane capacitance (Cap) were continuously monitored and recorded by applying the membrane test algorithms of Clampex 10 software (Axon Instruments, Foster City, CA, USA) throughout the experiment. Only cells with GΩ seal values and stable Ra and Cap values were considered for analysis. Data were acquired using an Axopatch 200A patch clamp amplifier (Axon Instruments), at a frequency of 5 kHz and filtered at 2 kHz. Recordings were digitized with a Digidata 1200 interface using Clampex 10 software. Electrophysiological data analyses were carried out using Clampfit 10 software (Molecular Devices, Sunnyvale, CA, USA) and with Origin 7 software (OriginLab Corporation, Northampton, MA, USA).

Statistical analysis

Statistical analyses were performed with R software (R Foundation for Statistical Computing, Vienna, Austria). Pooled data are expressed as the mean ± SEM. For the electrophysiology, myography and PLA, statistical comparisons between groups of data were carried out using a two-tailed Student's t test for unpaired data. $P < 0.05$ was considered statistically different.

In the case of the quantitative PCR data, a Student's t test for independent samples was used in the case of normal distributions (i.e. a Saphyro-Wilks test with $P > 0.05$). If this was not the case, a pairwise Mann–Whitney–Wilcoxon test (i.e. a non-parametric test) was applied to determine whether the differences between groups of data were statistically significant.

Results

We analysed the expression profile of TRPC channels in mesenteric, femoral and aorta VSMCs from BPN and BPH mice. The genes explored included all members of the TRPC family, as well as several control genes, such as calponin as a control for VSMCs, endothelial nitric oxide synthase as a control for endothelial cell contamination and ribosomal protein 18S (RP18S) as an endogenous control for the quantitative PCR. We explored both the relative abundance of the channel genes expressed in the normotensive VSMCs and the changes observed in BPH animals. The data are summarized in Fig. 1. We found mRNA expression of all TRPC channels but TRPC5 and TRPC7 (Fig. 1, left). Changes in expression upon hypertension (Fig. 1, right) are expressed as $\log2^{(-\Delta\Delta Ct)}$ so that positive values represent increased levels of expression compared with BPN, whereas negative values represent decreased expression (see Methods). In all cases, TRPC mRNA channel expression was higher in resistance (mesenteric) than in conduit (femoral or aorta) arteries, and significant differences in TRPC1 and TRPC3 expression were found in hypertensive mice. Expression of TRPC1 was decreased in mesenteric and aorta from BPH, whereas TRPC3 levels were higher in mesenteric and smaller in femoral.

Because TRPC expression was higher in resistance arteries, which functionally contribute more to blood pressure, and the increased TRPC3 expression was unique to mesenteric VSMCs from hypertensive mice, we decided to investigate the possible contribution of TRPC3 channels to the hypertensive phenotype using several pyrazole compounds (i.e. Pyr3, Pyr6 and Pyr10). Although Pyr3 and Pyr10 have been proposed as selective blockers of the DAG-activated TRPC channels, and particularly TRPC3, Pyr6 appears to exhibit a greater potency as inhibitor of Orai-mediated Ca^{2+} entry (Schleifer *et al.* 2012).

First, we tested the effect of these compounds on vessel tone performing pressure myography experiments in endothelium-denuded mesenteric arteries from BPN and BPH mice (Fig. 2). Pressurized arteries were pre-contracted with phenylephrine, and the application of 10 μM nifedipine (an LTCC blocker) at the

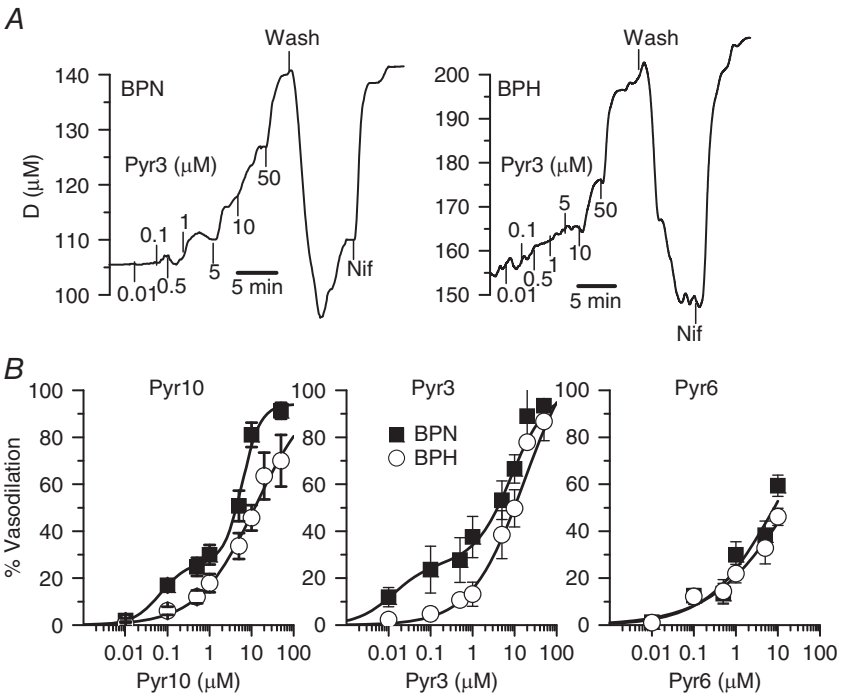

Figure 2. Effects of Pyr compounds on the vascular tone in BPN and BPH mesenteric arteries
A, representative examples of the effect of Pyr3 application at the indicated concentrations (in μM) on the external diameter of a BPN (left) and a BPH artery (right). In both cases, the arteries were pressurized to 70 mmHg and pre-contracted with bath application of 5 μM phenylephrine (Phe). Increased concentrations of Pyr3 were applied in the continuous presence of Phe. At the end of the experiment 10 μM nifedipine (Nif) was applied to determine the maximal diameter. *B*, dose–response effect of Pyr10, Pyr3 and Pyr6 in BPN (filled squares) and BPH (open circles) arteries. Data are normalized to the maximal diameter values obtained in the presence of nifedipine and expressed as percentage of relaxation (mean ± SEM; 5–9 arteries in each group). Data are fitted to Hill functions with apparent K_d values between 6 and 20 μM. For Pyr3 and Pyr10, the fitting of BPN data includes an additional high-affinity component representing 25% of the response and with apparent K_d values of 10 and 60 nM, respectively.

end of each experiment was used to determine the maximum diameter. Bath application of Pyr3 elicited a dose-dependent vasodilator response in mesenteric arteries (Fig. 2*A*) and smaller concentrations were needed to see a response in BPN. The same differences were observed with Pyr10. The whole dose–response curves are depicted in Fig. 2*B*. In both cases, BPN arteries have an apparent high-affinity component, which is responsible for ∼30% of the total response that was not present in BPH vessels. By contrast, the vasodilator effect of Pyr6 was less potent and there were no differences between BPN and BPH arteries (Fig. 2*B*). These data indicate that both Pyr3 and Pyr10 at concentrations ≤10 μM have a larger vasodilator effect in BPN arteries. It is reasonable to speculate that the high-affinity component represents the literature described specific blockage of TRPC3 channels, whereas the low affinity component, which is responsible for the full vasodilatation, is a result of some unspecific blockage. Therefore, these results would suggest that TRPC3 channels have a larger functional role in BPN arteries.

The effects of TRPC3 blockers were clearly not anticipated by the mRNA expression studies depicted in Fig. 1. Several hypotheses, including the absence of correlation between mRNA and protein changes, or differences in the blocking effect of Pyr3/10 compounds depending on the subunit composition of the TRPC tetramers, could explain this discrepancy. We decided to explore this possibility by characterizing the effect of Pyr10 on the non-selective cationic currents recorded in CHO cells expressing TRPC3, TRPC6 or TRPC3/6 channels. Currents of variable amplitude could be elicited in all experimental groups, as well as in mock-transfected CHO cells, in response to depolarizing ramps from −150 to +80 mV.

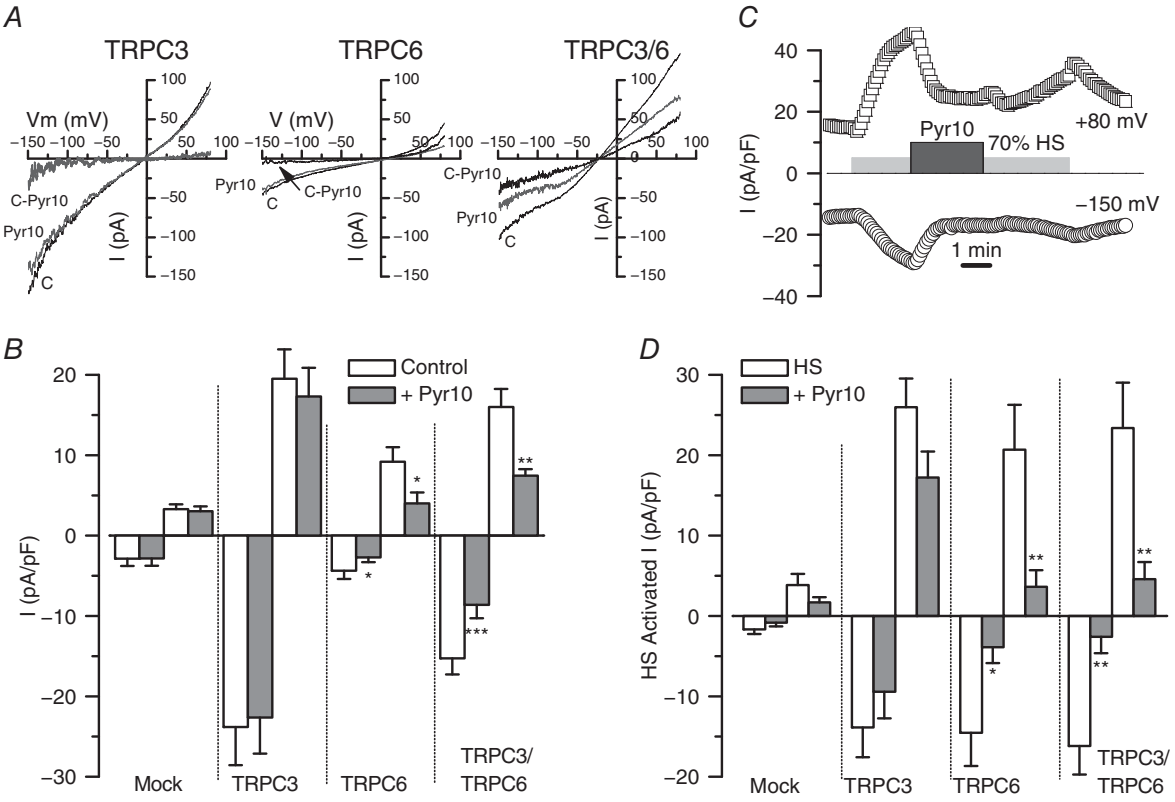

Figure 3. Functional contribution of TRPC3 and TRPC6 channels to basal and stretch-activated, non-selective cationic currents in CHO cells
A, representative examples of the traces recorded in the whole-cell configuration from unstimulated CHO cells transfected with TRPC3, TRPC6 and TRPC3/6 channels using ramp protocols from −150 mV to +80 mV. The effect of the application of Pyr10 (10 μM) in each case and the subtracted (C-Pyr), Pyr-10 sensitive current are also represented in the plots. *B*, lower bars plot shows average current densities (pA/pF) measured at −150 mV and +80 mV for each condition, as well as for untransfected CHO cells. Data are the mean ± SEM of seven to 23 cells in each condition. *C*, example of the experimental protocol used to explore the effect of Pyr10 on stretch-activated currents in a CHO cell transfected with TRPC3/6. The plot shows the time course of the current density recorded at −150 mV and +80 mV together with the time of application of the different stimuli. *D*, summary of Pyr10 effects on stretch-activated currents under all of the conditions explored. Bar plot shows average current densities elicited by application of a hypotonic solution (HS, 70% Standard$_e$ solution) and the inhibitory effect of Pyr10 (10 μM). Data are the mean ± SEM; 13–22 cells in each group.

Figure 3*A* shows the average current density obtained at −150 and +80 mV in all the experimental groups, together with representative examples of the currents obtained in TRPC3-, TRPC6- and TRPC3/6-transfected cells before and during the application of 10 μM Pyr10. The subtracted, Pyr10-sensitive currents are also shown. TRPC3-transfected cells had bigger currents than TRPC6-, and TRPC3/TRPC6-transfected cells showed an intermediate behaviour. Regarding the effect of Pyr10, the data showed that only currents from CHO cells expressing TRPC6 channels (alone or together with TRPC3) were sensitive to Pyr10. Average current densities at +80 and −150 mV, under control conditions or in the presence of Pyr10 (10 μM), are shown in Fig. 3*B*.

Because TRPC3 and TRPC6 mediated currents can be activated by several GPCR as well as by pressure-induced membrane stretch (Gonzales *et al.* 2014; Wilson & Dryer, 2014), we aimed to test the effect of Pyr10 on currents activated by some of these stimuli. To simulate a membrane stretch, we used a hypotonic stimulus (70% Standard$_e$ solution, HS) to activate the channels in CHO transfected cells. A typical experiment is depicted in Fig. 3*C* and the summary data obtained are shown in Fig. 3*D*. Application of HS elicited a reversible increase in the TRPC-mediated currents that was similar in the three conditions studied (TRPC3-, TRPC6- and TRPC3/6-transfected cells) and significantly much larger than that in mock-transfected CHO cells. These HS-induced currents, as found with basal currents, could be significantly inhibited by 10 μM Pyr10 only when TRPC6 channels were expressed.

These data suggest that Pyr10 blocks TRPC6 channels, and not TRPC3 (as reported previously), either as homo- or heteromultimers with other TRPC channels. The presence of heteromultimers between TRPC3 and TRPC6 channels in TRPC3/6-transfected cells was tested by co-immunoprecipitation experiments. Figure 4*A* shows immunocytochemical staining of TRPC3- and TRPC6- transfected cells with specific antibodies against TRPC3 and TRPC6 channels. The specificity of both antibodies, as well as the proper trafficking of the expressed proteins, is evident. Figure 4*B* shows a typical co-immunoprecipitation experiment, where TRPC6 or TRPC3 immunolabelling could be detected after immunoprecipitation of TRPC3/6-transfected cells using GFP-Trap beads to bind TRPC3-YFP fusion protein. Altogether, these sets of experiments indicate that Pyr10-sensitivity could be used as a tool to test the functional contribution of either TRPC6 or TRPC6 heteromultimers to ROC in native cells.

Because we lack a pharmacological tool to determine the presence and contribution of TRPC3 channels, we aimed to explore the blocking effect of intracellularly applied antibodies (Fig. 4*C*). Control experiments were carried out in non-transfected CHO cells using anti-TRPC3 or an indifferent antibody (against RFP; anti-RFP). No changes in the current amplitude could be observed in any case up to 10 min when recording on the whole-cell configuration of the patch clamp technique. Current amplitude of recordings from TRPC3-transfected cells was also stable up to 10 min when no antibody or anti-RFP antibody was added in the pipette solution, although a significant reduction was observed when dialysing the cell with anti-TRPC3. We confirmed that this blocking effect of anti-TRPC3 (or anti-TRPC6) was specific by exploring the antibodies effects on the HS-activated current (Fig. 4*D*). In TRPC3/C6-transfected cells, both antibodies led to a significant reduction of the current density, whereas only anti-TRPC3 (but not anti-RFP) inhibited HS activated currents in TRPC3-transfected cells.

All of the results presented so far provide support for the hypotheses that differences in Pyr10 sensitivity of BPN and BPH arteries could be a result of changes in the composition of the TRPC heteromultimers. Therefore, we aimed to obtain some insights on the subunit composition of the native TRPC channels in BPN and BPH VSMCs. We used the PLA assay technique to identify close associations between two TRPC3 subunits, two TRPC6 or one TRPC3 and one TRPC6 subunits. Figure 5A shows representative images obtained with this technique for each of the three combinations explored and in the two different cells studied (BPN and BPH VSMCs). Labelling with two different TRPC3 antibodies (C3-C3 combination), or dual labelling for TRPC3 and TRPC6 (C3-C6), produced significantly higher numbers of puncta per cell and total labelled area in BPH than in BPN cells. By contrast, labelling with two TRPC6 antibodies was significantly smaller in BPH cells. Average values of all the described combinations are depicted in the bar graph on the right of Fig. 5*A*. The possible associations detected for each combination (considering just one tetramer) are depicted in the scheme of Fig. 5*B*. The charts shown on the right group the data corresponding to the C3-C3 or C6-C6 combinations, representing the percentage of heteromultimers with more than a TRPC3 or TRPC6 subunit, respectively. Although more complex interpretations are possible, these data suggest that, in the hypertensive phenotype, there is a change in the composition of the TRPC3/6 tetramers, with a greater contribution of TRPC3 channels in the BPH cells.

We explored the functional correlate of these differences by analysing basal and receptor-activated cationic currents in freshly isolated VSMCs from BPN and BPH mice. Current amplitude at −150 mV was significantly larger in BPH cells (Fig. 6*B*). This difference remains when expressed it as current density (−8.1 ± 0.5 pA/pF in BPH *vs.* −6.4 ± 0.7 pA/pF in BPN) despite the larger size of BPH cells (16.9 ± 0.6 pF in BPH *vs.* 13.9 ± 0.5 pF in BPN) (Moreno-Domínguez *et al.* 2009). In addition

to differences in current size, there also were differences in Pyr10 and Pyr3 sensitivity, with the BPH cells being less sensitive to the drugs (Fig. 6*A* and *B*). These data suggest a decreased contribution of TRPC6 channels to the non-selective cationic conductance of BPH mesenteric VSMCs. Both results (i.e. the larger currents and the decrease of TRPC6 contribution) are compatible with a larger expression of TRPC3 channels in BPH cells. To confirm this, we explored the effect of intracellularly applied anti-TRPC3 antibodies on BPN and BPH cationic currents (Fig. 6*C*). Examples are shown of the time course of the current amplitudes at +80 and −150 mV in BPH cells in the presence of anti-RFP antibody (control; Fig. 6*C*, left) or anti-TRPC3 antibody in the pipette

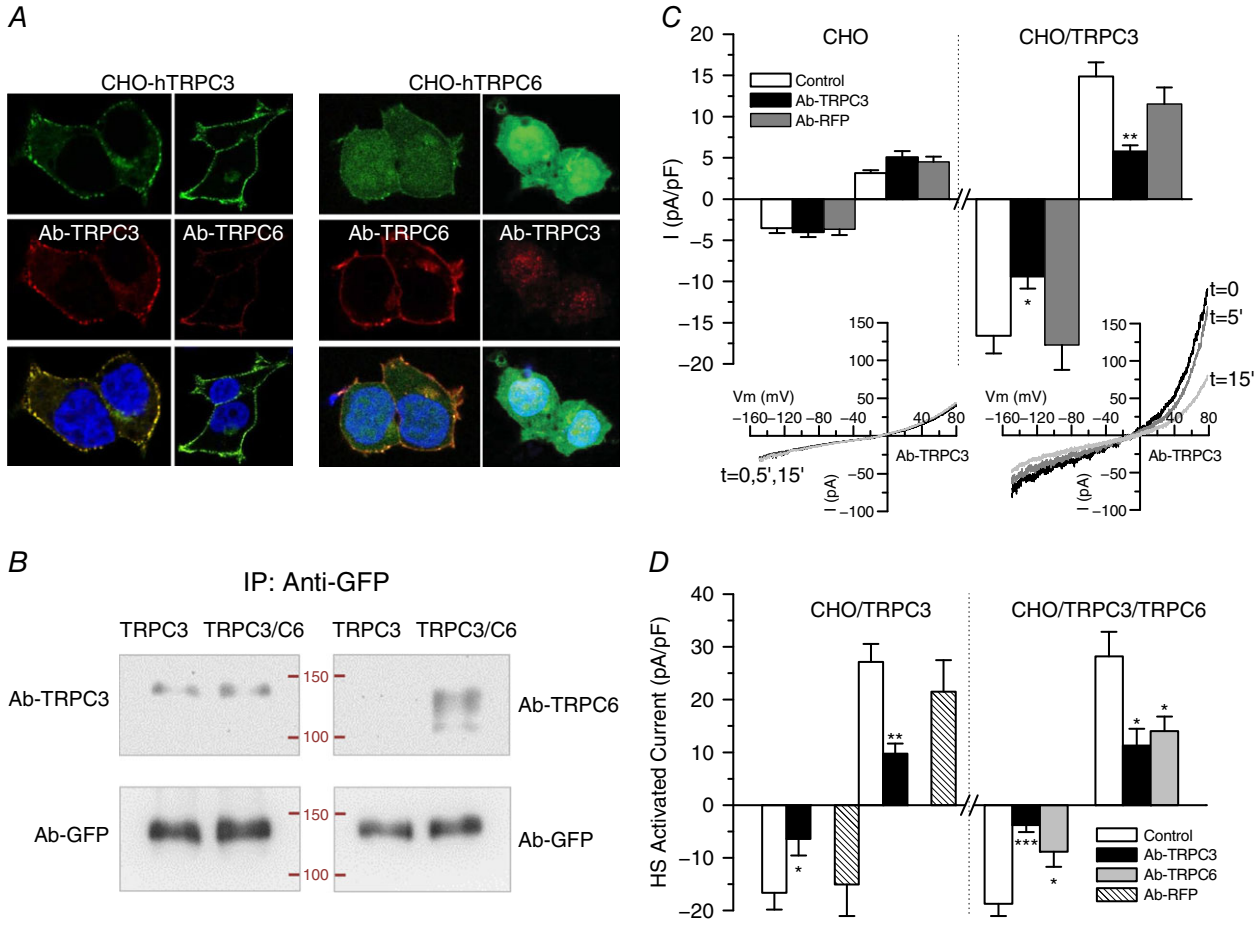

Figure 4. Use of antibodies to determine functional contribution, location and association of TRPC3 and TRPC6 channels in CHO cells

A, representative confocal images of immunolabelling with anti-TRPC3 and anti-TRPC6 of CHO cells transfected with TRPC3 (left) or TRPC6 (right). Immunostaining was predominant at the cell membrane and shows a good correlation with GFP-labelling for TRPC3 (a fusion protein). No cross-reactivity was observed in either case. *B*, TRPC3-GFP or TRPC3-GFP/TRPC6 cotransfected cells were immunoprecipitated with anti-GFP-trap and immunoblotted with GFP antibody (as a load control) or with anti-TRPC3 or anti-TRPC6 antibody. Labelling with anti-TRPC6 was detected on the cotransfected cells, demonstrating heteromultimeric association. Data are representative of two independent experiments. *C*, blocking effect of intracellularly applied antibodies on the cationic currents observed in transfected CHO cells. Average basal current density at −150 mV (open bars) and +80 mV (dashed bars) was obtained from whole-cell ramps applied every 5 s to control untransfected CHO cells and to cells transfected with TRPC3. The plots show the current density after 5–10 min of recording in control pipette solution or in the presence of the indicated antibodies. Each bar is the mean ± SEM of nine to 14 cells from at least four different experiments. The inset shows the current traces obtained at the indicated times in an untransfected CHO cell (left) or in a TRPC3-transfected CHO cell (right) with anti-TRPC3 antibody in the pipette solution. $^{*}p < 0.05$; $^{**}p < 0.01$ compared to CHO/TRPC3 control cells. *D*, the same protocol was used to explore the blocking effect of anti-TRPC3 or anti-TRPC6 on stretch-activated currents elicited from TRPC3 and TRPC3/C6 transfected cells upon exposure to the hypotonic solution (HS). The effects were calculated by subtracting basal, unstimulated currents and after 5–10 min of recording in control conditions or in the presence of the indicated antibodies. Data are the mean ± SEM, $n = 8$–10 cells.

solution (Fig. 6*C*, right), up to 10–12 min of recording. We monitored the stability of the recording conditions by checking cell capacitance and access resistance (data not shown) and holding current at −10 mV. The initial current amplitude was reduced by 25% after 5 min and by 39% after 10 min of recording when anti-TRPC3 was intracellularly applied, whereas no significant changes could be observed in control cells, either with an anti-RFP antibody or in the absence of antibodies. Average data obtained in VSMCs from BPN and BPH mice are depicted in Fig. 6*D*. The effect of anti-TRPC3 antibodies was only significant in BPH cells, again suggesting a greater contribution of TRPC3-containing channels to cationic currents in BPH VSMCs.

Finally, we also explored the amplitude of native currents in BPN and BPH VSMCs activated by several well defined agonists such as ATP (30 μM), UTP (50 μM) and phenylephrine (Phe 10 μM), as well as the DAG-permeable analogue OAG (100 μM) and also the blocking effects of Pry3 and/or Pyr10 (10 μM). Figure 7*A* shows the summary data. With the exception of UTP responses, which were significantly smaller in BPH VSMCs, the amplitude of the cationic currents elicited by all the other stimuli was not different between BPN and BPH cells. However, both preparations showed a remarkable difference when comparing the blocking effect of Pyr3/Pyr10 compounds. Although, in BPN cells, these drugs fully abolished the current activated by all the agonist studied, there is a fraction of this current that is not sensitive to Pyr3 (black bars) and/or Pyr10 (grey bars) in BPH cells. For example, in the case of ATP stimulation, although Pyr3/10 block almost completely the ATP-activated current in BPN VSMCs, the Pyr3/10-sensitive current represents only ~60% of this current in BPH VSMCs (Fig. 7*A*, right). Representative examples of the time course of the current amplitude at −100 mV and +40 mV in response to ATP alone or in combination with Pyr3 are shown in Fig. 7*B* (for a BPN cell) and Fig. 7*C* (a BPH cell).

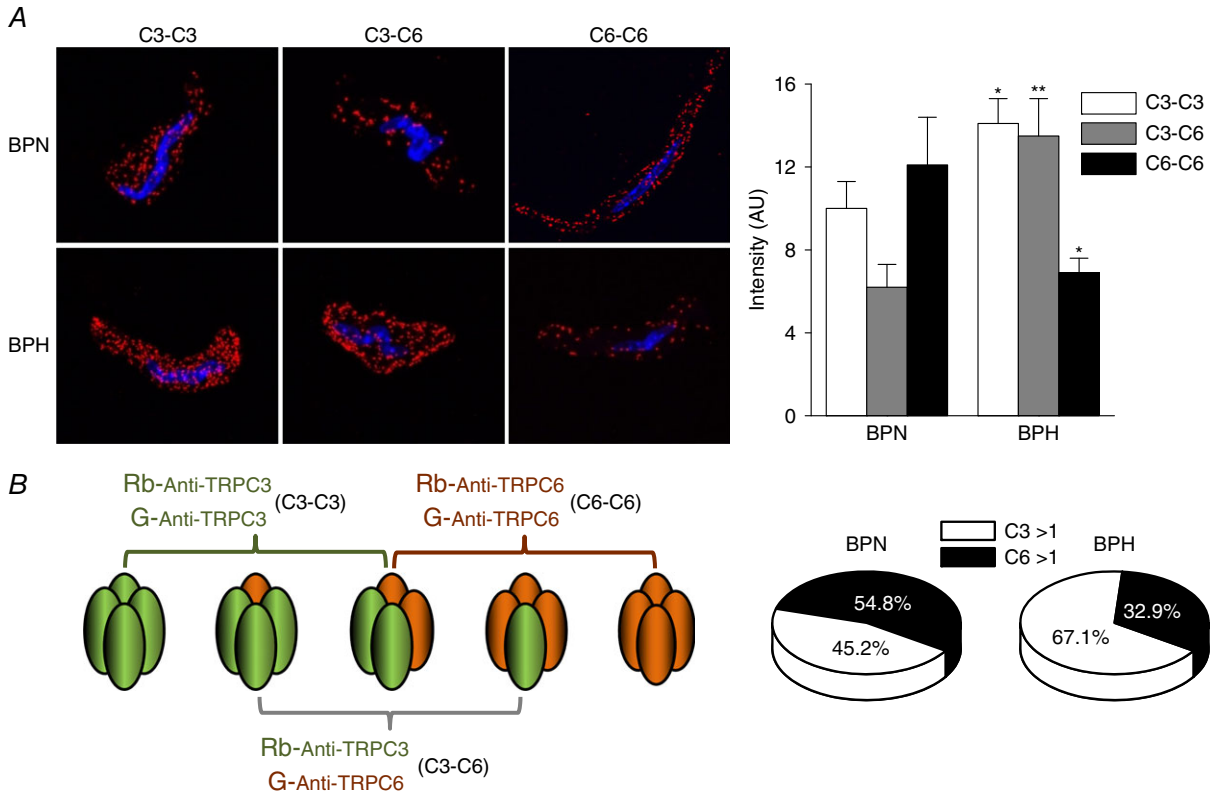

Figure 5. Differences in TRPC assembly in BPN and BPH mesenteric VSMCs
A, representative confocal images of the puncta density distribution using the PLA assay in BPN (upper) and BPH (lower) native VSMC cells. The bars plot shows the averaged density of puncta obtained in the three conditions represented in (*A*) for BPN and BPH cells. Data are the mean ± SEM; 36–64 cells in each group from four independent experiments. $^{*}p < 0.05$, $^{**}p < 0.01$ compared to the same condition in BPN. *B*, scheme of the possible associations between C3-C3, C6-C6 and/or C3-C6 subunits that can be recognized with each combination of antibodies used for the PLA assay. Following this scheme, the chart illustrates an interpretation of the data, considering 100% as the sum of the intensity of C3-C3 and C6-C6 groups and assuming that the C3-C6 group will be included in both. Accordingly, the C3-C3 group will contain associations with more than one C3 subunit (C3 > 1) and C6-C6 those with more than one C6 subunit (C6 > 1).

Discussion

In the present study, we have explored the hypothesis that TRPC3 and TRPC6 channels expressed in VSMCs may have a differential contribution to the regulation of vascular tone, which could be relevant for the changes in vascular reactivity associated with essential hypertension. This possibility was supported by the initial observation indicating a higher mRNA expression of those channels in resistance arteries (mesenteric *vs.* femoral or aorta). Furthermore, the changes in the mRNA expression levels of these channels when comparing VSMCs from BPN and BPH vessels are clearly different in resistance and conduit arteries (Fig. 1). Although the importance of either TRPC6 or TRPC3 channels in the vascular system has been demonstrated clearly over recent years (Earley & Brayden, 2015), the novelty of the present study relies on exploring the hypothesis that changes in these two channels upon hypertension determine a different composition of homo- and heterotetramers with discernible biophysical, pharmacological and functional properties.

Combining several methodological approaches and using both heterologously expressed channels and

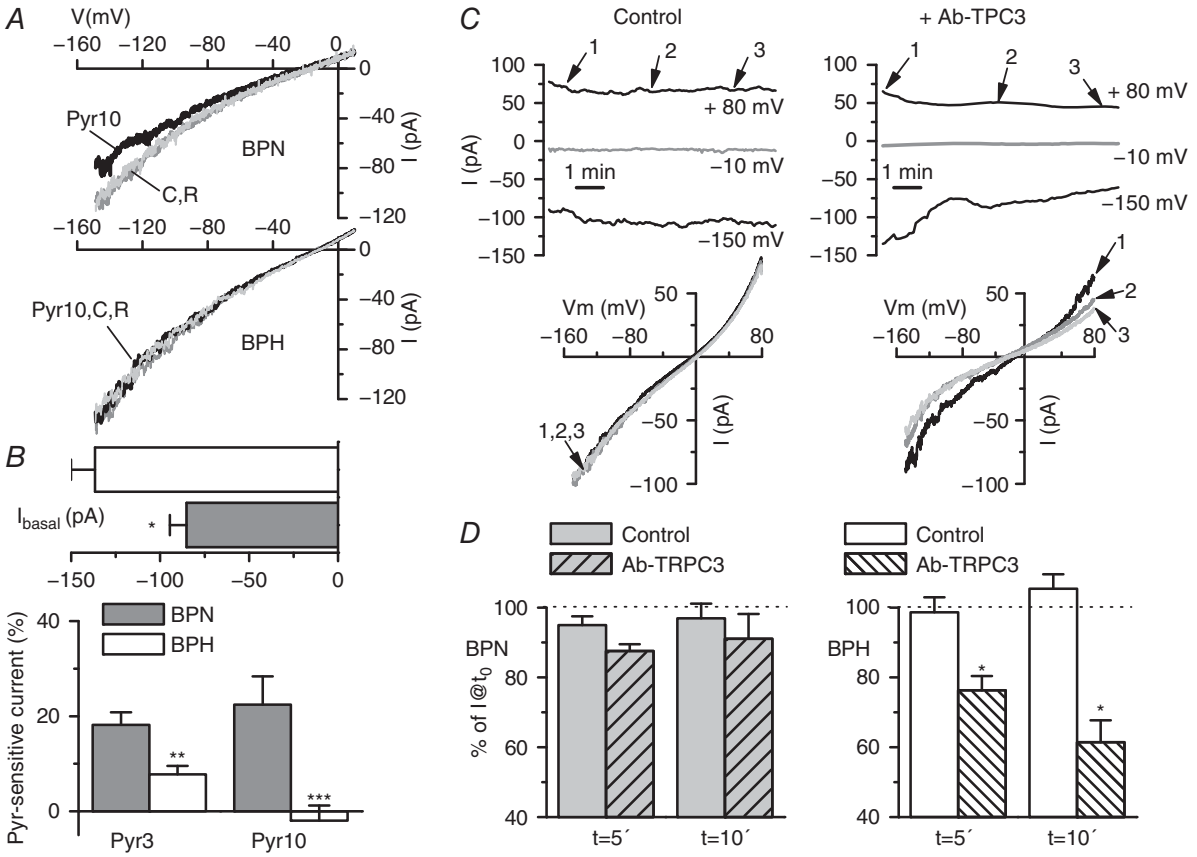

Figure 6. Characterization of basal cationic currents in BPH and BPN mesenteric VSMCs and effects of anti-TRPC3 antibody

A, basal cationic currents were obtained by voltage ramps in the presence of TRP external solution. The figure shows representative examples of current–voltage traces obtained in a BPN and a BPH mesenteric VSMC in control conditions (C), in the presence of 10 μM Pyr10 and after washout of the blocker (R). *B*, upper bar plot showing the current amplitude at −150 mV for both BPN and BPH cells (mean ± SEM, 40–60 cells in each group). The lower plot shows the average fraction of the Pyr3- or Pyr10-sensitive current at −150 mV in BPN (grey bars) or BPH cells (white bars). Each bar is the mean ± SEM of 10 cells (for Pyr3) and 23 cells (for Pyr10). *C*, representative examples of the time course of the currents elicited by voltage ramps in a BPH cell recorded with anti-RFP (left) or with anti-TRPC3 antibody (4 μg ml^{-1}) in the pipette solution (right). The plots show the current amplitude at −150 mV, +80 mV and at the holding potential (−10 mV, grey line). The time course of the cell capacitance and the access resistance were obtained simultaneously (not shown). Examples of the actual traces obtained with the ramp protocol at the time points of 0, 5 and 10 min (points 1, 2 and 3 in the graphs) are also depicted (bottom). *D*, average current amplitude at 5 and 10 min is represented as a fraction of the initial current amplitude both in control cells (solid bars) and in anti-TRPC3 treated cells (striped bars), for BPH (left plot) and BPN mesenteric VSMCs (right plot). Each bar is the mean ± SEM of seven to 14 cells in each group. For the control group, untreated cells and cells with anti-RFP antibody in the pipette solution were pooled together.

native cells, we conclude that TRPC3 and TRPC6 in BPH and BPN VSMCs show a different pattern of association (Fig. 8). VSMCs from BPH cells have a larger fraction of TRPC3-containing homo- and heterotetrameric channels with an increased basal activity, which can contribute to the more depolarized resting membrane potential observed in BPH VSMCs and to the increased vascular reactivity of BPH mesenteric arteries (Moreno-Domínguez *et al.* 2009). The larger basal cationic currents at negative potentials observed in BPH VSMCs were more sensitive to blockade with intracellularly applied anti-TRPC3 antibodies. The selectivity of this immunological blockade was confirmed in the heterologous system. In addition, BPH basal currents were less sensitive to Pyr10, which, in our hands, behaved as a selective blocker of TRPC6-containing channels.

In this regard, our work redefines the meaning of the pharmacological tools available for the study of TRPC3/6 channels. We found that the novel pyrazole compounds recently described as selective blockers of TRPC3 (mainly Pyr10 and also Pyr3) showed an increased selectivity for TRPC6-containing channels over TRPC3 homotetramers, in contrast to what has been described previously (Kiyonaka *et al.* 2009; Schleifer *et al.* 2012). Although the reported effect of these compounds on native TRPC3 channels (Kiyonaka *et al.* 2009; Koenig *et al.*

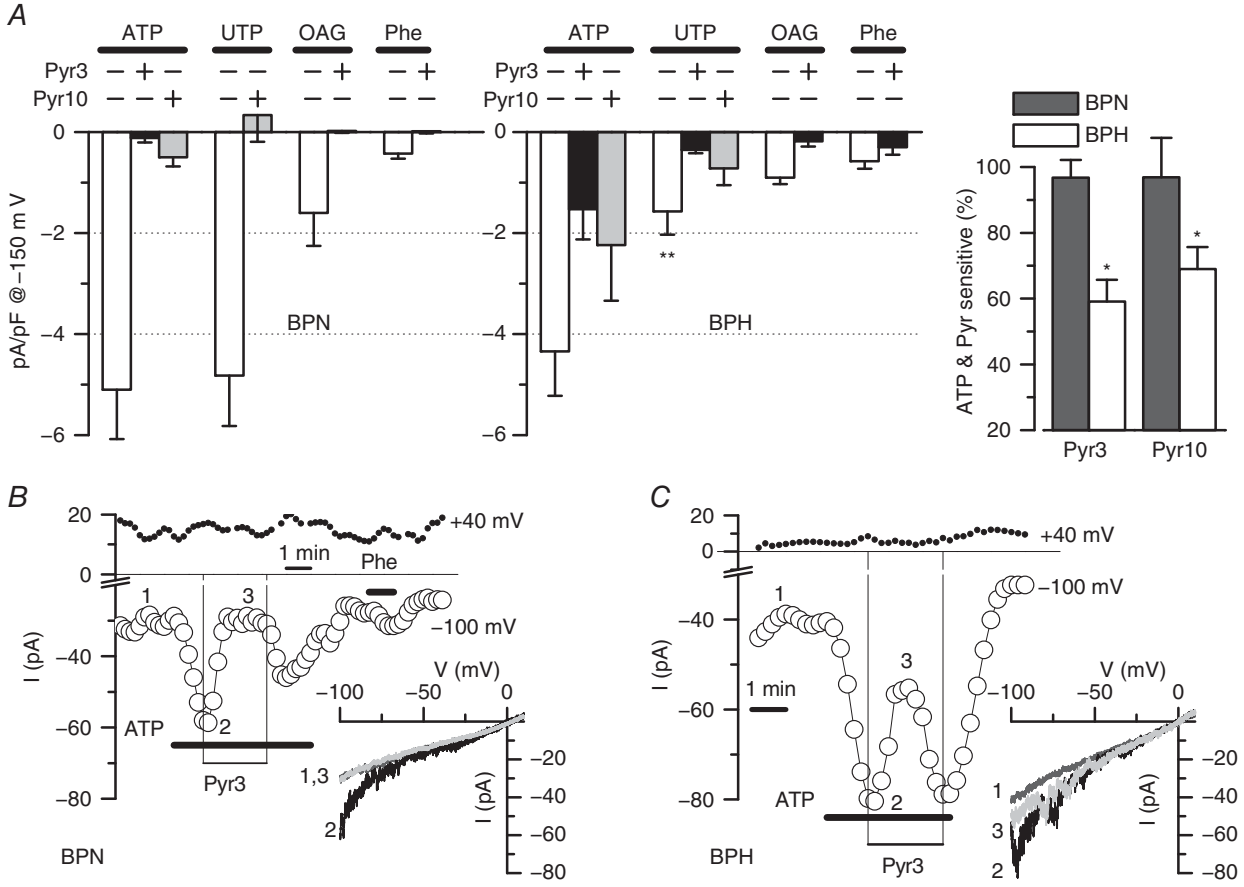

Figure 7. Effect of Pyr blockers on agonist-activated cationic currents in native VSMCs
A, summary data showing the current density at −150 mV of the current activated in the presence of ATP (30 μM), UTP (50 μM), OAG (100 μM) and phenylephrine (Phe, 30 μM) alone or in the presence of Pyr3 (10 μM) or Pyr 10 (10 μM) as indicated. Data were obtained from voltage ramps after subtracting basal, unstimulated currents. Data were obtained from BPN and BPH isolated mesenteric VSMCs. Blockers were applied in the presence of the agonists, and their effects were calculated after subtracting basal current as well. Agonist-induced currents are the average from 17–36 cells in each group, whereas the effect of the blockers was tested in 6–14 cells in each group. $^{**}p < 0.01$ compared with UTP-activated currents in BPN cells. The inset shows the fraction of the ATP-activated current that can be blocked by Pyr3 or Pyr10 in BPN (black bars) and BPH cells (white bars). $^{*}p < 0.05$ compared to UTP effect in BPN. *B* and *C*, representative examples of a BPN and a BPH cells that were stimulated with 30 μM ATP alone or with 10 μM Pyr3 as indicated in the graphs. The time course of the current amplitude at −100 mV (open circles) and +40 mV (filled circles) was obtained from voltage ramps applied every 5 s. Traces in control conditions (1) in the presence of ATP (2) or of ATP + Pyr3 (3) are shown in the inset. BPN cell was also challenged with 30 μM Phe as indicated.

2013) could be compatible with the presence of TRPC3/6 heterotetramers, we do not have a clear explanation for the disparities observed in the recombinant system, although several differences in the preparation and the methodology of the study can be highlighted. We have performed our characterization using TRPC3 overexpression in CHO cells and we have determined both basal and stretch-activated currents using electrophysiological techniques. By contrast, previous studies used TRPC3-transfected HEK293 (and/or HEK293T) cells and channel activity was measured by determining Ca^{2+} entry upon stimulation of endogenous muscarinic receptors with carbachol (Kiyonaka *et al.* 2009; Schleifer *et al.* 2012). It is possible that changes in the associated proteins endogenously expressed in the different cell lines used and/or changes in the response to blockers related to the specific activation pathway could contribute to the observed discrepancies. Moreover, and possibly more importantly, although we had analysed the acute effects of Pyr compounds that were applied to the external solution in the presence of the stimulus (for stretch- or agonist-activated currents), in these other

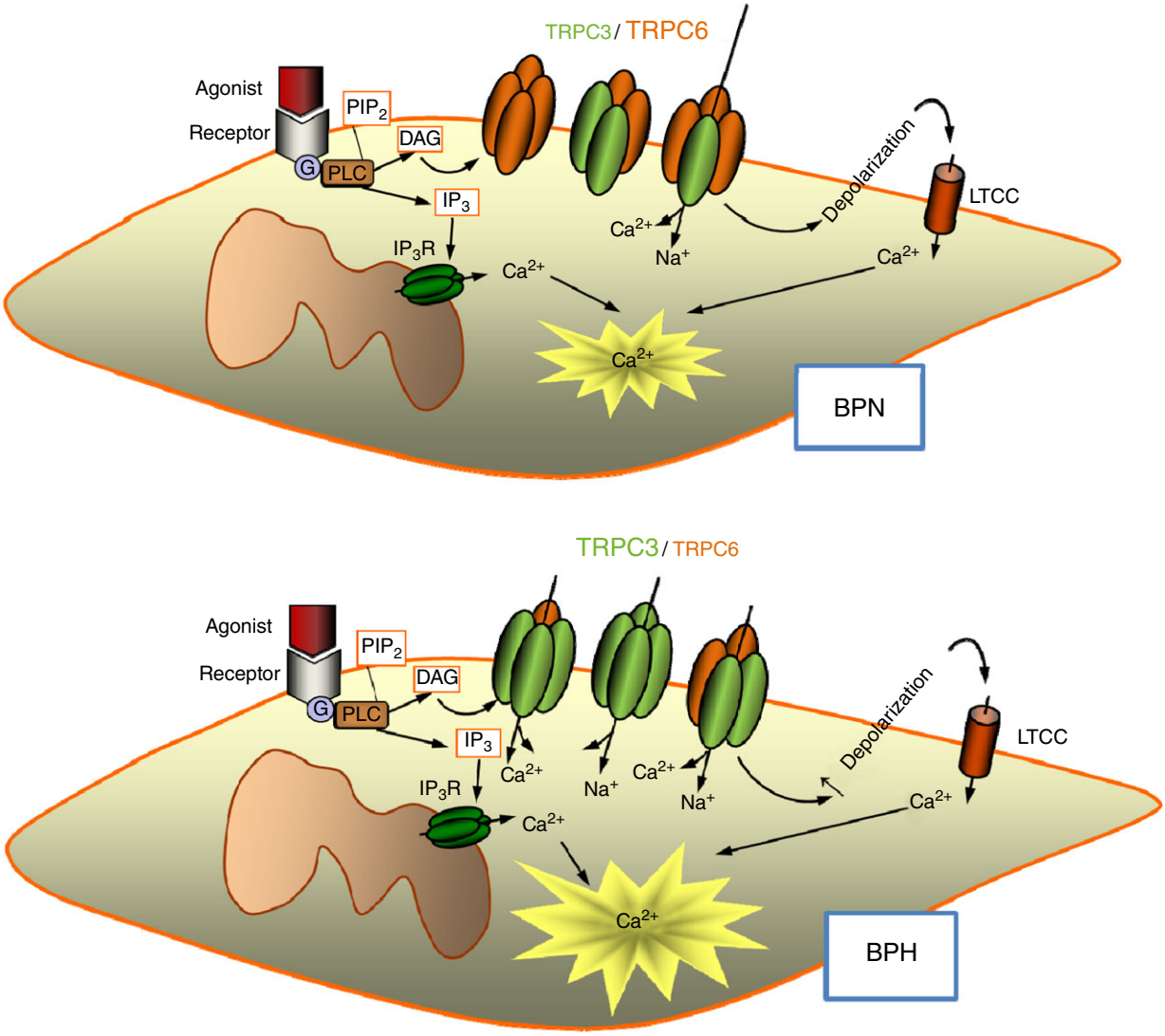

Figure 8. Diagram of the proposed changes in TRPC3/C6 composition upon hypertension
Homo- and heteromultimeric TRPC3/C6 channels contribute to basal cationic currents in VSMCs, thus modulating resting membrane potential and hence basal [Ca^{2+}] concentration and cell excitability. BPN cells may have a dominant expression of TRPC6 channels, associated with either homo- or heterotetramers, which show strong inward rectification. This will result in low basal currents at values around the resting membrane potential. In BPH cells, the increased expression of TRPC3 channels determines a change in the properties of heteromultimers, which will have now a larger proportion of TRPC3 subunits. TRPC3 channels show weak rectification, which will determine an increased basal current at negative potential contributing to cell depolarization, raising the [Ca^{2+}] concentration and increasing basal tone.

studies, the effects of Pyr3 on TRPC3-activated currents or TRPC3-dependent Ca^{2+} entry are determined upon chronic pre-treatment of the cells with Pyr3, which was always applied to the external solution previous to stimulation. Finally, the more detailed characterization of TRPC3 modulation (Kiyonaka *et al.* 2009) was carried out with Pyr3 because the more selective Pyr10 was not available at that time.

Some or several of these aspects may contribute to these largely unexpected differences on the sensitivity Pyr compounds of TRPC3 and TRPC6. In addition, our findings with the pharmacological blockade of TRPC3/6 channels could be reproduced both in heterologous and native systems with the use of blocking antibodies (Figs 4 and 6), providing an additional level of confidence to the results of the present study. This technique represents a powerful approach for the identification of the molecular correlates of native currents in the absence of more specific blockers, and also for defining the composition of heteromultimeric channel complexes (Sanchez *et al.* 2002; Moreno-Domínguez *et al.* 2009). We have been particularly careful with this group of experiments with intracellularly applied antibodies, both in the selection of the technically acceptable experiments and in the use of a large number of controls, including control antibodies for transfected cells and TRPC3/6 antibodies for untransfected cells.

Finally, our conclusions from the functional characterization of the TRPC-mediated cationic currents in native cells are supported by the results obtained with PLA. These studies indicated a larger proportion of TRPC3 subunits in BPH cells and a decreased expression of TRPC6. This observation is consistent with a larger number of TRPC3 homotetramers in these cells and/or heteromultimeric TRPC3/6 complexes with a larger proportion of TRPC3 subunits. Although these results would also be consistent with the formation of clusters of multimers containing only one TRPC3 subunit, based on the functional characterization of TRPC3/6 transfected cells, this latter possibility is doubtful.

TRPC channels show a high structural homology that favours the formation of heteromultimeric complexes, and this explains why the spectrum of biophysically and functionally distinct ROC or SOC exceeds what can be obtained with a single TRPC channel heterologously expressed. Because the composition of native TRPC complexes is poorly defined, the task of assigning a well-defined molecular correlate to receptor-activated cationic currents has proven difficult. Considering that many TRPC are often co-expressed in the same cell (Hofmann *et al.* 2002), heteromultimerization in addition to homomultimerization represents an attractive possibility. The presence of heteromultimeric TRPC6/C7 channels in vascular smooth muscle has been demonstrated using both biochemical and functional approaches (Maruyama *et al.* 2006). Interestingly, heteromultimeric TRPC6/C7 channels exhibit one property (modulation of current amplitude by changes in extracellular $[Ca^{2+}]$) that is distinct from homomultimeric TRPC6 or TRPC7, suggesting that these channel complexes are endowed with emergent properties. However, the evidence of TRPC subunit heteromultimerization was obtained using cultured A7r5 cells rather than native VSMCs. A better understanding of the mechanisms determining how TRPC subunits combine to form functional ion channel complexes is an essential prerequisite to evaluate their contribution to endogenous cation currents. In many cases, the studies using KO animals could help to define the role of the individual channels but, in the particular case of TRPC3 and TRPC6, these KO studies do not provide a unifying view of their individual role or the meaning of heteromultimeric associations. With respect to the innvestigation of mechanosensors, several studies using single, double and up to quadruple TRPC KOs conclude that TRPC functions involve combined activity of multiple TRPC proteins (Sexton *et al.* 2016). Although interfering with one single TRPC channels does not alter behavioural responses (Quick *et al.* 2012), double TRPC3/C6 KOs show sensory deficits that are augmented in quadruple KO (Sexton *et al.* 2016). These results indicate that TRPC3/C6 channels in sensory neurons show some functional redundancy. However, TRPC6 KO mice show a vascular phenotype as a result of a compensatory upregulation of VSMCs TRPC3 channels, which are not able to functionally replace TRPC6 channels (Dietrich *et al.* 2005), indicating that these two channels are not freely interchangeable and that they have distinct and non-redundant roles in the control of vascular tone. Because of this compensatory up-regulation of TRPC3 channels in VSMCs, the TRPC6 KO mice showed increased vascular reactivity and augmented mean blood pressure, which is in agreement with our present data. Importantly, our results confirm that the changes observed in the hypertensive animal accidentally created by Dietrich *et al.* (2005) when suppressing TRPC6 channels may be relevant to understand the mechanisms involved in the natural history of essential hypertension.

Finally, regarding TRPC3 channels, their expression has been reported to be upregulated in VSMCs in animal models of essential hypertension, such as the spontaneously hypertensive rat and the two-kidney, two-clip hypertensive rats (Liu *et al.* 2009; Wang *et al.* 2016). However, the study of concomitant changes in the expression of other TRPC channels has not received a systematic attention. There is only one recent report in which the role of upregulation of TRPC3 channels and downregulation of TRPC1 channels during hypertension and their contribution to changes in contractility is explored (Noorani *et al.* 2011), although these two changes

are studied and explained independently, with no attempt to link them to a different proportion of heteromultimeric TRPC channels. In this context, the present study provides a new paradigm for interpreting and better understanding many of the previous studies regarding the role of TRPC channels in vascular physiology and their contribution to altered vascular tone.

References

Adebiyi A, Thomas-Gatewood CM, Leo MD, Kidd MW, Neeb ZP & Jaggar JH (2012). An elevation in physical coupling of type 1 inositol 1,4,5-trisphosphate (IP3) receptors to transient receptor potential 3 (TRPC3) channels constricts mesenteric arteries in genetic hypertension. *Hypertension* **60**, 1213–1219.

Albert AP & Large WA (2006). Signal transduction pathways and gating mechanisms of native TRP-like cation channels in vascular myocytes. *J Physiol* **570**, 45–51.

Beech DJ, Muraki K & Flemming R (2004). Non-selective cationic channels of smooth muscle and the mammalian homologues of *Drosophila* TRP. *J Physiol* **559**, 685–706.

Cidad P, Moreno-Domínguez A, Novensá L, Roqué M, Barquín L, Heras M, Pérez-García MT & López-López JR (2010). Characterization of ion channels involved in the proliferative response of femoral artery smooth muscle cells. *Arterioscler Thromb Vasc Biol* **30**, 1203–1211.

Dietrich A, Chubanov V, Kalwa H, Rost BR & Gudermann T (2006). Cation channels of the transient receptor potential superfamily: their role in physiological and pathophysiological processes of smooth muscle cells. *Pharmacol Ther* **112**, 744–760.

Dietrich A, Mederos Y, Schnitzler M, Gollasch M, Gross V, Storch U, Dubrovska G, Obst M, Yildirim E, Salanova B, Kalwa H, *et al.* (2005). Increased vascular smooth muscle contractility in TRPC6–/– mice. *Mol Cell Biol* **25**, 6980.

Earley S & Brayden JE (2015). Transient receptor potential channels in the vasculature. *Physiol Rev* **95**, 645–690.

Gonzales AL, Yang Y, Sullivan MN, Sanders L, Dabertrand F, Hill-Eubanks DC, Nelson MT & Earley S (2014). A PLCg1-dependent, force-sensitive signaling network in the myogenic constriction of cerebral arteries. *Sci Signal* **7**, ra49.

Hofmann T, Obukhov AG, Schaefer M, Harteneck C, Gudermann T & Schultz G (1999). Direct activation of human TRPC6 and TRPC3 channels by diacylglycerol. *Nature* **397**, 259–263.

Hofmann T, Schaefer M, Schultz G & Gudermann T (2002). Subunit composition of mammalian transient receptor potential channels in living cells. *Proc Natl Acad Sci USA* **99**, 7461–7466.

Inoue R, Jensen LJ, Jian Z, Shi J, Hai L, Lurie AI, Henriksen FH, Salomonsson M, Morita H, Kawarabayashi Y, Mori M, Mori Y & Ito Y (2009). Synergistic activation of vascular TRPC6 channel by receptor and mechanical stimulation via phospholipase C/Diacylglycerol and phospholipase A2/ω-hydroxylase/ 20-HETE pathways. *Circ Res* **104**, 1399–1409.

Kiyonaka S *et al.* (2009). Selective and direct inhibition of TRPC3 channels underlies biological activities of a pyrazole compound. *Proc Natl Acad Sci USA* **106**, 5400–5405.

Koenig S, Schernthaner M, Maechler H, Kappe CO, Glasnov TN, Hoefler G, Braune M, Wittchow E & Groschner K (2013). A TRPC3 blocker, ethyl-1-(4-(2,3,3-trichloroacrylamide)phenyl)-5-(trifluoromethyl)-1H-pyrazole-4-carboxylate (Pyr3), prevents stent-induced arterial remodelings. *J Pharmacol Exp Ther* **344**, 33–40.

Linde CI, Karashima E, Raina H, Zulian A, Wier WG, Hamlyn JM, Ferrari P, Blaustein MP & Golovina VA (2012). Increased arterial smooth muscle Ca^{2+} signaling, vasoconstriction, and myogenic reactivity in Milan hypertensive rats. *Am J Physiol Heart Circ Physiol* **302**, H611–H620.

Liu D, Yang D, He H, Chen X, Cao T, Feng X, Ma L, Luo Z, Wang L, Yan Z, Zhu Z & Tepel M (2009). Increased transient receptor potential canonical type 3 channels in vasculature from hypertensive rats. *Hypertension* **53**, 70–76.

Livak KJ & Schmittgen TD (2001). Analysis of relative gene expression data using real-time quantitative PCR and the 2ˆ(-ΔΔCT) method. *Methods* **25**, 402–408.

Maruyama Y, Nakanishi Y, Walsh EJ, Wilson DP, Welsh DG & Cole WC (2006). Heteromultimeric TRPC6-TRPC7 channels contribute to arginine vasopressin-induced cation current of A7r5 vascular smooth muscle cells. *Circ Res* **98**, 1520–1527.

Mederos Y, Schnitzler M, Storch U, Meibers S, Nurwakagari P, Breit A, Essin K, Gollasch M & Gudermann T (2008). Gq-coupled receptors as mechanosensors mediating myogenic vasoconstriction. *EMBO J* **27**, 3092–3103.

Moreno-Domínguez A, Cidad P, Miguel-Velado E, López-López JR & Pérez-García MT (2009). De novo expression of Kv6.3 contributes to changes in vascular smooth muscle cell excitability in a hypertensive mice strain. *J Physiol* **587**, 625–640.

Nilius B & Honoré E (2012). Sensing pressure with ion channels. *Trends Neurosci* **35**, 477–486.

Noorani MMZ, Noel RC & Marrelli SP (2011). Upregulated TRPC3 and downregulated TRPC1 channel expression during hypertension is associated with increased vascular contractility in rat. *Front Physiol* **JUL**, 1–9.

Owens GK, Kumar MS & Wamhoff BR (2004). Molecular regulation of vascular smooth muscle cell differentiation in development and disease. *Physiol Rev* **84**, 767–801.

Quick K *et al.* (2012). TRPC3 and TRPC6 are essential for normal mechanotransduction in subsets of sensory neurons and cochlear hair cells. *Open Biol* **2**, 120068.

Reading SA, Earley S, Waldron BJ, Welsh DG & Brayden JE (2005). TRPC3 mediates pyrimidine receptor-induced depolarization of cerebral arteries. *Am J Physiol Hear Circ Physiol* **288**, H2055–H2061.

Sanchez D, Lopez-Lopez JR, Perez-Garcia MT, Sanz-Alfayate G, Obeso A, Ganfornina MD & Gonzalez C (2002). Molecular identification of Kva subunits that contribute to the oxygen-sensitive K^+ current of chemoreceptor cells of the rabbit carotid body. *J Physiol* **542**, 369–382.

Schlager G & Sides J (1997). Characterization of hypertensive and hypotensive inbred strains of mice. *Lab Anim Sci* **47**, 288–292.

Schleifer H, Doleschal B, Lichtenegger M, Oppenrieder R, Derler I, Frischauf I, Glasnov TN, Kappe CO, Romanin C & Groschner K (2012). Novel pyrazole compounds for pharmacological discrimination between receptor-operated and store-operated Ca(2+) entry pathways. *Br J Pharmacol* **167**, 1712–1722.

Senadheera S, Kim Y, Grayson TH, Toemoe S, Kochukov MY, Abramowitz J, Housley GD, Bertrand RL, Chadha PS, Bertrand PP, Murphy TV, Tare M, Birnbaumer L, Marrelli SP & Sandow SL (2012). Transient receptor potential canonical type 3 channels facilitate endothelium-derived hyperpolarization-mediated resistance artery vasodilator activity. *Cardiovasc Res* **95**, 439–447.

Sexton JE, Desmonds T, Quick K, Taylor R, Abramowitz J, Forge A, Kros CJ, Birnbaumer L & Wood JN (2016). The contribution of TRPC1, TRPC3, TRPC5 and TRPC6 to touch and hearing. *Neurosci Lett* **610**, 36–42.

Sharif-Naeini R, Dedman A, Folgering JHA, Duprat F, Patel A, Nilius B & Honor E (2008). TRP channels and mechanosensory transduction: Insights into the arterial myogenic response. *Pflügers Arch Eur J Physiol* **456**, 529–540.

Shin YC, Shin SY, So I, Kwon D & Jeon JH (2011). TRIP database: a manually curated database of protein-protein interactions for mammalian TRP channels. *Nucleic Acids Res* **39**, 356–361.

Tajada S, Cidad P, Moreno-Domínguez A, Pérez-García MT & López-López JR (2012). High blood pressure associates with the remodelling of inward rectifier K+ channels in mice mesenteric vascular smooth muscle cells. *J Physiol* **590**, 6075–6091.

Wang M, Tang YB, Ma MM, Chen JH, Hu CP, Zhao SP, Peng DQ, Zhou JG, Guan YY & Zhang Z (2016). TRPC3 channel confers cerebrovascular remodelling during hypertension via transactivation of EGF receptor signalling. *Cardiovasc Res* **109**, 34–43.

Wilson C & Dryer SE (2014). A mutation in TRPC6 channels abolishes their activation by hypoosmotic stretch but does not affect activation by diacylglycerol or G protein signaling cascades. *Am J Physiol Renal Physiol* **306**, F1018–F1025.

Yeon S-I, Kim JY, Yeon D-S, Abramowitz J, Birnbaumer L, Muallem S & Lee Y-H (2014). Transient receptor potential canonical type 3 channels control the vascular contractility of mouse mesenteric arteries. *PLoS ONE* **9**, e110413.

Additional information

Competing interests

The authors declare that they have no competing interests.

Author contributions

MTPG and JRLL designed the work. IAM, PC and MTPG performed the experiments and carried out the analysis and interpretation of the data. MTPG and JRLL wrote the manuscript and all authors revised it critically for important intellectual content. All authors approved the final version of the manuscript. All the experiments were conducted in MTPG and JRLL laboratories at the University of Valladolid.

Funding

The present study was supported by grants from the Ministerio de Economía y Competitividad (MINECO), Instituto de Salud Carlos III (RIC, RD12/0042/0006, Red Heracles) and Programa Estatal de Investigación (BFU2013-45867-R to JRLL and MTPG). I A-M is supported by the Junta de Castilla y León through the Fondo Social Europeo.

Acknowledgements

We thank Esperanza Alonso for excellent technical assistance and Drs Klaus Groschner (University of Graz) and Jason Yuan (University of Arizona) for their gift of TRPC3 and TRPC6 plasmids, respectively.